THE BIRTH AND THE FATE OF CLOSE AND WIDE BINARY STARS

by

Hsiang-Chih Hwang

A dissertation submitted to Johns Hopkins University

in conformity with the requirements for the degree of

Doctor of Philosophy

Baltimore, Maryland

August 2021

Abstract

Binary stars, where two stars are orbiting around a common center of mass, are at the core of modern astronomy. Since a significant fraction of stars are in multiple systems, binaries are now a critical component in all subfields, from star formation, to planet formation, to the reionization of the Universe shortly after the Big Bang. Close binaries are the origin of many exotic astronomical events, including type Ia supernovae which have been used to measure the accelerated expansion of the Universe. The recent detection of gravitational waves opens a new window to witness the mergers of black hole and neutron star binaries. On the other extreme, wide binaries are easily disrupted by gravitational perturbations, making them a unique tool to probe the visible and invisible Galactic structures. Therefore, a complete understanding of binary formation and evolution is critical to modern astronomy.

In my thesis, I use the revolutionary survey *Gaia* to reveal the birth and the fate of close and wide binary stars. Using the kinematic-dating method, I reveal the lifetime of contact binaries, providing key constraints on their formation and their death. I develop a comoving-search method to identify wide stellar companions around hot jupiter hosts, investigating the connection between the planet formation and the wide stellar companions. By combining

Gaia with a cutting-edge large spectroscopic survey, I report the first known relation between metallicity and the wide binary fraction. This relation suggests that the formation of wide binaries is more complicated than what was thought before. Following this direction, I conduct a detailed wide binary search in the Milky Way halo, further ruling out several hypotheses for wide binary formation. In the end, I conclude with the prospects of binary star research.

Thesis Committee

Primary Readers

Nadia Zakamska (Primary Advisor)
      Professor
      Department of Physics and Astronomy
      Johns Hopkins Krieger School of Arts and Sciences

Timothy Heckman
      Professor
      Department of Physics and Astronomy
      Johns Hopkins Krieger School of Arts and Sciences

Alternate Readers

Emanuele Berti
Professor
Department of Physics and Astronomy
Johns Hopkins Krieger School of Arts and Sciences

Sarah Hörst
Associate Professor
Department of Earth and Planetary Sciences
Johns Hopkins Krieger School of Arts and Sciences

Pablo Iglesias
Professor
Department of Electrical and Computer Engineering
Johns Hopkins Whiting School of Engineering

Acknowledgments

I thank my parents for supporting me throughout my life. I have always been an obnoxious child who does whatever he wants. I declined the medical school offer that was once their dream, and I did not pursue the Electrical Engineering career that was once my original undergraduate major, which they would have strongly preferred. Instead, I pursued my dream, astronomy. This decision was definitely not easy on them, and I can relate to them more and more as I mature. However, my parents continued to give me full support through all these years. Without them, I would not be the person I am today. I especially appreciate my mom for educating me. I can always hear her motto "do your best, and let God decide the rest" in my heart. I thank my dad for working hard to raise our family and for doing all the tedious tasks for me without any complaint, such as reading through my scholarship application in great detail. I thank my lifetime idol, my older brother, for everything he did. He looked after me when I was a kid, helped me when I had tensions with mom and dad, and continued to take care of me when I came to the States. I could not ask for a better family, so thank you and love you all very much.

I am deeply grateful to my thesis advisor, Professor Nadia Zakamska. When I was applying for graduate school, I contacted several professors I

was interested in, and your response was the longest one, even longer than the one I sent out (which was already very long). That was how I started working with you. When I was a first-year PhD student, I struggled a lot with my English writing. I still remember that you needed to correct nearly every sentence in my paper draft. I deeply appreciate your incredible patience with all my paper drafts and proposals. You are constantly encouraging and supportive. In the department's Christmas party in my first year, you told me that "writing is learnable", encouraging me to discover and exploit my own unlearnable characteristics. Without your help, I could not have gotten the Gardner fellowship or the HST proposal. You sacrificed nearly one week to take me to the Apache Point Observatory for my training, where you suffered from altitude sickness. You gave me full freedom to explore all the different kinds of science. It is incredible that in a single meeting, we can discuss science from quasars, supermassive black holes, Milky Way, binary stars, white dwarfs, young stellar objects, all the way to planets. You not only teach me how to do research, but also teach me how to advise students (Vedant, Evan, Gavin, Brandon, ...). It is impossible to list everything I feel grateful about to you, but I sincerely think that I have the best PhD advisor in the world.

My PhD career would not be successful without the help of many professors and scientists. I thank Tim Heckman for being the advisor of my second-year research project. I learned tremendously from your keen intuition about science. You could remember the plots I made months ago, and you could even identify bugs in the survey's pipeline by looking at my scatter

plots. I appreciate all kinds of scientific discussions with Kevin Schlaufman. Your wide range of knowledge significantly broadens the scope of my research. I am grateful to Rosie Wyse's advice throughout my PhD. Our close collaboration started back from my first year when I was a TA for your undergraduate Stellar Physics class, and I have learned tremendously from your insights since then. I thank my UIUC collaborators, Yue Shen and Xin Liu. You are my role models for balancing academic and family life. Without you, our VODKA project would not be successful. I thank Yuan-Sen Ting for always being extremely helpful with my research. You even read my draft when you had a severe fever. Your many data-driven techniques significantly changed my point of view in how to approach astronomical research.

Life in Baltimore would not be this joyful without all my friends at Hopkins. I thank Ai-Lei, Yi-Kuan, Ting-Wen for being close friends and for all our scientific discussions. I thank all my groupmates, especially Rachael and Kirsten, for giving me so much help and so many suggestions on various things. My lovely officemates at 115, in particular Erini, Jacob, and Cicero, I enjoyed those office times so much, including coffee, snacks, gossips, and science discussion. Thank you, Canon, Weichen, Bingjie, and Carol. We shared all the highs and lows together throughout our PhD careers, from TA training, lab, research exams, GBO, job applications, to defense. I will not forget our traditional RA treat, crab feasts, and Wednesday gatherings.

I thank all my Taiwanese folks in Baltimore. I thank everyone in Room 507 who made getting used to life in the States much easier. I thank everyone who has ever played badminton with me at the Recreation Center. It is an

honor for me to be the organizer of our badminton team. I did not live in college dorms before coming to the States, so I worried about whether or not I could live well with roommates. This concern turned out to be redundant because of my wonderful roommates, Szu-Jui, Nae-Chyun, and Ting-Wei Liao. Our weekly coffee hours were the key to maintaining sanity through the Covid time. Lastly, I am deeply thankful for meeting and having my girlfriend Ting-Wei Young in my life. You are constantly supportive with my research, reading all my paper drafts and emails and listening to all my presentations. You are always patiently listening to my murmurs about research ideas on our dates. You sacrifice numerous weekends to work with me at coffee shops and milk tea shops. Thank you for being on my side and beyond.

Table of Contents

6   Concluding Statement   **181**

List of Tables

List of Figures

Chapter 1

Introduction

We are truly fortunate that our Sun does not have any stellar companions. Otherwise, if the Sun had, or used to have, stellar companions, the formation environments of planets would be strongly perturbed, and the Earth and the human being might not come into existence. In fact, about 50% of Sun-like stars in the Milky Way have stellar companions (Duquennoy and Mayor, 1991). Therefore, it is lucky that we can enjoy our life on Earth with other planetary siblings crossing the sky.

Binaries, where two stars are orbiting around a common center of mass, have been known back in ancient human history. The resolved binary stars Mizar and Alcor in the Big Dipper (Ursa Major) are bright enough for naked eyes, and their separation of 0.2 deg was used as a vision test in the Arabic literature in the 13th century (and was known earlier). However, their physics of being bound as a physical binary was not known until the development of Isaac Newton's gravitation theory in the 17th century. Since then, together with the development of telescope technology, many other resolved binaries have been identified and studied.

Another type of binaries is found by their varying brightness due to eclipses, the so-called eclipsing binaries. These binaries have small separations such that their component stars are not resolved in ground-based telescopes due to the turbulence in the atmosphere. Due to their small separations, their orbital periods can be as small as one day. The binary origin of the first known eclipsing binary, Algol, was recognized back in 1783 by John Goodricke.

The modern ground-based and space-based observational techniques as well as large-field astronomical surveys significantly improve our understanding of binaries. Variability surveys include the Kepler mission, Optical Gravitational Lensing Experiment (OGLE), All-Sky Automated Survey for Supernovae (ASAS-SN), Zwicky Transient Facility (ZTF) have discovered hundreds of thousands of eclipsing binaries. The astrometry survey Gaia measures the parallaxes and proper motions for billions of stars (Gaia Collaboration et al., 2016; Gaia Collaboration et al., 2018a), resulting in one million wide binaries known today (El-Badry, Rix, and Heintz, 2021).

Binary stars continue to play a critical role in modern astronomy. Since a significant fraction of stars are in multiple systems (Duquennoy and Mayor, 1991; Duchêne and Kraus, 2013), binaries are a critical ingredient of astrophysics across in all subfields, from star formation, to planet formation, to the reionization of the Universe shortly after the Big Bang. With larger samples of binaries as well as better coverage of a wide range of binary separations, we finally have a more complete picture of binary demographics in terms of their separation distributions and mass dependence (Duquennoy and Mayor, 1991;

2

Figure 1.1: Stellar merger events that are associated with close binaries. Left: the kilonova from the merger of two neutron stars (image: ESA/Hubble Space Telescope). Middle: supernova 1994D (the bright spot on the lower left), which is spectroscopically confirmed as a type Ia supernova (image: Hubble Space Telescope). Right: stellar explosion V838 Mon in the Milky Way, whose origin may be a close binary (image: ESA/Hubble Space Telescope).

Raghavan et al., 2010; Duchêne and Kraus, 2013; Moe and Di Stefano, 2017).

Close binaries are the origin of many extraordinary events in the Universe (Fig. 1.1). Kilonovae arise coming from the mergers of double neutron stars, and gravitational waves from such an event were first detected in 2017 (Abbott et al., 2017). Type-Ia supernovae have been used to measure the accelerated expansion of the Universe (Riess et al., 1998), and they originate from the close binaries consisting of a white dwarf. Luminous red novae are produced in the merger of contact binaries on (or close to) the main sequence, with the first fascinating known case in the Milky Way captured in 2008 (Tylenda et al., 2011).

On the opposite end of the separation distribution, wide binaries are so weakly bound that they can serve as a unique probe of gravitational fields. Their orbits can be changed or disrupted due to gravitational interactions with other structures in the Milky Way (Bahcall, Hut, and Tremaine, 1985;

Weinberg, Shapiro, and Wasserman, 1987; Jiang and Tremaine, 2010). These structures can be molecular clouds, passing stars, or even passing black holes. Therefore, wide binaries have been used to constrain the nature of dark matter, ruling out the possibility that dark matter is compact objects (neutron stars and black holes) in the halo (Chaname and Gould, 2004; Quinn et al., 2009). Furthermore, orbital velocities of distant wide binaries can place independent constraints on the modified gravity theory (Hernandez, Jiménez, and Allen, 2012). Since gravity is the most mysterious force (so mysterious that it is not a force in general relativity), wide binaries provide a valuable gravity test on a large physical scale.

Numerous questions about binary stars remain unanswered. Many main-sequence close binaries have separations smaller than the size of pre-main-sequence stars. What mechanisms are responsible for their orbital shrinkage? Do they merge on the main-sequence or only after they evolve off the main-sequence? What do these mergers look like, and can we catch them in the act? What are the results of these mergers? What determines the wide binary fraction? How are these wide binaries formed and at what frequency? What are the signs of orbital modifications and disruptions by certain Galactic structures? Are they a probe of formation processes or more strongly dependent on the subsequent evolution? Answering these questions is critical to understanding binary stars, to their associated merger events, and to their application of probing the Milky Way.

In my thesis, I eager to fully understand the birth and the fate of close and wide binaries. In Chapter 2, I develop a kinematic-dating technique to measure

the age of contact binaries – close binary systems where two component stars touch each other. The age of binaries is notoriously difficult to measure. I use the cutting-edge kinematic-dating method enabled by modern astrometric data from Gaia to reveal the age evolution of contact binaries. The idea of kinematic dating is that older stars move faster than younger stars because older stars have experienced more gravitational jostles from other stars during their lifetime. With this method, I measure the birth and the merger time of contact binaries for the first time (Hwang and Zakamska, 2020), improving our understanding of the evolution of close binaries and revealing an unexpectedly short time to merger due to a yet-unknown process. I discuss the hypotheses for this process and potential for testing these hypotheses in Chapter 6.

In Chapter 3, I investigate the role of wide stellar companions in planet formation. In particular, I focus on a special planet population called "hot jupiters". These are giant gas planets, but unlike those in our solar system where Jupiter is 5 AU away from the Sun, these hot jupiters are located very close to their host stars, typically ten times closer than the orbit of Mercury. One proposed formation mechanism for hot jupiters is the three-body interaction under the perturbation of another stellar companion. I develop a method to search for wide stellar companions around hot jupiters, and used statistical analysis to determine whether hot jupiter hosts tend to have wide companions.

In Chapter 4, I study the formation of wide binaries in the Milky Way disk. Specifically, I investigate the metallicity dependence of the wide binary fraction. By combining Gaia data with the large spectroscopic survey LAMOST, I

use my comoving companion method to show that the wide binary fraction is strongly dependent on metallicity. I also demonstrate that younger stars have a higher wide binary fraction. These results suggest that multiple formation channels may be responsible for wide binaries. In Chapter 5, I further expand the investigation to wide binaries in the Milky Way halo. Since halo stars have very different stellar properties and evolution environments, the metallicity dependence of halo wide binary fraction provides key constraints on different hypotheses. Understanding wide binary formation is one of my key future work and is the foundation for using wide binaries to probe the Milky Way structures.

I conclude my thesis in Chapter 6, with discussion of the future prospects of binary star research.

Chapter 2

Lifetime of short-period binaries measured from their Galactic kinematics

As a significant fraction of stars are in multiple systems, binaries play a crucial role in stellar evolution. Among short-period (<1 day) binary characteristics, age remains one of the most difficult to measure. In this paper, we constrain the lifetime of short-period binaries through their kinematics. With the kinematic information from Gaia Data Release 2 and light curves from *Wide-field Infrared Survey Explorer* (WISE), we investigate the eclipsing binary fraction as a function of kinematics for a volume-limited main-sequence sample. We find that the eclipsing binary fraction peaks at a tangential velocity of $10^{1.3-1.6} \, \mathrm{km \, s^{-1}}$, and decreases towards both low and high velocity end. This implies that thick disk and halo stars have eclipsing binary fraction $\gtrsim 10$ times smaller than the thin-disk stars. This is further supported by the dependence of eclipsing binary fraction on the Galactic latitude. Using Galactic models, we show that our results are inconsistent with any known dependence of binary

7

fraction on metallicity. Instead, our best-fit models suggest that the formation of these short-period binaries is delayed by 0.6-3 Gyr, and the disappearing time is less than the age of the thick disk. The delayed formation time of $\gtrsim 0.6$ Gyr implies that these short-period main-sequence binaries cannot be formed by pre-main sequence interaction and the Kozai-Lidov mechanism alone, and suggests that magnetic braking plays a key role in their formation. Because the main-sequence lifetime of our sample is longer than 14 Gyr, if the disappearance of short-period binaries in the old population is due to their finite lifetime, our results imply that most ($\gtrsim 90\%$) short-period binaries in our sample merge during their main-sequence stage.

2.1 Introduction

Binaries are at the core of many exotic astronomical events in the Universe, including classical novae (Warner, 1995), red novae (Tylenda et al., 2011), type Ia supernovae (Whelan and Iben, Icko, 1973; Iben and Tutukov, 1984; Webbink, 1984), short gamma-ray bursts (Shibata and Taniguchi, 2006; Fong and Berger, 2013), binary black hole mergers (Abbott et al., 2016), and kilonovae (Abbott et al., 2017; Smartt et al., 2017; Cowperthwaite et al., 2017). A significant fraction of all stars are in binary and multiple systems (Duchêne and Kraus, 2013). Therefore, binary evolution plays a crucial role in the understanding of the Universe.

All the stellar binaries are once a main-sequence (MS) binary. While thousands of short-period (< 1 day) MS binaries have been found, they are not formed with such short separation because the radii of pre-MS stars are larger

than the MS stars. In fact, the initial separation of binaries is believed to be $\gtrsim 10\,\mathrm{AU}$ because the radius of an initial hydrostatic stellar core is $\sim 5\,\mathrm{AU}$ (Larson, 1969) and its fragmentation is unlikely (Bate, 1998; Bate, 2011). Therefore, short-period binaries must have gone through orbital migration to shrink the separation from $> 10\,\mathrm{AU}$ ($> 2000\,\mathrm{R_\odot}$) to a few $\mathrm{R_\odot}$.

Short-period binaries may have experienced several different processes to lose orbital angular momentum. At the pre-MS phase, the energy dissipation due to the interaction with the primordial gas may be able to produce binaries with separations down to $\sim 0.1\,\mathrm{AU}$ (Bate, Bonnell, and Bromm, 2002; Bate, 2009; Bate, 2012). This process takes place on a free-fall timescale, typically $\sim$Myr, and may be able to explain the formation of pre-MS binary stars with periods $> 1\,\mathrm{day}$ (Mathieu, 1994; Tohline, 2002).

During the MS phase, if a binary has a distant tertiary companion, the angular momentum of the inner binary can exchange with the outer tertiary companion, the so-called Kozai-Lidov mechanism (Kozai, 1962; Lidov, 1962). The inner binary separation can be reduced to a few stellar radii at the pericenter passages due to the high eccentricity excited by the Kozai-Lidov mechanism, and at that point the tidal friction is able to remove the angular momentum and shrink the orbit (Harrington, 1968; Kiseleva, Eggleton, and Mikkola, 1998; Eggleton and Kiseleva-Eggleton, 2001; Fabrycky and Tremaine, 2007). This process is often referred to as Kozai cycles with tidal friction (KCTF). If higher-order effects are taken into accounts, for example eccentric outer orbit and post-Newtonian effects, three-body interactions are more complicated and even chaotic (Naoz et al., 2013b; Naoz et al., 2013a; Naoz,

2016). The Kozai-Lidov mechanism is supported by observations that a large fraction of MS close binaries are in triple systems (Tokovinin, 1997; Pribulla and Rucinski, 2006; Tokovinin et al., 2006; Rucinski, Pribulla, and Kerkwijk, 2007). Furthermore, Borkovits et al., 2016 find that the distribution of mutual inclination between the inner binaries and the outer tertiaries shows a peak at $\sim 40°$, consistent with the prediction from KCTF (Fabrycky and Tremaine, 2007), although the other observed peak at $\sim 0°$ is not expected. Depending on the configuration of the triple stars and the initial conditions, KCTF may operate on a wide range of timescales, from $\lesssim 0.1\,\mathrm{Gyr}$ to several Gyr (Fabrycky and Tremaine, 2007; Perets and Fabrycky, 2009), until the orbits of the inner binaries are circularized.

If the binary separation is close enough (periods$\lesssim 5\,$days), magnetic winds become important in extracting angular momentum of binaries. Specifically, stars with masses $\lesssim 1.3\,\mathrm{M_\odot}$ possess subphotospheric convection zones that generate magnetic winds which take away the (rotational) angular momentum of the star. Due to the synchronization between the rotational and orbital periods in short-period binaries, the loss of angular momentum shrinks the orbit. Over a timescale of a few Gyr, magnetic winds are able to bring binaries to the contact phase (Stepien, 1995; Yakut, Kalomeni, and Tout, 2008; Van and Ivanova, 2019; Van, Ivanova, and Heinke, 2019).

The relative contribution of each process to the formation of short-period ($< 1\,$day) MS binaries is not yet clear. In particular, neither pre-MS disk migration nor KCTF during the MS can produce solar-type binaries within orbital periods $< 1\,$day. During the pre-MS phase, solar-mass stars accrete

most of their mass while slightly enlarged (a few $R_\odot$), and so disk migration might be able to produce close solar-type binaries down to periods of ~ 1 day, below which they would have merged (Hosokawa and Omukai, 2009). Hydrodynamical simulations show that pre-MS interaction is not able to produce binaries with separations $\lesssim 0.1\,AU$, although it can be due to the simulation resolution limit (Bate, Bonnell, and Bromm, 2002; Bate, 2009; Bate, 2012). The Kozai-Lidov mechanism encounters the difficulty that the majority of binaries with periods < 10 days have circular orbits (Latham et al., 2002; El-Badry et al., 2018), in which case the Kozai-Lidov mechanism is not effective. Probably only magnetic braking is able to bring solar-type binaries to orbital orbital periods < 1 day, but magnetic braking requires small initial period ($\lesssim 5\,$days) to be efficient.

If the ages of short-period binaries could be measured directly, ages could be used to constrain the mechanisms responsible for the orbital migration. By comparing with the MS lifetime, we can determine whether short-period binaries can survive for the entire MS lifetime. If the short-period binaries destruct or disappear at a particular age or at a particular stage of the stellar evolution, then we can constrain or identify the destruction process.

Age is notoriously difficult to measure for single stars. Furthermore, such methods, including isochrone fitting, stellar rotation, and chromosphere activity, are not valid anymore for short-period binaries because they may have undergone binary interaction and mass transfer. Kinematics is among the few reliable ways to probe the age of short-period binaries. The age-velocity dispersion relation has been well established for a variety of MS stars (Dehnen

11

and Binney, 1998; Nordström et al., 2004; Reid et al., 2009; Sharma et al., 2014). For disk stars, this relation may be the consequence of kinematic heating processes from giant molecular clouds, transient spiral arms, bars, and flyby satellite galaxies. Kinematics can also help separate the thin-disk, thick-disk, and halo stars. Because accelerations experienced by test particles are independent of their masses, we are able to directly compare the kinematics between single stars and binaries, and further infer their ages.

In this paper, we use Gaia Data Release 2 and the light curves from WISE to investigate the kinematics of short-period (< 1 day) eclipsing binaries. In Sec. 3.2, we describe the dataset, our sample selection, and our time-series analysis. In Sec. 4.3 we present our primary results of the relation between eclipsing binary fraction and kinematics. In Sec. 2.4, we investigate possible systematics and different sample selections. In Sec. 2.5, we use Galactic models and show that our results can be explained by a finite lifetime of eclipsing binaries. In Sec. 5.5, we discuss disk/halo difference, metallicity, and the implication from the lifetime of eclipsing binaries. We summarize in Sec. 5.6.

2.2   Sample Selection and Measurements

2.2.1   The parent Gaia sample

Our sample is selected from Gaia Data Release 2 (DR2; Gaia Collaboration et al. 2016; Gaia Collaboration et al. 2018a). Gaia is an optical all-sky survey which is obtaining photometry and astrometry for stars with magnitudes down to ~ 21 mag and radial velocities for select bright stars. Gaia DR2 was released on 25 April 2018, based on data collected between 25 July 2014 and 23 May 2016.

12

In Gaia DR2, broad-filter G-band magnitudes, blue-band BP magnitudes, red-band RP magnitudes, positions, parallaxes, and proper motions are available for ~ 1.33 billion objects and radial velocities for ~ 7 million stars, providing an unprecedented dataset on the phase-space distribution of stars in the Milky Way.

Our query for Gaia DR2 follows the one used in Gaia Collaboration et al., 2018b. Specifically, the mean flux divided by its error is is larger than 50 for G-band and larger than 20 for BP and RP bands. In Gaia DR2, BP and RP fluxes are not treated with deblending, so we apply a cut on `phot_bp_rp_excess_factor` to reduce the effect of crowded fields which makes the BP and RP bands unreliable (Evans et al., 2018; Arenou et al., 2018). `visibility_periods_used`> 8 is used to ensure that there are sufficient observations for deriving the astrometric solutions (Lindegren et al., 2018), and `parallax_over_error`> 10 is adopted to have well-measured parallaxes. We do not apply explicit cuts on relative proper motion uncertainties because that excludes objects having intrinsically low proper motions, which biases the kinematic results. Instead, we follow Gaia Collaboration et al., 2018b and use the unit error introduced by Lindegren et al., 2018 to avoid spurious astrometric solutions. Because we obtain the light curves from WISE, we cross-match Gaia DR2 and WISE using the Gaia DR2 cross-match catalog (Marrese et al., 2019). Our Gaia DR2 query is included in the Appendix.

We compute tangential velocities from proper motions and parallaxes provided by Gaia DR2. We do not use the radial velocities in Gaia DR2 because the radial velocity sample is ~ 100 times smaller. Furthermore, Gaia

DR2 does not report the radial velocities of double-line systems and objects having high radial velocity variations (Katz et al., 2019), which strongly biases the binary selection.

We correct the velocities by removing the solar motion and the differential rotation of the Galactic disk. We adopt the solar motion from Schönrich, Binney, and Dehnen, 2010 where $(U_\odot, V_\odot, W_\odot) = (11.1, 12.24, 7.25)\,\mathrm{km\,s^{-1}}$, with the convention that $U_\odot, V_\odot, W_\odot$ are oriented towards the Galactic center, the direction of Galactic rotation, and the north Galactic pole. Our sample is within 500 pc with a median of 380 pc, the local shear approximation described by Oort's constants is applicable. We remove the contribution from differential rotation of the Galactic disk using the Oort constants reported from Bovy, 2017: $A = 15.3\,\mathrm{km\,s^{-1}\,kpc^{-1}}$, $B = -11.9\,\mathrm{km\,s^{-1}\,kpc^{-1}}$, $C = -3.2\,\mathrm{km\,s^{-1}\,kpc^{-1}}$, $K = -3.3\,\mathrm{km\,s^{-1}\,kpc^{-1}}$. While this correction is only valid for disk stars and not for halo stars because halo stars are not rotating with the disk, but since the velocity correction of differential rotation is $< 10\,\mathrm{km\,s^{-1}}$, this (incorrect) correction is small for halo stars where the typical velocities are $> 100\,\mathrm{km\,s^{-1}}$. With the correction of the solar motion and the differential rotation of the Galactic disk, the tangential velocities (V_t) presented in this paper are the tangential components relative to the local Galactic rotation at the star's location.

2.2.2 Main sequence selection

Our MS selection is designed to satisfy several purposes: (1) the binary fraction is a strong function of mass and therefore color (Duchêne and Kraus, 2013).

Using a narrow color range reduces such mass dependence in our results. (2) On the blue end (BP−RP< 0.5 mag), there is contamination from pulsating stars like δ Scuti. (3) Stars leave the MS phase because of stellar evolution, so selecting long-lived (i.e. redder) MS stars helps to interpret kinematic results. (4) Because binaries are brighter than single stars, we aim to construct a volume-limited sample instead of a magnitude-limited sample to avoid systematics. For this reason, we cannot use MS stars that are too red because they are faint and the sample size would be small in a volume-limited sample.

To address all these points, we select an MS sample with absolute magnitude offsets $|\Delta G|$ < 1.5 mag and with 0.9 <BP−RP< 1.4, shown as the colored region in Fig. 5.4. The black dashed line in Fig. 5.4 is the spline fit to Pleiades, following Hamer and Schlaufman, 2019. Pleiades is a young, solar-metallicity open cluster with age $10^{8.04}$ years and [Fe/H]= −0.01 (Netopil et al., 2016), and ΔG is defined as the offset of absolute G magnitudes between the stars and Pleiades at the same BP−RP colors, where ΔG < 0 means that the star is brighter than Pleiades at the same color. Objects are defined as MS if they have $|\Delta G|$ < 1.5 mag. The 1.5 magnitude range is motivated by the fact that we want to include binaries, which are 0.75 mag brighter than single stars assuming equal luminosities and no occultations, and we also want to keep thick-disk and halo stars which are $\lesssim$ 1 mag fainter than Pleiades in the color range considered due to their lower metallicities.

The color selection of 0.9 <BP−RP< 1.4 is chosen to avoid the pulsating stars at BP−RP< 0.5, and to include most of the eclipsing binaries concentrated around BP−RP~ 1 in Fig. 2.2. From the PARSEC isochrone (Bressan et al.,

2012), the selection of BP−RP= 0.9-1.4 has masses ranging from 0.7 to $0.9\,M_{\odot}$, with temperatures 4500-5500 K, corresponding to late-G and K dwarfs. This selection ensures that their MS lifetime is longer than 14 Gyr.

2.2.3 Eclipsing binary sample from WISE

Because Gaia DR2 has not released the time series and the catalog of eclipsing binaries, we construct the eclipsing binary sample using two other ways. One is from the light curves of WISE, and the second is from the variability information in Gaia DR2. These two samples are complementary: the WISE sample has less contamination, while the Gaia sample is more complete in terms of the sky distribution and is not affected by the limits of period-finding algorithms.

The WISE eclipsing binary sample is constructed using *Wide-field Infrared Survey Explorer* (*WISE*; Wright et al. 2010). Our work requires a large sample and good cadences to recover short-period (< 1 day) eclipsing binaries, and WISE serves as an excellent dataset for this purpose. Since WISE is an all-sky survey, it provides a large cross match sample with Gaia. Furthermore, the orbital period of WISE satellite is ~ 1.6 hours, which is able to recover the MS eclipsing binaries, and this cadence is much better than most of the ground-based surveys. Its W1 (3.4 μm) and W2 (4.6 μm) bands have been collecting data since AllWISE in 2010 to NeoWISE in 2019, providing a long baseline to study the time series. In main-sequence regions and the color and parallax range of interest, we end up with ~ 1000 short-period eclipsing binaries in WISE, compared to only a few hundred targets in the Kepler eclipsing binary

catalog (Kirk et al., 2016) and the Catalina Sky Survey (Drake et al., 2014) under the same criteria.

The AllWISE source catalog provides `var_flg` which is a measure of the probability that an AllWISE source is variable in each WISE filter. Specifically, `var_flg` is an integer ranging from 0 to 9 such that $\sim 10^{-\mathtt{var\_flg}}$ is the probability that the observed WISE light curve is drawn from a non-variable population (Hoffman et al., 2012). Therefore, `var_flg`= 0 means non-variable and 9 indicates the highest probability of being variable. Out of the parent Gaia sample, we select targets where `var_flg`$\geq$ 5 in W1 band to further analyze their light curves, resulting $\sim$ 20,000 variable candidates. We do not consider other WISE bands because W2 has worse sensitivity, and W3 and W4 do not have single-epoch exposures in NeoWISE.

We download complete W1 light curves from AllWISE Multiepoch Photometry Table and NEOWISE-R Single Exposure (L1b) Source Table through NASA/IPAC Infrared Science Archive and perform time series analysis for variable candidates where `var_flg`$\geq$ 5. The W1 light curves from AllWISE and NeoWISE provide a total baseline of $\sim$ 9 years from 2010 to 2019. To ensure the photometric quality of single-epoch exposures, we follow the instruction of Cutri et al., 2011 to adopt the criteria of `saa_sep`> 0, `moon_masked`= 0, `qi_fact`> 0.9 for AllWISE[1], and `saa_sep`> 0, `moon_masked`= 0, `qi_fact`> 0.9, and `qual_frame`> 0.9 for NeoWISE[2]. AllWISE Multiepoch Photometry Database also contains some redundant photometric measurements, and we further exclude them by matching the source ID (source_id_mf) in AllWISE

---

[1]http://wise2.ipac.caltech.edu/docs/release/allwise/expsup/sec3_1.html
[2]http://wise2.ipac.caltech.edu/docs/release/neowise/expsup/sec2_3.html

and NeoWISE [3].

We use the periodogram of Multi-Harmonic Analysis of Variance (MHAOV; Schwarzenberg-Czerny 1996) to determine the periodicity in the light curves. MHAOV has good performance compared to other period-finding algorithms in terms of the accuracy against magnitude, sampling rates, quoted period, S/N ratios, number of observations, and different variability classes (Graham et al., 2013). We run MHAOV with three harmonics on the WISE variable candidates from $f_{\min} = 0.1\,\mathrm{day}^{-1}$ to $f_{\max} = 20\,\mathrm{day}^{-1}$ with $\mathit{\Delta}f = 1 \times 10^{-4}\,\mathrm{day}^{-1}$, or equivalently periods ranging from 0.05 day (1.2 hour) to 10 days. Chen et al., 2018 also measure the periods for WISE variables, but their minimum period in the periodogram is set to 0.143 day (3.4 hours). While this minimum period is safer because it is above the classical Nyquist period of 3.2 hours (i.e. two times of the WISE satellite's orbital period), it misses most of short-period MS eclipsing binaries. The Nyquist sampling theorem applies when the sampling is uniform, whereas WISE satellite does not observe targets uniformly due to the size of the field of view and the drift of the satellite's orbital plane (Mainzer et al., 2014). Thus WISE's slightly irregular sampling may help to recover periods below the classical Nyquist limit (VanderPlas, 2018). If the aliasing does happen, it results in an aliased peak in the periodogram. Therefore, aliasing only makes the measured period inaccurate but does not affect the fact that such source is a periodic variable. Since our main interest is in selecting short-period (< 1 day) eclipsing binaries but not their exact periods, aliasing does not affect our sample selection. Therefore, we adopt a minimum period in the periodogram smaller than the classic Nyquist limit to

---

[3]http://wise2.ipac.caltech.edu/docs/release/allwise/expsup/sec3_2.html

recover short-period MS eclipsing binaries. A more detailed investigation of the short-period WISE periodic variables will be presented in Petrosky et al. (in prep.).

For some eclipsing binaries, particularly contact binaries (W UMa binaries), their primary and secondary eclipses have similar depths so period-searching algorithms may not be able to distinguish the primary from secondary eclipses. Therefore, the period-searching algorithm may report a period that is two times smaller than the orbital period. We do not attempt to apply this factor of 2 correction, and we refer to the measured periods from periodograms as 'apparent periods', and keep in mind that the apparent periods may be two times smaller than the orbital periods of the binaries.

After time series analysis of the WISE variables, we use the following criteria to select the WISE eclipsing binary sample: (1) the peak in the MHAOV periodogram (Θ statistics) is larger than 200, meaning that a strong periodic signal is detected in the light curves; (2) there is at least one observation in every 0.05 phase in the phase-folded light curves, ensuring that the light curve is well-sampled; (3) even with the previous two criteria, there is an overdensity in the apparent periods at ~ 0.067 day, the orbital period of the WISE satellite. Therefore, we limit our sample to apparent periods > 0.07 day to avoid these spurious period measurements. These three criteria result in 2994 periodic variables from the parent Gaia sample (without the MS selection). We inspect their phase-folded light curves and confirm that these criteria provide a robust eclipsing binary sample.

Fig. 2.2 shows the apparent periods of the WISE periodic variables with

respect to the Gaia BP–RP colors. The red line is the theoretical minimum possible period for contact, equal-mass MS binaries. The red line is derived using PARSEC isochrone (Bressan et al., 2012) with an age of 9 Gyr and solar metallicity. The simple theoretical minimum possible apparent period is computed by $P_{apparent} = 0.5 P_{orbital} = \pi \sqrt{a^3 / G(M_1 + M_2)}$, where a is the semi-major axis of the binary, G is the gravitational constant, and M_1 and M_2 are the masses of the stars. We consider equal-mass binaries ($M_1 = M_2$) and use the Roche-lobe volume radius $R_L = 0.38a$ (Eggleton, 1983), where R_L is the volume radius of a star. By definition, the volume radius R_L equals to the radius of an undistorted star which is provided in the PARSEC isochrone. The overall trend of the solid red line in Fig. 2.2 represents the periods limited by the sizes of stars: bluer, larger stars have larger minimum periods while redder, smaller stars can have smaller periods.

Fig. 2.2 shows that our period measurements are in excellent agreement with the period limit of contact binaries, meaning that our WISE variable sample, if not all, is dominated by eclipsing binaries. Fig. 2.2 also emphasizes the need to search apparent periods below the classical Nyquist limit of 0.13 day, otherwise most of the eclipsing binaries having BP–RP> 1 would be missed. Some narrow gaps in apparent periods at multiples of the WISE's orbital period (0.13 day and 0.2 day) can be seen in the black points because the sampling is not sensitive to their periods. While aliasing can potentially downgrade our period accuracy, Fig. 2.2 shows that our results pass through the classic Nyquist limit at 0.13 day quite smoothly and recover a large number of low-mass eclipsing binaries below this limit. The blue end (BP–RP$\lesssim 0.5$)
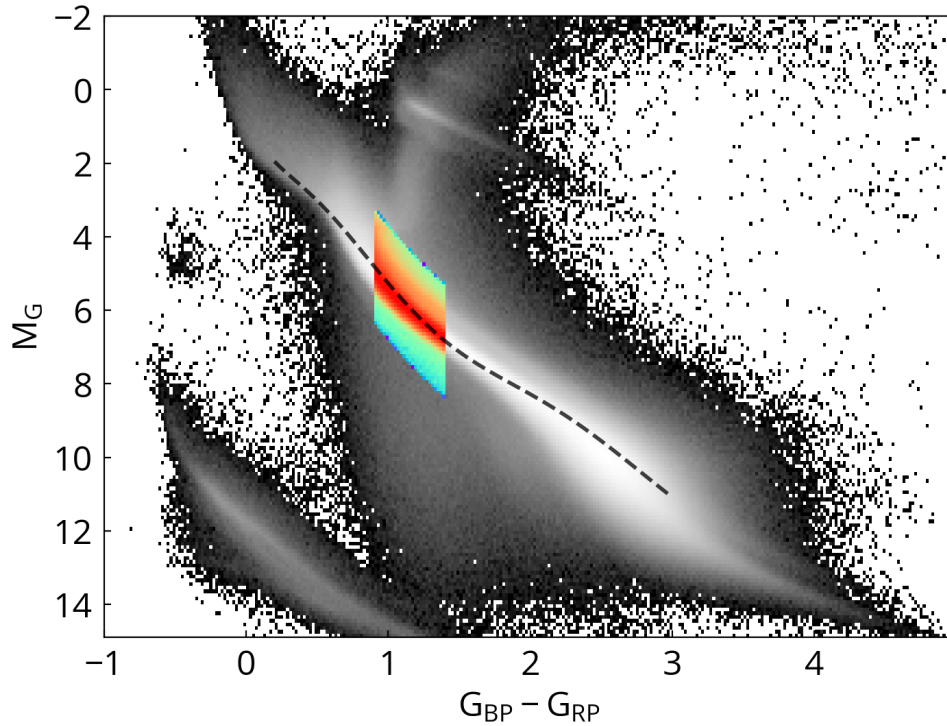
Figure 2.1: The H-R diagram demonstrating our selection. The x-axis is the Gaia BP–RP color, and the y-axis is the Gaia absolute G-band magnitude. The gray scale shows is the stars within 500 pc, and the color region indicates our main sequence sample. The dashed line is the spline fit of Pleiades.

overlaps the instability strip, so some of them may be δ Scuti variables (Gaia Collaboration et al., 2019). Type-II Cepheids are also located at the blue end (BP–RP $\lesssim$ 0.5), but their periods typically are longer than 1 day and are not seen in this plot.

2.2.4 Eclipsing binary sample from Gaia DR2

Here we construct another eclipsing binary sample using Gaia DR2 alone. While Gaia DR2 does not release the catalog and the light curves of eclipsing binaries, we can construct an indirect eclipsing binary sample from Gaia
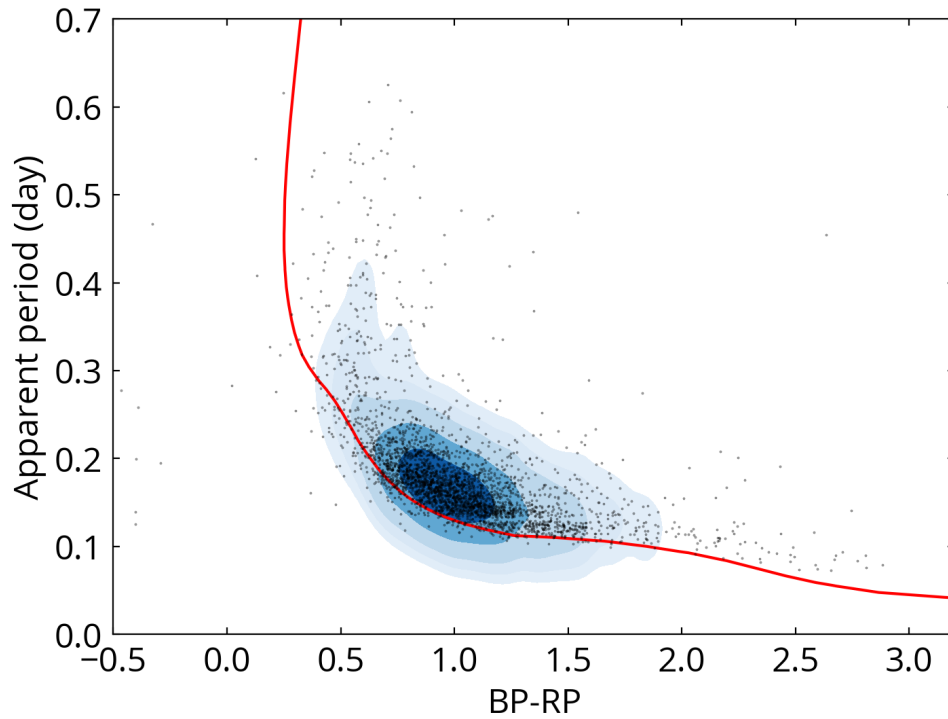
Figure 2.2: The distribution of apparent periods with respect to Gaia BP–RP color for the WISE periodic variables. The y-axis shows the apparent periods reported from periodograms, which typically are half of the orbital periods for short-period eclipsing binaries. The dots are the individual measurements, and the blue background is the Gaussian kernel density estimation where the bandwidths are chosen to present a smooth distribution. The red solid line shows the theoretical apparent periods (0.5×orbital periods) for contact, equal-mass binaries. The WISE variables agree very well with the red solid line, meaning that they are MS eclipsing binaries.

DR2. The variability information can be obtained from the photometric errors of Gaia DR2 (Gaia Collaboration et al., 2019). The photometric errors are calculated by

$$\texttt{phot\_g\_mean\_flux\_error} = \sigma_G/\sqrt{\texttt{phot\_g\_n\_obs}},$$

where σ_G is the standard deviation of the G-band fluxes. When a star passes through the field of view of the Gaia satellite, it goes through 9 astrometric field CCDs where each CCD has one G-band photometric measurement. This σ_G is the standard deviation of each CCD photometric measurement, which are obtained within the crossing time of a source over one CCD is ~ 4.4 seconds. Furthermore, as the Gaia satellite spins with a period of 6 hours, a source passes its two field of views separated by ~ 1.8 (or 4.2) hours. Therefore, σ_G also contains the information on variability on timescales of hours. Depending on the location of the sky, Gaia scans through the same target after several weeks (Evans et al., 2018; Riello et al., 2018). In our selection, we require that $\texttt{visibility\_periods\_used} > 8$, ensuring that there are enough visits to derive reliable astrometric solutions but also enough observations to measure photometric variability. In our Gaia sample with the MS cut, the median $\texttt{visibility\_periods\_used}$ is 13 and the median $\texttt{phot\_g\_n\_obs}$ (number of CCD photometric measurements contributing to G photometry) is 254.

Based on the photometric errors in the Gaia DR2, we compute σ_G and further $f_{G,raw} = \sigma_G/F_G$ for all the sources, where F_G is the mean flux in the G band. We refer to the dimensionless $f_{G,raw}$ as 'raw fractional variability' in the G band. While $f_{G,raw}$ contains the information about the variability of

stars, it has to be corrected for the magnitude-dependent instrumental errors (Evans et al., 2018). The instrumental fractional variability, $f_{G,inst}$, is computed from the running modes of f_G for our entire sample across the observed G-band magnitudes. Then the instrumentally corrected fractional variability is $f_G^2 = f_{G,raw}^2 - f_{G,inst}^2$. In this definition, f_G^2 may be negative, which means that such star does not have significant variability compared to the instrumental level. 95% of our MS sample is brighter than 14.8 mag in G-band, where the instrumental correction is $f_{G,inst} \sim 0.8\%$.

We use f_G^2 to identify eclipsing binaries in Gaia DR2. Fig. 2.3 shows the distribution of $\log(f_G^2)$ for the eclipsing binaries identified from WISE and for all MS stars located in the same region in the H-R diagram. The distribution of MS stars has a small excess at $\log(f_G^2) \sim -3$ and an enhanced tail at $\log(f_G^2) > -2$, suggesting two different origins for variability. By comparing with the WISE eclipsing binaries, we select stars having $\log(f_G^2) > -2$ (dashed line) as the eclipsing binary candidates. The excess at $\log(f_G^2) \sim -3$ is likely due to stellar rotation and the spots, ellipsoidal variations, and/or (semi-)detached binaries with longer orbital periods (Appendix 2.8.2). Particularly, we find that stars having $-2.5 < \log(f_G^2) < -2$ are significantly kinematically cooler than other stars, suggesting that they may be young stars where the spots are more active, or young binaries where the orbital periods are larger. A similar method has been used to obtain Gaia variability information to identify RR Lyrae stars (Belokurov et al., 2017) and sub-kpc dual quasar candidates (Hwang et al., 2020a).

This selection of eclipsing binaries is based on the assumption that eclipsing binaries are the dominant sources of variability on the MS in the color range considered. Although we do not have the information of periods for eclipsing binaries selected from Gaia DR2, we expect that short-period binaries dominate the sample because systems having shorter orbital periods have a higher probability of being eclipsing systems. Furthermore, eclipsing binaries with orbital periods > 1 day tend to be more detached and so vary in brightness only during eclipses, i.e., a smaller duty cycle of variability, which reduces their overall fractional variability. Indeed, in Appendix 2.8.2 we show that the majority of eclipsing binaries selected by Gaia fractional variability have orbital periods < 0.5 day. While it is still possible that some variability can be due to stellar rotations and flares, we argue that eclipsing binaries still dominate the number. One reason is that our criteria select objects with large variation amplitudes of $f_G^2 > 0.01$ (i.e. > 10%), which is unlikely to be due to spots.

2.2.5   Detectability as a function of parallax

After introducing the main-sequence selection and two eclipsing binary selections, we now determine the parallax (distance) cut to construct a volume-limited eclipsing binaries sample with the MS selection of $|\Delta G| < 1.5\,\mathrm{mag}$ and $0.9 <\mathrm{BP-RP}< 1.4$. Fig. 2.4 shows the fraction of stars that are short-period WISE eclipsing binaries as a function of parallax. If a star is too far so that it is not well detected in a single-exposure in WISE and therefore the periods cannot be well determined, we expect a steep decline in eclipsing binary
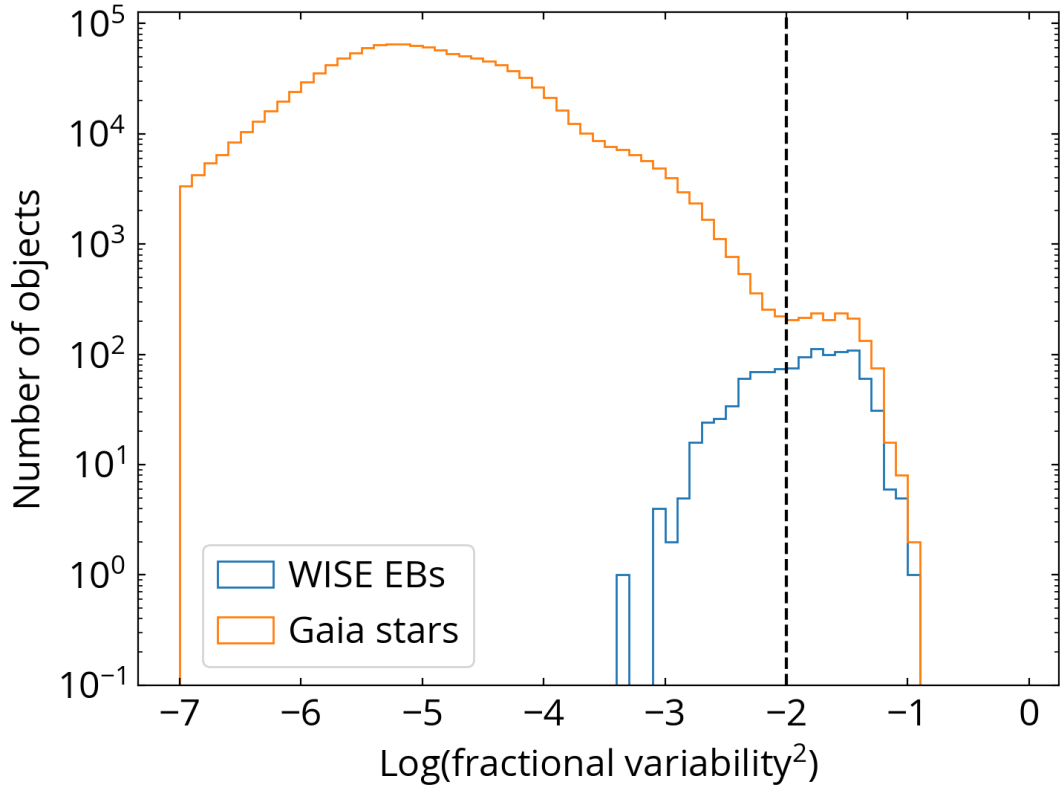
Figure 2.3: The distribution of fractional variability (f_G) for the Gaia main sequence sample and WISE eclipsing binaries. The excess of objects at $\log(f_G^2) \sim -3$ and > -2 two physical mechanisms for variability. By comparing with the WISE eclipsing binaries, we select Gaia stars having $\log(f_G^2) > -2$ (dashed line), i.e. variability > 10%, as the Gaia eclipsing binary sample.

fraction at a certain parallax. Instead, we see a flat dependence in Fig. 2.4, and the slight decrease at 2.5-3 mas parallaxes is likely consistent with the difference in eclipsing binary fraction between the thin disk and the older stars as discussed below.

With the criteria of $|\Delta G| < 1.5$ mag, $0.9 <$ BP$-$RP< 1.4, and parallax > 2 mas, we end up with 1081 WISE eclipsing binaries. All of them have apparent periods < 0.5 day. We do not correct for dust extinction because the Galactic models we use for comparisons with data includes the effects of extinction. At the limiting distance of 500 pc of our sample, the level of reddening (E(B$-$V)$<$ 0.2 mag) is small compared to the color range of our selection, and the level of extinction ($A_V < 0.8$ mag) does not affect the completeness of the volume-limited sample in our chosen magnitude range.

Fig. 2.4 also shows that the Gaia eclipsing binary fraction is consistent with WISE eclipsing binary sample and the detectability stays constant. With the criteria of $|\Delta G| < 1.5$ mag, $0.9 <$ BP$-$RP< 1.4, and parallax > 2 mas, we end up with 1545 eclipsing binaries from Gaia DR2.

2.2.6 General properties of our eclipsing binary selections

While we refer to our sample as eclipsing binaries, the variability may not only come from eclipses. The variability can also be the ellipsoidal modulation due to the strongly distorted stars. For WISE eclipsing binaries, we do not attempt to classify eclipsing binaries into subclasses based on their light curves, but Paczynski et al., 2006 show that eclipsing binaries with periods < 1 day consist of mostly contact binaries and some semi-detached binaries, and very few

27
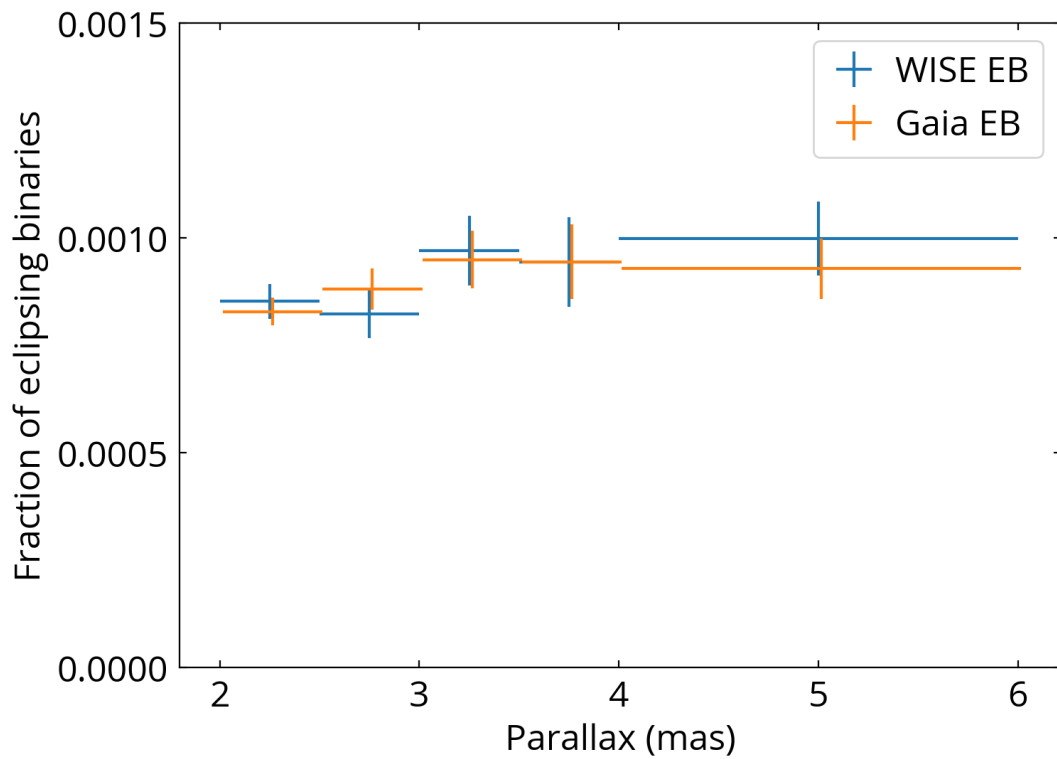
Figure 2.4: The fraction of eclipsing binaries as a function of parallax for the WISE and Gaia sample. The eclipsing binary fractions remain fairly flat over the entire range of parallax, meaning that we have not reached the limit of detectability of eclipsing binaries. We use parallax > 2 mas (i.e. within 500 pc) as our volume-limited sample.

detached binaries.

Both our WISE and Gaia eclipsing binary selections tend to select binaries with shorter periods because the probability of being eclipsed is higher, and also shorter-period systems are more likely to be contact binaries where photometric variability is stronger. By comparing with the Kepler eclipsing binaries (Kirk et al., 2016) in Appendix 2.8.2, we find that the majority of the Gaia eclipsing binaries have orbital periods < 0.5 day (or apparent periods < 0.25 day). Similarly, Fig. 2.2 shows that most of our WISE eclipsing binaries have apparent periods < 0.25 day, corresponding to orbital periods < 0.5 day. Since we are interested in eclipsing binary fraction as a function of kinematics, missing non-eclipsed short-period binaries only affects our sample completeness but does not bias the kinematic result.

2.2.7   Summary of the sample selection

Here we summarize our sample selection. Each of the WISE and Gaia samples has a parent MS sample and an eclipsing binary sample. The parent MS samples have the same selection as their corresponding eclipsing binary samples except without requiring variability or eclipses. For the WISE sample, the selection criteria are:

1. `parallax_over_error` > 10.

2. `phot_g_mean_flux_over_error` > 50.

3. `phot_rp_mean_flux_over_error` > 20.

4. `phot_bp_mean_flux_over_error` > 20.

5. `visibility_periods_used` > 8.

6. Cuts on `phot_bp_rp_excess_factor` following Gaia Collaboration et al., 2018b.

7. Cuts on unit errors following Gaia Collaboration et al., 2018b.

8. `parallax`> 2 mas (i.e. within 500 pc).

9. MS selection so that the absolute G-band magnitude relative to Pleiades is smaller than 1.5 mag ($|\varDelta G| < 1.5$).

10. A color selection of 0.9 <BP−RP< 1.4.

11. Every object has an AllWISE cross match.

12. AllWISE `cc_flags = 0000`, indicating no spurious signals in WISE images.

13. For the WISE eclipsing binary selection, we require that the peak in the MHAOV periodograms is larger than 200, at least one observation in every 0.05 phase in the phase-folded light curves, and apparent periods between 0.07 and 0.5 day.

The Gaia parent MS sample is selected using criteria (1)-(10), and the Gaia eclipsing binaries are selected further using $\log(f_G^2) > -2$.
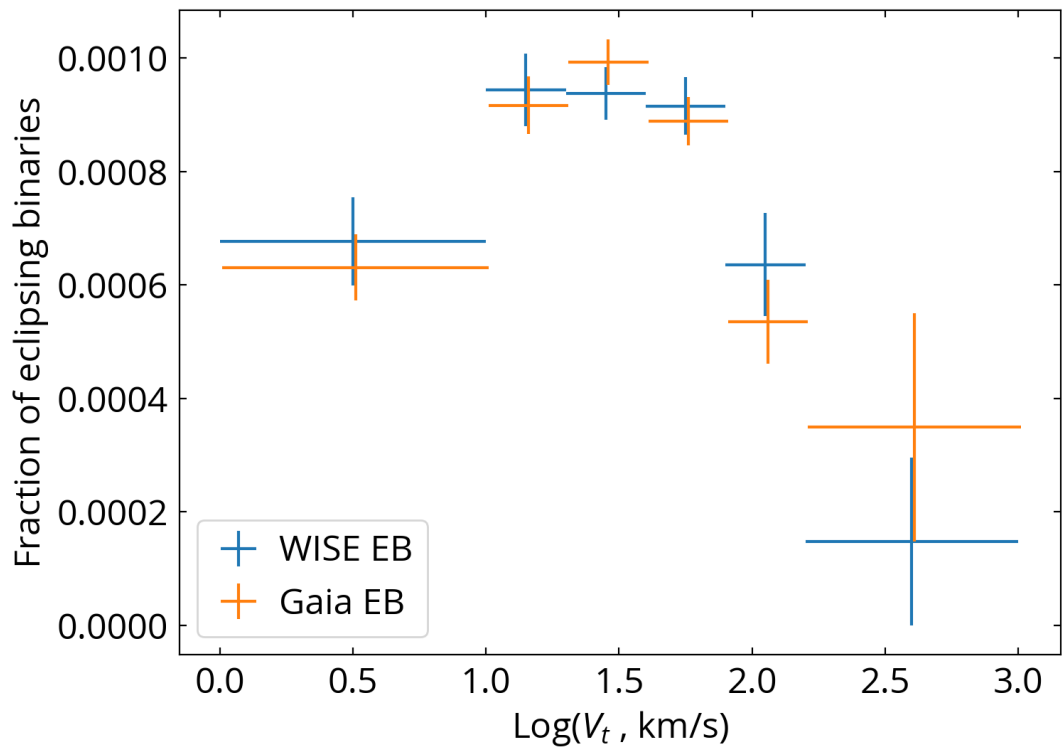
Figure 2.5: The fraction of short-period eclipsing binaries as a function of tangential velocity. The blue crosses use the eclipsing binaries selected from WISE, and the orange crosses are from Gaia DR2. The horizontal bars indicate the size of the bins, and the vertical bars are errors estimated using Poisson statistics. Both eclipsing binary samples show that the eclipsing binary fraction peaks at tangential velocity of $\sim 10^{1.3-1.6}$ km s^{-1}, and decreases toward both lower and higher velocities.

2.3 Eclipsing binary fractions as a function of kinematics

Fig. 2.5 presents the eclipsing binary fraction as a function of tangential velocity in the MS sample. Because WISE eclipsing binaries are easier to identify with more WISE scans and therefore may have different sky distribution as the WISE parent sample, we weigh the WISE result based on the sky distribution of WISE eclipsing binaries. Specifically, we bin the WISE eclipsing binaries by the galactic coordinates with steps of $\Delta l = 15 \deg$ and $\Delta b = 10 \deg$, and assign weights to each bin such that the parent sample has the same sky distribution as the WISE eclipsing binary sample while the total number of sources (i.e. the sum of the weights) remain unchanged. The error bars in Fig. 2.5 are estimated using the Poisson statistics assuming no errors from the weights. The difference between the unweighted and weighted result is small, within 0.4 of the error bars.

The WISE and Gaia eclipsing binary samples are in excellent agreement in Fig. 2.5: they show that the eclipsing binary fraction peaks at an intermediate tangential velocity ($\sim 10^{1.5} \, \mathrm{km \, s^{-1}}$), and decreases towards both low and high velocity end. With smaller error bars, the Gaia eclipsing binary sample constrains the peak to be in the bin of $10^{1.3-1.6} \, \mathrm{km \, s^{-1}}$. As elaborated in more detail in Section 2.6.1, the difference of eclipsing binary fraction cannot be explained by the smaller sizes of stars with lower metallicities. This is the primary result of this paper: the fraction of short-period binaries is a strong function of kinematics.

We perform the Anderson-Darling test to quantify the significance of

the difference in the distributions of tangential velocity between the sample of short-period eclipsing binaries and the comparison MS sample. The Kolmogorov-Smirnov test and the Anderson-Darling test give qualitatively the same result and here we quote the Anderson-Darling values because the Anderson-Darling test is more sensitive to tails of distributions. For WISE eclipsing binary sample, the p-value, the probability that two distributions are sampled from the same parent distribution, is 0.02. For Gaia eclipsing binary sample, the p-value is 6×10^{-4}. Therefore, the kinematic difference is statistically significant.

In principle, different velocity components (U, V, and W) may provide different kinematic information for eclipsing binaries. For example, the velocity component in the direction of galactic rotation (V component) would lag behind the disk as a result of asymmetric drift (Dehnen and Binney, 1998; Reid et al., 2009). However, since only tangential velocities are available for our sample, we find that decomposing the tangential velocity into U, V, and W component suffers strongly from the projection and does not provide statistically meaningful constraints. Therefore, we focus on the results of tangential velocities in this paper.

2.4   Potential systematics

Because binaries are brighter than single stars, using magnitude cut could bias the sample. We use a volume-limited sample without any explicit magnitude cut, and in Fig. 2.4 we show that the binary fractions remain fairly flat over the entire range of parallax considered, meaning that eclipsing binaries within
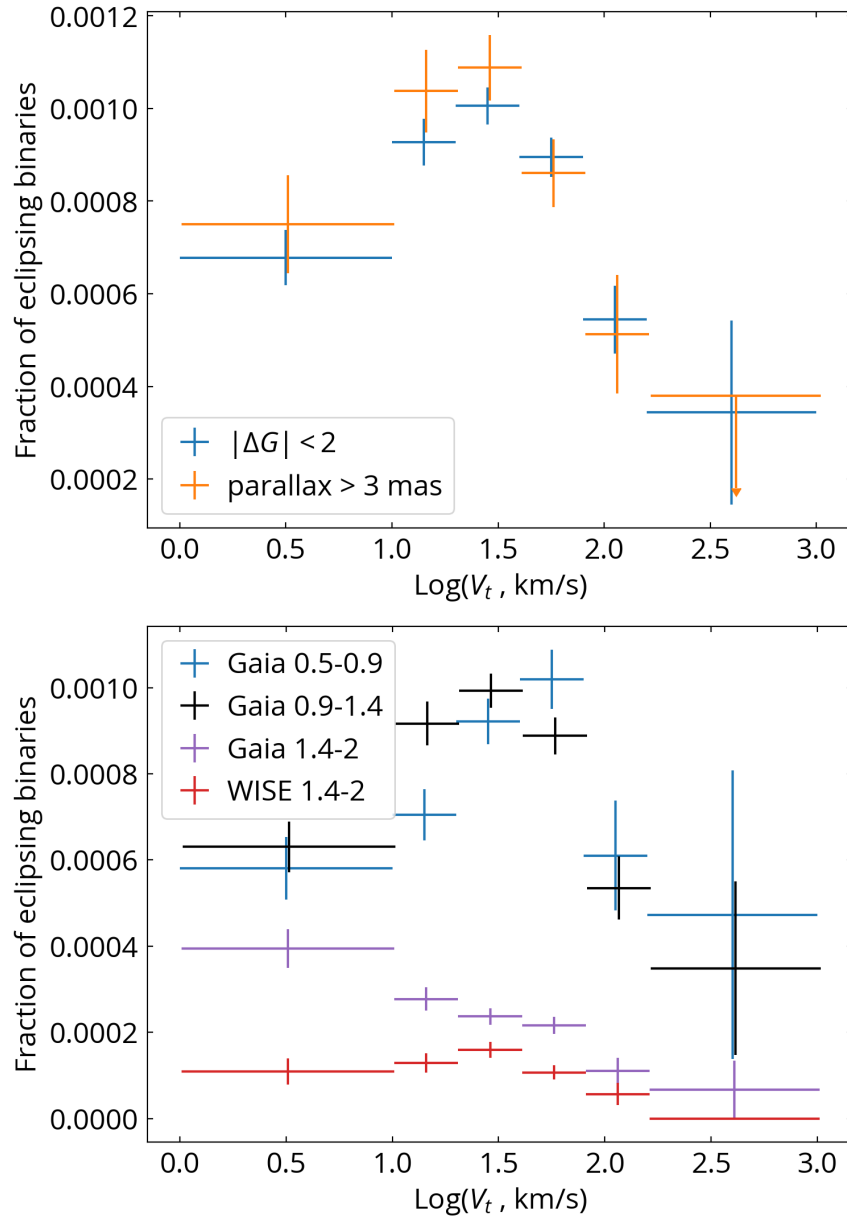
Figure 2.6: The same as Fig. 2.5, but with different sample selections. Top panel: Different MS selection of $|\Delta G| < 2$ mag (blue crosses) and parallax > 3 mas (orange crosses), using the Gaia eclipsing binary sample. Bottom panel: Different color selections. BP−RP=0.5-0.9 (blue crosses) and BP−RP=0.9-1.4 (black crosses) from the Gaia eclipsing binary sample agree with each other very well. BP−RP=1.4-2 from the WISE eclipsing binary sample also shows a similar trend but with a lower eclipsing binary fraction compared to the bluer color ranges. BP−RP=1.4-2 from the Gaia eclipsing binary sample has a peak at the low velocity end, which is likely due to the active flaring from young late-type dwarfs.

this distance range are well recovered. Furthermore, 95% of our MS sample are brighter than 14.8 mag in G-band while the limiting magnitude of Gaia DR2 is ~ 21 mag, our criteria for the mean flux divided by its error do not imply any implicit magnitude cut.

The excellent agreement between the WISE sample and Gaia sample in Fig. 2.5 means that our results are not affected by the WISE cross-match nor the limit of period-finding algorithms. Furthermore, the difference in the observing strategies of WISE and Gaia (and the resulting differences in the sky distribution of binaries) does not appear to affect our result. The dependence of the binary fraction on V_t cannot be explained by the covariance between velocity measurements and the variability. First of all, the tangential velocities are computed from proper motions and parallaxes with corrections from solar motions and the Galactic differential rotation, and there is no direct link to the photometry. If the observed dependence were due to the covariance between velocity and variability measurements, we would expect to see a monotonic relation in Fig. 2.5, which is not the case.

Gaia DR2 uses the standard deviation of individual flux measurements to estimate the flux errors, so variable sources like eclipsing binaries may have lower `phot_g_mean_flux_over_error` (also depends on the number of observations). Therefore, if a stricter cut for the mean flux divided by its error is used, the eclipsing binary sample may be reduced. However, this only affects the completeness level but not the kinematics, so it is not expected to change the observational trend in Fig. 2.5. To verify, we test a selection with the mean flux divided by its error only larger than 10 for G, BP and RP bands

35

(instead of 50, 20, and 20), resulting in ~ 10% more eclipsing binaries but not affecting the conclusion in Fig. 2.5.

The binaries in our sample only have separations of a few solar radii. For a solar-like contact binary at 100 pc, the maximum angular separation of the binary is ~ 0.1 mas, and the observed angular separation is even smaller due to the orbital motion and the viewing angle. Therefore, the resulting astrometric noise is ≪ 0.1 mas, which is below Gaia's astrometric precision (Lindegren et al., 2018). If the short-period binary has a tertiary companion, the additional orbital motion of the short-period binary around the companion may affect the astrometric solution. The level of this effect depends on the separation (and the orbital period) and the mass ratio between the inner binary and the tertiary companion. If the tertiary is comparable to the binary in brightness, we would actually not see much motion since the center of brightness would be relatively still, but such objects will be rare because the tertiary would be diluting the eclipses and we would be much less likely to identify such sources. If the tertiary is faint and therefore we mainly measure the motion of the inner binary, then outer orbital period needs to be short enough ($\lesssim 10$ yrs) to contribute significant orbital velocity to the inner binary, but also long enough (> 2 yrs of Gaia DR2's observation) so that the motion of the inner binary can still be described by the single-star model used by Gaia DR2's astrometric solutions. Therefore, there is a very limited parameter space for tertiary contamination to have a significant effect on our results.

In Fig. 2.6, we establish the robustness of results to differences in sample selection. In the top panel, we use the Gaia eclipsing binary sample to test

with a different MS selection of $|\Delta G| < 2$ mag, and also with a closer sample of parallax > 3 mas (i.e. within 333 pc). The results are nearly the same except that the fraction of binaries with parallax > 3 mas has larger error bars due to the smaller sample size. The results from the WISE eclipsing binary sample are similar so we do not repeat here.

In the bottom panel of Fig. 2.6, we test the fraction of eclipsing binaries with different color ranges, and therefore different mass ranges. We consider three BP−RP ranges: 0.5-0.9, 0.9-1.4 (the same in Fig. 2.5), and 1.4-2. The first two agree with each other very well. Interestingly, the eclipsing binary fraction in the color range of 0.5-0.9 seems to peak at a higher velocity ($V_t = 10^{1.6-1.9}$ km s^{-1}). The WISE eclipsing binary sample with BP−RP=0.5-0.9 also shows similar results to the Gaia sample, so we do not repeat here. This blue sample may have some contamination from δ Scuti variables, especially that a large fraction (up to ~ 70%) of stars located in the δ Scuti instability strip are pulsating, but most of them are variable on levels of a few mmag, below our variability sensitivity (Murphy et al., 2019). Indeed, within 751 eclipsing binaries in this color range, only 4 are identified as high-amplitude (> 0.1 mag) δ Scuti/SX Phoenicis from Gaia's non-public light curves (Rimoldini et al., 2019), so such contamination is small and does not affect the results.

The WISE eclipsing binary sample with BP−RP=1.4-2 (red crosses) shows a similar trend but with a lower eclipsing binary fraction compared to the bluer color ranges, which may be due to the combination of lower (eclipsing) binary fraction in low-mass stars (Duchêne and Kraus, 2013), the faintness of these stars, and their short periods below the classic Nyquist limit. The eclipsing

binary fraction from the Gaia eclipsing binary sample with BP–RP=1.4-2 (purple crosses) peaks at the lowest velocity bin, with perhaps a slightly flattened trend at $V_t \sim 10^{1.6}\,\mathrm{km\,s^{-1}}$. Because our Gaia eclipsing binary selection is based on the flux standard deviation but not the light curves, it is likely that this selection ends up with many actively flaring, young late-type stars. Due to the likely low completeness and high contamination of the reddest bin, we do not use it in our subsequent modeling.

2.5 The lifetime of eclipsing binaries from the galactic model

The kinematics in Fig. 2.5 may be linked to the age of the stars. When stars form in the disk, they have similar circular velocity (with some offset, Reid et al. 2009) as the disk initially. As time goes by, stars are perturbed by structures like giant molecular clouds, transient spiral arms, bars, and flyby satellite galaxies, resulting in a higher velocity dispersion when stars age. The age-velocity dispersion relation has been widely studied in literature (e.g. Nordström et al. 2004; Holmberg, Nordström, and Andersen 2009; Sharma et al. 2014; Cheng, Cummings, and Ménard 2019), and this relation is crucial for converting the kinematics into stellar ages.

Because the velocity dispersion monotonically increases with the stellar age, the average age of the stars in each tangential velocity bin in Fig. 2.5 is older with increasing velocities. Because the eclipsing binary fraction peaks at $10^{1.3-1.6}\,\mathrm{km\,s^{-1}}$ and drops at both lower and higher velocity ends, it means that the eclipsing binary fraction peaks at a certain stellar age, and is lower

for younger and older populations. As a first-order approximation, we parameterize the eclipsing binary fraction as a function of stellar age using three parameters: intrinsic eclipsing binary fraction (IEBF), the time when the eclipsing binaries form (t_0), and the time when the eclipsing binaries disappear (t_1). t_0 and t_1 determine the overall trend of eclipsing binary fraction versus kinematics, and IEBF adjusts the normalization but does not affect the trend.

Fully modeling Fig. 2.5 requires a complete description from the Galactic model, including the Galactic star formation rate history, number densities and kinematics for different stellar populations. We use the Gaia DR2 mock catalog produced by Rybizki et al., 2018. The Gaia DR2 mock catalog is generated using `Galaxia` (Sharma et al., 2011) that samples stars from a Besançon Galactic model (Robin et al., 2003) with a realistic 3D dust extinction map (Drimmel, Cabrera-Lavers, and Lopez-Corredoira, 2003; Marshall et al., 2006; Green et al., 2015; Bovy et al., 2016a; Bovy et al., 2016b). Because we do not correct for dust extinction in our samples, they can be directly compared with the Gaia DR2 mock catalog, although dust extinction within 500 pc is not a strong effect (typically $A_V < 0.8$ mag). The Gaia DR2 mock catalog also provides the ages and metallicities of the sampled stars, which is necessary for us to model the eclipsing binary lifetime.

We select stars from the Gaia DR2 mock catalog using the same color and absolute magnitude criteria as our sample, i.e. 0.9 <BP−RP< 1.4, $|\Delta G| < 1.5$, and parallax > 2 mas. The Gaia DR2 mock catalog itself does not simulate the stellar binaries, so for sources that are supposed to be binaries, their luminosities are underestimated by ≤ 0.75 mag. Our absolute magnitude

selection of $|\Delta G| < 1.5$ ensures that such systems are selected in both our eclipsing binary samples from observations and from the mock catalog. We assign weights to the stars in the mock catalog so that their sky distribution is the sample as our observational Gaia EB sample. The tangential velocities are corrected by removing the solar motion and the Galactic differential rotation.

We sample a grid of formation time (t_0) and disappearing time (t_1) shown in Fig. 2.7. For each combination of t_0 and t_1, we feed them into the Gaia DR2 mock catalog, and using the stellar ages recorded in the mock catalog, we compute the preliminary (preliminary because it has not considered the IEBF) eclipsing binary fractions weighted by the sky distribution as a function of tangential velocity. Then the preliminary eclipsing binary fractions are fit to the observed WISE-selected EB sample to determine the best-fit IEBF and the corresponding linear chi-squared costs, presented by the color coding in Fig. 2.7.

Fig. 2.7 shows that models with $t_0 = 0\,\mathrm{Gyr}$ and those with $t_1 \geq 12\,\mathrm{Gyr}$ can be rejected. We avoid using fits with 11 Gyr and 13 Gyr because these are the ages of thick-disk stars and halo stars in the mock catalog. We present some rejected examples in the left panel of Fig. 2.8. The observed drop of eclipsing binary fractions on the low-velocity end leads to rejection of models with $t_0 = 0\,\mathrm{Gyr}$ because such models can naturally only produce monotonically decreasing eclipsing binary fraction with increasing velocity (since the mean stellar ages monotonically increase with increasing velocity). On the other end of the distribution, models with $t_1 \geq 12\,\mathrm{Gyr}$ (i.e. when binaries can only disappear at an age above that of thick disk) make the eclipsing binary fraction

too high in the velocity bins $> 100\,\mathrm{km\,s^{-1}}$, for example the model (b) in the left panel of Fig. 2.8.

Fig. 2.7 presents the accepted models where $t_0 \sim 0.6\text{-}3\,\mathrm{Gyr}$ and $t_1 = 5\text{-}10\,\mathrm{Gyr}$, and the accepted t_0 and t_1 roughly follow a relation of $t_0 + 0.4t_1 \sim 5\,\mathrm{Gyr}$. Some examples of the accepted models are shown in the right panel of Fig. 2.8. They all successfully reproduce the overall trend of eclipsing binary fractions as a function of velocity.

The main uncertainty in these models lies in the Galactic descriptions used, including the star formation history, the adopted age-velocity dispersion relation, kinematics descriptions for different stellar populations (thin disk, thick disk, and halo), etc. These models are currently calibrated by the entirety of data from Galactic surveys. The number of free parameters involved is too large for us to investigate the uncertainty if a different Galactic description is used. Another uncertainty is the step-function-like lifetime model. While it is a reasonable first step, it is likely too simplistic. Because the uncertainties are mostly due to the model assumptions rather than due to measurement uncertainties, we do not pursue a best fit nor the Markov chain Monte Carlo procedure. Even though the modeling uncertainties are still unclear, the observed relation between eclipsing binary fraction and velocity can be successfully reproduced using the state-of-art Galactic descriptions.
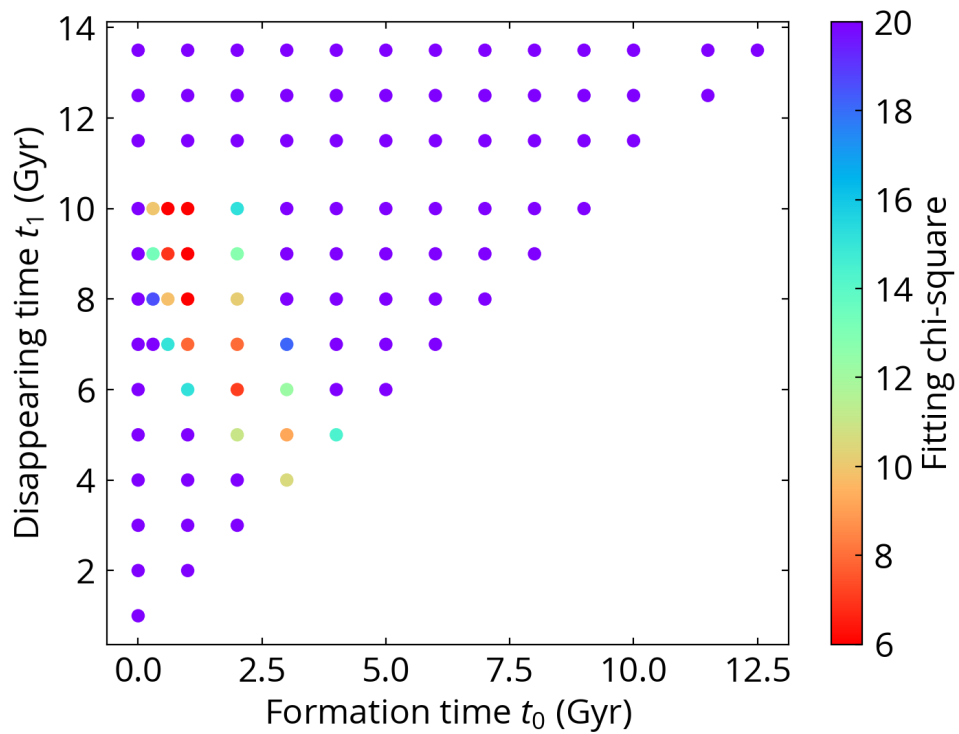
Figure 2.7: The model grids for the formation time (t_0) and disappearing time (t_1) of eclipsing binaries, color-coded by the chi-square of the best fit. The result constrains the formation time to be t_0 =0.6-3 Gyr and the disappearing time t_1 =5-10 Gyr, with accepted models roughly following the relation $t_0 + 0.4t_1 \sim 5$ Gyr.
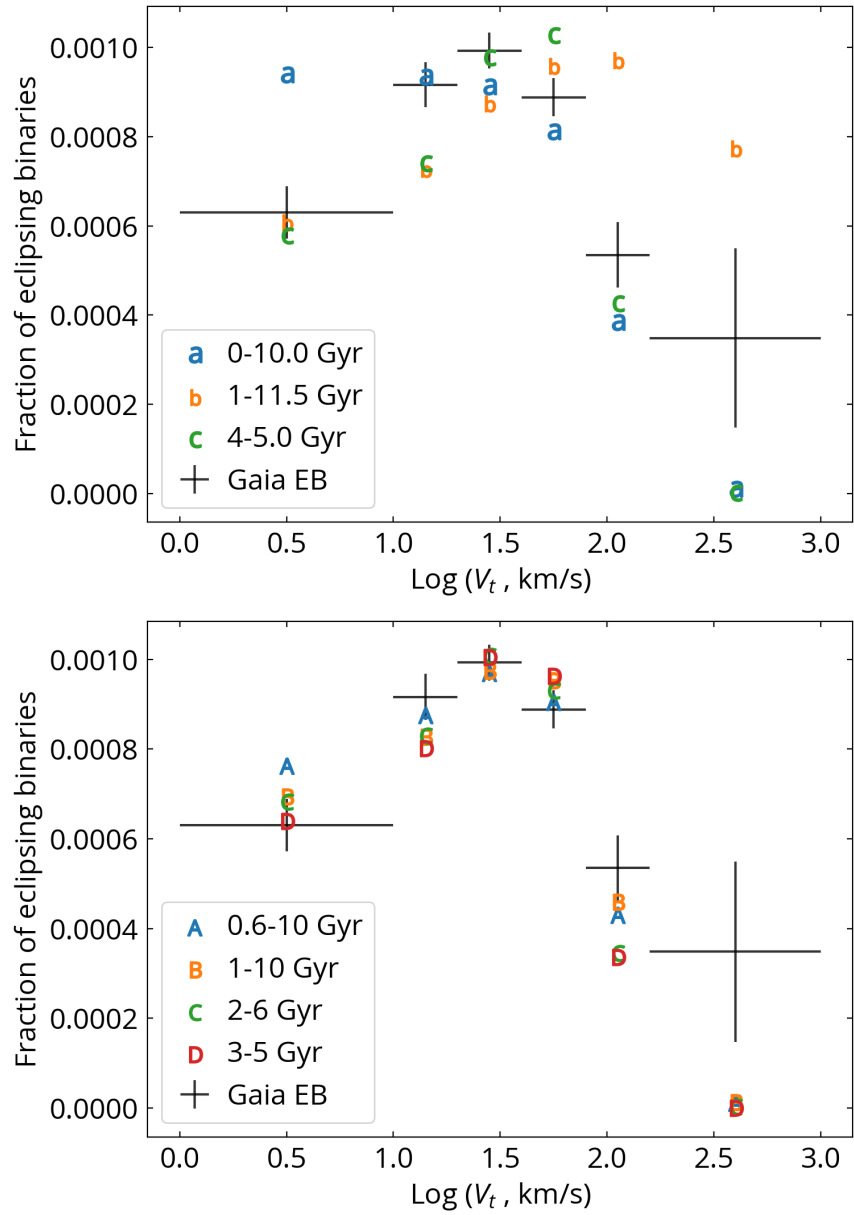
Figure 2.8: Examples of rejected models (left panel) and accepted models (right panel) for the lifetime of eclipsing binaries.

2.6 Discussion

2.6.1 Different properties between thin-disk, thick-disk and halo stars?

First, we attempt to determine if our results in Fig. 2.5 can be explained by the different eclipsing binary fractions in the thin-disk, thick-disk, and halo stars, without explicit consideration of stellar ages. Qualitatively, it is difficult because for $V_t < 100\,\mathrm{km\,s^{-1}}$, the sample is dominated by thin-disk stars and therefore a constant eclipsing binary fraction in thin-disk stars cannot explain the trend at $V_t < 100\,\mathrm{km\,s^{-1}}$ in Fig. 2.5. For $V_t > 100\,\mathrm{km\,s^{-1}}$, the thick-disk and halo stars start to dominate the sample so the decreasing eclipsing binary fraction might be linked to the different eclipsing binary fractions in different stellar populations.

The left panel of Fig. 2.9 presents the fractions of each stellar populations in each tangential velocity bins with the same selection in the H-R diagram as Fig. 5.4, weighted by the sky distribution of the Gaia eclipsing binary sample. The fractions of each stellar populations are derived from the Gaia Mock DR2 Catalog. The fractions of stellar populations in a tangential velocity bin can also be derived by considering the location distribution in the H-R diagram because thin-disk, thick-disk, and halo stars are located differently in the H-R diagram due to the difference in metallicity (e.g. Fig. 21 and 22 in Gaia Collaboration et al. 2018b). We use this method to obtain the fractions of each stellar populations from the Gaia data, with a similar result to that from the Gaia Mock DR2 Catalog. Fig. 2.9 shows that $> 90\%$ of the sample are thin-disk stars for $\log(V_t) < 10^{1.7}\,\mathrm{km\,s^{-1}}$, and $> 60\%$ are thick-disk stars for

$\log(V_t) > 10^{1.9}\,\mathrm{km\,s^{-1}}$. Halo stars become the dominant population ($> 50\%$) when $\log(V_t) > 10^{2.3}\,\mathrm{km\,s^{-1}}$, but the fraction of halo stars is reduced to 19% for $\log(V_t) > 10^{2.2}\,\mathrm{km\,s^{-1}}$.

The right panel of Fig. 2.9 shows the best-fit model that considers different eclipsing binary fractions for thin-disk, thick-disk, and halo stars. Because the halo stars only compose 19% of the sample in the highest velocity bin, its eclipsing binary fraction is not well constrained and hence we assume that the thick-disk stars and halo stars have the same eclipsing binary fractions during the fitting. The best-fit eclipsing binary fraction is $0.111 \pm 0.003\%$ for thin-disk stars, and $0.012 \pm 0.007\%$ for thick-disk and halo stars. Therefore, without the consideration of ages, the eclipsing binary fraction of thin-disk stars is ~ 10 times larger than the one of thick-disk and halo stars.

The best-fit model in the right panel of Fig. 2.9 is not able to reproduce the rising eclipsing binary fraction at $\log(V_t) < 10^{1.5}\,\mathrm{km\,s^{-1}}$. It is expected because thin-disk stars dominate in this velocity range and the model just reflects the eclipsing binary fraction of the thin-disk stars. Therefore, the eclipsing binary fraction of thin-disk stars cannot simply be a constant as a function of age.

The difference in eclipsing binary fractions between thin-disk stars and thick disk stars (and possibly halo stars) can be due to several factors. Because thick-disk and halo stars are older than thin-disk stars, the different eclipsing binary fraction may be the consequence of the eclipsing binary lifetime like Fig. 2.8. Thick-disk and halo stars are more metal-poor compared to thin-disk stars, and the effect of metallicity is discussed in the next section. Halo stars may be accreted from infalling satellite galaxies instead of forming in the

Milky Way, and therefore their formation environment can be different. The different eclipsing binary fractions might also result from the difference in physical properties between populations. For example, at fixed colors, metal-poor stars are smaller in size than metal-rich stars. Because the probability of being an eclipsing system is proportional to R/a, where R is the size of the star and a is the semi-major axis of the binary, smaller sizes of thick-disk stars might reduce the eclipsing binary fraction. However, we consider it unlikely. At the color of our sample, thick-disk stars are ~ 0.3 mag fainter than thin-disk stars, or a factor of ~ 0.87 smaller in the stellar radius. To reduce the eclipsing binary fraction by a factor of 10, thick-disk stars need to have a separation distribution 9 times wider than thin-disk stars. It is unlikely because that would make the period distribution of thick-disk stars ~30 longer than thin-disk stars.

The difference in the eclipsing binary fractions between the thin and thick disk is best demonstrated by the dependence of binary fraction on the Galactic height in Fig. 2.10. We slightly modify the sample selection here so that the sample remains complete to distances of ~ 1 kpc with sufficient statistical sample sizes. In this plot, the main-sequence sample is selected by $0.5 <$ BP–RP < 1.1, $|\varDelta G| < 1.5$, and parallax > 0.8 mas, and the eclipsing binaries are selected using $\log(f_G^2) > -2$. The Galactic height is computed by $d \times |\sin(b)|$, where d (inverse of parallaxes) is the distance of the star from the Sun and b is the Galactic latitude. Since we are interested in the change of eclipsing binary fractions on scales of > 100 pc, we do not correct for the height of the Sun above the Galactic plane, which is ~ 15 pc (Binney, Gerhard,

and Spergel, 1997; Widmark and Monari, 2019). We also show comparison with a $t_0 = 1\,\mathrm{Gyr}$ and $t_1 = 10\,\mathrm{Gyr}$ model, where we have modified the model in agreement with the selection used in Fig. 2.10.

Fig. 2.10 demonstrates that the eclipsing binary fraction decreases when the Galactic height $\gtrsim 300\,\mathrm{pc}$, where the thick-disk stars become increasingly dominant. This strengthens our conclusion that the thick disk has much lower eclipsing binary fraction than the thin disk. The increasing eclipsing binary fraction with increasing Galactic height at Galactic heights $< 300\,\mathrm{pc}$ is the consequence of the delayed formation of these short-period binaries. These trends are in excellent agreement with the model constructed independently based on the kinematic information. The strong dependence of short-period binary fraction on age, and consequently their kinematics and their Galactic height, explains the dependence on Galactic latitudes of eclipsing binary fraction seen in the literature (e.g. Prša et al. 2011; Slawson et al. 2011; Kirk et al. 2016).

Latham et al., 2002 find that there is no significant difference in the period distribution of spectroscopic binaries between disk stars and halo stars. Out of 156 objects with robust orbital solutions in their sample, the shortest period is 1.93 day, and only 7 (4.5%) have periods $< 10\,\mathrm{days}$. Therefore, it is likely that our results are different from theirs because we are probing a much shorter period population ($<1\,\mathrm{day}$) in which stronger evolutionary effects may be expected.

To summarize, while the declining eclipsing binary fraction at $\log(V_t) > 10^{1.5}\,\mathrm{km\,s^{-1}}$ suggests a much smaller eclipsing binary fraction in thick-disk and
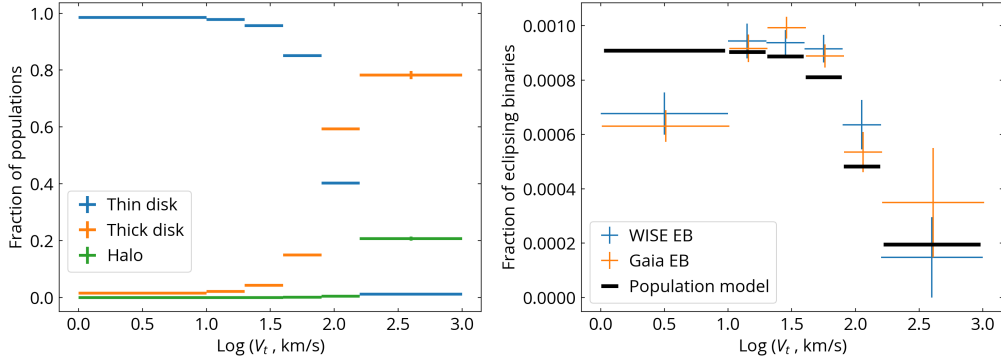
Figure 2.9: Left: fraction of the population (thin-disk, thick-disk, and halo stars) in each tangential velocity bin from the Galactic model. Right: eclipsing binary fraction versus tangential velocity, with a best-fit model (black horizontal bars) that considers different eclipsing binary fractions in each population. Age is not explicitly taken into account in the model. The best fit gives that the eclipsing binary fraction is ~ 10 times smaller in thick-disk (and probably halo) stars than in thin-disk stars. The population model can reproduce the observational trend on the high velocity end, but not on the low velocity end.

possibly halo stars, the rising eclipsing binary fraction at $\log(V_t) < 10^{1.5} \, \mathrm{km \, s^{-1}}$ is best explained by a delay in formation of eclipsing binaries compared to the formation of their components. We discuss possible causes for the delayed formation time and for the disappearing time in the following sections.

2.6.2 Metallicity

Recent studies have shown that the close-binary fraction (periods $< 10^4$ days; separation $<$ 10 AU) increases with decreasing stellar metallicity (Grether and Lineweaver, 2007; Yuan et al., 2015; Badenes et al., 2018; Moe, Kratter, and Badenes, 2019), consistent with formation of cose binaries due to disk fragmentation (Tanaka and Omukai, 2014). While our eclipsing binary sample has periods much shorter than their close binaries, we investigate if our results can be explained by the metallicity dependence.
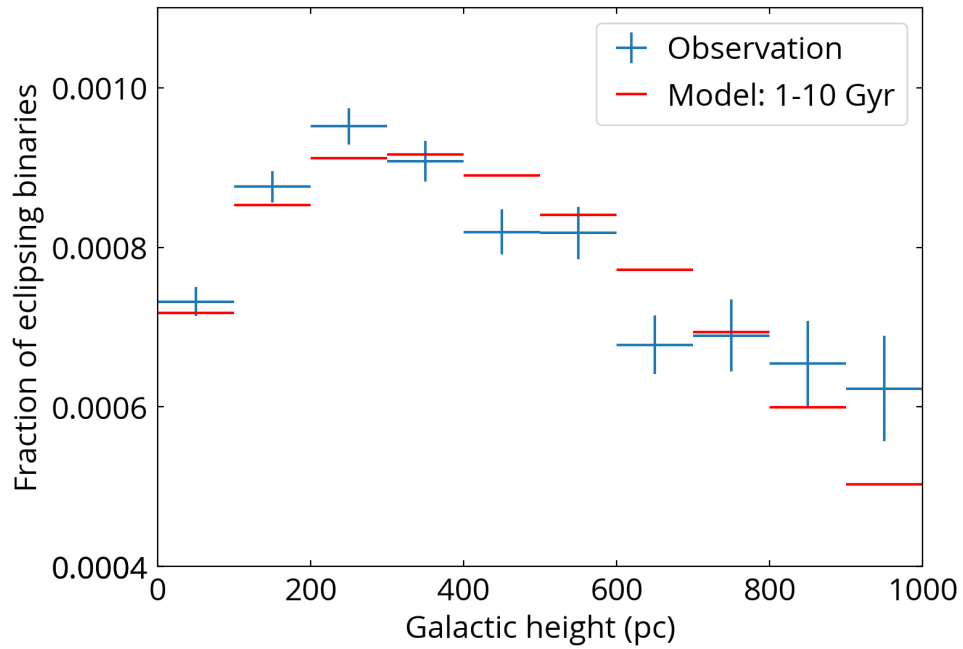
48

Figure 2.10: The eclipsing binary fraction as a function of the Galactic height. The blue crosses are the observational result where the horizontal segments indicate the bin sizes and the vertical segments are the errors of eclipsing binary fractions. The red horizontal bars are the model where the length of the bars is the bin size. The model uses a contact binary lifetime of 1 to 10 Gyr. The increasing eclipsing binary fraction with respect to Galactic latitudes at Galactic latitudes < 300 pc is due to the delayed formation of short-period binaries, and the deceasing eclipsing binary fraction at Galactic latitudes > 300 pc shows that the thick disk has a much lower eclipsing binary fraction.

Fig. 2.11 presents the models that take metallicity into account. We adopt the close binary fraction as a function of stellar metallicity from Moe, Kratter, and Badenes, 2019, and determine the normalization during the fitting (because not all close binaries are eclipsing binaries). The red triangles in Fig. 2.11 show the model that only includes metallicity effect but not age. The resulting binary fraction is inconsistent with the observation in two ways. First, for radial velocity $V_t < 10^{1.5}\,\mathrm{km\,s^{-1}}$, the metallicity-only model cannot reproduce the rising binary fraction as steep as the observation. This is because there is no strong metallicity-age relation for stellar ages $\lesssim 5\,\mathrm{Gyr}$ (Casagrande et al., 2011; Bensby, Feltzing, and Oey, 2014; Silva Aguirre et al., 2018). Second, the metallicity-only model does not have the decreasing binary fraction at velocity $V_t > 10^{1.6}\,\mathrm{km\,s^{-1}}$. Therefore, taking at face value the metallicity dependence by Moe, Kratter, and Badenes, 2019, our results cannot be explained by metallicity alone.

Fig. 2.11 also presents a model which includes both metallicity and age (orange squares). The adopted lifetime parameters are $t_0 = 1\,\mathrm{Gyr}$ and $t_1 = 8\,\mathrm{Gyr}$. The metallicity+age model shows a slight improvement in the velocity bin at $V_t = 100\,\mathrm{km\,s^{-1}}$ over the age-only model. Since this velocity bin is dominated by thick-disk stars, the goodness of the fit relies on the model descriptions, and therefore we do not favor the metallicity+age model because of its slight improvement.

We conclude that metallicity dependence is not able to explain the observational trends in eclipsing binary fraction versus kinematics. It is probably due to our sample focusing on the shortest period end, and mechanisms of
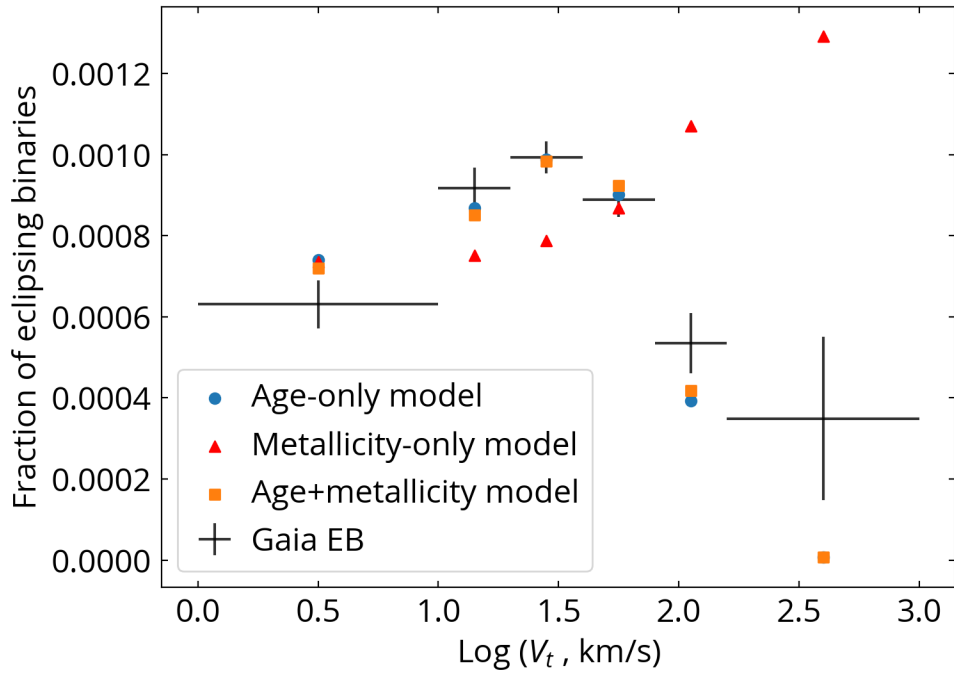
Figure 2.11: The eclipsing binary fraction versus tangential velocity, with models that take metallicity into account. The age-only model uses $t_0 = 1\,\text{Gyr}$ and $t_1 = 8\,\text{Gyr}$. The metallicity-only model (red triangles) cannot reproduce the observed trend.

orbital migration may make this sample more sensitive to the stellar ages. Binaries with longer periods (e.g. spectroscopic binaries) may not experience all the mechanisms of orbital migration, and therefore the effect of age is not prominent.

2.6.3 The formation of eclipsing binaries

Our results show that short-period eclipsing binaries form with a delay of $\gtrsim 0.6\,\text{Gyr}$. Because the size of pre-MS stars is much larger than zero-age MS stars, the separation between two stars in a binary must be larger than these eclipsing binaries in the beginning. Therefore, the formation delay is due to the orbital migration that a binary undergoes to lose the orbital angular

momentum until the orbital period is $\lesssim 1\,\mathrm{day}$.

Binaries can lose their orbital angular momentum through the energy dissipation in the pre-MS phase (Bate, 1998; Tohline, 2002; Moe and Kratter, 2018), through the angular momentum exchange with a distant tertiary and tidal effects (Kiseleva, Eggleton, and Mikkola, 1998; Fabrycky and Tremaine, 2007), and magnetic braking (Stepien, 1995). These mechanisms dominate different stages of orbital migration over different timescales.

Our estimated formation time of short-period binaries places strong constraints on the binary evolution theory. Because the pre-MS phase happens on a very short timescale ($\lesssim$ a few Myr), it does not fulfill the delayed formation time of $\sim 1\,\mathrm{Gyr}$. This means that short-period binaries cannot be produced only by the interaction in the pre-MS phase. The timescale of the Kozai-Lidov effect to produce short-period binaries depends on the initial conditions of the binary, including the initial separations and initial eccentricity of inner binary, ranging from $\sim\mathrm{Myr}$ to a few hundred Myr (Fabrycky and Tremaine, 2007; Perets and Fabrycky, 2009). Since the orbits of binaries are circularized at orbital periods of $\sim 10\,\mathrm{days}$ (Latham et al., 2002; El-Badry et al., 2018), it is difficult for the Kozai-Lidov mechanism to further reduce the orbital periods after that, and therefore other processes such as magnetic braking may be needed to complete the last step of orbital migration. Magnetic winds can bring detached binaries from periods of 5 days to contact binaries over a few Gyr (Stepien, 1995; Yakut, Kalomeni, and Tout, 2008). This timescale seems to agree with our constraint, but our upper limit of $\sim 3\,\mathrm{Gyr}$ for the formation time places a strong constraint on the possible parameter space.

While the delayed formation of short-period binaries is mostly determined by the magnetic braking, it does not mean that magnetic braking is the only process during the orbital evolution. In particular, because effective magnetic braking requires a small initial separation ($\lesssim 5$ day, Stepien 1995), pre-MS interaction and the Kozai-Lidov effect may still play an important role to bring binaries to orbital periods within ~ 5 days at an earlier stage.

Fig. 2.4 shows that the bluer color selection of BP−RP=0.4-0.9 has an eclipsing binary fraction peaking at a higher tangential velocity than the redder sample, indicating a potential mass dependence. While it requires a more detailed analysis, such mass dependence may be an important clue on the dominant orbital migration process. For example, magnetic winds require the presence of subphotospheric convection zones that are only in low-mass stars ($\lesssim 1.3\,M_\odot$). Therefore, if magnetic winds are the main cause for the delayed formation time in the color range of BP−RP=0.9-1.4, we may expect a longer delayed formation time for high-mass short-period binaries. The mass dependence of fragmentation during the proto-stellar phase may also play an important role (e.g. Kratter and Matzner 2006).

Our constraint of the formation time $\gtrsim 0.6\,$Gyr is consistent with observations that no short-period binaries ($P < 1$ day) are found in T Tauri stars and young clusters (Mathieu, 1994; Melo et al., 2001; Hebb et al., 2010). While short-period eclipsing binaries are easy to detect if they exist, none is found with periods < 1 day in Hyades and Pleiades (Torres, 2003; David et al., 2015; David et al., 2016), and only one is found in Praesepe (Rucinski, 1998; Zhang, Deng, and Lu, 2009). Further investigation is required to determine the true

eclipsing binary fraction in open clusters for comparison with our results. His-torically, RS Cha, with an orbital period of 1.67 days, was the shortest-period pre-MS eclipsing binary (Alecian et al., 2007), but Kepler K2 observations of Upper Scorpius (age of 5-7 Myr) have recently revealed three shorter period pre-MS eclipsing binaries EPIC 204506777, 203476597, and 202963882 where the orbital periods are 1.63, 1.44, and 0.63 days, respectively (David et al., 2019). The latter system is composed of two low-mass stars with $0.29\,M_\odot$ and $0.20\,M_\odot$, much lighter than our sample.

2.6.4 The disappearance of eclipsing binaries

In Sec. 2.6.1, we show that thick-disk and halo stars dominate the sample for $\log(V_t) > 10^{1.9}\,\mathrm{km\,s^{-1}}$, and a factor of ~ 10 smaller eclipsing binary fraction in thick-disk and halo stars can explain the observed declining eclipsing binary fraction at the high-velocity end. One possibility is that the eclipsing binary lifetime is shorter than the MS lifetime of these thick-disk and halo stars, making the eclipsing binary fraction in these populations much smaller compared to thin-disk stars. In this scenario, our results suggest that the disappearing time is between 5-10 Gyr, depending on the formation time. Although the disappearing time is not well constrained, we discuss some possible scenarios that limit the lifetime of eclipsing binaries.

Contact binaries may end up as stellar mergers. Tylenda et al., 2011 report a stellar merger of a contact binary V1309 Scorpii, although its progenitor is probably at the beginning of the red giant branch and not a MS considered here. The merging product may eventually become a blue straggler (Robertson

and Eggleton, 1977). By using binary evolutionary models, Stepien and Kiraga, 2015 show that some contact binaries can merge and become blue stragglers within the age of globular clusters ($\leq 13\,\mathrm{Gyr}$), and they suggest that this formation track may constitute a substantial fraction of all blue stragglers in globular clusters.

Our sample of BP−RP=0.9-1.4 has a MS lifetime longer than 14 Gyr. If the declining eclipsing binary at $\log(V_t) > 10^{1.9}\,\mathrm{km\,s^{-1}}$ is due to the stellar mergers of contact binaries, our results imply that the majority of short-period MS binaries are destroyed before the age of the thick disk ($\sim 11\,\mathrm{Gyr}$) and before the end of their own MS lifetime. This scenario can be tested by searching for high-velocity merging products, for example field blue stragglers.

A few other possibilities may reduce the binary fraction in old stars. One possibility is that their lower metallicity makes the orbital migration more inefficient, for example by suppressing the formation of triples, but this interpretation is disfavored by Moe, Kratter, and Badenes, 2019 where they show that the triple star fraction increases with decreasing metallicity. Alternatively, these old stars were originally in binaries with more massive stars, which have evolved into compact objects (white dwarfs, neutron stars, or black holes) and therefore only the originally less-massive stars are visible now. It is not impossible because O- and B- binaries with periods < 20 days seem to favor modest mass ratios ($q \sim 0.5$; Moe and Di Stefano 2017). If some of the high-velocity stars in our sample indeed have invisible companions with periods < 20 days, the radial velocity variation is on orders of $\sim 10\,\mathrm{km\,s^{-1}}$, which is detectable by Gaia's radial velocity measurements.

2.6.5   Interpretation of the formation time and disappearing time

Our results are consistent with the age estimate of contact binaries in literature. Kinematic studies show that the age of contact binaries is of several Gyr (Guinan and Bradstreet, 1988; Bilir et al., 2005). Yildiz, 2014 estimate the age of ~ 4.5 Gyr for W UMa binaries based on the stellar model (Yildiz and Dogan, 2013) and kinematics. These estimates are consistent with our formation time and disappearing time.

One distinction between this work and the literature is that we constrain the formation time and the disappearing time, not just the average age of eclipsing binaries. We emphasize that the formation time and disappearing time of short-period binaries are constrained in an average sense because of the use of the simple lifetime model. Our results do not imply that all eclipsing binaries form and disappear at the same time. In fact, it is very likely that the formation time itself is a wide distribution because the orbital migration processes, especially the Kozai-Lidov mechanism, is sensitive to the initial conditions (e.g. Perets and Fabrycky 2009).

Because the formation time and disappearing time are derived in an average sense, their difference $(t_1 - t_0)$ may not directly reflect the lifetime of the contact phase. Such timescale of the contact phase is rather uncertain, with some estimates ranging from 0.1 Gyr (Veer, 1979; Eggen and Iben, 1989) to ~ 10 Gyr (Mochnacki, 1981). If the contact phase is short (< 1 Gyr), then $t_1 - t_0$ is mainly related to the distribution of the formation time. If the contact phase can last for $>$ a few Gyr, $t_1 - t_0$ may be able to constrain the timescale of the

contact phase.

2.6.6   Alternative explanations?

In this section, we explore other possibilities that might explain the result. First, our results cannot be explained by different binary properties in different mass of young clusters because typical 1-D velocity dispersion in young clusters is $\lesssim 10\,\mathrm{km\,s^{-1}}$ (e.g. Larsen, Brodie, and Hunter 2004) while our result shows that eclipsing binary fraction peaks at $\sim 30\,\mathrm{km\,s^{-1}}$.

When binaries evolve to contact binaries, their surface temperatures may change, and the mass transfer may alter their eclipse depths and light curve profiles (Yakut and Eggleton, 2005; Stepien and Gazeas, 2012), moving them into or out of our sample selection. The color evolution from detached to contact binaries is a long-standing open question, and in some models the effective temperature of contact binaries oscillates without reaching an equilibrium (the thermal relaxation oscillation model; Lucy 1968; Flannery 1976; Webbink 1976; Yakut and Eggleton 2005).

While it is difficult to quantify these effects at the moment, we argue that our results are not strongly affected by such color evolution. (1) Among close binaries, there is an excess of nearly equal-mass binaries, so called twins (Tokovinin, 2000; Pinsonneault and Stanek, 2006; Raghavan et al., 2010). Among wider binaries with primary masses 0.8-1.2 $\mathrm{M_\odot}$ and $P = 10^{0.5-1.5}$ day, the fraction of nearly equal ($q > 0.95$) binaries is $\sim$ 38% (Moe and Di Stefano, 2017), and it is likely to be even larger at shorter periods. When these nearly equal-mass binaries evolve to contact binaries, they do not experience

significant color evolution. (2) Consider an effective observed temperature T_{eff} of an unresolved, detached binary defined as $R_1^2 T_1^4 + R_2^2 T_2^4 = (R_1^2 + R_2^2) T_{\text{eff}}^4$, where R_1 and R_2 are the radii and T_1 and T_2 are the temperatures of the two component stars, respectively. With the scaling relation of $R \propto M^{0.8}$ and $T \propto M^{0.54}$ for low-mass stars and M is the mass of a star (Lamers and Levesque, 2017), the minimum observed temperature happens at $T_{\text{eff}} = 0.8 T_1$ when $q = 0.6$. For a smaller mass secondary star ($q < 0.6$), T_{eff} increases toward T_1 because the light coming from the secondary becomes negligible. During the contact phase, one extreme case is that two stars reach the same temperature $T_{\text{contact}} = T_1$ from T_{eff}, then it results a maximum color change of $\Delta BP-RP \sim 0.5$ (from the simulated colors in PARSEC isochrones). In reality, $T_{\text{contact}} < T_1$ and the color change is smaller ($\Delta BP-RP < 0.5$). If our kinematic result is due to the color evolution, it means that the result would depend on how wide our color selection is. We test our result with a color selection of $BP-RP = 0.5\text{-}1.5$ and the result remains the same, and therefore our result is not the consequence of such color evolution.

Another selection effect is unresolved tertiary companions. If the unresolved tertiary contributes non-negligible fluxes, it may change the apparent color of the binary and/or reduce the photometric variability, which would affect our selection. However, if the effect of unresolved tertiary companions is not a strong function of age (and therefore kinematics), then it only reduces the completeness of our sample without biasing the results.

There is one interesting scenario where unresolved tertiary companions

have an age dependence, in the sense that there is an excess of short-lived, unresolved tertiary companions around the short-period main-sequence binaries. In this case, we would only see the short-period binary after the short-lived, unresolved tertiary companion dies, which would explain the increasing eclipsing binary fraction at the low-velocity end in Fig. 2.5. From our model, the lifetime of these short-lived tertiary companions needs to be shorter than $3\,\mathrm{Gyr}$, corresponding to stellar masses $> 1.5\,\mathrm{M}_\odot$. This scenario contradicts previous studies which show that most of the tertiary companions are lighter than the total mass of the inner binaries (Tokovinin et al., 2006; Borkovits et al., 2016). This scenario would also imply that nearly all short-period binaries have close white dwarf companions, which has not been reported.

Another scenario is that the tertiary companion is at a short separation from the inner binary at the young age and is blended with it, but becomes more widely separated afterwards. When the Kozai cycle stops, the mutual inclination between the inner binary and the outer tertiary companion tends to get stuck at a certain value (Fabrycky and Tremaine, 2007), making the tertiary companion slightly farther compared to random orientation. However, such difference in projected separations is marginal and cannot explain the steep increase of eclipsing binary fraction at the low-velocity end. Alternatively, the tertiary companions may migrate outwards due to the gravitational perturbations from passing stars, e.g., in the natal open cluster environment (Zakamska and Tremaine, 2004). This may be in line with El-Badry et al., 2019 who suggest such orbital migration to explain the excess of nearly equal-mass binaries with separations of a few thousand AU. However, it implies that

nearly all our older short-period binaries should have bright resolved tertiary companions, while we only find 20% of our sample having resolved comoving companions with projected separations of 10^{2-5} AU. Therefore, this scenario seems unlikely.

These alternative scenarios try to explain the increasing eclipsing binary fraction at the low-velocity end. Based the arguments above, they all seem unlikely, and none of them can explain the decreasing eclipsing binary fraction at the high-velocity end. Therefore, we consider the lifetime of short-period binaries to be the best explanation for our results.

2.7 Conclusions

In this paper, we investigate the kinematics of short-period ($< 1\,\mathrm{day}$) main-sequence eclipsing binaries. We construct two samples of eclipsing binaries: one from the time series analysis of WISE light curves, and the other from the photometric variations in Gaia DR2. These two eclipsing binary samples are complementary to each other: WISE eclipsing binary sample has nearly no contamination, while Gaia eclipsing binary sample has a more homogeneous sky distribution and is not affected by the limitations of period-finding algorithms. We carefully investigate the potential effects from different selection criteria, and require a volume-limited sample instead of magnitude-limited since binaries are brighter than singles. With the kinematics from Gaia DR2, we present the following findings:

1. Our primary result is that the eclipsing binary fraction peaks at tangential velocity $V_t = 10^{1.3-1.6}\,\mathrm{km\,s^{-1}}$ and decreases towards both low and

high velocity ends (Fig. 2.5).

2. Since thick-disk and halo stars dominate at high velocity ($V_t > 100\,\mathrm{km\,s^{-1}}$), our results imply that the eclipsing binary fraction is at least ~ 10 times smaller in thick-disk and halo stars compared to thin-disk stars (Fig. 2.9). This is further supported by the decreasing eclipsing binary fraction when the Galactic latitude $\gtrsim 300\,\mathrm{pc}$ (Fig. 2.10).

3. The relation between eclipsing binary fraction and kinematics is best explained by the lifetime of eclipsing binaries (Fig. 2.7 and 2.8). By using Galactic models, we constrain the formation time (t_0) of eclipsing binaries to be between 0.6 and 3 Gyr and the disappearing time (t_1) to be between 5 and 10 Gyr, where t_0 and t_1 are related through $t_0 + 0.4t_1 \sim 5\,\mathrm{Gyr}$. The lower eclipsing binary fraction in thick-disk and halo stars may be a consequence of the finite lifetime of eclipsing binaries.

4. While the pre-MS interaction and the Kozai-Lidov mechanism may help to shrink the binary orbits at an earlier stage, the delayed formation time of $0.6 - 3\,\mathrm{Gyr}$ means that short-period binaries cannot form directly from these two scenarios. The timescale is more consistent with magnetic braking, but the upper limit of $\sim 3\,\mathrm{Gyr}$ provides a strict constraint for the theory.

5. The disappearance of eclipsing binaries may be due to their mergers within the MS lifetime. This scenario may be tested by studying the kinematics of the merging products, if they can be identified in survey data.

2.8 Appendix

2.8.1 Gaia query

Here is the query for selecting eclipsing binaries from Gaia DR2 used in this paper:

```
SELECT
  gaia.*,
  allwise.w1mpro, allwise.w2mpro, allwise.w3mpro, allwise.w4mpro,
  allwise.cc_flags, allwise.var_flag
FROM gaiadr2.gaia_source AS gaia
```

```
LEFT JOIN gaiadr2.allwise_best_neighbour AS allwisexmatch
  ON gaia.source_id = allwisexmatch.source_id
LEFT JOIN gaiadr1.allwise_original_valid AS allwise
  ON allwise.allwise_oid = allwisexmatch.allwise_oid
WHERE
  gaia.parallax_over_error > 10 AND
  gaia.phot_g_mean_flux_over_error>50 AND
  gaia.phot_rp_mean_flux_over_error>20 AND
  gaia.phot_bp_mean_flux_over_error>20 AND
  gaia.phot_bp_rp_excess_factor <
1.3+0.06*power(gaia.phot_bp_mean_mag-gaia.phot_rp_mean_mag,2) AND
  gaia.phot_bp_rp_excess_factor >
1.0+0.015*power(gaia.phot_bp_mean_mag-gaia.phot_rp_mean_mag,2) AND
  gaia.visibility_periods_used>8 AND
  gaia.parallax >= 2.
```

2.8.2   Comparison with the Kepler eclipsing binary catalog

In this appendix, we investigate how our eclipsing binary selection, especially in the Gaia-only sample where we do not have light curves, compares with the published Kepler eclipsing binaries. We cross-match the Kepler eclipsing binary catalog (Kirk et al., 2016) with Gaia DR2 with a matching radius of 1 arcsec, and exclude objects that have multiple Gaia matches, ending up with 2721 Kepler eclipsing binaries. The cross-match shows that 95% of them have

parallaxes < 2 mas. To compare our MS eclipsing binary selection with the Kepler catalog, we use the following criteria: (1) 0.9 <BP−RP< 1.4, $|\Delta G| < 1.5$, and parallax > 0.5 mas, resulting in 665 sources.

Fig. 2.12 shows the Gaia fractional variability versus the orbital periods in the Kepler eclipsing binary catalog. We use the light curve morphology measurements from Kirk et al., 2016 to roughly classify the variables into eclipsing binaries (solid circles) where `morphology`< 0.8 and ellipsoidal variables (open circles) where `morphology`> 0.8. Eclipsing binaries (solid circles) are color-coded by their `morphology`, and usually `morphology`< 0.5 are detached binaries, `morphology`= 0.5-0.7 are semi-detached binaries, and `morphology`= 0.7-0.8 are contact binaries. Our Gaia eclipsing binary selection criterion ($\log(f_G^2) > -2$) is above the orange solid line in the plot. For sources where the Gaia fractional variability is below the instrumental level (Sec. 2.2.4), we place them at the bottom of the plot (−5 on the vertical axis). Most of our Gaia-Kepler eclipsing binaries (85/86) have orbital periods < 0.5 day (apparent periods < 0.25 day), and most of them are contact binaries where `morphology`= 0.7-0.8.

The Kepler eclipsing binary fraction (including ellipsoidal variables) of orbital periods < 1 day and cooler K stars (temperatures between 4000-5000 K, similar to our main sample) is 0.4%, which is ∼ 4 times higher than our Gaia EB sample. The difference is due to several factors. (1) First, our Gaia EB selection is more sensitive to contact binaries with orbital periods < 0.5 day, and insensitive to (semi-)detached binaries with orbital periods > 0.5 day; (2) Second, Kepler is able to recover more low-amplitude ellipsoidal variables at
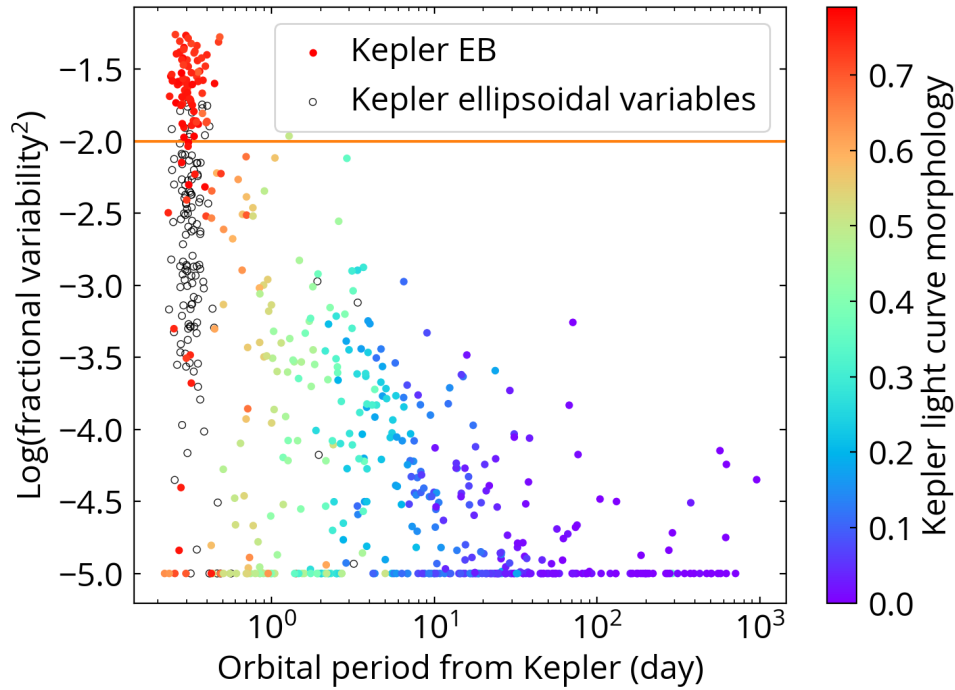
Figure 2.12: Comparison between fractional variability from Gaia DR2 and Kepler orbital periods. The Kepler sample is divided into eclipsing binaries (solid circles) and ellipsoidal variables (open circles). The solid circles are color-coded by the Kepler light curve morphology measurements (Kirk et al., 2016), and contact binaries usually have values between 0.7 and 0.8. Our Gaia eclipsing binary selection mainly selects contact binaries with orbital periods < 0.5 day.

orbital periods < 0.5 day. Once we account for these differences, we find that our eclipsing binary fraction is consistent with Kepler.

It is difficult to compare the WISE eclipsing binary selection with the Kepler eclipsing binary catalog because Kepler eclipsing binaries are more distant and most of them are below or close to WISE's single-exposure sensitivity. However, Fig. 2.3 and Fig. 2.4 have shown that the properties of WISE eclipsing binaries are in general similar to Gaia eclipsing binary selection, so the conclusions from the comparison between the Kepler eclipsing binaries and Gaia eclipsing binaries also apply to the WISE eclipsing binary sample.

Chapter 3

Very wide companion fraction from Gaia DR2: a weak or no enhancement for hot jupiter hosts, and a strong enhancement for contact binaries

There is an ongoing debate on whether hot jupiter hosts are more likely to be found in wide binaries with separations of $\gtrsim 100$ AU. In this paper, we search for comoving, very wide companions with separations of $10^3 - 10^4$ AU for hot jupiter hosts and main-sequence contact binaries in Gaia DR2, and compare the very wide companion fractions with their object-by-object-matched field star samples. We find that $11.9 \pm 2.5\%$ of hot jupiter hosts and $14.1 \pm 1.0\%$ of contact binaries have companions at separations of $10^3 - 10^4$ AU. While the very wide companion fraction of hot jupiter hosts is a factor of 1.9 ± 0.5 larger than their matched field star sample, it is consistent, within $\sim 1\sigma$, with that of matched field stars if the matching is only with field stars without close companions (within ~ 50 AU) as is the case for hot jupiter hosts. The very

wide companion fraction of contact binaries is a factor of 3.1 ± 0.5 larger than their matched field star sample, suggesting that the formation and evolution of contact binaries are either tied to or correlated with the presence of wide companions. In contrast, the weak enhancement of very wide companion fraction for hot jupiter hosts implies that the formation of hot jupiters is not as sensitive to those environment properties. Our results also hint that the occurrence rates of dual hot jupiter hosts and dual contact binaries may be higher than the expected values from random pairing of field stars, which may be due to their underlying metallicity and age dependence.

3.1   Introduction

The discovery of the first exoplanet orbiting a sun-like star, 51 Pegasi b, presents a significant challenge to planet formation theories based on our Solar System (e.g. Mayor and Queloz 1995; Rasio et al. 1996). While the giant planets of the Solar System may have somewhat migrated (Morbidelli et al., 2012), they likely formed in the cooler outer regions of the protoplanetary disc where the icy material facilitated rapid core growth to accrete massive gaseous atmospheres before the disk dissipated. In contrast, 51 Pegasi b is the prototypical 'hot jupiter', with a mass roughly half that of jupiter but with an orbital separation from the host star of about 7 times smaller than that of Mercury. 25 years after the discovery of 51 Pegasi b, the formation of hot jupiters remains an open question.

There are three main hot jupiter formation theories: in situ formation, disk migration, and high-eccentricity tidal migration (Dawson and Johnson, 2018).

In the in situ formation scenario, hot jupiters form at their current locations. This scenario was believed to be challenging because both gravitational instability and core accretion are difficult to operate at hot jupiters' close-in locations (Rafikov, 2005; Rafikov, 2006), but recent study suggests that in situ formation is still possible under certain conditions (Bodenheimer, Hubickyj, and Lissauer, 2000; Batygin, Bodenheimer, and Laughlin, 2016; Boley, Granados Contreras, and Gladman, 2016; Lee and Chiang, 2016). In the disk migration scenario, hot jupiters form at larger separations and migrate to their current location under the torque from the protoplanetary disk (Goldreich and Tremaine, 1980; Lin and Papaloizou, 1986; Lin, Bodenheimer, and Richardson, 1996; Nelson et al., 2000; Ida and Lin, 2008).

In the high eccentricity migration scenario, the hot jupiter forms at a large separation from the host star, is driven into a high-eccentricity orbit, and undergoes tidal circularization which leaves the planet in its small, circular orbit. The eccentricity excitation may be caused by planet-planet scattering (Rasio and Ford, 1996; Weidenschilling and Marzari, 1996; Ford and Rasio, 2006; Chatterjee et al., 2008; Jurić and Tremaine, 2008), or Kozai-Lidov interactions (Kozai, 1962; Lidov, 1962) with an other planet (Naoz et al., 2011) and/or with a stellar companion (Wu and Murray, 2003; Fabrycky and Tremaine, 2007; Naoz, Farr, and Rasio, 2012).

The occurrence of stellar companions around hot jupiter hosts provides a constraint on the formation of hot jupiters. If Kozai-Lidov interactions with stellar companions represent a significant channel for hot jupiter formation, then stellar companions should be common around hot jupiter hosts. At an

earlier evolutionary stage, the presence of stellar companions can affect the environment of the protoplanetary disk and the planet formation (Kraus et al., 2012).

There has been extensive work on measuring the incidence of stellar companions to hosts of hot jupiters (Knutson et al., 2014; Endl et al., 2014; Piskorz et al., 2015; Bryan et al., 2016; Evans et al., 2016; Belokurov et al., 2020b), but whether hot jupiter hosts have a higher wide companion fraction is still an ongoing debate. Ngo et al. (2016) conduct a direct imaging search for companions to hot jupiter systems and find that for companions with separations between 50 and 2000 AU, hot jupiter hosts have a companion fraction 2.9 times higher than that of the field stars from Raghavan et al., 2010, with a significance of $4.4\,\sigma$. They argue that $> 80\%$ of these companions are not able to induce Kozai-Lidov oscillations because the oscillation timescale is too long, and therefore the enhanced companion occurrence may instead be linked to the formation environment of the gas giants.

However, Moe and Kratter, 2019 point out that such enhanced companion fraction of hot jupiter hosts may be a consequence of several selection effects. First, they argue the field star sample from Raghavan et al., 2010 is not ideal for the hot jupiter hosts used in Ngo et al., 2016 because these two samples have slightly different mass and metallicity, and the field star sample is not complete.

Second, observations have shown that fewer hot jupiter hosts have close stellar companions at separations $\lesssim 50\,\mathrm{AU}$ compared to the field stars (Wang et al., 2014b; Wang et al., 2014a; Kraus et al., 2016; Matson et al., 2018; Ziegler

et al., 2019). This may be the result of the shorter life-time of protoplanetary disks in binaries compared to those around single stars (Kraus et al., 2012; Kraus et al., 2016). Specifically, hot jupiter hosts have a very small companion fraction within 50AU – only $4\%^{+4\%}_{-2\%}$ (Ngo et al., 2016). In contrast, field stars with a similar mass and metallicity have a companion fraction within 50AU of $40 \pm 6\%$ (Moe and Kratter, 2019). In the absence of any other physical mechanisms, the lower close companion fraction of hot jupiter hosts would result in a higher wide companion fraction compared to the field stars. After having accounted for this bias, Moe and Kratter, 2019 argue that hot jupiter hosts do not have an enhanced wide companion fraction compared to the field stars.

In this paper, we examine the very wide companion fraction at separations of $10^3 - 10^4$ AU around hot jupiter hosts and main-sequence contact binaries using Gaia data. We search for comoving and colocated companions to hot jupiter hosts, contact binaries, and to field stars down to Gaia's spatial resolution limit. By using Gaia, we are able to compare the companion fraction between different populations based on the same dataset, without dependence on external data and models.

In this paper, we refer to companions with separations of $< 50\,$AU as close companions, those of $50 - 2000\,$AU as wide companions, and those of $10^3 - 10^4$ AU as very wide companions. This paper is structured as follows. Section 3.2 describes our sample selection and the search of comoving companions. Section 4.3 presents our main results. We discuss the results in Section 5.5 and conclude in Section 5.6.

3.2   Sample selection and method

3.2.1   Selection of hot jupiter hosts

We use the sample of main sequence hot jupiter hosts whose selection is described in Hamer and Schlaufman (2019). Briefly, hot jupiters were selected from the confirmed planets table of the NASA Exoplanet Archive using the fiducial definition from Wright et al. (2012), planets having $P < 10$ days and $M \sin i > 0.1 \, M_{\mathrm{Jup}}$. Most ($\sim 90\%$) of these hot jupiters were discovered by transiting surveys and further confirmed by follow-up radial-velocity observations. Therefore, no contamination from false-positive eclipsing binaries is expected. This is important because an exoplanet sample from radial velocity surveys may be biased because exoplanet radial velocity surveys may exclude spectroscopic binaries (Moe and Kratter, 2019). In transiting surveys, the presence of a close companion may dilute the transit depths and potentially bias an exoplanet sample, but Moe and Kratter, 2019 show that hot jupiters are relatively immune to this effect because of their deep and frequent transits. The Gaia DR2 designations of these hot jupiter hosts were then obtained from SIMBAD. The sample was limited to hosts having good astrometry using the quality cuts described in Appendix 1 of Hamer and Schlaufman (2019). Individual line-of-sight reddening values were calculated for each star by interpolating the three-dimensional reddening map from Capitanio et al. (2017) and integrating the interpolated grid along the line of sight to calculate a total $E(B - V)$ reddening. $E(B - V)$ was converted to Gaia reddening $E(\mathrm{BP-RP})$ and extinction A_G, using the mean extinction coefficients from Casagrande

71

and VandenBerg (2018). Evolved hot jupiter hosts were excluded by removing hosts which fall more than one magnitude above an empirical fit to the Pleiades in the $(BP − RP)$–M_G plane. Among the 338 main-sequence hot jupiter hosts from Hamer and Schlaufman, 2019, we further limit the sample to parallaxes > 2.5 mas (distances < 400 pc) for better companion completeness. As explained in the later sections, we remove targets where no matched field stars are found or in a comoving group, ending up with 193 hot jupiter hosts.

3.2.2 Selection of main-sequence contact binaries

Short-period binaries are often compared to hot jupiters because historically both their formations are speculated to be due to the Kozai-Lidov interactions (e.g. Fabrycky and Tremaine, 2007). Furthermore, a direct comparison of wide companion fractions between short-period binaries and hot Jupiters (Moe and Kratter, 2019) provides a probe of the different formation processes across the mass gap of $4 − 9\,M_J$ (Schlaufman, 2018). Therefore, in this paper we compare the companion fraction between main-sequence hot jupiter hosts, main-sequence contact binaries and field stars.

We use the sample of contact binaries whose selection is detailed in Hwang and Zakamska, 2020. They used the fractional variability from Gaia Data Release 2 (DR2; Gaia Collaboration et al. 2016; Gaia Collaboration et al. 2018a) to select high-amplitude (> 10%) variables, which are dominated by contact binaries on the main sequence. They selected main-sequence objects using $|\varDelta G| < 1.5$ mag, where $\varDelta G$ is defined as the offset of absolute G magnitudes

between the stars and Pleiades at the same BP−RP colors (Hamer and Schlaufman, 2019). Other photometric and astrometric quality criteria employed in this work are the same as those used in Hwang and Zakamska, 2020. By comparing with the Kepler eclipsing binary catalog (Kirk et al., 2016), Hwang and Zakamska, 2020 show that this method efficiently selects main-sequence contact binaries with orbital periods < 0.5 day. In this paper, we use a color cut of BP−RP=0.5-1.5 mag to avoid blue pulsating stars and red M-dwarf flaring stars (Gaia Collaboration et al., 2019).

With all selections discussed above, we further limit the main-sequence contact binary sample to parallaxes > 2.5 mas (i.e. within 400 pc), remove targets if we cannot identify a matched field star, and remove targets in comoving groups explained in the later sections. We end up with 1333 main-sequence contact binaries.

3.2.3 Control field star sample

For each target sample (hot jupiter host sample or main-sequence contact binary sample), we select a field star sample that matches object-by-object in several properties. Specifically, for each target star (hot jupiter host or a contact binary), we search a field star such that: (1) it is > 10 pc away from the target star (assuming the pair has the same parallax as the target star), and it is < 20 deg from the target star; (2) the BP−RP color difference is < 0.05 mag; (3) the parallax difference with the target star is < 10%; (4) the tangential velocity difference with the target star is < 10 km s^{-1}; (5) the field star satisfies the Gaia selections explained in Sec. 3.2.2. The tangential velocity used here has been

corrected for the solar motion (Schönrich, Binney, and Dehnen, 2010) and the Galactic differential rotation using the Oort's constants reported by Bovy, 2017. To improve statistics, for each hot jupiter host, we find four matched field stars, where the mutual separations of four matched field stars are all $> 10\,\mathrm{pc}$ (assuming the same parallax as the target star). We exclude hot jupiter hosts from the sample if four matched field stars are not found. Because the contact binary sample is sufficiently large, only one field star is matched to one contact binary. Every control field star is matched to exactly one target.

By matching the properties described above, we ensure that the sample of the target stars (hot jupiter hosts or contact binaries) and the corresponding matched field star sample have similar distributions of masses, sky distributions, Galactic latitudes, and kinematics. Since the stellar age is strongly correlated with the kinematics (Dehnen and Binney, 1998; Nordström et al., 2004; Reid et al., 2009; Sharma et al., 2014), we expect that the kinematic ages of the target sample and the matched field star sample are also similar. This is important because the occurrence of both hot jupiters and contact binaries has strong stellar age dependence (Hamer and Schlaufman, 2019; Hwang and Zakamska, 2020). Matching the Galactic latitudes is crucial because the contact binary fraction is much lower in the thick disk than in the thin disk (Hwang and Zakamska, 2020).

The hot jupiter occurrence rate is correlated with stellar metallicity (Gonzalez, 1997; Santos, Israelian, and Mayor, 2004; Fischer and Valenti, 2005). Therefore, ideally, we may also want to match metallicity for the control field stars. Although we match the masses, Galactic latitudes, and kinematics,

which are all correlated with metallicity, there is no guarantee that the metallicity is exactly the same as the hot jupiter host sample. However, in this paper we focus on the very wide companions ($10^3 - 10^4$ AU), and it is has been shown that the solar-type binary fraction beyond > 200 AU is independent of metallicity (El-Badry and Rix, 2019; Moe, Kratter, and Badenes, 2019). Therefore, metallicity plays a relatively minor role in our investigation of very wide companions.

3.2.4 Comoving companion search

We search for very wide comoving companions with projected separations up to 10^6 AU (4.8 pc). We start with a selection of nearby stars, from which we further select the comoving companions. For each target star (hot jupiter host, contact binary, or field star), we select its nearby stars where (1) either the parallax difference < 0.2 mas or the difference of line-of-sight distance (inverse of parallax) is < 20 pc; (2) projected physical separations < 20 pc assuming all nearby stars have the same parallaxes as the target star. Furthermore, we require that the candidate comoving companion meet all criteria in Sec. 3.2.2, except that we do not apply criteria on Gaia DR2 parameters `phot_rp_mean_flux_over_error`, `phot_bp_mean_flux_over_error`, `phot_bp_rp_excess_factor`, BP–RP, and ΔG since these criteria may exclude faint companions (like M dwarfs) and we are interested in identifying comoving companions of all stellar types.

For the nearby stars selected following this procedure, we then compute the projected relative velocity between two stars using their proper motion
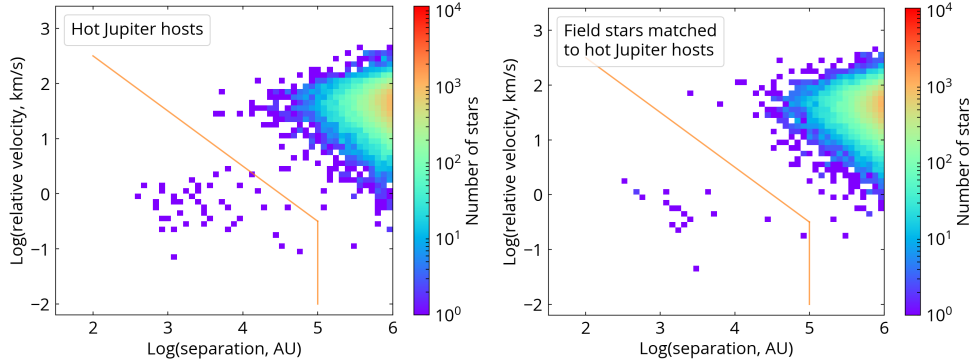
Figure 3.1: Search of comoving companions around hot jupiter hosts (left) and their matched field stars (right). The x-axis is the physical separations projected on the sky assuming the mean of the two parallaxes, and the y-axis is the projected relative velocity. The upper-right distribution corresponds to the physically unrelated nearby stars, while the lower-left is the comoving companions. The solid line is the empirical demarcation line to isolate the comoving companions. Although 4 matched field stars are used for each hot jupiter host, here we only show the same number of field stars and hot jupiter hosts for better comparison.

difference and their mean parallax. The projected physical separations are recomputed but now using the mean parallax of two stars. We use projected physical separations instead of 3-D physical separations because the 3-D physical separations are dominated by the parallax uncertainty.

We remove targets (hot jupiter hosts, contact binaries, and their matched field stars) that are in clusters or comoving groups, because they may contaminate the comoving companion search. Specifically, we remove target stars that have ≥ 100 nearby stars within the separations of 10^{5-6} AU and relative velocities of $< 10\,\mathrm{km\,s^{-1}}$. This only removes $\lesssim 1\%$ of the samples and therefore does not affect the main results.
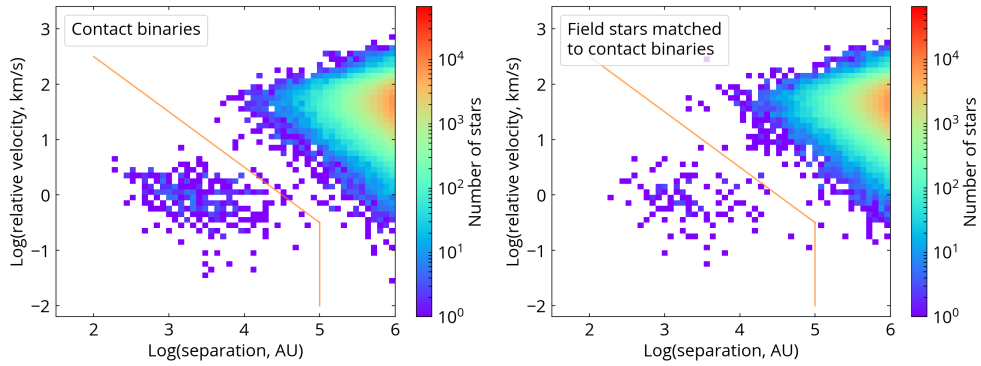
Figure 3.2: Similar to Fig. 3.1, but here for main-sequence contact binaries (left) and their matched field stars (right). Every contact binary has one matched field star.
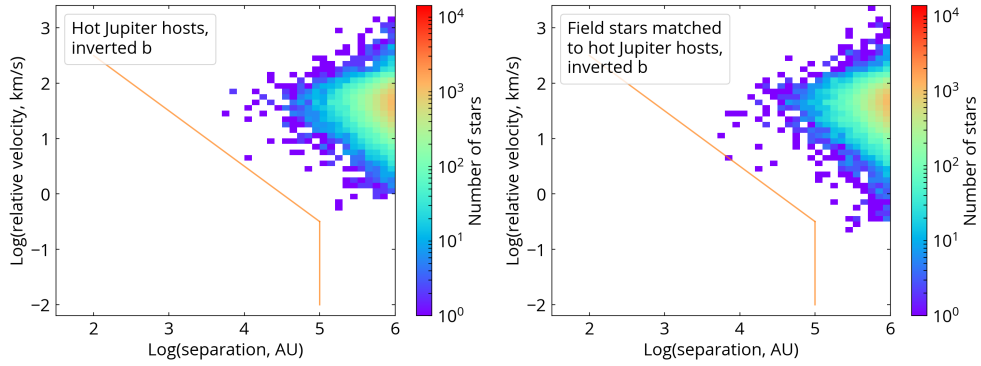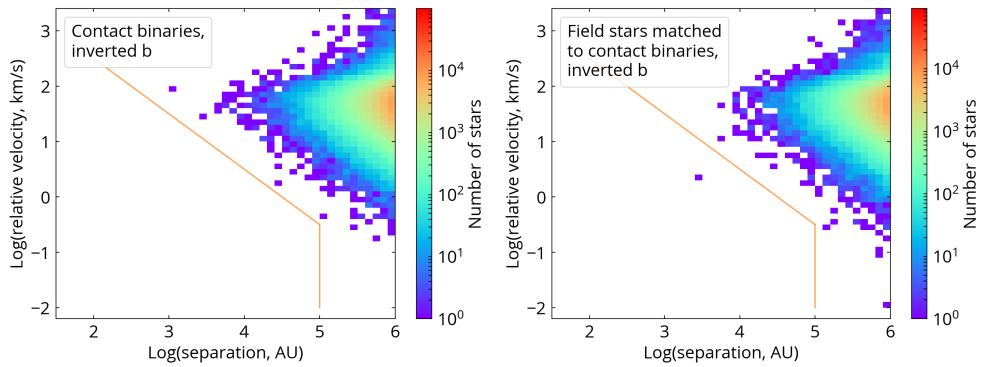

**Figure 3.3:** Contamination tests for hot jupiter hosts (left) and their matched field stars (right) by inverting their Galactic latitudes. The axes are the same as Fig. 3.2. Although 4 matched field stars are used for each hot jupiter host, here we only show the same number of field stars and hot jupiter hosts for better comparison.

Figure 3.4: Contamination tests for main-sequence contact binaries (left) and their matched field stars (right) by inverting their Galactic latitudes.
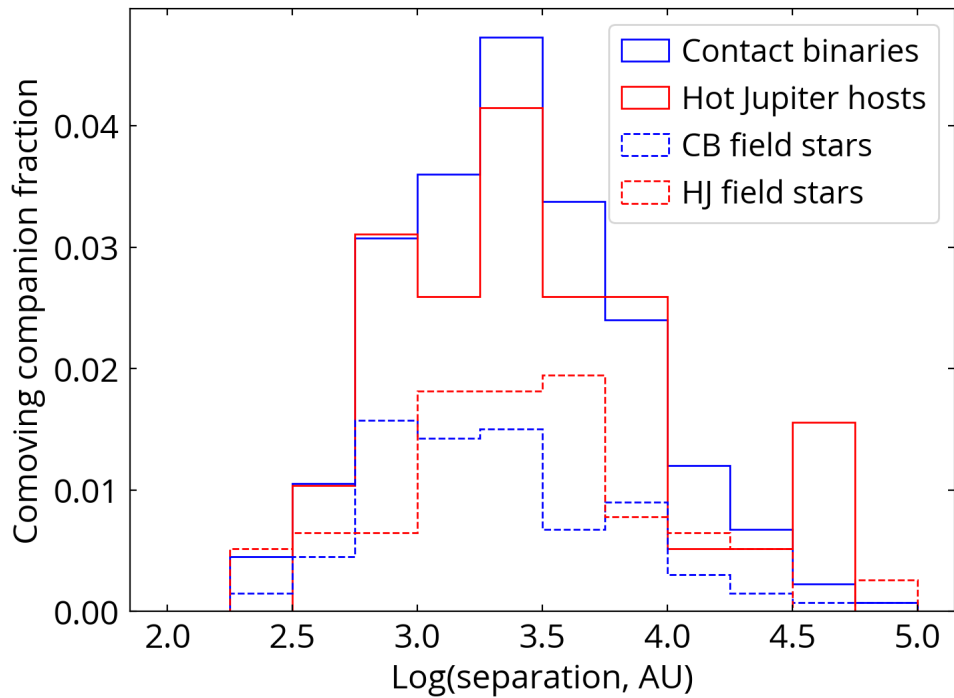
Figure 3.5: The distributions of projected separations for the comoving companions around hot jupiter hosts, main-sequence contact binaries, and their matched field stars. For separations $< 10^3$ AU, the sample starts to suffer from incompleteness due to Gaia photometry. The separations of $10^3 - 10^4$ AU is secure for the investigation of wide comoving companions.

3.2.5   Selection of very wide comoving companions

Fig. 3.1 and Fig. 3.2 show the distributions of relative velocity versus projected physical separation of nearby sources for hot jupiter hosts and contact binaries, respectively. In these plots, the over-density at the upper-right corner is the chance projection stars, and the over-density at the lower-left corner is the comoving companions of the target stars. The triangular shape of the chance projections is because in the log-log space of relative velocity and physical separation, the number of chance projections increases as a power of 2 with respect to separation. The number of chance projections increases as a power of 2 with respect to the velocity in the low velocity limit of the Maxwellian-like velocity distribution (the velocity difference in Fig. 3.1 and Fig. 3.2 contains two dimensions of velocity). At the high velocity limit of the Maxwellian-like distribution, the number of chance projections decreases exponentially. Therefore, the constant number of chance projection follows a slope of −1 at low velocities.

The orange solid line in Fig. 3.1 and Fig. 3.2 is an empirical demarcation line that isolates the comoving companions from the chance projection stars. Specifically, this demarcation line has a relative velocity of $10^{1.5}\,\mathrm{km\,s^{-1}}$ at a projected separation of $10^3\,\mathrm{AU}$ and a slope of −1 in the log-log space, and removes objects beyond $10^5\,\mathrm{AU}$. The slope of the demarcation line ensures that it is parallel to the chance projection stars so that the contamination level is not a strong function of the separation.

Given the Gaia DR2 sensitivity down to ∼ 20 mag in G-band, our search for comoving companions is complete down to an absolute G-band magnitude

of 12 mag within 400 pc. When selecting comoving companions, we adopt a conservative cut that the comoving companions have G-band absolute magnitudes brighter than 11.5 mag. Therefore, we should detect most of the stellar objects, except for late M dwarfs and old white dwarfs. Since the hot jupiter hosts in wide binaries and wide solar-type binaries have statistically consistent stellar mass-ratio distributions (Moe and Kratter, 2019), the incompleteness at the faintest end does not affect our result.

In Fig. 3.3 and Fig. 3.4, we test the level of contamination from the random background stars by flipping the sign of the Galactic latitudes of the targets (Shaya and Olling, 2011; Jiménez-Esteban, Solano, and Rodrigo, 2019). In addition, we flip the sign of the proper motion in the direction of galactic latitudes after removing the solar motion and the differential rotation from the Galactic disk. The tests show that 0, 1, 0, 1 chance projection stars fall into our selection (below the orange demarcation line and a separation between $10^3 - 10^4$ AU) for hot jupiter hosts, the field stars matched for hot jupiter hosts, contact binaries, and the field stars matched for the contact binaries, respectively. The contamination from the chance projection stars is mainly due to the targets at low Galactic latitudes. This level of contamination does not significantly affect our main results.

Fig. 3.5 shows the separation distribution of the comoving companions selected using the demarcation line. The comoving companion fraction on the vertical axis is computed from the number of comoving companions in each separation bin divided by the total number of the sample. We remove targets (field stars) and their corresponding field stars (targets) if more than

one comoving companions are found. Specifically, none of hot jupiter hosts and the field star samples has 2 resolved comoving stars. In contrast, a significantly higher fraction (7/1333) of contact binaries have 2 comoving stars, providing further constraints on the formation of contact binaries and their wide companions (Hwang et al. in preparation). Overall, multiple comoving systems are rare so removing them does not affect the results.

We find one known dual hot jupiter host, WASP-94 A and B (Neveu-Vanmalle et al., 2014; Teske, Khanal, and Ramírez, 2016), and one known dual contact binary, BV Dra and BW Dra (Batten and Hardie, 1965), and one newly discovered dual binary. In our procedure, we count the separations of these dual systems twice, but it does not change the main result if we exclude them or count their separations once.

We provide two machine-readable tables, one for the hot jupiter hosts and the other one for the contact binaries, with their corresponding wide companions that are used in Fig. 3.5. The tables contain (1) the Gaia DR2 `source_id` of hot jupiter hosts and contact binaries; (2) the Gaia DR2 `source_id` of their companions; (3) their physical separations in AU. Dual systems appear two times in the table.

Since we require reliable BP−RP colors for the targets (not for the companions), our spatial resolution is limited by Gaia's BP- and RP-band photometry because Gaia DR2 uses a window of $3.5 \times 2.1\,\mathrm{arcsec}^2$ to measure the total flux in BP- and RP-bands, i.e. applies no deblending. For pairs with separations $\lesssim 2\,\mathrm{arcsec}$, their BP and RP fluxes may be affected by the companion and may be excluded by the `phot_bp_rp_excess_factor` criteria. Therefore, our

Table 3.1: Very wide companion fraction ($10^3 - 10^4$ AU) for hot jupiter hosts and contact binaries.

	Hot jupiter hosts	Contact binaries
Very wide companion fraction ($10^3 - 10^4$ AU)	11.9±2.5% (23/193)	14.1±1.0% (188/1333)
Field star values	6.3±0.9% (49/772)	4.5±0.6% (60/1333)
Enhancement compared to the field values	1.9±0.5	3.1±0.5
Enhancement expected from the lack of close companions	1.4 ± 0.3	1.0

secure spatial resolution is 2 arcsec, and because we limit our sample to be within 400 pc, we are able to probe the very wide comoving companions with separations > 800 AU.

The contact binary sample and two field star samples all show a steady decline of the companion fractions toward larger separations, but the hot jupiter sample has an enhanced comoving companion fraction at $\sim 10^{4.5}$ AU. While it may be due to the contamination from chance projection, the contamination test (Fig. 3.3) shows that < 1 contamination is expected at this separation. However, there are only three sources in the bin at $\sim 10^{4.5}$ AU, and therefore it suffers from small-number statistics and its significance requires a larger sample to confirm.

We conclude that separations of $10^3 - 10^4$ AU is the secure separation range to investigate in Gaia DR2, and we define the very wide companion fraction as the fraction of a sample that have comoving companions at separations of $10^3 - 10^4$ AU. In the next section, we investigate the very wide comoving fraction in hot jupiter hosts and contact binaries.

3.3 Results

In this section, we start with the presentation of the observed very wide companion fractions in Sec. 3.3.1. We then compute how the lack of close companions may affect the very wide companion fractions in Sec. 3.3.2. We compare the observed quantities with the enhancement due to the lack of close companions in Sec. 3.3.3.

3.3.1 Observed very wide companion fractions

Table 3.1 presents the very wide comoving companion fractions for hot jupiter hosts, contact binaries, and their matched field stars. Specifically, 11.9±2.5% (23/193) of hot jupiter hosts and 6.3±0.9% (49/772) of their matched field stars have companions at separations of $10^3 - 10^4$ AU. For main-sequence contact binaries and their matched field stars, 14.1±1.0% (188/1333) and 4.5±0.6% (60/1333) have very wide comoving companions. The ratios of the observed comoving fraction to the field value is 1.9±0.5 and 3.1±0.5 for the hot jupiter hosts and main-sequence contact binaries, respectively.

3.3.2 Expected enhancement of very wide companion fraction due to the lack of close companions

Moe and Kratter, 2019 point out that the seemingly enhanced wide companion fraction of hot jupiter hosts compared to the field stars may be the consequence of the lack of close companions (< 50 AU) to the hot jupiter hosts. As an extreme example, if all the stars were in stellar binary systems with a wide range of separations and hot jupiters could not form in binaries with separations

< 1000 AU, then we would find that all hot jupiter hosts have wide stellar companions at separations > 1000 AU, i.e. an enhanced very wide companion fraction compared to the field stars. Therefore, an ideal comparison sample of the field stars for the hot jupiter hosts would be those field stars that do not have close companions within ∼ 50 AU. Unfortunately, it is not possible to select such a sample at the present time: such stellar pairs are too close to be spatially resolved, photometric selection on the color-magnitude diagram is rarely precise enough to distinguish a single from a binary with a high mass ratio, and the use of high-precision radial velocity surveys strongly reduce the sample size. Therefore, there is no way to evaluate the fraction that have a companion within ∼ 50 AU in our field star samples.

As we are unable to find comparison objects without close companions, we test the hypothesis that the hot jupiter hosts are a random sampling of the field stars except that hot jupiter hosts avoid systems with close companions. If there were no triple systems, this statement is equivalent to having the same the companion separation distribution for hot jupiter hosts and for the field stars at separations $\gtrsim$ 50 AU. If there are triples, the companion separation distributions of hot jupiter hosts and field stars are not the same, because avoiding systems with close separations also affects the companions at large separations.

Under such hypothesis, we compute the expected enhancement of companion fraction at separations between s_0 and s_1 due to the lack of close

companions, denoted as $\mathcal{E}^{\text{HJ}}(s_0,\ s_1)$:

$$\mathcal{E}^{\text{HJ}}(s_0,\ s_1) =$$

$$\frac{F^{\text{HJ}}(s_0,\ s_1)}{F^{\text{field}}(s_0,\ s_1)} = \frac{B^{\text{HJ}}(s_0,\ s_1) + T^{\text{HJ}}(s_0,\ s_1)}{B^{\text{field}}(s_0,\ s_1) + T^{\text{field}}(s_0,\ s_1)}, \tag{3.1}$$

where $F^{\text{HJ}}(s_0,\ s_1)$ is the companion fraction of hot jupiter hosts at separations between s_0 and s_1; $B^{\text{HJ}}(s_0,\ s_1)$ is the fraction of hot jupiter hosts that are in binary systems with separations between s_0 and s_1; and $T^{\text{HJ}}(s_0,\ s_1)$ is the companion fraction with separations between s_0 and s_1 contributed by triple systems. For field stars, similar definitions are used for $F^{\text{field}}(s_0,\ s_1)$, $B^{\text{field}}(s_0,\ s_1)$, and $T^{\text{field}}(s_0,\ s_1)$.

We first calculate the expected enhancement of companion fraction ($\mathcal{E}^{\text{HJ}}_{\text{no triple}}$) in the case with no triples, i.e. $T^{\text{HJ}} = T^{\text{field}} = 0$. We use *close* to denote the separations smaller than 50 AU, *wide* to denote the separations between 50 and 2000 AU, and *very wide* to denote the separations between 10^3 and 10^4 AU. From Equation 3.1, we have $\mathcal{E}^{\text{HJ}}_{\text{no triple}}(wide) = B^{\text{HJ}}(wide)/B^{\text{field}}(wide)$. We further define a function $\mathcal{S}^{\text{HJ}}(s_0, s_1) \equiv B^{\text{HJ}}(s_0, s_1)/(1 - B^{\text{HJ}}(close))$ and similarly for $\mathcal{S}^{\text{field}}(s_0, s_1)$. Then under the hypothesis that the shapes of the companion separation distributions of hot jupiter hosts and field stars are the same beyond 50 AU, we have $\mathcal{S}^{\text{HJ}}(wide) = \mathcal{S}^{\text{field}}(wide)$. Therefore, $\mathcal{E}^{\text{HJ}}_{\text{no triple}}(wide) = B^{\text{HJ}}(wide)/B^{\text{field}}(wide) = [\mathcal{S}^{\text{HJ}}(wide)(1 - B^{\text{HJ}}(close))]/[\mathcal{S}^{\text{field}}(wide)(1 - B^{\text{field}}(close))] = (1 - B^{\text{HJ}}(close))/(1 - B^{\text{field}}(close))$. With $F^{\text{HJ}}(close) = B^{\text{HJ}}(close) = 0.04$ (Ngo et al., 2016) and $F^{\text{field}}(close) = B^{\text{field}}(close) = 0.40$ (Moe and Kratter, 2019), the expected enhancement for very wide companion fractions is $\mathcal{E}^{\text{HJ}}_{\text{no triple}}(wide) =$

$(1 - 0.04)/(1 - 0.40) = 1.6$. Thus in the case of no triples, there is an apparent enhancement of companion fraction which is independent of the chosen separation range once it is $> 50\,\mathrm{AU}$, and therefore $\mathcal{E}_{\mathrm{no\ triple}}^{\mathrm{HJ}}(\mathrm{wide}) = \mathcal{E}_{\mathrm{no\ triple}}^{\mathrm{HJ}}(\mathrm{very\ wide})$. This is an example that the (very) wide companion fraction of hot jupiter hosts may be enhanced compared to that of the field star sample due to the lack of close companions in hot jupiter hosts which are common in the comparison sample of field stars.

The contribution of companion fraction from triples can be written as

$$T^{\mathrm{HJ}}(s_0,\ s_1) =$$

$$T_{\mathrm{in},0}^{\mathrm{HJ}}(s_0,\ s_1) + T_{\mathrm{in},1}^{\mathrm{HJ}}(s_0,\ s_1) + T_{\mathrm{out},1}^{\mathrm{HJ}}(s_0,\ s_1), \tag{3.2}$$

where $T_{\mathrm{in},0}^{\mathrm{HJ}}(s_0,\ s_1)$ is the fraction of hot jupiter hosts that are in the inner binary of triples with inner separations between s_0 and s_1; $T_{\mathrm{in},1}^{\mathrm{HJ}}(s_0,\ s_1)$ is the fraction of hot jupiter hosts that are in the inner binary of triples with outer separations between s_0 and s_1; and $T_{\mathrm{out},1}^{\mathrm{HJ}}(s_0,\ s_1)$ is the fraction of hot jupiter hosts that are in the outer tertiary of triples with outer separations between s_0 and s_1. Similar definitions apply to $T_{\mathrm{in},0}^{\mathrm{field}}(s_0,\ s_1)$, $T_{\mathrm{in},1}^{\mathrm{field}}(s_0,\ s_1)$, and $T_{\mathrm{out},1}^{\mathrm{field}}(s_0,\ s_1)$ for field stars.

Triples tend to make the enhancement of companion fraction ($\mathcal{E}$) smaller than the case without triples. For example, if there is a triple with inner separation $< 50\,\mathrm{AU}$ and an outer separation of $5000\,\mathrm{AU}$, then this system would contribute a very wide companion to field stars through $T_{\mathrm{in},1}^{\mathrm{field}}(very\ wide)$, but not to hot jupiter hosts through $T_{\mathrm{in},1}^{\mathrm{HJ}}(very\ wide)$ because its small inner separation prevents the formation of a hot jupiter. An accurate estimate of $T^{\mathrm{HJ}}(s_0,\ s_1)$

is challenging because it requires a good understanding of the distributions of inner and outer separations and their correlation.

By taking the contribution of triples into account, Moe and Kratter, 2019 estimate the expected enhancement of companion fraction due to the lack of close companions to be $\mathcal{E}^{HJ}(\text{wide}) = 1.32 \pm 0.25 \ (0.37 \pm 0.07/0.28 \pm 0.05)$ for wide binaries. For very wide companions investigated in this paper, $\mathcal{E}^{HJ}(\text{very wide})$ may not be exactly the same as $\mathcal{E}^{HJ}(\text{wide})$, depending on difference of the triple contribution in these two separation ranges. However, with current limited understanding of the correlation between inner and outer separations, we estimate that $\mathcal{E}^{HJ}(\text{very wide}) \sim \mathcal{E}^{HJ}(\text{wide})$ to leading order.

The unresolved inner binaries of triples may also enhance the (very) wide companion fractions. Unresolved binaries have two times higher probability of having a hot jupiter than single stars, simply because there are two stars in an unresolved binary. If there exists a significant number of triples with unresolved inner separations ($\lesssim 1000\,\text{AU}$ in our case) and resolved outer separations ($> 1000\,\text{AU}$ in our case), then hot jupiter hosts may have an enhanced wide companion fraction because they are more likely to be found in the inner binaries of triples. With some realistic binary fraction and triple fraction, we estimate that this effect would result in an enhancement of companion fraction of $10 - 20\%$, and may be smaller if hot jupiter hosts tend to have fewer close companions. Combined with the effect of the lack of close companions, the expected enhancement of very wide companion fraction is $\mathcal{E}^{HJ}(\text{very wide}) = 1.4 \pm 0.3$ for hot jupiter hosts, and we tabulate this number in the bottom row of Table 3.1.

Unlike hot jupiter hosts where a lack of close companions is observed within ~50 AU, close binaries only show a lack of companions within ~ 1 AU (Tokovinin et al., 2006; Gies et al., 2012; Tokovinin, 2014b). Therefore, while the lack of close companions enhances the wide companion fraction for hot jupiter hosts, such effect is negligible for contact binaries (Moe and Kratter, 2019), and we tabulate $\mathcal{E}^{\mathrm{CB}}(\text{very wide}) = 1.0$ in the bottom row of Table 3.1 for the contact binaries.

3.3.3 A weak or no enhancement for hot jupiters, and a significant enhancement for contact binaries

Compared to $\mathcal{E}^{\mathrm{HJ}}(very\ wide) = 1.4 \pm 0.3$, our measured enhancement factor of 1.9 ± 0.5 for hot jupiter hosts suggests that there is no or a weak enhancement at $\sim 1\sigma$ significance. Therefore, the enhanced very wide companion fraction from hot jupiter hosts is consistent, within $\sim 1\sigma$, with the fact that they lack close companions. Confirming the weak enhancement requires a larger hot jupiter host sample in the future.

Compared to $\mathcal{E}^{\mathrm{CB}}(very\ wide) = 1.0$, our measured enhancement factor of 3.1 ± 0.5 for main-sequence contact binaries shows that there is a significant enhancement at a 4σ significance. This enhancement cannot be explained by the lack of close companions, and therefore some other physical mechanisms are needed to explain the connection between contact binaries and their very wide companions.

3.4 Discussion

3.4.1 Very wide companions play a minor role in the orbital migration

Close binary fraction increases with decreasing metallicity, but (very) wide binary fraction with separations $\gtrsim 200\,\mathrm{AU}$ is weakly dependent on the metallicity (Moe, Kratter, and Badenes, 2019; El-Badry and Rix, 2019). Therefore, the enhanced very wide companion fraction around contact binaries is not due to their metallicity.

The very wide companions investigated in this paper are not able to induce significant orbital migration in the proto-contact binaries and proto-hot jupiter systems through the classical Kozai-Lidov mechanism. For a companions at a separation of $10^3\,\mathrm{AU}$, it can induce the Kozai-Lidov oscillation only when the inner binaries have a separation $\gtrsim 5\,\mathrm{AU}$, which is set by the requirement that the oscillation timescale needs to be shorter than the timescale of the relativistic pericenter precession (Fabrycky and Tremaine, 2007). Therefore, these very wide companions are not able to bring the inner proto-hot jupiter system and proto-contact binaries to their current separations ($< 0.1\,\mathrm{AU}$).

When the outer orbit is eccentric, it can trigger a higher-order octuple effect, called the eccentric Kozai-Lidov effect (Naoz et al., 2013b; Naoz, 2016). The eccentric Kozai-Lidov effect typically enhances the efficiency of forming hot jupiters (Naoz, Farr, and Rasio, 2012) and close binaries (Naoz and Fabrycky, 2014). Although the octuple timescale is not well quantified due to the chaotic nature of the eccentric Kozai-Lidov effect, it is typically longer than the classical Kozai-Lidov effect (Naoz, 2016). Therefore, the very wide

companions are not able to contribute much to the orbital migration through the eccentric Kozai-Lidov effect either.

Another possibility is that the very wide companions were initially located at a smaller separation where they can induce strong Kozai-Lidov oscillations, and they migrated outward at a later time. This scenario is also suggested by El-Badry et al., 2019 where they find an excess of equal-mass stellar binaries out to separations of $\sim 10^3$ AU. Because equal-mass binaries are mainly formed from disk fragmentation at close separations ($\lesssim 100\,$AU), they argue that the observed equal-mass wide binaries are formed with close separations and further widened by dynamical interactions in their birth environments. However, such excess of equal-mass binaries at $\sim 10^3$ AU is only $\sim 5\%$ in the field. It is not yet clear if this outward migration is a dominant path for the very wide companions around contact binaries. Further investigation on the mass ratios between the contact binaries and their very wide companions may be able to constrain this scenario.

If the Kozai-Lidov mechanism is a dominant formation channel for contact binaries, we would expect them to have companions with smaller separations to trigger the Kozai-Lidov oscillations. Then following the same argument as Section 3.3.2, we would expect a lower very wide companion fraction for contact binaries because of their enhanced close companion fraction. Instead, our result shows that contact binaries have an enhanced very wide companion fraction, suggesting that either the Kozai-Lidov mechanism is not a dominant formation channel for contact binaries, or there is another mechanism producing a significant number of very wide companions around contact binaries

that compensate for the effect of the enhanced close companion fraction.

To sum up, these very wide companions play a minor role in the orbital migration of the inner systems unless they have undergone a significant outward orbital migration. Therefore, the very wide companions are more likely to be indicative of their formation environment.

3.4.2 Formation environment of very wide companions, hot jupiter hosts, and contact binaries

Because the binding energy of very wide binaries is small, they are sensitive to the environment of their birth place. Several mechanisms have been proposed for the formation of wide binaries. Turbulent core fragmentation may be able to form binaries with separations from a few hundred to a few thousand AU (Offner et al., 2010; Lee et al., 2017). Binaries with separations of 10^3-10^5 AU can form through the dissolution of star clusters (Kouwenhoven et al., 2010; Moeckel and Clarke, 2011), the disintegration of unstable compact triples (Reipurth and Mikkola, 2012), and pairing of adjacent pre-stellar cores (Tokovinin, 2017). In terms of timescales, turbulent core fragmentation and the paring of adjacent cores take place at an age of $\lesssim 1\,\mathrm{Myr}$ during the pre-stellar phase. It takes a longer time (from 10 to a few hundred Myr) for a cluster to dissolve and for a compact triple to unfold.

Wide binaries may be disrupted over time through the gravitational interaction with closely passing stars, molecular clouds, invisible objects, and the Galactic tides (Heggie, 1975; Bahcall, Hut, and Tremaine, 1985; Weinberg, Shapiro, and Wasserman, 1987; Chaname and Gould, 2004; Jiang and

Tremaine, 2010). Such disruption takes place on timescales of several Gyr, and most binaries with separations $< 10^4$ AU are not disrupted within the age of the Milky Way (Weinberg, Shapiro, and Wasserman, 1987; Andrews et al., 2012). Even if the wide binaries are disrupted, two stars can still stay in an unbound comoving pair at separations of $\sim 100\,\text{pc}$ for several Gyr because of the small relative velocity (Jiang and Tremaine, 2010; Oh et al., 2017). Therefore, most of the very wide companions investigated here are stable over the age of the Milky Way and the disruption events play a relatively minor role.

The enhanced very wide companion fraction around contact binaries suggests that (proto-)contact binaries are more likely to form in the environments that produce wide systems. For the scenario where wide companions are formed from the dissolution of star clusters, it means that the formation of contact binaries is sensitive to the cluster properties (Kouwenhoven et al., 2010). If wide companions are formed from the disintegration of compact triples, then it implies that (proto-)contact binaries may be the product of such formation. If the very wide companions are formed from the enhanced turbulent core fragmentation due to certain environmental properties (which may also tend to produce compact multiples), then it suggests contact binaries are also more likely to form in such environment.

In contrast, the weak or no enhancement of very wide companion fraction around hot jupiter hosts suggests that hot jupiter formation has different dependence on the formation environment as the contact binaries. Moe and Kratter, 2019 use the different wide companion enhancements between hot jupiter hosts and close binaries to support the idea that hot jupiters are formed

from core accretion and (sub-)stellar objects are formed from gravitational instability, coinciding with the mass gap of 4-9 M_J found by Schlaufman, 2018. The very wide companions investigated here are more sensitive to the birth environment, and the weak or no enhancement of very wide companion fraction around hot jupiter hosts indicates that hot jupiter host formation may be insensitive to larger-scale properties of the birth environment, including the cluster properties and the efficiency of turbulent core fragmentation.

3.4.3 The frequency of dual hot jupiter hosts and double contact binaries

The probability of finding a hot jupiter host (contact binary) in the companion of a hot jupiter host (contact binary) seems to be higher than the occurrence rate of hot jupiters (contact binaries) in the field. Although the sample is small, we find one dual hot jupiter host (two hot jupiter hosts) among 22 hot jupiter hosts that have very wide companions. This ~ 9% of hot jupiter occurrence rate (we double count the dual hot jupiter host because that preserves correct statistical properties for inference) in the comoving companions of hot jupiter hosts is much higher than the 0.5 – 1% occurrence rate in the field (Mayor et al., 2011; Wright et al., 2012; Fressin et al., 2013; Santerne et al., 2016; Zhou et al., 2019). Similarly, we find 2 double contact binaries out of 188 contact binaries that have very wide companions. This ~ 2% occurrence in the very wide companions is also significantly higher than the 0.1% occurrence in the field using the same selection method (Hwang and Zakamska, 2020). Our results hint that the occurrence rate of hot jupiters and contact binaries in the comoving companions may be about one order-of-magnitude higher than that

in the field. In other words, the occurrence rates of dual systems are higher than the expected values from random pairing of field stars. However, the current sample size of dual systems is still very small so future larger samples are needed to further confirm these results.

Tokovinin, 2014b also finds an enhanced occurrence rate of 2+2 systems (quadruples consisting of two close stellar binaries) and suggests that these systems were formed by some special process. The disintegration of dynamically unstable compact multiples (Reipurth and Mikkola, 2012) may also help the formation of double contact binaries, but not for dual hot jupiter hosts. Here we propose another scenario where the enhanced occurrence rate of dual systems is due to the co-chemical (components have similar metallicities) and the co-eval (components have similar ages) nature of the components of wide binaries. Andrews, Chanamé, and Agüeros, 2018 show that the components of wide binaries with separations $< 4 \times 10^4$ AU have similar metallicities and elemental abundances within measurement uncertainties (see Kamdar et al. 2019 for larger separations). Therefore, if we find a wide companion around a hot jupiter host, then because hot jupiter hosts tend to have higher metallicities (Gonzalez, 1997; Santos, Israelian, and Mayor, 2004; Fischer and Valenti, 2005) and the components of wide binaries have similar metallicities (Andrews, Chanamé, and Agüeros, 2018), we would expect that the wide companion of a hot jupiter host also has a higher metallicity and therefore a higher chance of hosting a hot jupiter, resulting in an enhanced occurrence rate of dual hot jupiter hosts. The close binary fraction is dependent on the metallicity (Moe, Kratter, and Badenes, 2019), and the contact binary fraction is also a function

of the stellar age due to their orbital migration and merger (Hwang and Za-kamska, 2020), and therefore such metallicity and age dependence of contact binaries can also result in the higher occurrence rate of dual contact binaries.

3.5 Conclusions

In this paper we investigate the very wide comoving fractions with separations of $10^3 - 10^4$ AU around hot jupiter hosts and main-sequence contact binaries using Gaia DR2. We further compute the enhancement of very wide companion fractions by comparing with their matched field star samples. We present the following findings:

1. $11.9 \pm 2.5\%$ of hot jupiter hosts and $14.1 \pm 1.0\%$ of contact binaries have companions at separations of $10^3 - 10^4$ AU. Compared to the matched field star samples, the very wide companion fractions are enhanced by a factor of 1.9 ± 0.5 and 3.1 ± 0.5 for hot jupiter hosts and contact binaries, respectively (Table 3.1).

2. The measured fraction of very wide companions for hot jupiter hosts is consistent, within $\sim 1\sigma$, with that for matched field stars once we take into account the observational bias in the comparison sample introduced by the lack of close companions to hot jupiter hosts. In contrast, the strong enhancement of very wide companions around contact binaries is highly statistically significant, and there must be a physical mechanism connecting the inner short-period binary with its very wide companion.

3. We argue that the very wide companions are indicative of the formation

environments. The enhanced very wide companion fraction around contact binaries suggests that contact binary formation is sensitive to their formation environment, e.g. the star cluster properties, the efficiency of fragmentation, and/or compact multiples. The weak or no enhancement of very wide companion fraction around hot jupiters implies that the formation of hot jupiters is more tied to their host-star properties instead of large-scale formation environments.

4. The probability of finding a hot jupiter host (contact binary) in the companion of a hot jupiter host (contact binary) seems to be about an order of magnitude larger than the occurrence rate of hot jupiters (contact binaries) in the field, which may be due to the underlying metallicity and age dependence of hot jupiters and contact binaries. Larger samples are needed to better quantify such occurrence rates.

Chapter 4

The non-monotonic, strong metallicity dependence of the wide-binary fraction

The metallicity dependence of the wide-binary fraction in stellar populations plays a critical role in resolving the open question of wide binary formation. In this paper, we investigate the metallicity ([Fe/H]) and age dependence of the wide-binary fraction (binary separations between 10^3 and 10^4 AU) for field F and G dwarfs within 500 pc by combining their metallicity and radial velocity measurements from LAMOST DR5 with the astrometric information from Gaia DR2. We show that the wide-binary fraction strongly depends on the metallicity: as metallicity increases, the wide-binary fraction first increases, peaks at [Fe/H]$\simeq 0$, and then decreases at the high metallicity end. The wide-binary fraction at [Fe/H]$= 0$ is about two times larger than that at [Fe/H]$= -1$ and [Fe/H]$= +0.5$. This metallicity dependence is dominated by the thin-disk stars. Using stellar kinematics as a proxy of stellar age, we show that younger stars have a higher wide-binary fraction at fixed metallicity

97

close to solar. We propose that multiple formation channels are responsible for the metallicity and age dependence. In particular, the positive metallicity correlation at [Fe/H]< 0 and the age dependence may be due to the denser formation environments and higher-mass clusters at earlier times. The negative metallicity correlation at [Fe/H]> 0 can be inherited from the similar metallicity dependence of close binaries, and radial migration may play a role in enhancing the wide-binary fraction around the solar metallicity.

4.1   Introduction

Wide binaries are weakly bound, as such they are sensitive to the gravitational perturbations in the Milky Way and have been used to investigate the visible and invisible Galactic structures (Heggie, 1975; Bahcall and Soneira, 1981; Bahcall, Hut, and Tremaine, 1985; Weinberg, Shapiro, and Wasserman, 1987; Chaname and Gould, 2004; Yoo, Chaname, and Gould, 2004; Quinn et al., 2009; Jiang and Tremaine, 2010). Wide binaries may also be able to probe the dark matter substructure in dwarf galaxies (Peñarrubia et al., 2016). Furthermore, a significant fraction of stars are in binaries and multiple systems (Abt and Levy, 1976; Duquennoy and Mayor, 1991; Fischer and Marcy, 1992; Duchêne and Kraus, 2013), and about half of wide binaries (separations $a > 1000\,\text{AU}$) are the outer binaries of high-order hierarchical systems (Raghavan et al., 2010; Tokovinin, 2014a; Tokovinin, 2014b; Moe and Di Stefano, 2017), so understanding the formation of wide binaries is crucial for the formation of hierarchical systems and the implications for both large-scale and small-scale Galactic structures.

The formation of wide binaries is still not well understood. They are unlikely to form by capture of random field stars, due to the low stellar density in the field (e.g. Goodman and Hut 1993). This is further supported by the similarity of the chemical compositions of the wide binary components with separations $\lesssim 1$ pc$\sim 2 \times 10^5$ AU (Andrews, Chanamé, and Agüeros, 2018; Andrews et al., 2019; Hawkins et al., 2020), indicating that the components of wide binaries are born together, and several mechanisms have been proposed for their formation. For example, turbulent core fragmentation can form binaries with separations from ~ 100 AU to ~ 1000 AU (Padoan and Nordlund, 2002; Fisher, 2004; Offner et al., 2010). Binaries with separations of $10^3 - 10^5$ AU can be formed through the dynamical unfolding of compact triples (Reipurth and Mikkola, 2012), the dissolution of star clusters (Kouwenhoven et al., 2010; Moeckel and Clarke, 2011), or by the random pairing of adjacent pre-stellar cores (Tokovinin, 2017).

Many observational efforts have been directed at constraining the formation of wide binaries. Several young (< a few Myr) wide binaries have been found (e.g. Kraus et al. 2011; Pineda et al. 2015; Tobin et al. 2016b; Lee et al. 2017), supporting the proposal that wide binaries can be formed during the pre-main sequence phase, through turbulent core fragmentation and/or the pairing of pre-stellar cores. However, it is known that the wide-binary fraction is higher in pre-main sequence stars compared to that of field stars (Ghez, Neugebauer, and Matthews, 1993; Köhler et al., 2000). Furthermore, the separation distribution of binaries in low-density star-forming regions (Simon, 1997; Kraus and Hillenbrand, 2009; Tobin et al., 2016a; Joncour, Duchêne, and

Moraux, 2017) is found to be flatter than that of main-sequence field binaries (Tokovinin and Lépine, 2012; El-Badry and Rix, 2018). It has been argued that these differences may arise from the different formation environments and/or ages in the current young star-forming regions compared to those of the field stars (Kroupa, 1995; Kraus and Hillenbrand, 2009). Therefore, it remains challenging to directly infer the formation of field wide binaries from the multiplicity in young star-forming regions alone.

Theory has suggested that wide binaries can form from the dissolution of clusters (Kouwenhoven et al., 2010; Moeckel and Clarke, 2011), which similar to the turbulent core fragmentation and the random pairing of pre-stellar cores, is also environment-dependent. In this scenario, wide binaries are formed by the pairing of initially unbound stars when the cluster rapidly expands after gas expulsion. The formation timescale of wide binaries in this case correlates with how fast the gas is dispersed, which is of the order of ~10 Myr (Lada and Lada, 2003; Bastian et al., 2005; Fall, Chandar, and Whitmore, 2005; Mengel et al., 2005). Kouwenhoven et al., 2010 show that the dissolution of lower-mass clusters results in a higher wide-binary fraction because the lower velocity dispersion increases the pairing probability in the phase space. Observational studies find a lower wide-binary fraction in open clusters than that of the low-density star-forming regions and the field (Bouvier, Rigaut, and Nadeau, 1997; Deacon and Kraus, 2020). Since the surviving open clusters are usually at the massive end of the cluster mass function, these results are most likely due to that the high-density environments reduce the wide binary formation within the clusters. Therefore, the wide-binary fraction resulting

directly from the cluster dissolution remains not well constrained.

Besides forming from the dissolution of clusters, wide binaries can also form through the dynamical unfolding of compact triples. Three stars are initially formed in a compact, unstable configuration, and the subsequent dynamical evolution can bring one component closer and push the other component further away, and if it is not ejected entirely, the object appears as a wide binary (Reipurth and Mikkola, 2012). This scenario is supported by that these wide systems are frequently members of higher-order multiples (Law et al., 2010; Allen et al., 2012; Elliott and Bayo, 2016), and that main-sequence contact binaries have a factor of 3 higher wide companion fraction at separations > 1000 AU than that of the field stars (Hwang et al., 2020b). However, the importance of the dynamical unfolding to form wide binaries is still debated. In particular, this scenario should lead to outer companions with eccentric orbits, but Tokovinin, 2020 shows that the eccentricity distribution of wide binaries is close to thermal, inconsistent with the dynamical unfolding explanation.

With the multiple interconnected formation channels, the exact explanation remains elusive despite decades of research. This situation is drastically changing with the advent of recent large spectroscopic surveys. In particular, metallicity dependence of binary fraction measured from these surveys is proving useful in disentangling binary formation. In terms of close binaries, recent studies have shown that the close-binary fraction is anti-correlated with metallicity (Grether and Lineweaver, 2007; Raghavan et al., 2010; Yuan et al., 2015; Badenes et al., 2018; Moe, Kratter, and Badenes, 2019; El-Badry

and Rix, 2019; Mazzola et al., 2020). This finding supports the scenario that close binaries are formed via disk fragmentation and the lower-metallicity disks are more prone to fragmentation (Kratter and Matzner, 2006; Tanaka and Omukai, 2014; Moe, Kratter, and Badenes, 2019; Tokovinin and Moe, 2020). Alternatively, radiation hydrodynamical simulations from Bate, 2019 suggest that the anti-correlation between close-binary fraction and metallicity could also be explained by the fact that lower metallicities facilitate all kinds of small-scale fragmentation (disk, filament, and core fragmentation), not just disk fragmentation. Regardless of their exact physical explanations, it has been proposed that such metallicity dependence of the close-binary fraction may ultimately be passed on to their final products – blue stragglers (Wyse, Moe, and Kratter, 2020).

While the studies of close binaries have reached more consensus, the metallicity dependence of the wide-binary fraction is less conclusive, with competing conclusions from various studies (Zapatero Osorio and Martin, 2004; Zinnecker, Köhler, and Jahreiß, 2004; Rastegaev et al., 2008; Jao et al., 2009; Lodieu, Osorio, and Martin, 2009; Zhang et al., 2013; Ziegler et al., 2015). In a recent study, El-Badry and Rix, 2019 investigate the binary fraction as a function of separation and metallicity. They use Gaia DR2 to establish the comoving pair sample within 200 pc (El-Badry and Rix, 2018), and combine it with wide-field spectroscopic surveys, including LAMOST, RAVE, APOGEE, GALAH, and Hypatia. They find an emergence of an anti-correlation between the binary fraction and metallicity at separations $a < 200\,\text{AU}$, while the binary fraction at $a \gtrsim 200\,\text{AU}$ remains relatively constant with respect to metallicity.

The authors conclude that a significant fraction of binaries with $a < 200\,\mathrm{AU}$ are formed by disk fragmentation while binaries with $a \gtrsim 200\,\mathrm{AU}$ may be formed from turbulent core fragmentation which has a weaker dependence on metallicity.

In this paper, we revisit the metallicity dependence of field wide binaries ($a = 10^3 - 10^4\,\mathrm{AU}$) using the LAMOST and Gaia DR2 datasets. Our sample consists of stars out to $500\,\mathrm{pc}$, important for inclusion of sufficient numbers of the thick-disk and halo stars. By doubling the sample size compared to El-Badry and Rix, 2019 and, more importantly, dissecting the kinematics of these stars as age proxy which is left unexamined in El-Badry and Rix, 2019, we are able to investigate metallicity and age effects and better constrain both the formation and evolution scenarios for wide binaries.

Through out the paper, we refer to wide binaries as those with separations between 10^3 to $10^4\,\mathrm{AU}$. While we adopt the notation 'binary' for our multiple systems, we caution that some of them might be actually unresolved higher-order multiples. The paper is organized as follows. Section 4.2 describes the LAMOST and Gaia datasets and the method of searching for comoving companions. Section 4.3 presents our main result that the wide-binary fraction is strongly dependent on the metallicity. We discuss the implications for the wide binary formation in Section 5.5 and conclude in Section 5.6.

4.2 Sample selection and method

4.2.1 LAMOST and metallicity measurements

Our sample is selected from The Large Sky Area Multi-Object Fiber Spectro-scopic Telescope (LAMOST; Deng et al. 2012; Zhao et al. 2012). In its final data release of the LAMOST Phase I (2011–2017) survey, LAMOST DR5 has released optical $(3700 - 9000\text{Å})$ low-resolution spectra $(R \sim 1800)$ for about 10 million stars, providing a rich dataset for Galactic archaeology.

We use the A/F/G/K stars catalog from LAMOST DR5 (v3). Its metallicity ([Fe/H]) is derived from the LAMOST Stellar Parameter pipeline (LASP; Wu et al. 2011b; Wu et al. 2011a) and the data-driven Payne pipeline (DD-Payne; Xiang et al. 2019). LASP fits the observed spectrum using a full spectrum fitting package ULySS (Université de Lyon Spectroscopic analysis Software; Koleva et al. 2009). Specifically, each observed spectrum is fit to a grid of model spectra based on the ELODIE library (Prugniel and Soubiran, 2001; Prugniel et al., 2007) to derive T_{eff}, $\log g$, and [Fe/H].

The Payne is designed to measure multiple elemental abundances where the model spectra are emulated with neutral networks (Ting et al., 2019). When combined with data-driven models with theoretical prior, the Payne can be applied to low-resolution spectra $(R \sim 1000)$ to derive reliable elemental abundances, a method that has been dubbed the name Data-Driven Payne, or DD-Payne (Ting et al. 2017b; Ting et al. 2017a, see also Ness et al. 2015; O'Briain et al. 2020). Based on this, Xiang et al., 2019 train the spectral model using the

LAMOST stars where the stellar labels have been derived from other high-resolution surveys like GALAH (De Silva et al., 2015) and APOGEE (Majewski et al., 2017). DD-Payne provides a final product with stellar parameters ($T_{\rm eff}$, $\log g$, V_{mic}) and 16 elemental abundances.

By comparing the metallicity measured by LASP and DD-Payne, we find that LASP metallicities are systematically higher than DD-Payne metallicities by 0.07 dex, with a standard deviation of 0.07 dex. The 0.07 dex offset between LASP and DD-Payne does not strongly correlate with metallicity. Since LASP metallicities are calibrated to the ELODIE spectral library and DD-Payne ties the metallicity to APOGEE, this systematic offset might be due to the different abundance scale used by ELODIE and APOGEE (M. Xiang, private communication). Otherwise, the small scatter of 0.07 dex shows that the metallicities of LASP and DD-Payne are in good agreement. Since we focus on the relative trend of the wide-binary fraction with respect to metallicity, the accuracy of the absolute values of metallicities is not the main concern.

4.2.2   Gaia and the comoving companion search

We use Gaia Data Release 2 (DR2) to search for the comoving companions around the LAMOST stars. Gaia DR2 provides broad-filter G-band magnitudes, blue-band BP magnitudes, red-band RP magnitudes, sky positions, parallaxes, and proper motions for 1.33 billion objects and radial velocities for 7 million stars (Gaia Collaboration et al., 2016; Gaia Collaboration et al., 2018a), resulting in an unprecedented dataset for the phase-space information of the Milky Way.

We cross-match the LAMOST catalog with Gaia DR2 using a matching radius of 2 arcsec. When an object has multiple visits by LAMOST, we only keep the one with the highest signal-to-noise ratio (SNR) in SDSS g-band. For LAMOST stars where multiple Gaia sources are matched, we keep the one with the smallest separation. If one Gaia source_id is matched to multiple LAMOST designations, which most of the time is due to the repeated LAMOST designation naming, we keep the one with the highest SNR in SDSS g-band.

The comoving companion searching method is detailed in Hwang et al., 2020b. Briefly, for each target star, we select a nearby star sample where the stars have similar parallaxes (either parallax difference < 0.2 mas, Gaia DR2's typical parallax errors, or the line-of-sight distance difference < 20 pc) as the target star. Then between the target star and each nearby star, we compute the two-dimensional relative velocity (proper motion difference divided by the mean parallax of the two stars) on the sky and the projected separation. We do not consider the component along the line of sight because that involves the parallax difference of two stars, which is dominated by the parallax measurement errors. The physical projected distance remains accurate because it does not involve the parallax difference of the two stars. In the remaining paper, the relative velocity and separation refer to the projected quantities (except for the total velocity v_{tot} explained in Sec. 4.2.6 that uses the radial velocity component). The comoving companions are well separated from the chance projection stars in the relative velocity-separation space, and we use an empirical demarcation line introduced in Hwang et al., 2020b to select comoving companions.

To exclude contamination from open clusters or comoving groups, we exclude stars that belong to aggregates with more than 50 stars within separation $10^5 - 10^6$ AU and relative velocity $< 10 \, \mathrm{km \, s^{-1}}$. This only excludes 0.4% of the targets and does not have a strong impact on our result. For the ease of interpretation and counting, we further exclude targets that have more than one comoving companion, which affects only 0.1% of the sample.

4.2.3   Selection criteria for the main sample

To ensure that the LAMOST pipeline metallicity (LASP) are reliable for our targets, we require that their spectral SNR per pixel be >50 in the SDSS g-band. For DD-Payne metallicity, we require that their spectral SNR per pixel > 50 in the SDSS g-band and the fitting quality flag `QFLAG_CHI2==good`. We limit our sample to the effective temperature between 5000 and 7000 K and surface gravity $\log g > 3.7$. For DD-Payne, we require that `TEFF_FLAG==good` and `LOGG_FLAG==good`. Based on the spectral type classified by LASP, 94% of the selected sample are F and G dwarfs.

After cross-matching with Gaia DR2, we limit our sample to parallaxes > 2 mas (distances within 500 pc). We further exclude unreliable photometric and astrometric measurements following the criteria in the Appendix B in Gaia Collaboration et al., 2018b, except that we relax the criteria on BP and RP fluxes. These criteria require that the S/N of Gaia G band larger than 50, the parallax over error > 10, the visibility periods > 8, and an astrometric quality criteria introduced in the Appendix C of Lindegren et al., 2018. We do not apply any criteria for BP and RP fluxes because BP and RP photometry has a

worse spatial resolution than G band (Evans et al., 2018), and also BP and RP have inferior sensitivity than G-band, which may affect the detection of faint companions. We use the same criteria for the nearby star sample where the comoving companion is searched.

With these selections and the removal of sources in comoving groups, we end up with 257,560 stars with LASP metallicity, and 247,669 with DD-Payne metallicity. They share 243,823 stars in common. LASP and DD-Payne are essentially the same sample of stars with two alternative [Fe/H] determinations. Tables of these wide binaries are available electronically, and their information is detailed in Appendix 4.6.2.

4.2.4   Computing the wide-binary fraction

In this study, we adopt a conservative angular resolution of 2 arcsec, corresponding to 1000 AU at 500 pc, i.e., we consider only wide binaries with separations of two stars to be at least 1000 AU. This choice is motivated by several factors. Gaia G-band uses PSF-fitting photometry, and its spatial resolution is ~ 0.5 arcsec in DR2 (Arenou et al., 2018). Furthermore, we find that the number of comoving pairs decreases at angular separations $\lesssim 1.5$ arcsec, which may be due to the worse quality of astrometric measurements in the presence of a nearby source. Also, the diameter of LAMOST fibers is 3.3 arcsec (Zhao et al., 2012). Therefore, two stars with an angular separations $\lesssim 3.3/2$ arcsec would be located in a single fiber, which may affect metallicity measurements.

We define the wide-binary fraction (WBF) to be

$$WBF = N_{\mathrm{companion}}/N_{\mathrm{LAMOST}}, \tag{4.1}$$

where N_{LAMOST} is the number of LAMOST stars, and $N_{\text{companion}}$ is the number of LAMOST stars that have one comoving companion in Gaia at 10^3 to 10^4 AU.

In most cases, LAMOST does not observe both stars due to its random subsampling. The random subsampling does not affect our definition of wide binaries since we only require one of two stars to have LAMOST observations (and both stars have Gaia phase space information). Nonetheless, the metallicity of the two stars, individually, might not be accessible. Here we assume that both stars have the same metallicity and adopt the metallicity from the stellar component with LAMOST measurements. We argue that this assumption is justified because previous studies have shown that wide binaries with separations $\lesssim 10^4$ AU have nearly identical elemental abundances (Andrews, Chanamé, and Agüeros, 2018; Andrews et al., 2019; Hawkins et al., 2020), and simulations have suggested that most pairs with separations $\lesssim 10^6$ AU and small relative velocities ($\lesssim 2\,\text{km/s}$) are conatal (Kamdar et al., 2020). Due to turbulent mixing, conatal stars from the same gas cloud are expected to be homogeneous in metallicity (Feng and Krumholz, 2014).

One possible bias is the higher detection rate of fainter companions for less distant targets. Therefore, when computing $N_{\text{companion}}$, we only consider companions that have absolute G-band magnitudes < 10, where our companion search is complete across the entire distance range of the sample. This criterion removes most of white dwarf companions, which may induce an age dependence of $N_{\text{companion}}$ if young, bright white dwarfs are detected but old, faint white dwarfs are not. This is not a strong effect because white dwarf-main sequence pairs are more than ten times less frequent than main sequence-main

sequence pairs (El-Badry and Rix, 2018). The absolute magnitude criterion also excludes faint M dwarf companions, but because the lifetime of M dwarfs is longer than the age of Universe, this does not induce age dependence.

We select a sub-sample within 100 pc to test the completeness. In this sub-sample, without the absolute magnitude constraint for the companions, the wide-binary fraction is $7.12 \pm 0.70\%$. This is consistent with Raghavan et al., 2010 where they measure that $7 \pm 1\%$ of solar-like stars within 25 pc have companions at separations between 10^3 to 10^4 AU. With an additional cut on absolute G-band magnitudes < 10 mag, the wide-binary fraction of our 100-pc sample is reduced to $3.73 \pm 0.51\%$, where 84% of the excluded companions are faint M dwarfs and 16% are white dwarfs. The wide-binary fraction (with the absolute magnitude cut on the companions) of our full 500-pc sample is 2.98 ± 0.03, in good agreement with the 100-pc sample ($1.5\,\sigma$). This illustrates that the companions with absolute G-band magnitudes < 10 mag are well detected within 500 pc. The $1.5\,\sigma$ difference may arise from the different metallicity regime probed at larger distances and the slightly reduced completeness of Gaia sources at angular separations close to 2 arcsec (Arenou et al., 2018). In the Appendix, we test with larger binary separations and show that our results are robust against the possible incompleteness at small angular separations.

Values of N_{LAMOST} and $N_{\mathrm{companion}}$ may weakly depend on the distance because of the spatial resolution. For example, in the case of triple stars, the counting of N_{LAMOST} and $N_{\mathrm{companion}}$ is different depending on whether the inner binary of a hierarchical triple is resolved or not. Specifically, if

the inner binary is unresolved, then this triple system would be considered as a binary during the counting; if the inner binary is resolved, the system would be considered as one having multiple comoving companions and hence are excluded in our counting. Nonetheless, the contribution of marginally resolved hierarchical triples (those only resolved at small distances) is expected to be small and should not affect our conclusions.

With the absolute magnitude criterion for the companions, we end up with 7,671 (7,266) comoving pairs with separations of 10^3-10^4 AU for the LASP (DD-Payne) sample. Among them, there are 330 pairs (660 LAMOST stars) where both stars in the pair were observed by LAMOST. Some of these pairs have been studied to show that the components of wide binaries have similar metallicity and elemental abundances (Andrews, Chanamé, and Agüeros, 2018; Andrews et al., 2019). Since the definition of our wide-binary fraction is essentially the probability that a randomly selected star is in a wide binary system, the proper statistics requires that we account for both LAMOST stars in N_{LAMOST} and $N_{\mathrm{companion}}$ even if they belong to the same pair. LAMOST targeting does not depend on the binarity of stars (Carlin et al., 2012), and therefore no direct systematics is inherited from the targeting.

4.2.5   Contamination test

We test the contamination of our comoving search by flipping the sign of the Galactic latitude and the proper motion in the direction of Galactic latitude of the LAMOST stars. The comoving search for a given LAMOST star only considers the Gaia sources nearby its flipped location and does not include
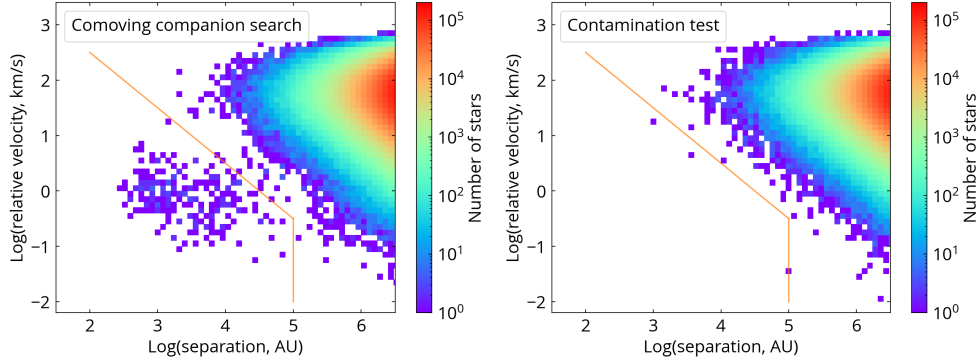
Figure 4.1: The comoving companion search (left) and the contamination test (right) for 4000 randomly selected LAMOST stars, where 2000 of them have [Fe/H]< −0.75 and the other 2000 have [Fe/H]> 0. The contamination test flips the sign of the Galactic latitude and the proper motion in the direction of Galactic latitude; therefore, all pairs in the right panel are chance projection. The orange solid line is the empirical selection for comoving companions. The level of contamination from chance projection plays a negligible role in our results.

other flipped LAMOST stars. Thus, the flipped LAMOST stars have similar surrounding stellar densities as their original locations, but now all nearby stars are chance projection. We randomly select 2000 LAMOST stars with [Fe/H]< −0.75 and 2000 with [Fe/H]> 0 to investigate if the contamination level depends on the metallicity. We ensure that the sky regions of the flipped LAMOST stars are covered by Gaia DR2 with visibility periods > 8. The solar motion and the Galactic disk differential rotation contribute different proper motions depending on the sky location, which need to be taken into account in the contamination test. We remove their contributions to proper motions using the local shear approximation (Olling and Dehnen, 2003) with the solar motion from Schönrich, Binney, and Dehnen, 2010 and the Oort constants from Bovy, 2017. Therefore, the solar motion and the disk differential rotation do not contribute the relative velocity in the contamination test.

Fig. 4.1 shows the comoving search result of the 4000 LAMOST stars (left) and their contamination test (right). The orange line is the empirical demarcation line designed to have a similar slope as the chance projection (Hwang et al., 2020b), and we only consider wide binaries at separations between 10^3 and 10^4 AU in this paper. Among these 4000 LAMOST stars, 105 of them have wide companions in the left panel (with the absolute magnitude cut on the companions), and only one chance projection in the right panel (there are other two chance-projection pairs below the demarcation line, but their separations are not between 10^3 and 10^4 AU). Therefore, the contamination level is about two order-of-magnitude smaller than the wide-binary fraction regardless of the metallicity. This contamination is lower than in Hwang et al., 2020b (which is purely based on Gaia) because most of the LAMOST stars are located in lines-of-sight towards the outer disc (Zhao et al., 2012). In short, the level of contamination from chance alignments plays a negligible role in our results.

The astrometric measurements may be affected by the presence of subsystems. For example, the orbital motion (Belokurov et al., 2020b) and the photometric variability (Hwang et al., 2020a) of the unresolved systems may induce astrometric noise. The presence of a marginally resolved source (angular separations of a few ×0.1 arcsec) also downgrades the astrometric measurement quality because of the non-point-spread-function light profile (Hwang et al., 2020a). The blending of unresolved spectra may result in unreliable or flagged metallicity. These possibilities would reduce the completeness of the wide binaries that have subsystems; however, they are unlikely to affect our results

significantly. First, the parameter space for (marginally) unresolved systems to have corrupted astrometric measurements due to the orbital motions or photometric variability is narrow, especially that the angular separation of such system needs to be large and the orbital or photometric timescale needs to be comparable or shorter than Gaia's temporal baseline. Second, these possibilities affect parallaxes more than the proper motions because most of our sample have parallaxes close to 2 mas, while their median total proper motions is about 20 mas yr^{-1}. This is the reason we use a more relaxed parallax criterion in the comoving companion search (either parallax difference < 0.2 mas or the line-of-sight distance difference < 20 pc). A more relaxed parallax criterion may result in a higher contamination, but Fig. 4.1 shows that the contamination level remains negligible. Third, if our results are due to the presence of subsystems, then we would expect our results to change for a sample at different distances and for wide binaries with different separations. In the Appendix 4.6.1, we show that our conclusions remain unchanged when different selection criteria are used.

4.2.6   Distinguishing thin disk, thick disk, and halo stars

We consider two methods to distinguish the thin disk, thick disk, and halo stars: (1) the maximum Galactic height of the Galactic orbits (maximum vertical excursion, z_{max}); and (2) total 3-dimensional velocity (v_{tot}), computed from the projected velocity from Gaia and the radial velocity from LAMOST LASP, with respect to the local standard of rest (Schönrich, Binney, and Dehnen, 2010). We use galpy[1] (Bovy, 2015) to derive the z_{max} of the Galactic

---

[1]http://github.com/jobovy/galpy
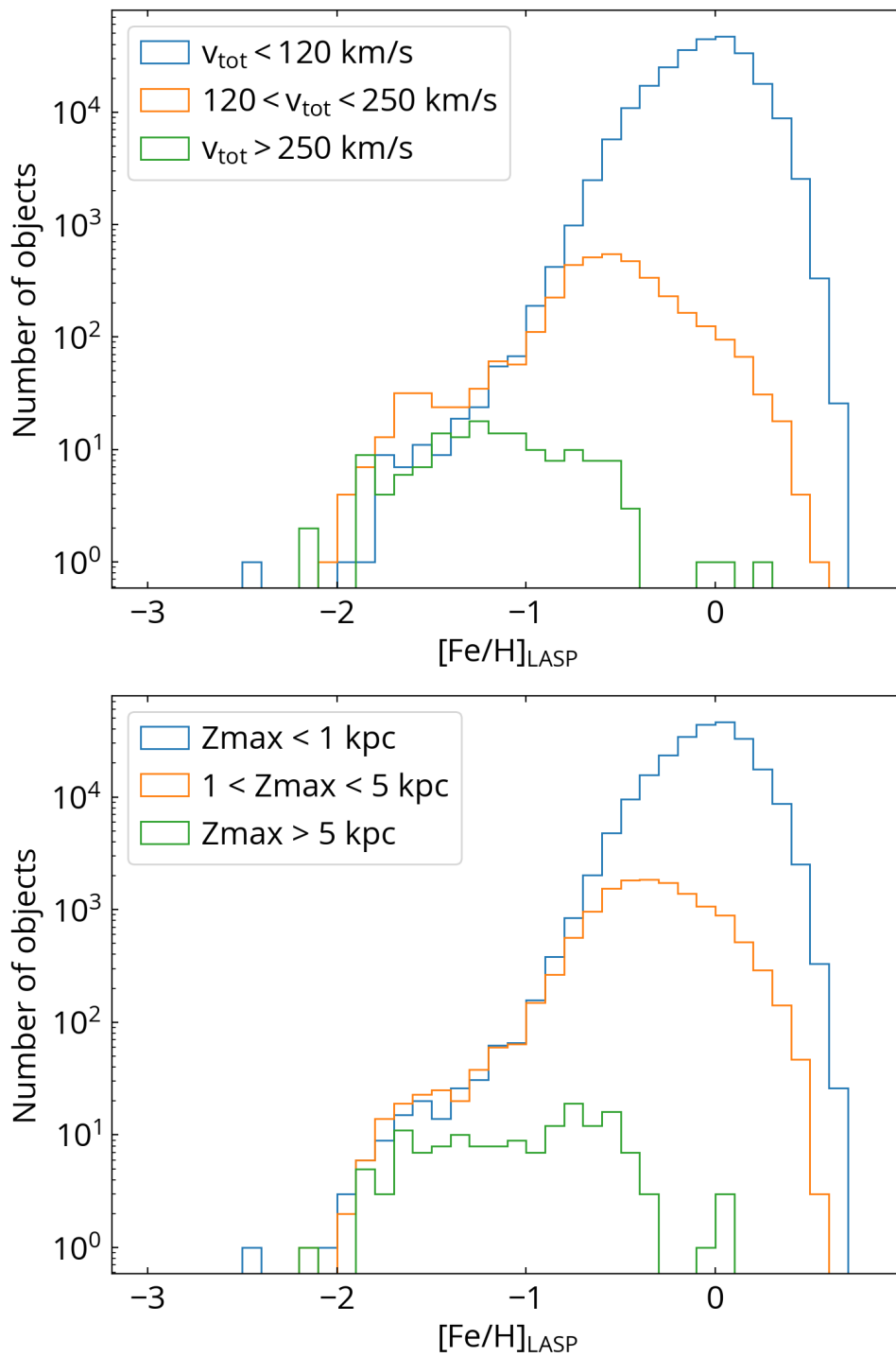
Figure 4.2: The LASP metallicity distribution for the thin-disk, thick-disk, and halo stars, selected using total velocity (top) and the maximum Galactic height (bottom).

orbits. Specifically, we use the fast estimation of orbit parameters via the Stäckel approximation, and the estimation for z_{max} is precise to a level better than $\sim$ 1% (Mackereth and Bovy, 2018). We use the Milky Way potential `MWPotential2014` from Bovy, 2015 and a solar motion with respect to the local standard of rest from Schönrich, Binney, and Dehnen, 2010.

We use the Gaia DR2 mock catalogue (Rybizki et al., 2018) to test our selection for thin-disk, thick-disk, and halo stars. The Gaia DR2 mock catalogue is generated using `Galaxia` (Sharma et al., 2011) that samples stars from the Besançon Galactic model (Robin et al., 2003). To match the properties of our LAMOST F- and G dwarfs, we select main-sequence mock stars with 0.6 <BP-RP< 1.1 and parallax > 2 mas. Following Hwang and Zakamska, 2020, we assign weights to the mock stars so that they have a similar sky distribution as our LAMOST sample. Then we use `galpy` to derive the z_{max} for the mock stars.

Using Gaia DR2 mock catalogue, we find that 91% of v_{tot} < 120 km s^{-1} stars belong to the thin disk, 87% of 120 < v_{tot} < 250 km s^{-1} stars belong to the thick disk, and 88% of v_{tot} > 250 km s^{-1} stars belong to the halo. For the z_{max} selection, 92% of z_{max} < 1 kpc stars are thin disk, 80% of 1 < z_{max} < 5 kpc are thick disk, and 35% of z_{max} > 5 kpc are halo stars. Therefore, we consider v_{tot} as a better selection for the halo sample than z_{max}. Their metallicity distributions are shown in Fig. 4.2. The low-metallicity tail at [Fe/H]< −1 in the thin-disk stars may be partially contributed by the contamination from the thick-disk stars. By using the v_{tot} (z_{max}) selection, we have 7602 (7335), 67 (334), and 2 (2) wide binaries in the thin disk, thick disk, and halo respectively. We caution

readers for the results for the halo in this study due to its small sample, and one of the z_{max}-selected halo wide binaries has [Fe/H]=−0.46 and is likely a thick disk contaminant.

4.3 The metallicity and age dependence of the wide-binary fraction

Fig. 4.3 shows the wide-binary fraction as a function of stellar metallicity. The black points use the LASP metallicity, and the blue points use the metallicity derived by DD-Payne. The metallicity bins span from [Fe/H]= −2 to +0.5 and are indicated by the ticked line at the bottom of Fig. 4.3, with the markers located at the center of each metallicity bin. The bin sizes and the numerical values are available in Appendix 4.6.3. The black and the blue points are slightly offset horizontally for clarity. Error bars of the wide-binary fractions are Poisson uncertainties.

The overall metallicity dependence is similar for LASP metallicity and DD-Payne metallicity: the wide-binary fraction first increases with increasing metallicity, peaks at [Fe/H]≃ 0, and then decreases at the high metallicity end. The metallicity where the wide-binary fraction peaks is slightly different between LASP and DD-Payne, which is likely due to the systematic metallicity offset of 0.07 dex between LASP and DD-Payne (Sec. 4.2.1). Otherwise, our result is robust over different metallicity pipelines. We focus on the results using LASP metallicity for the rest of the figures, and we do not find significant difference from those using DD-Payne metallicity.

We perform the Kolmogorov-Smirnov test to quantify the significance of
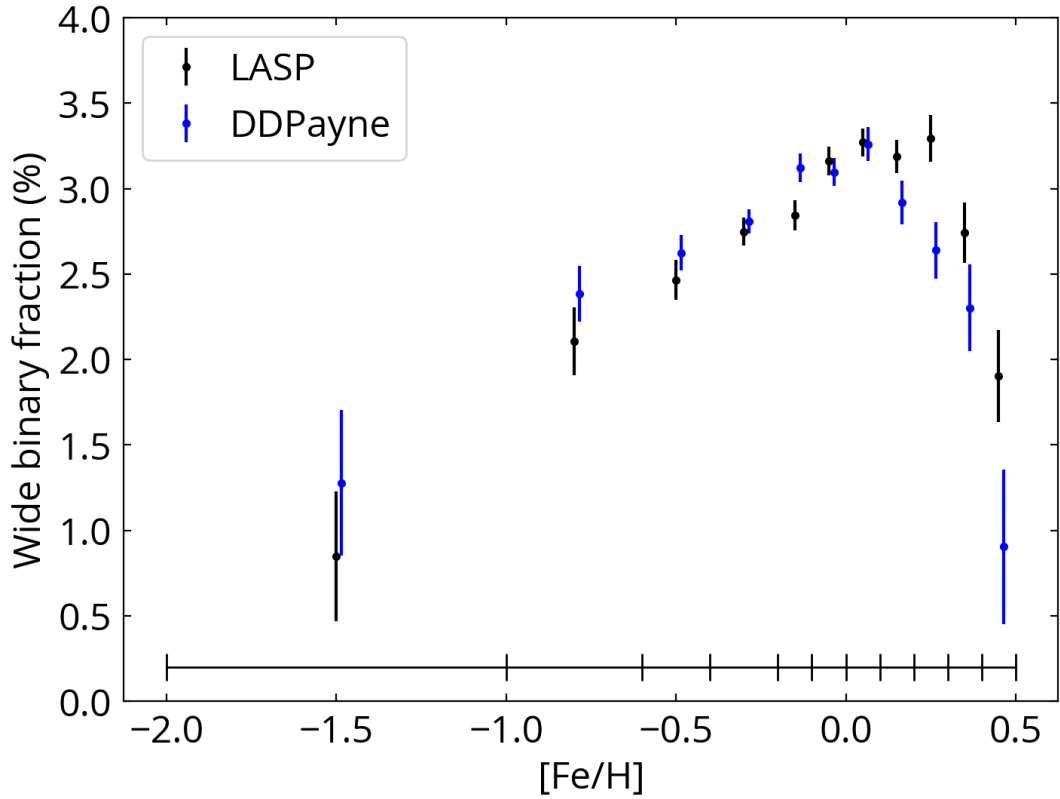
Figure 4.3: The metallicity dependence of the wide-binary fraction (10^3-10^4 AU). The black points use the [Fe/H] derived from LAMOST Stellar Parameter pipeline (LASP), and the blue points use the LAMOST [Fe/H] measured by DD-Payne. The black and the blue points are slightly offset along the horizontal axis for clarity. The ticks at the bottom show the bin size, and the markers are located at the center of the bin. Both results show that, as [Fe/H] increases, the wide-binary fraction first increases at low [Fe/H], peaks at [Fe/H]$\simeq 0$, and then decreases at high [Fe/H].
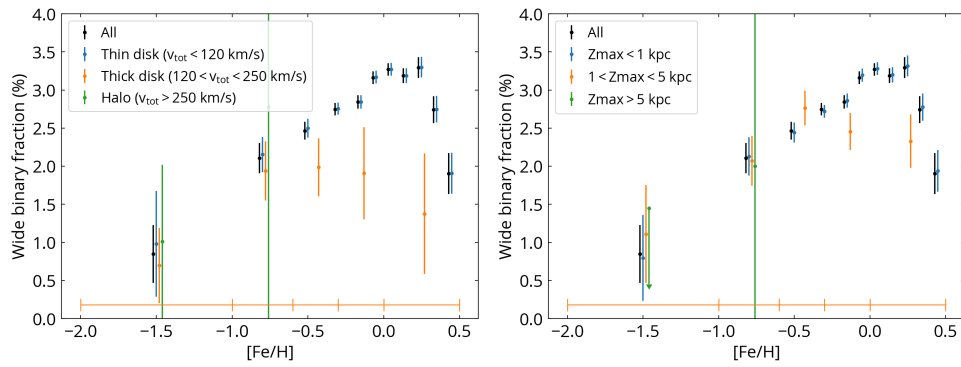
Figure 4.4: The metallicity dependence of the wide-binary fraction in the thin disk, thick disk, and halo. The LASP metallicity is adopted here, and results from DD-Payne are similar. For comparison, the black points show the same result from Fig. 4.3. The bin size of the thin-disk sample is the same as Fig. 4.3, and that of the thick-disk and halo samples is shown as the ticked orange line at the bottom. The left panel uses the total velocity to select different populations, and the right panel uses the maximum Galactic height of the orbits. The results of these two selections are in good agreement with each other. The metallicity dependence of wide binaries is dominated by the thin-disk stars. The wide-binary fraction of the thick disk follows a similar trend as the thin disk at low [Fe/H], and then become flat with increasing metallicity at [Fe/H]> −0.5. The wide-binary fraction in the halo is not well constrained due to small number statistics.
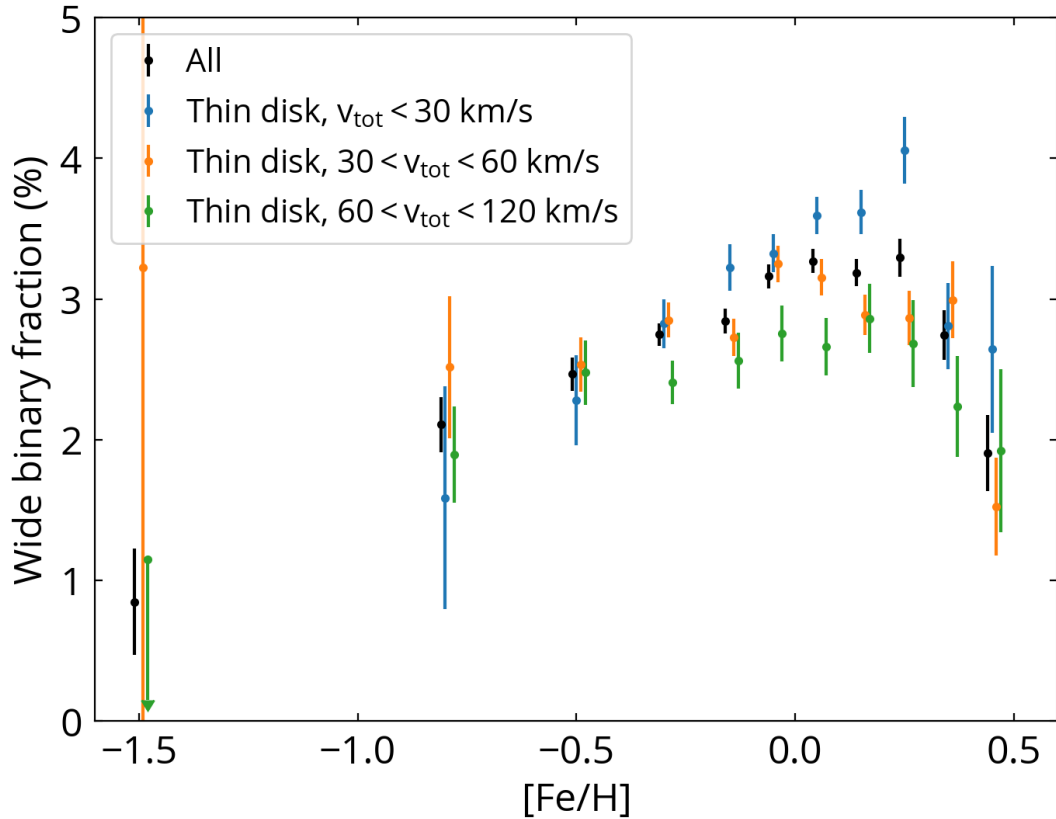
Figure 4.5: The wide-binary fraction as a function of metallicity for the thin-disk stars in bins of total velocity. Points are slightly offset horizontally for clarity. For comparison, the black points show the result from all stars in Fig. 4.3. The velocity is a proxy of the stellar age, where older stars typically exhibit larger velocities. The wide-binary fraction of the low-velocity (young) stars has a stronger metallicity dependence.
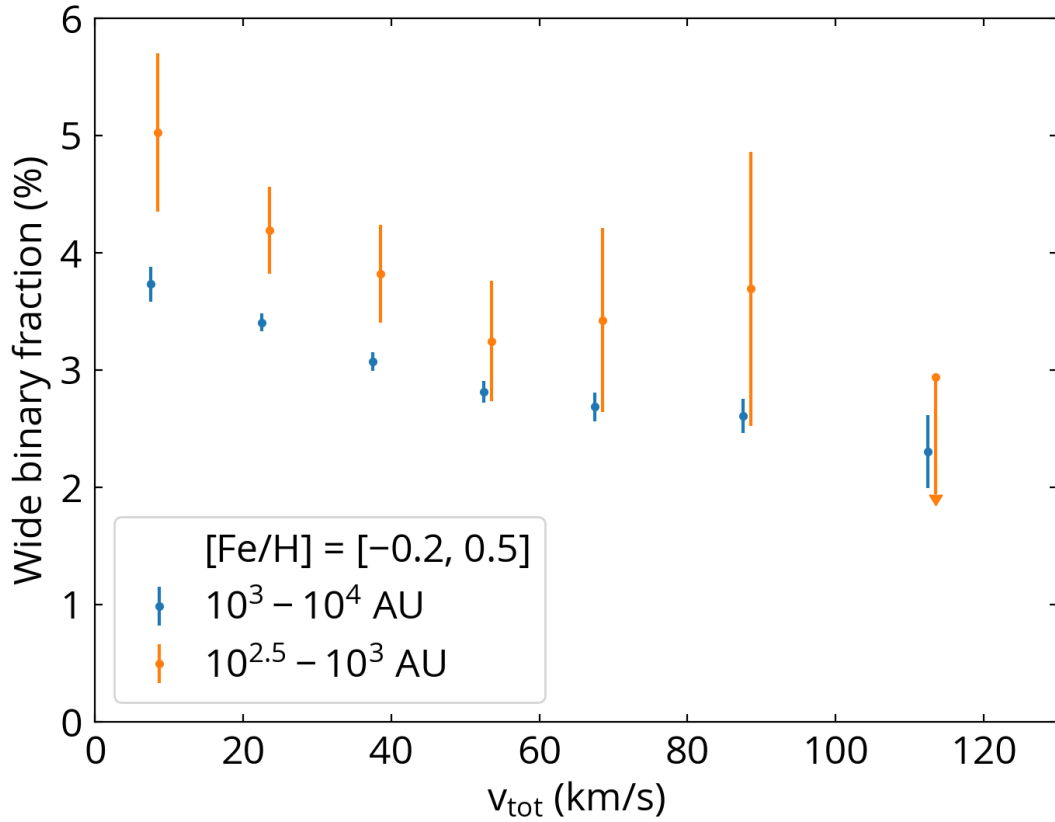
Figure 4.6: The relation between the wide-binary fraction and the total velocity, where the total velocity is a proxy of stellar age. Here we only consider [Fe/H] between −0.2 and +0.5. The wide-binary fraction shows a prominent decrement with increasing velocity (and hence increasing stellar age) at $v_{tot} < 50 \, \text{km s}^{-1}$. This age dependence is also present in the wide binaries with smaller separations of $10^{2.5}$ AU.

the difference in the metallicity distributions between the stars with wide companions and the entire main sample (with criteria described in Sec. 4.2.3). The p-value, the probability that two metallicity distributions are sampled from the same parent distribution, is 2×10^{-10}. Therefore, the difference is statistically significant, suggesting that wide binaries show robust metallicity dependence and are not a randomly drawn subsample of the parent distribution.

Since different populations may dominate at different metallicities, we further divide the sample into thin-disk, thick-disk, and halo stars using the total velocity (left panel) and the z_{max} (right panel) in Fig. 4.4. For comparison, the black points are the LASP points from Fig. 4.3. For the thin-disk samples, we adopt the same metallicity bins as for the full sample (black points), and we use larger metallicity bins (the ticked orange line at the bottom of Fig. 4.4) for the thick-disk and halo samples to reduce the Poisson uncertainties. Overall, the velocity-selected samples are in agreement with the z_{max}-selected samples. The thin-disk sample shows a similar trend as in Fig. 4.3, meaning that the global metallicity dependence is dominated by the thin disk stars, which constitutes a large fraction of the LAMOST sample. The thick-disk sample follows the metallicity relation of the thin-disk stars at [Fe/H]$<$ -0.4. At [Fe/H]$>$ -0.4, the wide-binary fraction of the thick-disk sample is much lower than that of the thin disk. The halo sample has a wide-binary fraction of $\lesssim 1.5\%$ in the metallicity bin of $-2 <$[Fe/H]< -1. While it is consistent with the wide-binary fractions in the thin-disk and thick-disk stars at the same metallicity, the wide-binary fraction in the halo is not well constrained given that there are only two wide binaries in the halo sample.

Directly age-dating main-sequence stars is difficult, and in most cases, impossible. However, kinematics of main-sequence stars nonetheless gives a *statistical* estimate of the ages, especially for the thin-disk stars because their dynamical evolution is mostly secular (Dehnen and Binney, 1998; Nordström et al., 2004; Reid et al., 2009; Sharma et al., 2014; Ting and Rix, 2019). Hence, in Fig. 4.5, we use total velocities to investigate the stellar age dependence of the wide-binary fraction in the thin disk as a function of metallicity. Here we select thin-disk stars by $z_{max} < 1\,\text{kpc}$ and bin the sample into the low-velocity ($v_{tot} < 30\,\text{km}\,\text{s}^{-1}$), the middle-velocity ($30 < v_{tot} < 60\,\text{km}\,\text{s}^{-1}$), and the high-velocity ($60 < v_{tot} < 120\,\text{km}\,\text{s}^{-1}$) sample.

Fig. 4.5 shows that wide-binary fractions of all velocity sub-samples have a similar metallicity trend, but such metallicity dependence is strongest in the low-velocity, young sample. In the metal-poor regime ($[\text{Fe/H}] \lesssim -0.5$), the wide-binary fractions of stars are about the same, irrespective of their velocity. In contrast, the lowest-velocity sample has a higher wide-binary fraction at $[\text{Fe/H}] \sim 0$ than that of the higher-velocity samples. This result also means that the metallicity dependence of the wide-binary fraction in the thin disk is not due to the varying levels of contamination from the thick-disk stars with respect to metallicity, in which case we would expect a weaker metallicity dependence in the low-velocity thin-disk sample where the contamination is the lowest.

Fig. 4.5 demonstrates that younger stars have a higher wide-binary fraction, especially at $[\text{Fe/H}] \sim 0$. However, we caution that Fig. 4.5 does not necessarily mean that there is a metallicity-dependent age evolution for wide binaries,

because each metallicity bin may have different age distributions. It is possible that the lack of age evolution in the metal-poor regime ([Fe/H]< −0.5) is simply because these metallicity bins lack young stars (e.g. Casagrande et al. 2011; Lin et al. 2020).

To explore the stellar age dependence further, in Fig. 4.6 we investigate the wide-binary fraction as a function of total velocity. We also present the wide-binary fraction for separations between $10^{2.5}$ and 10^3 AU, where we apply a parallax cut > 6.3 mas for the sample so that $10^{2.5}$ AU corresponds to the angular resolution of 2 arcsec. Furthermore, we adopt an absolute G-band magnitude criterion of 12.5 mag for the $10^{2.5}$-10^3 AU case. The result is similar but noisier if we use the original criterion of 10 mag. Here we only consider metallicity between −0.2 and 0.5 because they cover a wider age distribution compared to the metal-poor stars. In case that massive companions may induce additional age dependence, we test the selection by requiring that the companions be fainter than the LAMOST stars, and the result remains nearly the same.

Fig. 4.6 shows that stars having $v_{tot} < 50\,\mathrm{km\,s^{-1}}$ have a higher wide-binary fraction with separations down to $10^{2.5}$ AU. Based on the Gaia DR2 mock catalogue (Rybizki et al., 2018) which sample mock stars from the Besançon Galactic model (Robin et al., 2003), the total velocity of $\sim 50\,\mathrm{km\,s^{-1}}$ corresponds to a mean stellar age of $\sim 5\,\mathrm{Gyr}$. Therefore, the wide-binary fraction seems to be higher in younger stars with ages $\lesssim$ a few Gyr.

4.4 Discussion

We have found that in the thin disk, the wide-binary fraction increases with metallicity at $[Fe/H] \lesssim 0$, and then decreases with metallicity in the super-solar regime. Furthermore, based on the kinematics, the enhanced wide-binary fraction at $[Fe/H] \simeq 0$ is age dependent, with a higher wide-binary fraction in younger stars. In the following sections, we compare these results to those from past studies, and seek an interpretation that would simultaneously explain the metallicity and age dependence of the wide-binary fraction.

4.4.1 Comparison with previous work

In the pre-Gaia era, some studies concluded that the wide-binary fraction was relatively independent of metallicity (Zapatero Osorio and Martin, 2004; Zinnecker, Köhler, and Jahreiß, 2004), while some found a lower wide-binary fraction for metal-poor stars (Rastegaev et al., 2008; Jao et al., 2009; Lodieu, Osorio, and Martin, 2009; Zhang et al., 2013; Ziegler et al., 2015). Moe, Kratter, and Badenes, 2019 argued that a lower wide-binary fraction of the metal-poor stars from high-resolution imaging studies may be a selection effect, because photometric selection of metal-poor stars may exclude unresolved metal-poor binaries since they are brighter than the metal-poor single stars and may be considered as metal-rich single stars. Our results do not involve any photometric estimates of metallicity and are free from such selection effect.

In the Gaia era, with proper motions and parallaxes available for billions of stars, a large sample of comoving pairs has been made possible (Oh et al.,

2017; El-Badry and Rix, 2018; Jiménez-Esteban, Solano, and Rodrigo, 2019). In particular, El-Badry and Rix, 2019 study the metallicity dependence of wide binaries with separations from 50 to 50,000 AU by combining the comoving pair sample from Gaia DR2 and wide-field spectroscopic surveys. For binaries with separations $\gtrsim$ 250 AU, they conclude that the binary fraction remains constant with respect to metallicity.

Our sample bears some similarities to the one from El-Badry and Rix, 2019, but here we complement the study by expanding the sample to 500 pc. Their sample is restricted within 200 pc. Therefore, we have a larger sample at larger distances, which strongly improves the constraints on the thick-disk and halo stars at the low-metallicity end. Our sample enables us to further dissect the wide-binary fraction as a function of metallicity and age, while El-Badry and Rix, 2019 do not take the kinematics and ages into account.

While our findings of the strong metallicity dependence for the wide-binary fraction seem at odds with their conclusion, El-Badry and Rix, 2019 do comment that there is a slight excess of wide binaries at [Fe/H]$\simeq$ 0, consistent with our results. They suspect that such excess may be due to the age effect such that old wide binaries are disrupted by gravitational perturbations from other stars and molecular clouds. In the following section, we investigate this possibility in detail, and will argue that gravitational perturbations are unlikely to play a dominant role.

4.4.2 Wide binary disruption

When time passes, wide binaries may be disrupted by passing stars, molecular clouds, and Galactic tidal fields (Bahcall, Hut, and Tremaine, 1985; Weinberg, Shapiro, and Wasserman, 1987; Chaname and Gould, 2004; Yoo, Chaname, and Gould, 2004; Quinn and Smith, 2009; Jiang and Tremaine, 2010). Binaries with wider separations are easier to be disrupted due to the weaker binding energy. In particular, given the stellar density in the solar neighborhood, theoretical estimates show that binaries with separations $> 0.1\,\mathrm{pc}$ ($2 \times 10^4\,\mathrm{AU}$) would be disrupted within $10\,\mathrm{Gyr}$ (Weinberg, Shapiro, and Wasserman, 1987). Therefore, fewer binaries with separations $> 10^4\,\mathrm{AU}$ are expected in the old disk stars (Bahcall and Soneira, 1981; Retterer and King, 1982; Weinberg, Shapiro, and Wasserman, 1987). Tian et al., 2020 may detect this effect in their 'halo sample' selected by the high tangential velocities ($> 85\,\mathrm{km\,s^{-1}}$), and the authors argue that their results cannot be explained by the binary disruption due to the low density in the halo. While this hints that there might be other effects beyond gravitational perturbations which shape the wide-binary fraction, we note that their results might not be conclusive, as a tangential velocity cut at $> 85\,\mathrm{km\,s^{-1}}$ likely results in predominantly old thin-disk stars and thick-disk stars, instead of halo stars.

While the disruption of binaries by the gravitational perturbations (passing stars, molecular clouds, and Galactic tidal fields) may be able to make the wide-binary fraction lower in the metal-poor stars because they are on average older, this explanation alone is at odds with some results presented in this study. First, theoretical arguments have shown that the disruption lifetime of

10^3 AU binaries is $\sim 100\,\mathrm{Gyr}$, much longer than the age of Universe (Weinberg, Shapiro, and Wasserman, 1987). Furthermore, if binary disruption were to play an important role, we expect wider binaries should be preferentially disrupted. However, our data do not show a significant difference in the age evolution between $10^{2.5-3.0}$ AU and 10^{3-4} AU binaries (Fig. 4.6). Also, binary disruption is not able to explain the anti-correlation between wide-binary fraction and metallicity at [Fe/H]> 0. Therefore, we conclude that the age and metallicity dependence of the wide-binary fraction cannot solely be explained by binary disruption.

4.4.3 Wide binary formation and evolution

Since wide binary disruption cannot be the whole story, here we investigate whether the metallicity and age dependence arise from wide binary formation. Wide binaries with separations of 10^3-10^4 AU can be formed through multiple channels, including the turbulent core fragmentation (Padoan and Nordlund, 2002; Fisher, 2004; Offner et al., 2010), dynamical unfolding of unstable compact triples (Reipurth and Mikkola, 2012; Elliott and Bayo, 2016), the dissolution of star clusters (Kouwenhoven et al., 2010; Moeckel and Clarke, 2011), and the pairing of adjacent pre-stellar cores (Tokovinin, 2017). However, not all of these channels can provide the observed metallicity and age dependence of the wide-binary fraction.

4.4.3.1 The negative metallicity dependence

We first tackle the decrease of the wide-binary fraction with metallicity at [Fe/H]> 0. The dynamical unfolding of compact triples may be able to explain such metallicity dependence. In this scenario, triple stars are born in compact, unstable configurations, and then they evolve to a hierarchical architecture with one companion scattered into a wide orbit (Reipurth and Mikkola, 2012). As a result, the formation of wide binaries is influenced by the occurrence of close binaries, so the metallicity dependence of the wide binaries is inherited from the formation of compact systems through disk and other small-scale fragmentation. If wide companions were preferentially formed via this scenario, then the wide-binary fraction would follow a similar metallicity dependence as close binaries. Indeed, close binaries also show a declining occurrence rate as a function of metallicity (Grether and Lineweaver, 2007; Raghavan et al., 2010; Yuan et al., 2015; Badenes et al., 2018; Moe, Kratter, and Badenes, 2019; El-Badry and Rix, 2019; Mazzola et al., 2020), as is observed for the super-solar metallicity sample in this study. This may be in line with the excess of equal-mass binaries ('twin' binaries) at separations > 1000 AU, which also suggests that these wide binary twins are formed at close separations initially ($a < 100\,\text{AU}$) and then their orbits are widened by the dynamical interaction with the birth environments (El-Badry et al., 2019).

The connection between wide companions and close binaries is supported by other observational studies. For instance, 96% of close binaries with orbital periods < 3 days have tertiary companions (Pribulla and Rucinski, 2006; Tokovinin et al., 2006). Hwang et al., 2020b find that the occurrence rate of

the wide companions at 10^3-10^4 AU around main-sequence contact binaries is a factor of 3 higher compared to that of the field stars. Conversely, about half of wide pairs with separations of 10^3-10^4 AU are hierarchical multiples (Raghavan et al., 2010; Moe and Di Stefano, 2017; Moe and Kratter, 2019).

The enhanced occurrence rate of tertiary companions around close binaries possibly suggests that tertiary companions play a critical role in the orbital migration of the inner binary through the Kozai-Lidov mechanism, where the outer tertiary companion excites the high eccentricity of the inner binary (Kozai, 1962; Lidov, 1962; Kiseleva, Eggleton, and Mikkola, 1998; Eggleton and Kiseleva-Eggleton, 2001; Eggleton and Kisseleva-Eggleton, 2006; Fabrycky and Tremaine, 2007; Naoz et al., 2013b; Borkovits et al., 2016). Nonetheless, noting that the Kozai-Lidov mechanism is only effective under certain inner-to-outer separation ratios and mutual inclinations, it remains unclear whether this mechanism can be responsible for the majority of those triple systems consisting of close binaries (Moe and Kratter, 2018; Hwang and Zakamska, 2020; Hwang et al., 2020b). Alternatively, the enhanced occurrence rate of tertiary companions may be a result of compact multiple stars forming from disk fragmentation (Tokovinin and Moe, 2020), then the occurrence of these wide companions would follow the similar anti-correlation with metallicity as the close binaries, in line with the scenario of dynamical unfolding of compact triples.

To sum up, we argue that the negative metallicity dependence of the wide-binary fraction is inherited from that of the close-binary fraction through the dynamical unfolding of triple stars. Nonetheless, the metallicity dependence

of the wide-binary fraction is clearly non-monotonic. It raises a question why this anti-correlation is only present at [Fe/H]> 0, while that of the close-binary fraction spans from [Fe/H]= −3 to +0.5. This implies that there is another limiting factor dominating the wide binary formation at the metal-poor regime, which we investigate in detail in the next section.

4.4.3.2 The positive metallicity dependence

During the pre-main sequence phase (ages < a few Myr), wide binaries can form through the turbulent core fragmentation and the random pairing of adjacent pre-stellar cores. While the wide-binary fractions from these two mechanisms are not explicitly dependent on metallicity, as is shown in the hydrodynamical simulations (Bate, 2005; Bate, 2014; Bate, 2019), wide binaries themselves are sensitive to the formation environments. In particular, most if not all stars form in clustered environments (Lada and Lada, 2003), and about 20-30% of stars originate from bound clusters (Bressert et al., 2010; Kruijssen, 2012; Chandar et al., 2017). Environments with a higher stellar density have small stellar separations, making wide binaries more difficult to survive. Furthermore, the higher velocity dispersion accompanied by the higher stellar density makes the random pairing less likely. Indeed, observational studies have found that wide-binary fractions are higher in the low-density star-formation regions compared to the higher-density clustered environment (Simon, 1997; Kraus and Hillenbrand, 2009; Tobin et al., 2016a; Elliott and Bayo, 2016; Joncour, Duchêne, and Moraux, 2017; Deacon and Kraus, 2020). Therefore, density of the formation environment plays a critical role in the wide binary formation (e.g. Marks, Kroupa, and Oh 2011; Marks and Kroupa

2011; Marks and Kroupa 2012).

When the gas is removed after $\sim 10\,\mathrm{Myr}$ (Bastian et al., 2005; Fall, Chandar, and Whitmore, 2005; Mengel et al., 2005), the cluster expands in response to the change in the gravitational potential (Goodwin and Bastian, 2006; Goodwin, 2009). At this cluster dissolution phase, two unbound stars that are originally close in the phase space may pair together and become a wide binary (Kouwenhoven et al., 2010; Moeckel and Clarke, 2011). Using Monte Carlo and N-body simulations, Kouwenhoven et al., 2010 further find that the wide-binary fraction decreases strongly with increasing cluster mass, where the main driving factor may be associated with the increasing velocity dispersion that makes two stars less likely to pair in the phase space.

In the earlier Universe, star formation environments tend to have a higher pressure and density than the present day, and high-mass clusters are preferentially formed in such environments (Harris and Pudritz, 1994; Elmegreen and Efremov, 1997; Kravtsov and Gnedin, 2005; Kruijssen, 2014; Ma et al., 2020). A higher-density environment reduces the wide binary formation from the turbulent core fragmentation and the random pairing of adjacent pre-stellar cores, and also fewer wide binaries can form from the dissolution of higher-mass clusters. As a result, the wide-binary fraction would be lower in the older stars, which explains the age dependence in Fig. 4.5 and Fig. 4.6. Furthermore, because metal-poor stars are on average older stars, this naturally explains the positive correlation between the wide-binary fraction and metallicity.

132
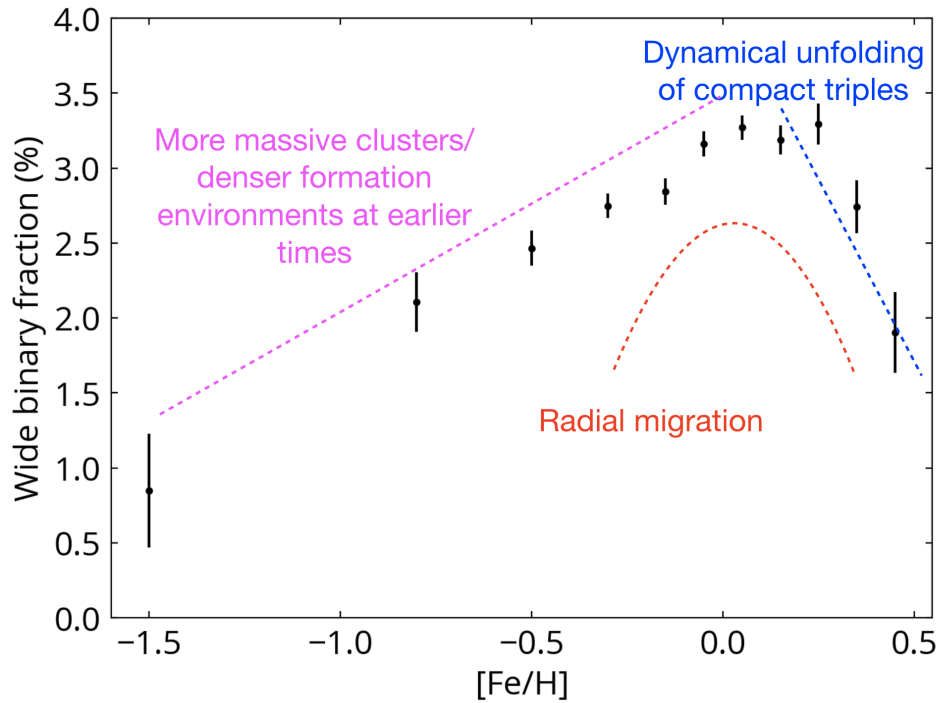
Figure 4.7: Schematic illustration of the metallicity dependence of various proposed wide binary formation channels in this study. The observed metallicity dependence (black points) is likely the consequence of multiple formation channels of wide binaries. The dashed lines show the metallicity trend of the proposed mechanisms, and their values and slopes are only for schematic illustration. The dynamical unfolding of compact triples (blue line) follows the metallicity anti-correlation of the close-binary fraction. The trend at $[Fe/H] < 0$ can be due to that the density of the formation environments and the cluster mass are higher at earlier times (pink line). The environmental effect ceases to play a role at the high metallicity because the formation time is similar at $[Fe/H] > 0$, and therefore the anti-correlation from the dynamical unfolding of triple stars manifests itself at high metallicities. Radial migration may also play a role in enhancing the wide-binary fraction around the solar metallicity (red line).

4.4.4 A holistic view and future outlook

So far we have discussed various wide binary formation channels and how they may or may not induce metallicity and age dependence in the observed wide-binary fraction. In reality, these mechanisms must all play a role in varying degrees. It is unlikely that our result can be explained by only one mechanism. In particular, no one formation mechanism can explain the non-monotonic relation between metallicity and the wide-binary fraction.

Fig. 4.7 summarizes the metallicity dependence of the wide binary formation channels, and we propose that the observed metallicity and age dependence are caused by the combination these formation mechanisms. Briefly, the higher stellar density in the star formation environments and the dissolution of higher-mass clusters at an earlier time result in the lower wide-binary fraction in the older stars and the positive metallicity correlation at [Fe/H]$\lesssim$ 0. The metallicity dependence of dynamical unfolding of compact triples follows the anti-correlation between metallicity and the close-binary fraction, which may explain the declining wide-binary fraction at the super-solar metallicity regime. The values and slopes of the lines in Fig. 4.7 are only for schematic illustration.

The reason that the positive metallicity correlation of wide-binary fraction ceases at [Fe/H]= 0 may be that the mean stellar age is similar at [Fe/H]= 0 and = 0.5 (Casagrande et al., 2011; Bensby, Feltzing, and Oey, 2014; Silva Aguirre et al., 2018). Since their formation times are similar, there is no much difference in their formation environments. As the environmental effect ceases to play a dominant role, the anti-correlation with metallicity inherited from the

close-binary fraction manifests itself at the regime of super-solar metallicity.

If the negative correlation with metallicity is due to the dynamical unfolding of compact triples, it is not directly obvious why it only applies to [Fe/H]> 0 and does not extend to [Fe/H]< 0. One possibility is that at [Fe/H]< 0, dense environments disrupt the wide binaries or prohibit their formation in the first place. Another challenge for the dynamical unfolding of compact triples to explain the metallicity dependence at [Fe/H]> 0 is that both the wide-binary fraction and the close-binary fraction (Moe, Kratter, and Badenes, 2019) decreases by a factor of 2 from [Fe/H]= 0 to [Fe/H]= 0.5. If the metallicity dependence of the wide-binary fraction is inherited from the close-binary fraction, it implies that nearly all wide binaries at [Fe/H]> 0 are associated with the close binary formation. Therefore, it is possible that there are other mechanisms, like radial migration explained below, that also shape the metallicity dependence at [Fe/H]> 0.

Given that the wide-binary fraction conspicuously peaks around the solar metallicity, close to the current metallicity of the interstellar medium in the solar neighborhood, it is natural to speculate if the metallicity trend in the wide-binary fraction is due to the radial migration of stars in the Milky Way. Stars that do not have solar metallicities were preferentially formed elsewhere and then radially migrated to the solar neighborhood (e.g. Wojno et al. 2016; Minchev et al. 2018; Han et al. 2020). If the radial migration process can disrupt wide binaries, it would result in a lower wide-binary fraction at low and high [Fe/H]. For example, if a wide binary is trapped at the corotation resonance of a spiral arm, there could be a close destructive interaction between the wide

binary and a high-density clump. The migration timescales across the disk are several Gyr (e.g. Frankel et al. 2018; Frankel et al. 2020), which may explain the inferred age dependence of the wide-binary fraction in Fig. 4.6. However, as discussed in Sec. 4.4.2, the disruption timescale of a 1000-AU wide binary is longer than the age of the Universe, so we consider the disruption by radial migration processes unlikely to explain the metallicity dependence.

Even if radial migration processes do not directly disrupt wide binaries, radial migration may still play a role in shaping the metallicity dependence of the wide-binary fraction. For stars with super-solar metallicities in the solar neighborhood, they were formed in the inner Milky Way and then migrated to their current location (Kordopatis et al., 2015; Wojno et al., 2016; Han et al., 2020). The higher stellar density at the inner Milky Way lowers the wide-binary fraction, and therefore we would expect a lower wide-binary fraction for stars with higher super-solar metallicities. Similarly, stars with sub-solar metallicities may have a wide-binary fraction different from that of solar-metallicity stars due to radial migration. If there is a higher probability of radial migration for stars with more circular orbits (i.e. populations with cooler kinematics), as proposed by Daniel and Wyse, 2018, then the derived age estimates for this population of radial migrators will be biased low. We include radial migration in Fig. 4.7, and future work is needed to determine the relative importance of the scenarios listed in Fig. 4.7.

Finally, for the entire population (irrespective of metallicity), the wide-binary fraction of the thick-disk stars is lower than that of the thin-disk stars, and that of the halo stars is marginally lower than the thick-disk stars (Fig. 4.4).

However, the age distribution of the thin-disk stars is different from the thick-disk and halo stars. Silva Aguirre et al., 2018 show that the age distribution of the low-α-element disk (thin disk) peaks at 2 Gyr, while the high-α-element disk (thick disk) peaks at 11 Gyr. Halo stars in the solar neighborhood are also 11 Gyr old (e.g. Jofre and Weiss 2011; Kalirai 2012). Therefore, the lower wide-binary fraction in the thick-disk and halo stars may be due to that they are older than the thin-disk stars. This suggests that their wide-binary fractions are likely driven by the same effect as the thin-disk stars, which is mostly determined by the formation environments at the different time.

In this study, we propose that multiple formation mechanisms are responsible for the metallicity and age dependence of the wide-binary fraction. Several lines of future work may be able to further constrain their individual contributions. First, different formation mechanisms predict different mass-ratio distributions. For example, the mass ratio distribution from cluster dissolution is consistent with random pairing (Kouwenhoven et al., 2010), while that of the dynamical unfolding of compact triples is not (Reipurth and Mikkola, 2012). Therefore, an investigation in the mass ratios of wide binaries as a function of metallicity may shed light on the underlying formation mechanisms. Second, a statistical study of wide binary eccentricity (e.g. Tokovinin and Kiyaeva 2016) as a function of metallicity may be helpful, because dynamical unfolding of compact triples leads to more eccentric outer orbits. However, the interpretation may be complicated, because multiple mechanisms may be at work at the same time, and these wide companions from dynamical unfolding may interact with their formation environments, altering their eccentricity. Also,

spectroscopic age estimates for giants via C/N-related features in spectra (e.g. Martig et al. 2016; Ting and Rix 2019) can further constrain the age evolution of wide binaries.

4.5 Conclusions

In this paper, we investigate the metallicity and age dependence of the wide-binary ($a = 10^3$-10^4 AU) fraction. Specifically, we use the metallicity and radial velocity from LAMOST DR5 combined with the astrometric information from Gaia DR2 to measure the wide-binary fraction of field F and G dwarfs. Our findings include:

1. Wide-binary fraction strongly depends on the metallicity (Fig. 4.3). As metallicity increases, wide-binary fraction first increases, peaks at [Fe/H]$\simeq$ 0, and then decreases at the high metallicity end. The wide-binary fraction at [Fe/H]= 0 is about two times larger than that at [Fe/H]= −1 and [Fe/H]= +0.5. Such metallicity dependence is dominated by the thin-disk stars (Fig. 4.4).

2. The wide-binary fraction is further dependent on the stellar age, with younger stars having a higher wide-binary fraction (Fig. 4.5, Fig. 4.6).

3. Our results suggest that multiple formation channels may be responsible for the formation of wide binaries, resulting in the metallicity and age dependence of the wide-binary fraction (Fig. 4.7). Binaries of 10^3-10^4 AU are unlikely to be disrupted by the gravitational perturbations on the relevant timescale. The positive correlation between the wide-binary

fraction and metallicity at [Fe/H]< 0 may be due to that the density of formation environments and the cluster masses are higher at earlier times, lowering the wide-binary fraction at the low-metallicity end. This also explains the age dependence that younger stars have a higher wide-binary fraction. The anti-correlation between metallicity and the wide-binary fraction at [Fe/H]> 0 can be inherited from the similar anti-correlation of the close-binary fraction through the dynamical unfolding of compact triples. Radial migration may also enhance the wide-binary fraction around the solar metallicity in the solar neighborhood.

---

[2]http://www.astropy.org

2018).

4.6 Appendix

4.6.1 Tests of different selection criteria

In Fig. 4.8, we investigate how our results depend on the selection criteria. Based on the selection described in Sec. 4.2.3, we change a certain criterion and check how it affects the resulting metallicity dependence of the wide-binary fraction. The LASP metallicity is used. The black points are the main LASP result in Fig. 4.3. For better visual comparison, we present the wide-binary fraction scaled to 1 at [Fe/H]= 0 for the vertical axis in Fig. 4.8. Different tests are slightly offset along the horizontal axis for clarity. The metallicity bins are the same as in Fig. 4.3. We change the following criteria for each test. (1) We select sample with parallax > 5 mas (blue), i.e. distances within 200 pc. (2) Instead of wide binary separations between 10^3 to 10^4 AU, we only consider those with separations between 3000 AU and 10^4 AU (orange). These wide binaries have angular separations > 6 arcsec. (3) Since (wide) binary properties depend on the primary mass, we require that the LAMOST stars be the primary of the wide binaries, i.e. the G-band magnitude of the LAMOST star is brighter than that of the companion star ($G_0 < G_1$, green). (4) A narrower temperature range of 5000-6000 K is used (red) to investigate the mass dependence across the entire metallicity range.

All the tests in Fig. 4.8 have a similar metallicity trend as in Fig. 4.3, supporting that our conclusions are robust against the selection details and other

140

potential systematics. Test (1) shows that a similar metallicity trend can already be seen with a sample within 200 pc, with much larger errors. This result emphasizes the need for a larger sample out to 500 pc. The binary angular separations in test (2) are > 6 arcsec, implying that our conclusion is not affected by the reduced source completeness at small separations. Test (3) shows that the metallicity dependence is nearly the same when we require that the LAMOST stars are the primaries of the wide binaries. The result of test (4) remains similar when a narrower temperature (and therefore mass) range is used, meaning that the metallicity dependence of the wide-binary fraction is not due to the different mass distribution across the metallicity.

4.6.2 Catalogs of wide binaries

We provide two catalogs electronically for wide binaries with LASP and DD-Payne metallicities, respectively. These wide binaries are the sample used in Fig. 4.3, and they follow the selection criteria detailed in Sec. 4.2.3. Table 5.2 tabulates the descriptions for the catalogs. Fields starting with the prefix '0_' are the information for the LAMOST stars, and those starting with the prefix '1_' are for the wide companions. Pairs where both stars were observed by LAMOST have two entries in the catalogs.

4.6.3 Tables of numerical data

We tabulate the numerical data used in Fig. 4.3, 4.4, and 4.5 in Table 4.2, 4.3, 4.4, and 4.5.
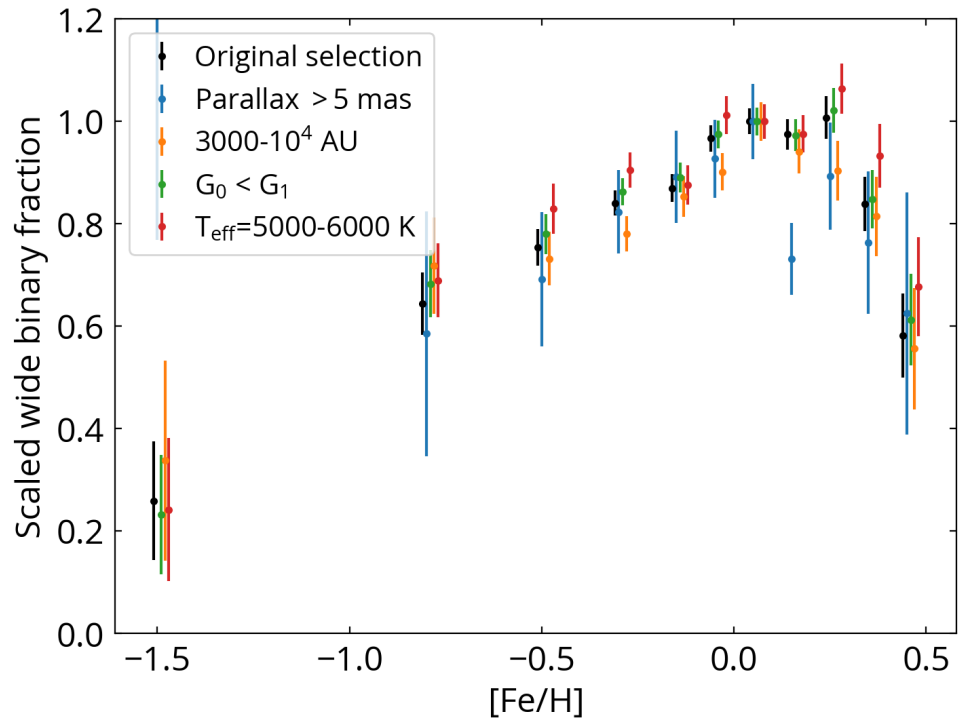
Figure 4.8: The test of different selection criteria. The black points show the original result from Fig. 4.3, and other colors show the results when one certain selection criterion is changed. The points are offset horizontally for clarity. These tests agree well with our main result, supporting that our conclusions are robust against different selection details.

Table 4.1: Descriptions for the wide binary catalogs.

Field	Description
0_source_id	Gaia DR2 source_id of the LAMOST star
0_ra	Right ascension of the LAMOST star from Gaia DR2 (J2015.5; deg)
0_dec	Declination of the LAMOST star from Gaia DR2 (J2015.5; deg)
0_parallax	Parallax of the LAMOST star from Gaia DR2 (mas)
0_parallax_error	Uncertainty in 0_parallax from Gaia DR2 (mas)
0_pmra	Proper motion in right ascension direction of the LAMOST star from Gaia DR2 (mas yr^{-1})
0_pmra_error	Uncertainty in 0_pmra (mas yr^{-1}) from Gaia DR2
0_pmdec	Proper motion in declination direction of the LAMOST star from Gaia DR2 (mas yr^{-1})
0_pmdec_error	Uncertainty in 0_pmdec (mas yr^{-1}) from Gaia DR2
0_g	Apparent G-band magnitude of the LAMOST star from Gaia DR2 (mag)
0_designation[a]	LAMOST designation from the LASP catalog
0_starid[b]	Star ID from the DD-Payne catalog
0_feh	Iron abundance of the LAMOST star measured by LASP or DD-Payne (dex)
0_teff	Effective temperature of the LAMOST star measured by LASP or DD-Payne (K)
0_logg	Surface gravity of the LAMOST star measured by LASP or DD-Payne (log cgs)
0_vtot	Total velocity (v_{tot}) with respect to the local standard of rest ($\mathrm{km\,s^{-1}}$)
0_zmax	The maximum Galactic height of the Galactic orbits, z_{max} (kpc)
1_source_id	Gaia DR2 source_id of the companion star
1_ra	Right ascension of the companion star from Gaia DR2 (J2015.5; deg)
1_dec	Declination of the companion star from Gaia DR2 (J2015.5; deg)
1_parallax	Parallax of the companion star from Gaia DR2 (mas)
1_parallax_error	Uncertainty in 1_parallax from Gaia DR2 (mas)
1_pmra	Proper motion in right ascension direction of the companion star from Gaia DR2 (mas yr^{-1})
1_pmra_error	Uncertainty in 1_pmra (mas yr^{-1}) from Gaia DR2
1_pmdec	Proper motion in declination direction of the companion star from Gaia DR2 (mas yr^{-1})
1_pmdec_error	Uncertainty in 1_pmdec (mas yr^{-1}) from Gaia DR2
1_g	Apparent G-band magnitude of the companion star from Gaia DR2 (mag)
separation	Physical separation of the wide binary (AU)
rel_vel	Relative velocity of the wide binary projected on the sky ($\mathrm{km\,s^{-1}}$)

[a] This field is only in the LASP wide binary catalog. [b] This field is only in the DD-Payne wide binary catalog.

Table 4.2: Numerical data for Fig. 4.3

[Fe/H] bin	(-2.0, -1.0)	(-1.0, -0.6)	(-0.6, -0.4)	(-0.4, -0.2)	(-0.2, -0.1)	(-0.1, 0.0)
LASP	0.85±0.38%	2.11±0.20%	2.47±0.12%	2.75±0.08%	2.84±0.09%	3.16±0.08%
	(5/590)	(113/5364)	(434/17599)	(1174/42705)	(1015/35699)	(1418/44847)
DD-Payne	1.28±0.43%	2.38±0.16%	2.63±0.10%	2.81±0.07%	3.12±0.08%	3.10±0.08%
	(9/704)	(209/8765)	(653/24872)	(1595/56745)	(1388/44481)	(1440/46499)

[Fe/H] bin	(0.0, 0.1)	(0.1, 0.2)	(0.2, 0.3)	(0.3, 0.4)	(0.4, 0.5)
LASP	3.27±0.08%	3.19±0.10%	3.29±0.14%	2.74±0.17%	1.90±0.27%
	(1535/46935)	(1079/33854)	(593/17998)	(246/8968)	(50/2626)
DD-Payne	3.26±0.10%	2.92±0.13%	2.64±0.17%	2.30±0.25%	0.90±0.45%
	(1104/33853)	(527/18056)	(255/9659)	(82/3561)	(4/442)

Table 4.3: Numerical data for Fig. 4.4, left

[Fe/H] bin	(-2.0, -1.0)	(-1.0, -0.6)	(-0.6, -0.4)	(-0.4, -0.2)	(-0.2, -0.1)	(-0.1, 0.0)
$v_{tot} < 120\,\mathrm{km\,s^{-1}}$	0.98±0.69% (2/204)	2.15±0.23% (87/4038)	2.50±0.12% (414/16562)	2.76±0.08% (1161/42136)	2.85±0.09% (1011/35534)	3.17±0.08% (1418/44723)
[Fe/H] bin	(0.0, 0.1)	(0.1, 0.2)	(0.2, 0.3)	(0.3, 0.4)	(0.4, 0.5)	
$v_{tot} < 120\,\mathrm{km\,s^{-1}}$	3.27±0.08% (1533/46838)	3.19±0.10% (1078/33785)	3.30±0.14% (593/17966)	2.75±0.18% (246/8950)	1.91±0.27% (50/2622)	
[Fe/H] bin	(-2.0, -1.0)	(-1.0, -0.6)	(-0.6, -0.3)	(-0.3, 0.0)	(0.0, 0.5)	
120-250 $\mathrm{km\,s^{-1}}$	0.70±0.49% (2/287)	1.94±0.39% (25/1290)	1.99±0.38% (27/1359)	1.91±0.60% (10/524)	1.38±0.79% (3/218)	
$> 250\,\mathrm{km\,s^{-1}}$	1.01±1.01% (1/99)	2.78±2.78% (1/36)				

Table 4.4: Numerical data for Fig. 4.4, right

[Fe/H] bin	(-2.0, -1.0)	(-1.0, -0.6)	(-0.6, -0.4)	(-0.4, -0.2)	(-0.2, -0.1)	(-0.1, 0.0)
$z_{max} < 1\,\mathrm{kpc}$	0.80±0.56% (2/251)	2.13±0.25% (72/3383)	2.44±0.13% (347/14206)	2.72±0.08% (1065/39130)	2.86±0.09% (982/34315)	3.20±0.09% (1399/43765)
[Fe/H] bin	(0.0, 0.1)	(0.1, 0.2)	(0.2, 0.3)	(0.3, 0.4)	(0.4, 0.5)	
$z_{max} < 1\,\mathrm{kpc}$	3.28±0.08% (1510/46041)	3.20±0.10% (1067/33339)	3.32±0.14% (587/17707)	2.78±0.18% (245/8824)	1.94±0.27% (50/2578)	
[Fe/H] bin	(-2.0, -1.0)	(-1.0, -0.6)	(-0.6, -0.3)	(-0.3, 0.0)	(0.0, 0.5)	
1-5 kpc	1.11±0.64% (3/270)	2.07±0.33% (40/1931)	2.76±0.23% (144/5211)	2.45±0.24% (103/4196)	2.33±0.35% (44/1889)	
$z_{max} > 5\,\mathrm{kpc}$	< 1.44% (0/69)	2.00±2.00% (1/50)				

Table 4.5: Numerical data for Fig. 4.5

[Fe/H] bin	(-2.0, -1.0)	(-1.0, -0.6)	(-0.6, -0.4)	(-0.4, -0.2)	(-0.2, -0.1)	(-0.1, 0.0)
$v_{tot} < 30\,\mathrm{km\,s^{-1}}$	< 11% (0/9)	1.59±0.79% (4/252)	2.28±0.32% (51/2238)	2.83±0.17% (263/9308)	3.22±0.17% (375/11633)	3.33±0.14% (595/17888)
30-60 $\mathrm{km\,s^{-1}}$	3.23±3.23% (1/31)	2.52±0.50% (25/994)	2.53±0.19% (172/6786)	2.85±0.12% (550/19287)	2.73±0.13% (435/15944)	3.25±0.13% (613/18863)
60-120 $\mathrm{km\,s^{-1}}$	< 1.15% (0/87)	1.89±0.34% (31/1636)	2.48±0.23% (117/4724)	2.41±0.15% (246/10218)	2.56±0.20% (170/6635)	2.76±0.20% (191/6928)
[Fe/H] bin	(0.0, 0.1)	(0.1, 0.2)	(0.2, 0.3)	(0.3, 0.4)	(0.4, 0.5)	
$v_{tot} < 30\,\mathrm{km\,s^{-1}}$	3.59±0.13% (736/20481)	3.62±0.16% (525/14509)	4.06±0.24% (291/7174)	2.81±0.30% (85/3027)	2.64±0.59% (20/757)	
30-60 $\mathrm{km\,s^{-1}}$	3.15±0.13% (599/18991)	2.89±0.14% (405/14022)	2.86±0.19% (220/7680)	3.00±0.27% (121/4040)	1.52±0.35% (19/1246)	
60-120 $\mathrm{km\,s^{-1}}$	2.66±0.20% (173/6499)	2.86±0.25% (136/4753)	2.68±0.31% (76/2831)	2.23±0.36% (39/1745)	1.92±0.58% (11/572)	

Chapter 5

Wide binaries in the Galactic halo from the H3 survey

Halo wide binaries play a key role in understanding of wide binary formation and the nature of dark matter. By using Gaia EDR3, we search for resolved wide binary companions in the H3 survey, a large spectroscopic survey that targets for ~ 200, 000 stars and ~ 20% of them are halo stars. We identify 968 high-confidence wide binary candidates. Based on their Galactic kinematics, about 50 of them are halo wide binaries and many of them are likely associated with the accreted *Gaia*-Sausage-Enceladus dwarf galaxy. We show that the wide binary fraction in the disk decreases toward the low metallicity end. Once the metallicity is controlled, the halo wide binary fraction is consistent with that of the disk stars. Furthermore, no dependence of the wide binary fraction on α abundance is found. These results suggest that the metallicity is the main driver of the wide binary fraction, and our leading explanation is that lower-metallicity formation environments tend to have higher stellar densities that disrupt wide binaries. Our results further imply that disrupted globular clusters do not contribute to a significant fraction of the halo.

5.1 Introduction

Because wide binaries are weakly bound, they can be disrupted by the gravitational interaction with other structures in the Milky Way. In particular, halo wide binaries can constrain the nature of dark matter (Chaname and Gould, 2004; Quinn et al., 2009). Orbital velocities of distant wide binaries can place independent constraints on the modified gravity theory (Hernandez, Jiménez, and Allen, 2012). Furthermore, with many disrupted accreted galaxies revealed by the Gaia mission (Belokurov et al., 2018; Helmi et al., 2018; Belokurov et al., 2020a; Helmi, 2020) and large spectroscopic surveys (Conroy et al., 2019b; Naidu et al., 2020), halo wide binaries provide a different view of the formation environments of these progenitor dwarf galaxies in the early Universe.

Halo wide binaries are vital to understanding wide binary evolution. Wide binaries in the disk may be disrupted by molecular clouds, passing stars, and Galactic tides (Retterer and King, 1982; Bahcall, Hut, and Tremaine, 1985; Weinberg, Shapiro, and Wasserman, 1987; Jiang and Tremaine, 2010). In contrast, halo wide binaries are less likely to be disrupted by molecular clouds and passing stars because they spend most of their lifetime outside the disk. Even when the halo wide binary passes through the disk, its high spatial velocity makes the passage time short, and so it is less likely to be disrupted (Weinberg, Shapiro, and Wasserman, 1987). Therefore, a detailed comparison between the properties of disk and halo wide binaries is able to reveal the gravitational interactions in the Milky Way.

Recent studies have shown that the majority of wide binaries at around

solar metallicities have similar chemical abundances within measurement uncertainties (Andrews, Chanamé, and Agüeros, 2018; Andrews et al., 2019; Hawkins et al., 2020; Nelson et al., 2021). The chemical homogeneity among these wide binaries suggests that these wide binaries are co-natal (Kamdar et al., 2020), resulting from a well-mixed interstellar medium in their formation environments (Feng and Krumholz, 2014). The level of chemical homogeneity among these wide binaries is one key test for chemical tagging (Andrews, Chanamé, and Agüeros, 2018; Andrews et al., 2019; Hawkins et al., 2020), a promising technique to reconstruct the formation history of the Milky Way using chemical abundances (Freeman and Bland-Hawthorn, 2002; Ting, Conroy, and Goodman, 2015). However, this assumption has not been tested at low metallicities ([Fe/H]< −1), which is of particular importance for old disk stars and the halo. Therefore, assembling a sample of low-metallicity wide binaries is critical for testing chemical tagging in this metallicity regime.

The metallicity dependence of the wide binary fraction is crucial for understanding wide binary formation. Our recent study shows that the wide binary fraction in the disk peaks at the solar metallicity and decreases both the low- and high-metallicity ends (Hwang et al., 2021). We propose several hypotheses that may explain the metallicity dependence, including the different stellar density in the formation environments at different Universe ages, the dynamical unfolding of compact triples, and the radial migration of Galactic orbits. Since halo wide binaries are probing a different part of the parameter space, their metallicity dependence is helpful to constrain these possible scenarios.

Despite of the wide applications, halo wide binaries have been challenging to identify in the past. First, the density of halo stars is low compared to that of the disk in the solar neighborhood, less than 0.2 per cent of local stars (Helmi, 2008). Therefore, assembling a large halo star sample is not straightforward in the first place. Second, identifying a resolved companion as the wide binary companion is challenge before the Gaia era. Even the Gaia mission provides the proper motions and parallaxes for billions of stars (Gaia Collaboration et al., 2016), most of the wide binary samples are still limited within 1 kpc (El-Badry and Rix, 2018; Hartman and Lépine, 2020; El-Badry, Rix, and Heintz, 2021), where the number of halo stars is insufficient to place a useful constraint on the halo wide binary fraction (Hwang et al., 2021).

In this paper, we overcome these difficulties by having a customized wide binary search for halo stars in the H3 survey. H3 survey is a large spectroscopic survey targeting specifically for the halo stars (Conroy et al., 2019a). It is expected to have ~200,000 stars at the end of the survey, and about 40,000 of them are kinematic halo stars. Since most of the H3 stars are more than 1 kpc away, we optimize the wide binary method for the H3 stars to maximize the resulting information.

The paper is structured as follows. Section 5.2 describes the H3 and Gaia dataset and the general criteria for the sample. Section 5.3 details the methods of wide binary search and presents their results. Section 5.4 explores the properties of the selected wide binary candidates and investigates the metallicity dependence of the wide binary fraction. We then discuss the implications in Section 5.5 and conclude in Section 5.6. Throughout the paper, we use 'wide

binaries' and 'wide binary candidates' interchangeably when we refer to the selected wide binaries, because there is always some non-zero probability that our wide binaries are not genuine. We also use 'metallicity' and 'iron abundance' ([Fe/H]) interchangeably. We use the notation 'binary' even if some of them may have unresolved companions and therefore are in fact triples or higher-order multiples.

5.2 Sample selection

5.2.1 H3 survey

The H3 ('Hectochelle in the Halo at High Resolution') survey is a high-resolution spectroscopic ($R \approx 23,000$) survey targeting for halo stars (Conroy et al., 2019a). The survey is conducted by the 6.5-m MMT with a wavelength coverage of 5150-5300Å. The survey has been collecting data since 2017. The main selection of H3 is composed of the following criteria: (1) $15 < r < 18$ where r is the $r-$band magnitude from Pan-STARRS (Chambers et al., 2016; Flewelling et al., 2016); (2) $\pi - 2\sigma_\pi < 0.5$ mas where π and σ_π are parallaxes and parallax uncertainties from Gaia Data Release 2 (Gaia Collaboration et al., 2018a); (3) $|b| > 30°$ to avoid disk stars; (4) declination $> -20°$ to be observable from MMT. The H3 survey has secondary selections targeting for stellar streams, K giants, blue horizontal branch stars, and RR Lyrae. This simple selection of magnitudes and parallaxes provides an unbiased view of the distant Milky Way.

The stellar parameters are measured from the H3 spectra using MINESweeper (Cargile et al., 2020). MINESweeper is a Bayesian framework that incorporates

149

the information from H3 spectra, broadband photometry, and priors like Gaia parallaxes to fit a model based on model based on the `MIST` (v2.0) stellar isochrones (Dotter, 2016; Choi et al., 2016). Cargile et al., 2020 show that the stellar parameters of benchmark stars and clusters measured by `MINESweeper` are in good agreement with literature values. In this paper, we use the radial velocities, distances, iron abundances ([Fe/H]), alpha-element abundances ([α/Fe]), extinction (A_V) measured from `MINESweeper`.

In this paper, we use the H3 data from `rcat_V3.0.2.d20201005_MSG.fits`. We require `flag==0` and signal-to-noise (S/N) ratios > 3 to avoid unreliable stellar parameter measurements. Targets from the Sagittarius stream selection (`Sgr_FLAG==1` and those from the stream tiles (tileID starting with 'tb') are excluded. Most of the targets were observed by H3 one time. For stars that were observed by H3 multiple times, we use the entries with highest signal-to-noise ratios. These selections result in a parent sample of 101,667 unique H3 stars for wide binary search.

5.2.2   Gaia survey

Gaia is an all-sky survey that provides optical broad-band photometry and high-precision astrometric measurements (Gaia Collaboration et al., 2016). Gaia Early Data Release 3 (EDR3) (Gaia Collaboration et al., 2020) was released in December 2020, with parallaxes and proper motions available for 1.5 billion sources down to Gaia G-band magnitudes of $\sim$ 21 mag. Gaia also measures the radial velocities for bright stars ($G < 15$), but most halo stars are fainter than this magnitude limit. This is one of the H3 survey's motivations to observe a

large number of halo stars below 15 mag.

We use Gaia EDR3 to search for the comoving companions around the H3 stars. Because H3 target selection uses Gaia's parallaxes and because Gaia obtains astrometric solutions using parallaxes and proper motions at the same time, all H3 targets have proper motions from Gaia.

The goal of this paper is to search for H3 stars' wide companions that have nearly identical Gaia proper motions as the H3 targets. We query a field star sample from Gaia EDR3 to conduct the wide binary search. For this field star sample, we only require that their proper motions be available in Gaia EDR3 (`astrometric_params_solved==` 31 or 95). We do not apply any criteria on magnitudes and astrometric quality indicators (e.g. `ruwe`) to maximize the chance finding the companions. Our wide binary selection compares the proper motions for each pair, which implicitly requires good astrometric quality. It is inevitable that we may miss some genuine wide binaries because some of their stars have worse astrometric quality, but chances are extremely low for a chance-alignment pair to be selected as a wide binary because of their bad astrometric quality.

Gaia EDR3's ability to resolve pairs starts dropping significantly at 0.7", and at 0.5"separations about 50% of pairs can be spatially resolved (Fabricius et al., 2020). We do not use Gaia's BP-RP colors for our wide binary selection, but we do use them to understand the properties of the selected wide binaries. When BP-RP colors are used in the analysis, we require their `bp_flux_over_error` and `rp_flux_over_error` to be larger than 10. Unlike G-band photometry, BP and RP fluxes do not have de-blending treatment and

therefore their fluxes can be affected by nearby sources within about 2″(Riello et al., 2020). To ensure that BP-RP colors are not strongly affected by the nearby sources, we apply an additional criterion of `phot_bp_rp_excess_factor`< 1.4 when BP-RP colors are used in the analysis.

5.2.3 Orbital parameter calculations

We measure the parameters for Galactic orbits, especially the total energy (E_{tot}) and the angular momentum along the Galactic z-direction (L_z), using `Gala` v1.1 (Price-Whelan et al., 2020). During the calculations, we use the Galactocentric frame from `Astropy` (Robitaille et al., 2013; Astropy Collaboration et al., 2018): Sun's Galactocentric radius R_0 = 8.122 kpc (Gravity Collaboration et al., 2019), solar motion with respect to the local standard of rest [$V_{R,\odot}$, $V_{\phi,\odot}$, $V_{Z,\odot}$]=[−12.9, 245.6, 7.78] km s^{-1}(Drimmel and Poggio, 2018), and Sun's current Galactic height $Z_\odot$ = 20.8 pc (Bennett and Bovy, 2019). The Milky Way potential `MilkyWayPotential` (Bovy, 2015) is adopted. Using different Milky Way potential models does not change the results significantly (Naidu et al., 2020). A right-handed coordinate is used, and thus a star on a prograde (retrograde) orbit has a negative (positive) L_z.

The observational inputs for orbital parameter calculations are the radial velocities and distances measured from H3 spectra using `MINESweeper`, and celestial coordinates and proper motions measured from Gaia EDR3. Following Naidu et al., 2020, to obtain robust orbital parameters, when we use E_{tot} and L_z in the analysis, we require that (i) $|E_{tot}|/\sigma_{E_{tot}} > 3$ and $|L_z|/\sigma_{L_z} > 3$; or (ii) $\sigma_{E_{tot}} < 0.1 \times 10^5$ km^2 s^{-2} and $\sigma_{L_z} < 0.5 \times 10^3$ kpc km s^{-1}. The first condition

is a normal 3-σ uncertainty cut, and the second condition is to ensure that we keep halo stars with small L_z in the sample. Out of 101,667 H3 stars, 99,564 (97.9 per cent) of them satisfy these kinematic criteria.

5.3 Wide binary search

For a solar-mass wide binary with a semi-major axis of $> 1000\,\text{AU}$, its orbital Keplerian velocity is $< 0.7\,\text{km s}^{-1}$. Therefore, for a genuine wide binary, we expect its member stars to have nearly identical proper motions and, if they do not have unresolved close companions, similar radial velocities. Our wide binary search method depends on whether the radial velocities from H3 are available for both paired stars. Because of the fiber allocation limit, H3 stars are at least 20 arcsec away from other H3 targets. In Sec. 5.3.1, we search for wide binaries among the H3 stars where radial velocities are available for both paired stars, and in Sec. 5.3.2 we search for wide binaries without radial velocity information.

One key measurement for the wide binary search is the proper motion difference, δPM, of a pair. This is computed by

$$\delta PM = \sqrt{(\text{pmra}_1 - \text{pmra}_0)^2 + (\text{pmdec}_1 - \text{pmdec}_0)^2},\qquad(5.1)$$

where pmra_i and pmdec_i are the Gaia EDR3 proper motions in right ascension direction ($\mu_\alpha \cos\delta$) and in declination direction (μ_δ) for star i ($= 0$ or 1), respectively. With Gaia's proper motion precision at the relevant magnitudes, the typical uncertainties of δPM is $\sim 0.1\,\text{mas yr}^{-1}$, depending on the exact errors of the proper motions. The relative velocity difference projected in the

plane of sky is $\delta V = 4.7 \times \delta PM \times d$, where δV is in units of $\mathrm{km\,s^{-1}}$, δPM is in $\mathrm{mas\,yr^{-1}}$, and d is the heliocentric distance of the pair in kpc. Therefore, for a wide binary at 1 to 10 kpc, Gaia can measure their projected orbital velocity δV with uncertainties of $0.5 - 5\,\mathrm{km\,s^{-1}}$. This precision is sufficient to distinguish the genuine wide binaries where the orbital velocities are $< 1\,\mathrm{km\,s^{-1}}$ from random chance-alignment pairs where the typical velocity differences are several hundred $\mathrm{km\,s^{-1}}$ for the thick-disk and halo stars.

5.3.1   Selection A: when both stars were observed by H3

If there is a wide binary population among the H3 pairs (where both stars were observed by H3), we would expect an enhanced population with radial velocity difference at zero. Fig. 5.1 shows the radial velocity difference for the H3 pairs with different angular separations. To reduce the number of chance-alignment pairs, we only consider pairs where the parallax differences are within $3\,\sigma_\pi$. For pairs with $\delta PM < 0.5\,\mathrm{mas\,yr^{-1}}$ and separations $< 90\,\mathrm{arcsec}$ (blue line), there is an enhanced clustering with radial velocity differences $< 2\,\mathrm{km\,s^{-1}}$ (vertical dashed line), suggesting the presence of wide binaries among these pairs. The distribution of radial velocity differences for pairs with separations between 90 and 180 arcsec (orange) does not have significant enhancement at zero, and is similar to that of the chance alignment pairs (selected by $\delta PM > 5\,\mathrm{mas\,yr^{-1}}$, green histogram). Therefore, even with low proper motion differences, pairs with separations $> 90\,\mathrm{arcsec}$ are dominated by chance alignments.

We experiment with a few other selections and see if such wide binary

signal remains. We find that the enhancement at zero RV difference is still present, although weaker, for pairs with $\delta PM < 0.5$ mas yr^{-1} and separations between 60 and 90 arcsec. Therefore, there are wide binaries extending beyond 1 arcmin in the sample. We experiment with a selection of δPM between 0.5 and 1 mas yr^{-1}, but no significant wide binary signal at RV difference at zero is found.

Based on Fig. 5.1, we select wide binary candidates by (1) proper motion differences < 0.5 mas yr^{-1}; (2) angular separations < 90 arcsec; and (3) radial velocity differences < 2 km s^{-1}. With the SNR cut larger than 3 for both stars in a pair, these selections result in 7 wide binary candidates. 6 more wide binaries are included if the SNR cut is relaxed to 2. By comparing with the distribution of radial velocity difference for chance alignment in Fig. 5.1, we estimate that at most one of them might be a chance-alignment pair. We refer to this selection as *Selection A*, and the relevant numbers are summarized in Table 5.1.

All these wide binary candidates have angular separations between 20 and 90 arcsec, where the lower limit is caused by the H3's fiber allocation and the upper limit is due to our selection. Based on the distance measurements from MINESweeper, they have binary separations of $10^{4.5-5.5}$ AU. This result demonstrates the existence of wide binaries with separations up to $\sim 10^5$ AU in the H3 data.

Our selection only uses a rather relaxed criterion for parallaxes by requiring the parallax differences within $3\sigma_\pi$. It turns out that 6 of the 7 wide binaries have parallax differences within $0.7\sigma_\pi$, and the remaining one has a $1.2\sigma_\pi$

difference, far below the $3\sigma_\pi$ criterion. The small differences in the parallaxes of the selected candidates strongly suggest that most of these wide binaries are genuine.

Fig. 5.2 compares the iron abundances of member stars in the 7 wide binaries. Only 3 of them have iron abundances within 1σ of each other, and the other four all have iron abundance differences more than 2σ. Although the conclusion is still limited by its small number statistics, the inconsistent iron abundances may be due to surface abundance evolution (Dotter et al., 2017) or different evolution stages.

5.3.2 Selection B: when one star was observed by H3

For every H3 target, we search for their resolved wide companion in Gaia within 60 arcsec. In most of the cases, only the H3 target has radial velocity available, so we cannot compute radial velocity difference among the pair to help the selection. Most H3 targets are distant (> 1 kpc) and therefore we do not have precise distances inferred from the Gaia parallaxes for H3 targets. The distance precision measured from MINESweeper is not sufficient to distinctly separate the wide binary population from the random chance-alignment pairs in the relative velocity-physical separation space. Without distances, proper motion differences and angular separations cannot be converted to velocity difference and physical separations. Compared to the comoving companion search using relative velocities and physical separations, using proper motion difference and angular separation would have a higher level of contamination, and its searching sensitivity depends more on the distance of the targets.
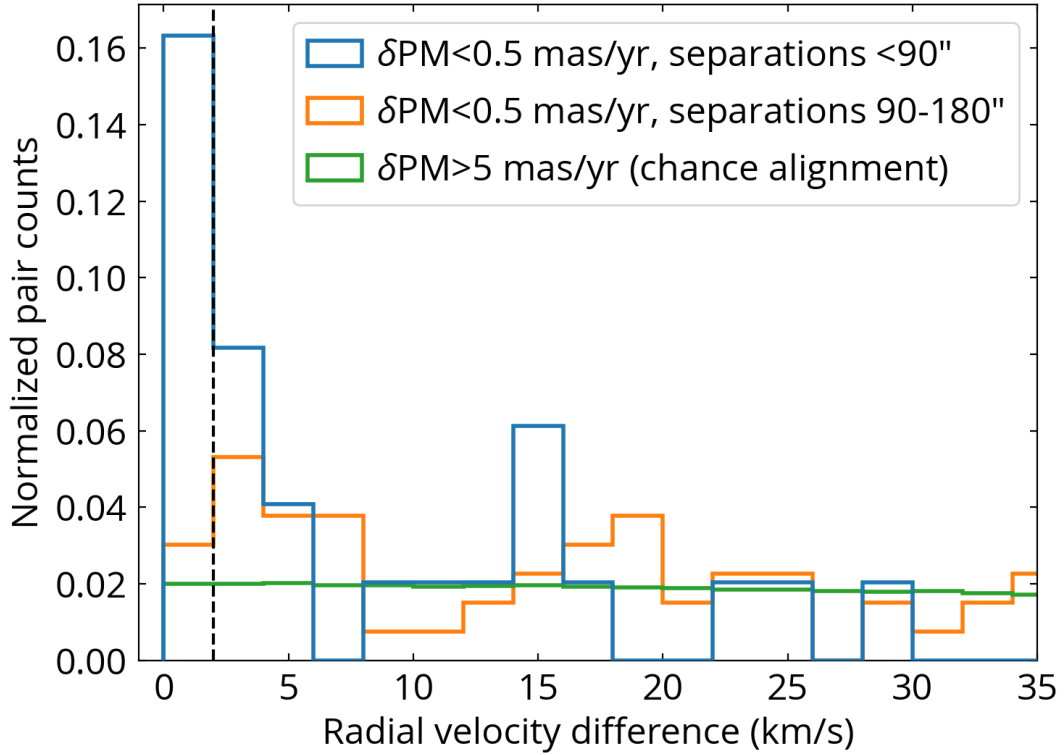
Figure 5.1: The radial velocity differences among the pairs where both stars were observed by H3. The orange, green, and red histograms show the results for the low-proper-motion-difference sample at different angular separations. The blue histogram shows the radial velocity differences of the chance-alignment pairs selected by high proper motion differences ($\delta PM > 5 \, \text{mas} \, \text{yr}^{-1}$). The low-proper-motion-difference sample at small angular separations shows a significant enhancement at zero radial velocity difference, indicative of the existence of wide binary population. The vertical dashed line marks $2 \, \text{km} \, \text{s}^{-1}$, the criterion used in our selection.
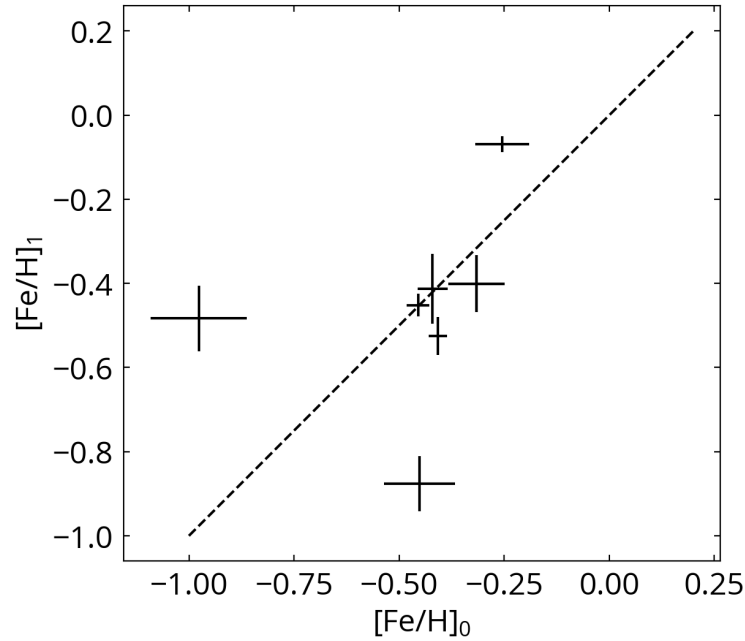
Figure 5.2: The difference in the iron abundance ([Fe/H]) of both components of the wide binary from Selection A.

Fig. 5.3 (left panel) shows the proper motion differences and angular separations of all the pairs consisting of H3 stars. To reduce the contamination, we require that the parallax difference of the pair is consistent within $3\sigma_\pi$. An enhanced population with separations < 10 arcsec and proper motion differences $\lesssim 1 \, \mathrm{mas\,yr^{-1}}$ can be seen, indicative of the resolved wide binary populations. The rest of the pairs are chance projection.

To better quantify the contamination from the chance-alignment pairs, we conduct a test by offsetting the H3 targets' Galactic latitudes by 1 degree (and the coordinates of field stars remain the same) and redo the wide binary search. Pairs consisting of two H3 targets are excluded. Therefore, all the pairs from this test are chance-alignment pairs. The result is shown in Fig. 5.3, middle panel. This contamination test well reproduces the chance-alignment

pairs in the left panel, except that the left panel has an additional wide binary population at small angular separations and small proper motion differences.

In the right panel of Fig. 5.3, we compute the chance alignment probability (CAP) in each two-dimensional bin. Specifically, CAP in every bin is calculated by the number of pairs in the middle panel divided by the number of pairs in the left panel. The right panel of Fig. 5.3 shows that the wide binaries can be selected by small proper motion differences with CAP less than 10% out to 30 arcsec. There still seems to have CAP less than 20% at low proper motion differences and separations larger than 30 arcsec, but it may be due to the shot noise caused by the low number counts so we do not focus on them.

We adopt an empirical straight line (the dashed lines in Fig. 5.3) in the log(proper motion difference)-separation space to select the high-confidence wide binaries. Specifically, This straight line starts from PMD = 1.6 mas yr^{-1} at 0 separation to PMD= 0.1 at 30 arcsec. This selection results in 961 wide binary candidates, and the contamination test in the middle panel of Fig. 5.3 suggests that ~ 24 (3 per cent) of them may be chance-alignment pairs.

5.4   Properties of wide binaries

5.4.1   H-R diagram

Fig. 5.4 shows the H-R diagram of the wide binaries, where the absolute G-band magnitudes are computed using the distances measured from MINESweeper. Most of the wide binaries identified here are main-sequence stars, and some are located on the giant branch. The companions scatter more around the main sequence track because they are fainter and more likely to have unreliable

159
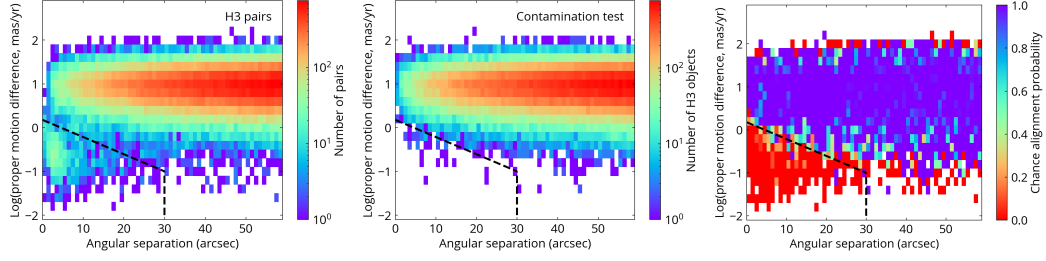
Figure 5.3: The wide binary search in the proper motion difference-angular separation space. Left: the distribution for all the pairs consisting of an H3 star. In addition to the chance-alignment pairs dominating at the upper-right part, there is an enhanced wide binary population with small proper motion differences and small angular separations. Middle: the contamination test where the H3 stars' Galactic latitudes are offset by 1 arcmin. Therefore, all the pairs in this panel are chance-alignment pairs. Right: the chance-alignment probability computed from the left and middle panel. Based on the chance-alignment probability, we use an empirical selection (the dashed lines in the three panels) to select high-confidence wide binaries.

colors.

For a genuine wide binary, we would expect both component stars to be located on the same isochrone with the same metallicity. To investigate this, we use the [Fe/H] and [α/Fe] measured from the H3 stars and see whether the companion stars are located close to the corresponding MIST isochrone in the H-R diagram. We define color deviation Δ(BP-RP) by:

$$\Delta(BP - RP)_i = (BP - RP)_i - (BP - RP)_{iso,i},\tag{5.2}$$

where $(BP - RP)_i$ is the observed Gaia BP-RP color for star i, and $(BP - RP)_{iso}$ is the expected BP-RP color from the MIST isochrone for the star. Specifically, we compute the MIST isochrone using brutus [1] given the measured [Fe/H], [α/Fe], and A_V of the H3 star, assuming a stellar age of 10 Gyr. Then for the star of interest (H3 star or its companion), $(BP - RP)_{iso,i}$ is computed from

---

[1] https://github.com/joshspeagle/brutus

the isochrone given the absolute G-band magnitude of the star. The last step requires that an absolute magnitude only maps to a single BP-RP value, which is satisfied for the main-sequence phase and part of the giant phase. Because the isochrone has included the extinction A_V, the resulting $\Delta(BP - RP)_i$ is extinction corrected.

Fig. 5.5 shows the distribution of $\Delta(BP - RP)$ for the H3 stars, companion stars, and the chance-alignment stars. The H3 stars are concentrated at $\Delta(BP - RP)_{H3} = 0$, which is expected because this is how MINESweeper uses broadband photometry and MIST isochrone to derive relevant quantities like distances. The $\Delta(BP - RP)_{companion}$ is also highly clustered around 0, indicating that these companions are located close to the expected isochrone. The deviation of $\Delta(BP - RP)_{companion}$ from being exactly at 0 may be due to the uncertainties in their photometry (especially that most of the companions are fainter than the H3 stars), the presence of unresolved companions around the H3 stars or the companions (while isochrones assume that they are single stars), or that they are not genuine wide companions. For comparison, chance-alignment pairs selected by proper motion differences $> 5\,\mathrm{mas\,yr^{-1}}$ have $\Delta(BP - RP)_{companion}$ with a wide range of scatter and does not concentrate around a certain value. Fig. 5.5 supports that the majority of the wide binary candidates are indeed genuine wide binaries.
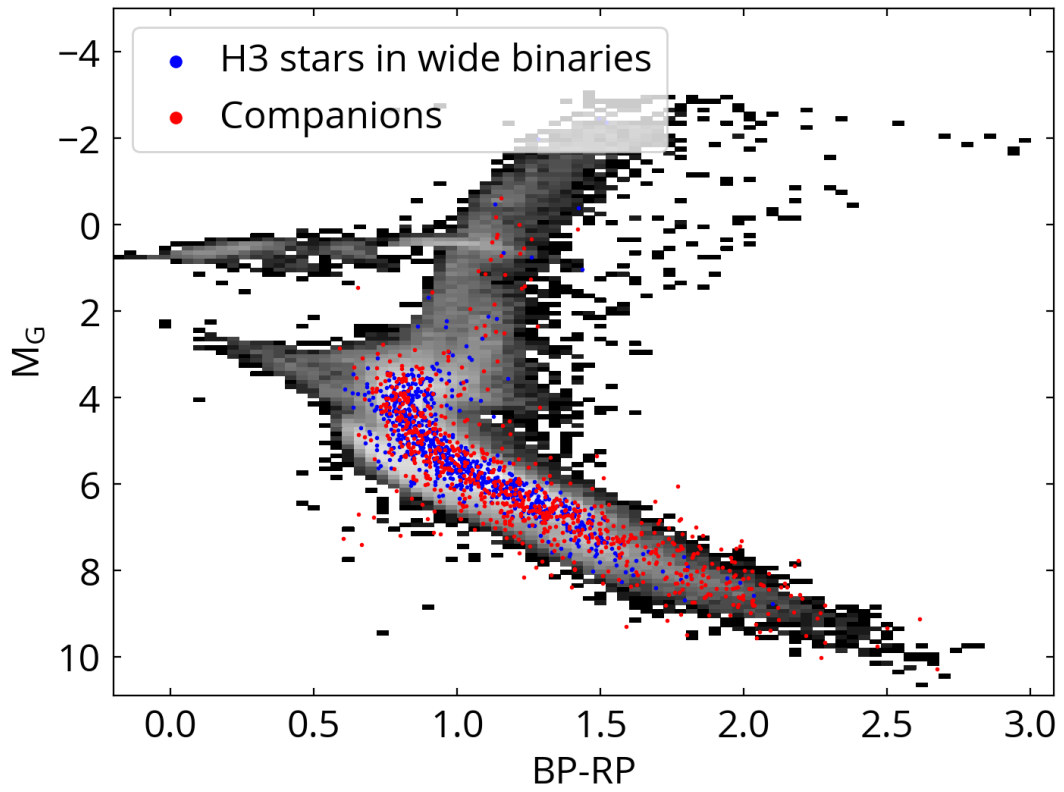
Figure 5.4: The H-R diagram of the wide binaries. The red points show the H3 targets in the wide binaries, and the blue points are the companions. Most of the wide binaries are main-sequence stars.
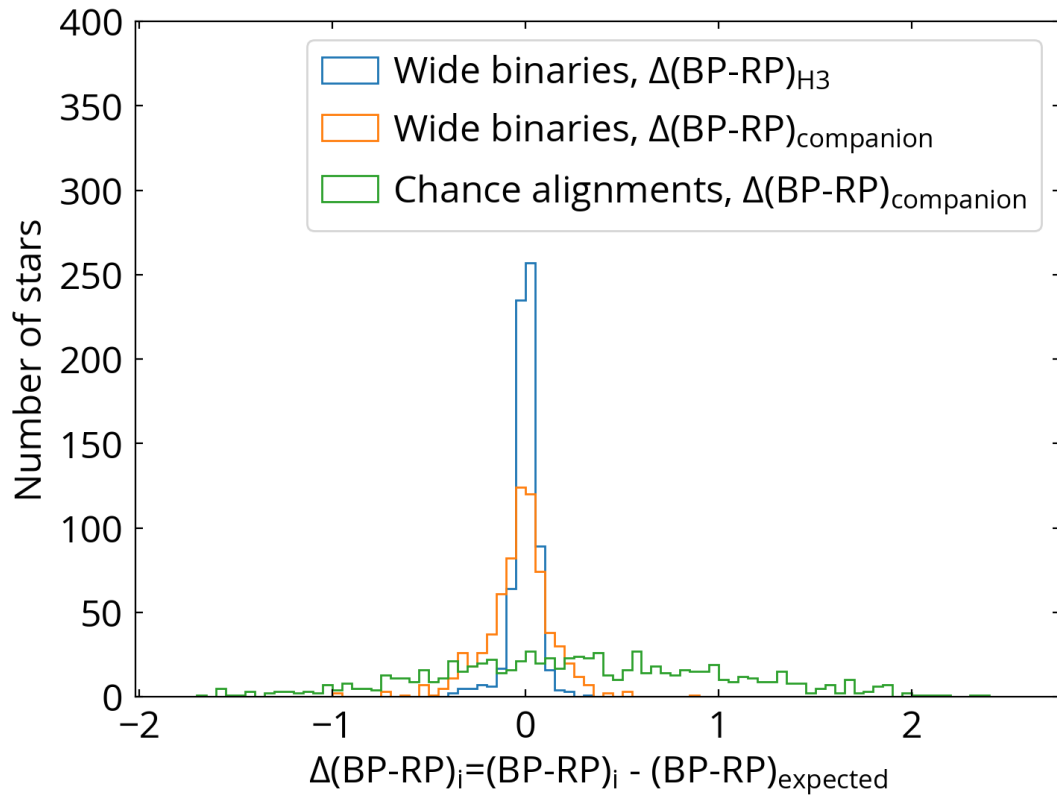
Figure 5.5: The distribution of color deviation $\varDelta(BP - RP)$, defined in Eq. 5.2. The color deviation of the companions are strongly concentrated around 0, meaning that they are located at the reasonable region in the H-R diagram. In contrast, the companions from chance-alignment pairs have a wide range of color deviations. This comparison supports that most of the wide binaries are genuine and are not chance-projection pairs.
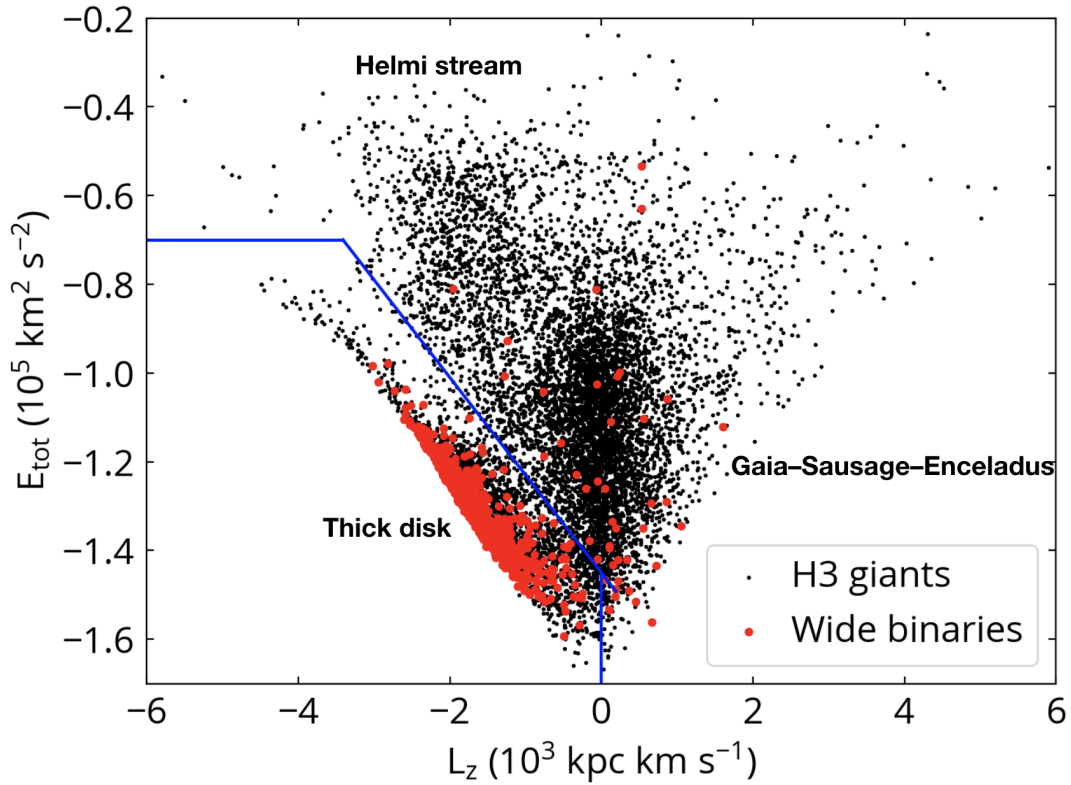
Figure 5.6: The Galactic orbits of stars in the E_{tot}-L_z space. The H3 giant stars (black points) illustrate the kinematic substructures in the halo, with texts highlighting the prominent structures. The wide binaries are shown as red points. Blue wedge is the empirical demarcation line used to distinguish the disk and halo stars. Most of the wide binaries are in the disk. There are about 50 halo wide binaries, and many of them can be associated with the accreted Gaia-Sausage-Enceladus dwarf galaxy.

5.4.2 Galactic kinematics

Fig. 5.6 shows the H3 giants (black points) and the wide binaries (red points) in the E_{tot}-L_z space. We apply the criteria detailed in Sec. 5.2.3 to have reliable kinematic measurements, resulting in 951 wide binaries. The distance distributions vary in the E_{tot}-L_z space. In particular, the (thick) disk stars are on average closer to the Sun than the halo stars. Therefore, using the H3 giants alone (selected by $\log g < 3.5$) presents a relatively unbiased view with respect to the distances of the substructures in the halo out to ~ 50 kpc (Naidu et al., 2020). Several structures are present in Fig. 5.6, including high-α disk (thick disk), in-situ halo, and other substructures that can be connected to previous accretion events like Sagittarius and *Gaia*-Sausage-Enceladus, as detailed in Naidu et al. 2020. For the wide binary sample, we do not apply the $\log g$ criterion. As a result, compared to the H3 giants, a larger number of main-sequence wide binaries are located in the disk locus in Fig. 5.6. It is particularly interesting that several wide binaries have E_{tot} and L_z associated with halo substructures, especially *Gaia*-Sausage-Enceladus, in Fig. 5.6.

We use the E_{tot}-L_z plane to separate the halo and thick disk populations. The blue solid line in Fig. 5.6 is our empirical demarcation line, with thick disk stars located in the lower-left part and the halo stars for the rest. The disk-star selection is: (1) $E_{tot} < -0.7 \times 10^5 \, \text{km}^2 \, \text{s}^{-2}$; and (2) $L_z < 0$; and (3) $E_{tot,5} < -1.45 - 0.22 L_{z,3}$, where $E_{tot,5} = E_{tot}/(10^5 \, \text{km}^2 \, \text{s}^{-2})$ and $L_{z,3} = L_z/(10^3 \, \text{kpc} \, \text{km} \, \text{s}^{-1})$. With this selection, we have 1151 (95%) thick-disk wide binaries and 60 (5%) halo wide binaries from Selection B. All wide binaries from Selection A belong to the disk.

5.4.3 The metallicity dependence of the wide binary fraction

To investigate the metallicity dependence of the wide binary fraction, we need to make sure that the sample properties are similar across the metallicity. In particular, lower-metallicity stars are more likely to be halo stars and may be located at larger distances. Therefore, a lower wide binary occurrence rate at lower metallicities may result from the fact that binaries at larger distances are more difficult to resolve due to the spatial resolution limit, and also their companions may be too faint to be detected in Gaia with good astrometric measurements. Furthermore, different mass range is probed at different distances because lower-mass main-sequence stars may be too faint at larger distances. Therefore, to compare the wide binary fraction at different metallicity, we need to ensure that these property distributions (e.g. distances) are similar across the metallicity range of interest.

We use the halo sample as the benchmark sample, and use a Monte-Carlo method to construct several disk samples with different metallicities where their properties are star-by-star matched to the halo sample. Specifically, we have one disk sample where the metallicities of the disk stars are star-by-star matched to the halo sample with Δ[Fe/H]< 0.2, referred to as 'metallicity-matched disk sample'. In addition, we have other 5 disk samples where their [Fe/H] are in the bins of [-3, -2, -1, -0.5, 0, 0.5]. In this analysis, only wide binaries from Selection B are used.

These disk star samples are assembled by star-by-star matching to the halo star sample's properties. Specifically, for a given halo star, its matched disk

stars have (1) distance differences < 10% of the halo star's distance, and (2) BP-RP color differences < 0.2 mag. The former criterion ensures that the matched disk star sample has the same distance distribution as the halo sample, and the latter criterion is to select a disk sample with similar color and therefore mass distribution. Then, the [Fe/H] criterion is imposed depending on the type of the disk sample. Then among the disk stars that satisfy these matching criteria, we randomly assign one of them to that specific halo star. Therefore, for one halo star, there are 6 matched disk stars with different metallicity criteria. If any one of the matched disk star is not found, then that specific halo star is excluded.

The parent halo sample consists of 20912 stars. Because of the poor detectability of wide binaries and the difficulty of finding a matched disk star at large distances, we require that the halo stars have distances < 5 kpc, reducing the sample size to 11462. Then we search for the disk stars that matched to the halo star sample. In the end, 11373 halo stars have successful matched disk stars. 89 halo stars are excluded because not all matched stars are found, mostly because their distances are too large (> 4 kpc) or too small (< 1 kpc). Then in every halo and disk sample, we compute its wide binary fraction, which is the number of wide binaries in the sample divided by the total number of the sample (i.e. 11373).

While we do not explicitly match the α abundances, the resulting samples turn out to have similar mean α abundances. Except for the disk sample at [Fe/H]> 0 that has a mean [α/Fe] of 0.122 ± 0.001, other disk samples and the halo sample have mean [α/Fe] between 0.2 and 0.3. Therefore, the dependence

on α abundance plays a minor role when we investigate the iron abundance dependence among these samples. The dependence on α abundance will be investigated further in Sec. 5.4.4.

Fig. 5.7 shows the wide binary fraction as a function of metallicity for the halo and disk samples. The [Fe/H] values are the mean metallicities in each sample, and the errors of the wide binary fraction are the Poisson uncertainties. For comparison, we overplot the results from Hwang et al., 2021 where our 500-pc sample is dominated by the thin-disk stars, with [Fe/H] values indicating the centers of the bins. The wide binary fraction from Hwang et al., 2021 is multiplied by an arbitrary factor of 0.2 for better visual comparison. The wide binary fractions from this work and Hwang et al., 2021 can only be compared in a relative sense (i.e. the overall metallicity trend) but not in an absolute sense, because they use samples that have different range of wide binary separations and different detection limit for the companions.

Fig. 5.7 shows that the wide binary fraction in the disk decreases towards the low-metallicity end. This is similar to the trend from Hwang et al., 2021, but now this work extends the trend down to [Fe/H]= −3 where the nearby sample of Hwang et al., 2021 does not have any statistical power. On the other hand, the H3 sample has a limited number of stars at [Fe/H]> 0 and cannot investigate the decreasing metallicity trend at the high-metallicity end that appears in the result from Hwang et al., 2021. Therefore, the results of the H3 survey are highly complementary to the previous studies.

In Hwang et al., 2021, we attempt to differentiate the thick-disk stars and halo stars using total 3-dimensional velocities and the maximum Galactic

heights. We find that, as the entire population (regardless of the metallicity difference), the wide binary fraction of the halo stars is lower than that of the thick disk. But at a fixed metallicity, the wide binary fraction of the halo seems consistent with that of the thick disk. However, there are only two possible halo wide binaries in Hwang et al., 2021, so the conclusion is still limited by small number statistics.

Here with a better kinematic selection and a larger halo wide binary sample, we are in a better position to investigate the difference (or not) between the disk and the halo sample. We find that the wide binary fraction of halo stars is consistent with that of the disk stars where the metallicities are matched. This suggests that metallicity is the main driver of the wide binary fraction, and that the disk and halo stars do not have significantly different wide binary fraction once the metallicity is controlled.

In Fig. 5.7 , we use the observed surface metallicity, but the surface metallicity may change over stellar evolution. Even on the main sequence, surface metallicity can change as much as 0.5 dex due to atomic diffusion and gravitational settling (Dotter et al., 2017). We investigate this effect by using initial metallicity computed based on the model from Dotter et al., 2017, and the results remain similar to Fig. 5.7.

5.4.4 Alpha abundances

We use a star-by-star matching method similar to Sec. 5.4.3 to investigate the α abundance dependence of the wide binary fraction. To ensure that our sample covers a wide range of α abundances, we focus on the disk sample
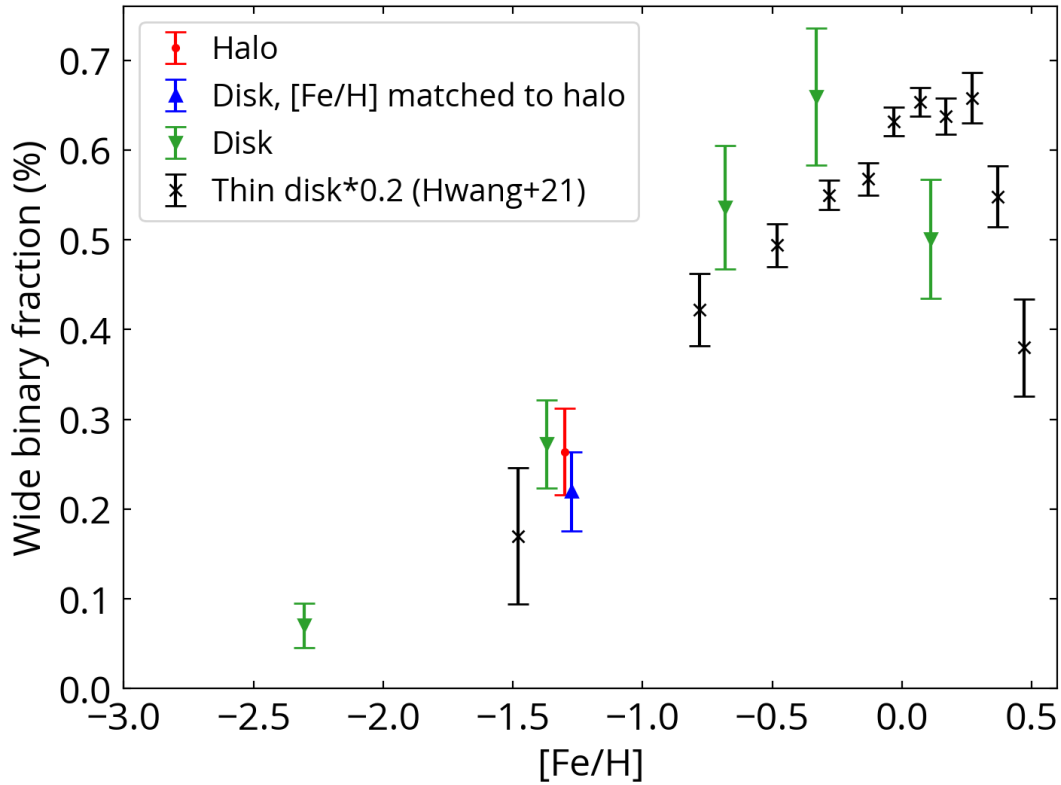
Figure 5.7: The wide binary fraction as a function of metallicity. The blue, orange, and green markers show the results from this study, with [Fe/H] values indicating the mean metallicity in each sample. The blue point is the wide binary fraction for the halo stars, and the orange point is that for the disk stars where their metallicities are star-by-star matched to the halo stars. The green points are the disk stars matched to halo stars but with different metallicities. The black points show the results from a thin-disk-dominated local sample (Hwang et al., 2021), where the [Fe/H] values are the centers of each metallicity bin. This plot shows that the wide binary fraction decreases towards the low-metallicity end. Also, the wide binary fractions of the halo and the disk are consistent once their metallicities are controlled.

with [Fe/H] between -1 and -0.5, using the disk star selection from Sec. 5.4.2. Then this sample is binned into 5 sub-samples by [α/Fe] from 0 to 0.5 with a step of 0.1 dex. The sub-sample with [α/Fe] between 0 and 0.1 is used as the benchmark sample, and we construct the star-by-star matching sample from other sub-samples. Specifically, for a given star in the benchmark sample, its matched stars in other sub-samples have (1) distance differences $< 10\%$, (2) BP-RP color differences < 0.2 mag, and (3) [Fe/H] differences < 0.1. Therefore, for a star in the benchmark sample (i.e. [α/Fe] between 0 and 0.1), it has 4 matched stars in different α abundance bins. If any of 4 matched stars is not found, we discard the star from the benchmark sample. After this procedure, we end up with 2346 disk stars in each [α/Fe] bin, and all these bins have similar distance distributions, color distributions, and [Fe/H] distributions. Then the wide binary fraction is computed in each bin by dividing the number of wide binaries found in Section B by the total number of stars in each sample.

Fig. 5.8 presents the wide binary fraction in the disk stars as a function of α abundance. The absolute values of wide binary fractions in this plot should not be directly compared to those in Fig. 5.7 because they use different benchmark samples and therefore have different distance distributions. Fig. 5.8 shows that the wide binary fraction does not significantly depend on α abundances, with the relative change in the wide binary fraction less than $\sim 20\%$ across the entire range of α abundances.
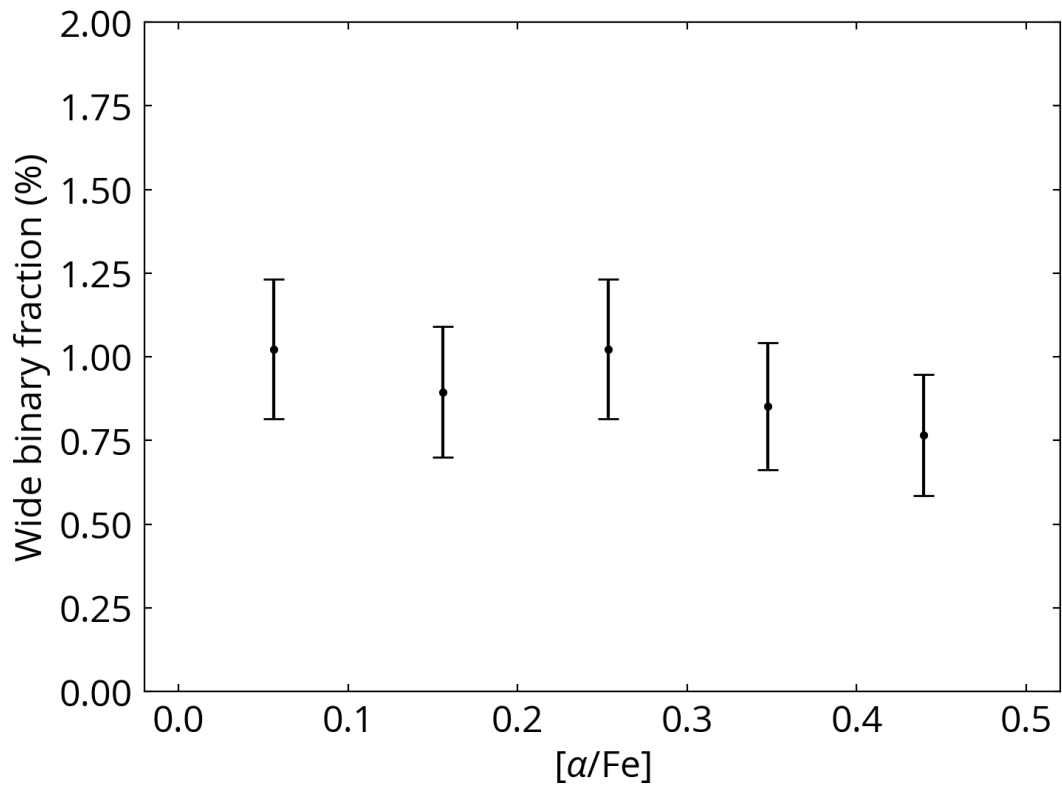
Figure 5.8: The wide binary fraction versus α-element abundance, where the iron abundances are controlled in each bin. The wide binary fraction is consistent with no dependence on α-element abundance.

Table 5.1: Summary of the selected wide binary candidates.

	Selection A	Selection B
Angular separations	20-60 arcsec	< 30 arcsec
Binary separations	$10^{4.5-5.5}$ AU	10^{3-5} AU
Number of wide binaries	7	961
Chance-alignment probability	< 1 pair	$4.6 \pm 0.7\%$
Number of halo/disk stars	0/7	50/909

5.4.5 Summary of the wide binary search and catalog

Table 5.1 provides the summary of the selected wide binary candidates. There are 7 wide binaries candidates from Selection A (Sec. 5.3.1) and 1000 from Selection B (Sec. 5.3.2). Selection A selects wide binaries with larger angular separations of $20 - 60$ arcsec (and therefore larger binary separations), and Selection B selects those with angular separations < 30 arcsec. Based on the kinematics, about 50 wide binaries are halo wide binaries.

We provide an electronic catalog for the wide binaries. Table 5.2 tabulates the descriptions for the catalog. Fields starting with the prefix '0_' are the information for the H3 stars, and those starting with the prefix '1_' are for the companions.

5.5 Discussions

5.5.1 Comparison with the literature

In the pre-Gaia era where high-precision parallaxes are not available for most of the stars, the reduced proper motion diagram is used to distinguish high-velocity halo stars from disk stars and to identify halo wide binaries. The

Table 5.2: Descriptions for the wide binary catalog.

Field	Description
method	The wide binary selection method.
0_source_id	Gaia EDR3 source_id of the H3 star
0_ra	Right ascension of the H3 star from Gaia EDR3 (J2016.0; deg)
0_dec	Declination of the H3 star from Gaia EDR3 (J2016.0; deg)
0_parallax	Parallax of the H3 star from Gaia EDR3 (mas)
0_parallax_error	Uncertainty in 0_parallax from Gaia EDR3 (mas)
0_pmra	Proper motion in right ascension direction of the H3 star from Gaia EDR3 (mas yr^{-1})
0_pmra_error	Uncertainty in 0_pmra (mas yr^{-1}) from Gaia EDR3
0_pmdec	Proper motion in declination direction of the H3 star from Gaia EDR3 (mas yr^{-1})
0_pmdec_error	Uncertainty in 0_pmdec (mas yr^{-1}) from Gaia EDR3
0_g	Apparent G-band magnitude of the H3 star from Gaia EDR3 (mag)
0_H3_ID^a	H3 id for the H3 star
0_FeH	Iron abundance of the H3 star measured by H3 (dex)
0_Teff	Effective temperature of the H3 star measured by H3 (K)
0_logg	Surface gravity of the H3 star measured by H3 (log cgs)
0_Vrad	Radial velocity of the H3 star measured by H3 (km s^{-1})
0_dist_adpt	Heliocentric distances of the H3 star measured by H3 (kpc)
0_Etot	Total orbital energy of the H3 star (10^5 km^2 s^{-2})
0_Etot_err	Uncertainty in 0_Etot (10^5 km^2 s^{-2})
0_Lz	Orbital momentum along the Galactic z-axis of the H3 star (10^3 kpc km s^{-1})
0_Lz_err	Uncertainty in 0_Lz (10^3 kpc km s^{-1})
1_source_id	Gaia EDR3 source_id of the companion star
1_ra	Right ascension of the companion star from Gaia EDR3 (J2016.0; deg)
1_dec	Declination of the companion star from Gaia EDR3 (J2016.0; deg)
1_parallax	Parallax of the companion star from Gaia EDR3 (mas)
1_parallax_error	Uncertainty in 1_parallax from Gaia EDR3 (mas)
1_pmra	Proper motion in right ascension direction of the companion star from Gaia EDR3 (mas yr^{-1})
1_pmra_error	Uncertainty in 1_pmra (mas yr^{-1}) from Gaia EDR3
1_pmdec	Proper motion in declination direction of the companion star from Gaia EDR3 (mas yr^{-1})
1_pmdec_error	Uncertainty in 1_pmdec (mas yr^{-1}) from Gaia EDR3
1_g	Apparent G-band magnitude of the companion star from Gaia EDR3 (mag)
1_H3_ID^a	H3 id for the companion star
1_FeH^a	Iron abundance of the companion star measured by H3 (dex)
1_Teff^a	Effective temperature of the companion star measured by H3 (K)
1_logg^a	Surface gravity of the companion star measured by H3 (log cgs)
1_Vrad^a	Radial velocity of the companion star measured by H3 (km s^{-1})
1_dist_adpt^a	Heliocentric distances of the companion star measured by H3 (kpc)
separation	Angular separation of the wide binary (arcsec)
pm_diff	Proper motion difference of the wide binary (mas yr^{-1})

^{a} These fields are only available for selection method==A.

reduced proper motion diagram uses proper motions as a proxy for distances because closer stars have larger proper motions, and halo stars are more separated because of their lower metallicities and higher spatial velocities (Salim and Gould, 2002). Using this method, previous studies have found 100-200 halo(-like) wide binary candidates (Chaname and Gould, 2004; Quinn and Smith, 2009; Allen and Monroy-Rodríguez, 2014; Coronado et al., 2018), and use them to constrain the mass of massive compact halo objects (Yoo, Chaname, and Gould, 2004; Quinn et al., 2009; Monroy-Rodríguez and Allen, 2014).

Reduced proper motion diagram uses photometry to distinguish halo and disk stars. However, lower-metallicity stars have higher close binary fraction (Moe, Kratter, and Badenes, 2019), plus that close binaries are more likely to have resolved wide companions (Hwang et al., 2020b), halo wide binaries selected from reduced proper motion diagram may preferentially exclude systems with unresolved companions. In contrast, since the wide binary selections used in this work depend only on the astrometry and not on photometry, our selections are not affected by unresolved companions. Also, reduced proper motion diagram can confuse halo stars with high-velocity thick-disk stars.

Gaia provides high-precision astrometry for billions of stars (Gaia Collaboration et al., 2016), making the search for a large number of wide binaries possible (Oh et al., 2017; El-Badry and Rix, 2018; Jiménez-Esteban, Solano, and Rodrigo, 2019; Hartman and Lépine, 2020). Using Gaia EDR3, El-Badry, Rix, and Heintz, 2021 have cataloged about a million wide binaries within 1 kpc. By

cross-matching this catalog the with median-resolution ($R \sim 1800$) LAMOST survey DR6 (Deng et al., 2012; Zhao et al., 2012) and using LAMOST's radial velocities to compute E_{tot} and L_z , we find that there are 50 halo wide binaries that satisfy the halo selection from Sec. 5.4.2 and SNR > 10 in g-band from LAMOST. We repeat the same procedure for the median-resolution ($R \sim 2000$) SEGUE DR9 (Yanny et al., 2009), ending up with 16 halo wide binaries with SNR > 10.

The 50 halo wide binaries and ~900 disk wide binaries found in this paper feature the largest wide binary sample with high-resolution spectroscopy. In addition to radial velocities that enable precise kinematic measurements, the high-resolution spectroscopy further provides reliable chemical abundances that are critical for the understanding of wide binary formation and evolution.

5.5.2 Origin of the iron-abundance dependence

Wide binary disruption by passing stars and other Galactic structures are unlikely to play an important role in our results. Most of the wide binaries from Hwang et al., 2021 have separations of $\sim 1000\,\mathrm{AU}$. The disruption timescale for these wide binaries is $\sim 100\,\mathrm{Gyr}$ (Weinberg, Shapiro, and Wasserman, 1987). The wide binaries identified in this paper have longer separations than Hwang et al., 2021 (a median separation of $7700\,\mathrm{AU}$), but their surrounding stellar densities are also much lower than Hwang et al., 2021, resulting a similar disruption timescale. Since their disruption timescales are longer than the age of Universe, the iron-abundance dependence of the wide binary fraction is not due to wide binary disruption over their lifetime.

Hwang et al., 2021 show that the wide binary fraction of thin-disk stars peaks around [Fe/H]= 0 and decreases towards both low and high metallicity ends. We propose several possibilities to explain such metallicity dependence. The positive correlation between the metallicity and the wide binary fraction at [Fe/H]< 0 may be due to the denser formation environments in the earlier Universe that tend to disrupt the wide binaries. At [Fe/H]> 0, The anti-correlation between metallicity and the wide binary fraction may be due to that some wide binaries are formed from the dynamical unfolding of compact triples (Reipurth and Mikkola, 2012; Elliott and Bayo, 2016), and thus they inherit the metallicity dependence from the close binary fraction (Raghavan et al., 2010; Yuan et al., 2015; Badenes et al., 2018; Moe, Kratter, and Badenes, 2019; El-Badry and Rix, 2019). The radial migration of Galactic orbits (Sellwood and Binney, 2002) may also cause such non-monotonic metallicity dependence, either due to different formation environments at different galactocentric radii or that the enhanced interaction with high-density gas clumps disrupt the wide binaries.

Halo wide binaries are particularly useful to decipher the origin of the metallicity dependence of wide binary fraction. For example, most of the halo stars do not experience the radial migration. Therefore, if the metallicity dependence of the wide binary fraction is due to radial migration which is more important for disk stars, we would expect a different wide binary fraction in the halo. The sample used in Hwang et al., 2021 is dominated by kinematic thin-disk stars, and no more than two wide binaries are likely to be halo. Therefore, we cannot constrain the halo wide binary fraction in the

177

previous work.

Now with the H3 data, we can compare the wide binary fraction between the disk and the halo. Our results suggest that iron abundance is the main driver for the wide binary fraction (Fig. 5.7), instead of their origin (disk versus halo) nor α abundance (Fig. 5.8). This rules out radial migration as the dominant driver for the metallicity dependence of the wide binary fraction.

After ruling out the radial migration scenario, our leading hypothesis for the iron abundance dependence of the wide binary fraction is that the formation environments are denser at lower [Fe/H], which are more disruptive for wide binaries. This is possible because studies have found that the star formation environments have higher pressures and densities at higher redshifts, and also higher-mass clusters tend to form in such environments (Harris and Pudritz, 1994; Elmegreen and Efremov, 1997; Kravtsov and Gnedin, 2005; Kruijssen, 2014; Ma et al., 2020).

5.5.3   Implications for the halo

There is an ongoing debate on whether disrupted globular clusters play an important role in the stellar halo. Because wide binaries cannot survive in globular clusters due to the extremely high stellar density, disrupted globular clusters would lower the halo wide binary fraction if they contribute to a significant fraction of the halo.

Our result finds that the wide binary fraction of the halo is consistent with that of the disk (Fig. 5.7). Assuming that the original halo wide binary fraction (i.e. halo stars that are not from globular clusters) is the same as the disk and

the wide binary fraction from disrupted globular clusters is zero, our result implies that the disrupted globular clusters contribute less than ~ 50% of the halo. This is consistent with other studies where they find ~ 10% of halo are related to disrupted globular clusters (Martell and Grebel, 2010; Martell et al., 2011; Martell et al., 2016; Koch, Grebel, and Martell, 2019).

Our halo sample, selected to be within 5 kpc from the Sun, is dominated by the accreted *Gaia*-Sausage-Enceladus dwarf galaxy (Naidu et al., 2020), and many of our halo wide binaries have kinematics associated with it (Fig. 5.6). With a similar argument, our result suggests that the globular clusters of *Gaia*-Sausage-Enceladus do not dominate the total number of accreted stars from *Gaia*-Sausage-Enceladus.

5.6   Conclusions

Halo wide binaries play a critical role in constraining the nature of dark matter and wide binary formation. In this paper, we search for wide binaries in the H3 survey. Our findings include:

1. Depending on the availability of radial velocities, we use two selection methods to search for wide binaries (Fig. 5.1, Fig. 5.3). Our search results in a total of 968 wide binary candidates with binary separations ranging from 10^3 to 10^6 AU. The results are summarized in Table 5.1. This is the largest wide binary sample with high-resolution ($R > 10,000$) spectroscopy.

2. Their companions are located at the reasonable locations in the H-R diagram (Fig. 5.5), supporting that most of them are genuine wide binaries instead of chance-alignment pairs.

3. Based on the Galactic kinematics, we separate the wide binaries into disk and halo population (Fig. 5.6), resulting in a sample of 50 halo wide binaries and many of them have kinematics associated with the accreted *Gaia*-Sausage-Enceladus dwarf galaxy.

4. By using the Monte-Carlo method to control for the distance and metallicity, we show that the wide binary fraction in the halo is consistent with that in the disk (Fig. 5.7). Also, the wide binary fraction in the disk decrease toward the low-metallicity end (Fig. 5.7). We do not find a significant dependence of the wide binary fraction on α abundance (Fig. 5.8).

5. Our results imply that radial migration plays a minor role in the metallicity dependence of the wide binary fraction. The remaining promising explanation for such metallicity dependence is that lower-metallicity formation environments have higher stellar densities that tend to disrupt wide binaries, thus lowering the wide binary fraction.

6. Since wide binaries are unlikely to survive in globular clusters, the fact that we find a similar wide binary fraction in the halo as that of the disk suggests that disrupted globular clusters do not contribute to a significant fraction of the stellar halo.

Chapter 6

Concluding Statement

In this thesis, I make significant progress on improving our understanding of the birth and the fate of close and wide binary stars. I develop a kinematic-dating technique to track the lifetime of main-sequence contact binaries. I find that contact binaries form at the age of $\sim 1\,\text{Gyr}$ (Hwang and Zakamska, 2020). The formation time provides a powerful constraint on their formation mechanisms. 1 Gyr formation timescale is too long for pre-main-sequence interaction and the three-body interaction through the Kozai-Lidov mechanism, and is more consistent with the timescale of magnetic braking. Therefore, our results suggest that magnetic braking plays a critical role in the formation of contact binaries. My results also show that these contact binaries merge within their main-sequence lifetime, implying an appreciable number of merger remnants in our Milky Way.

Using the astrometric information from the cutting-edge survey *Gaia*, I develop a comoving-search method to study the role of wide stellar companions in the formation of hot jupiters and contact binaries (Hwang et al., 2020b). Specifically, I measure the wide companion fractions (the fraction of

the sample that has stellar companions at $10^3 - 10^4$ AU) for the hot jupiter host sample and contact binary sample, and compare these fractions with the field star sample. I find that both hot jupiter hosts and contact binaries have higher wide companion fractions than that of the field stars by a factor of 2 and 3, respectively. The enhanced wide companion fraction of hot jupiter hosts can be explained by their lack of close stellar companions, and therefore no obvious connection between the wide stellar companions and formation of hot jupiters is found. In contrast, the enhanced wide companion fraction of contact binaries suggests that the formation of these close binaries is associated with their wide companions through, for example, the dynamical unfolding of compact triples.

I report the first known relation between the wide binary fraction and metallicity, providing a critical clue on the formation and evolution of wide binaries (Hwang et al. 2021, Fig. 4.7). The non-monotonic metallicity dependence may be due to the different formation environments at different times, the dynamical unfolding of compact triples, radial migration of Galactic orbits, or their combinations. To further constrain these hypotheses, I conduct a systematic search for wide binaries in the Milky Way's halo. Because halo stars have very different properties (metallicities, ages, and formation and evolution environments) than disk stars, they are particularly useful to test our hypotheses. Using this sample, I present a metallicity dependence from halo wide binaries that is similar to the disk stars (Fig. 5.7). Since halo stars do not experience Galactic radial migration, we can conclude that Galactic radial migration does not play an important role in the metallicity dependence

of wide binary fraction at the low-metallicity. Therefore, the lower wide binary fraction at lower metallicities is most likely a consequence of the denser environments in the earlier Universe.

In the years to come, I will continue to investigate the life of binary stars. First, I will examine the mass dependence of the lifetime of contact binaries, which will prove if magnetic braking is the dominant formation channel. Second, I will search for contact binaries about to merge based on their rapid period changes. Then I will search for the remnant of contact binary mergers, especially using their unusually blue colors and rapid stellar rotations. For wide binaries, I am currently developing a new technique to measure one of binary star's fundamental parameter, eccentricity. The eccentricity will inform us of wide binary formation and the subsequent evolution. All I mention here is a subset of binary search, and there are more binary stars coming outside of the Milky Way through their gravitational waves and mergers. Therefore, I am sincerely looking forward to the bright future lighten by binary stars.

References

Abbott, B. P. et al. (2016). "Binary Black Hole Mergers in the first Advanced LIGO Observing Run". In: *Physical Review X* 6.4, p. 041015. ISSN: 2160-3308. DOI: 10.1103/PhysRevX.6.041015. arXiv: 1606.04856.

Abbott, B. P. et al. (2017). "GW170817: Observation of Gravitational Waves from a Binary Neutron Star Inspiral". In: Phys. Rev. Lett. 119.16, p. 161101. ISSN: 0031-9007. DOI: 10.1103/PhysRevLett.119.161101.

Abt, H. A. and S. G. Levy (1976). "Multiplicity among solar-type stars". In: ApJS 30, p. 273. ISSN: 0067-0049. DOI: 10.1086/190363. URL: https://ui.adsabs.harvard.edu/abs/1976ApJS...30..273A/abstract.

Alecian, E. et al. (2007). "Calibration of the pre-main sequence RS Cha binary system". In: A&A 465, pp. 241–248. DOI: 10.1051/0004-6361:20065822. arXiv: 0610947 [astro-ph].

Allen, Christine and Miguel A. Monroy-Rodríguez (2014). "An improved catalog of halo wide binary candidates". In: ApJ 790.2, p. 158. DOI: 10.1088/0004-637X/790/2/158. arXiv: 1406.5164. URL: http://arxiv.org/abs/1406.5164http://dx.doi.org/10.1088/0004-637X/790/2/158.

Allen, Peter R. et al. (2012). "Low-mass Tertiary Companions to Spectroscopic Binaries. I. Common Proper Motion Survey for Wide Companions Using 2MASS". In: AJ 144.2, p. 62. ISSN: 0004-6256. DOI: 10.1088/0004-6256/144/2/62.

Andrews, Jeff J., Julio Chanamé, and Marcel A. Agüeros (2018). "Wide binaries in Tycho-Gaia II: Metallicities, abundances and prospects for chemical tagging". In: MNRAS 473.4, pp. 5393–5406. ISSN: 13652966. DOI: 10.1093/mnras/stx2685. arXiv: 1710.04678.

Andrews, Jeff J. et al. (2012). "Common Proper Motion Wide White Dwarf Binaries Selected From The Sloan Digital Sky Survey". In: ApJ 757.2, p. 170. DOI: 10.1088/0004-637X/757/2/170. arXiv: 1209.0175. URL: http://arxiv.org/abs/1209.0175http://dx.doi.org/10.1088/0004-637X/757/2/170.

Andrews, Jeff J. et al. (2019). "Using APOGEE Wide Binaries to Test Chemical Tagging with Dwarf Stars". In: ApJ 871.1, p. 42. ISSN: 1538-4357. DOI: 10.3847/1538-4357/aaf502. arXiv: 1811.12032.

Arenou, F. et al. (2018). "Gaia Data Release 2: Catalogue validation". In: A&A 616, A17. arXiv: 1804.09375.

Astropy Collaboration et al. (2018). "The Astropy Project: Building an inclusive, open-science project and status of the v2.0 core package". In: AJ 156.3, p. 123. DOI: 10.3847/1538-3881/aabc4f. arXiv: 1801.02634. URL: http://arxiv.org/abs/1801.02634http://dx.doi.org/10.3847/1538-3881/aabc4f.

Badenes, Carles et al. (2018). "Stellar Multiplicity Meets Stellar Evolution And Metallicity: The APOGEE View". In: ApJ 854, p. 147. ISSN: 0004-637X. DOI: 10.3847/1538-4357/aaa765. arXiv: 1711.00660.

Bahcall, J. N., P. Hut, and S. Tremaine (1985). "Maximum mass of objects that constitute unseen disk material". In: ApJ 290, p. 15. ISSN: 0004-637X. DOI: 10.1086/162953.

Bahcall, J. N. and R. M. Soneira (1981). "The distribution of stars to V = 16th magnitude near the north galactic pole - Normalization, clustering properties, and counts in various bands". In: ApJ 246, p. 122. ISSN: 0004-637X. DOI: 10.1086/158905.

Bastian, N. et al. (2005). "The star cluster population of M 51 II. Age distribution and relations among the derived parameters". In: A&A 431.3, pp. 905–924. ISSN: 00046361. DOI: 10.1051/0004-6361:20041078. URL: http://dx.doi.org/10.1051/0004-6361:20041078.

Bate, M. R., I. A. Bonnell, and V. Bromm (2002). "The formation mechanism of brown dwarfs". In: MNRAS 332.3, pp. L65–L68. ISSN: 0035-8711. DOI: 10.1046/j.1365-8711.2002.05539.x. arXiv: 0206365 [astro-ph].

Bate, Matthew R. (1998). "Collapse of a Molecular Cloud Core to Stellar Densities: The First Three-dimensional Calculations". In: ApJ 508.1, pp. L95–L98. ISSN: 0004637X. DOI: 10.1086/311719.

Bate, Matthew R. (2005). "The dependence of the initial mass function on metallicity and the opacity limit for fragmentation". In: MNRAS 363.2, pp. 363–378. ISSN: 00358711. DOI: 10.1111/j.1365-2966.2005.09476.x. URL: https://ui.adsabs.harvard.edu/abs/2005MNRAS.363..363B/abstract.

Bate, Matthew R. (2009). "Stellar, brown dwarf and multiple star properties from hydrodynamical simulations of star cluster formation". In: MNRAS 392.2, pp. 590–616. ISSN: 00358711. DOI: 10.1111/j.1365-2966.2008.

14106.x. arXiv: 0811.0163. URL: http://arxiv.org/abs/0811.0163http://dx.doi.org/10.1111/j.1365-2966.2008.14106.xhttps://academic.oup.com/mnras/article-lookup/doi/10.1111/j.1365-2966.2008.14106.x.

Bate, Matthew R. (2011). "Collapse of a molecular cloud core to stellar densities: the formation and evolution of pre-stellar discs". In: MNRAS 417.3, pp. 2036–2056. ISSN: 00358711. DOI: 10.1111/j.1365-2966.2011.19386.x.

Bate, Matthew R. (2012). "Stellar, brown dwarf and multiple star properties from a radiation hydrodynamical simulation of star cluster formation". In: MNRAS 419.4, pp. 3115–3146. ISSN: 00358711. DOI: 10.1111/j.1365-2966.2011.19955.x. arXiv: 1110.1092.

Bate, Matthew R. (2014). "The statistical properties of stars and their dependence on metallicity: The effects of opacity". In: MNRAS 442.1, pp. 285–313. ISSN: 13652966. DOI: 10.1093/mnras/stu795. arXiv: 1405.5583.

Bate, Matthew R. (2019). "The statistical properties of stars and their dependence on metallicity". In: MNRAS 484.2, pp. 2341–2361. ISSN: 13652966. DOI: 10.1093/mnras/stz103. arXiv: 1901.03713.

Batten, A. H. and R. H. Hardie (1965). "ADS 9537-A Pair of Eclipsing Binaries." In: AJ 70, p. 666. ISSN: 00046256. DOI: 10.1086/109609.

Batygin, Konstantin, Peter H. Bodenheimer, and Gregory P. Laughlin (2016). "In Situ Formation and Dynamical Evolution of Hot Jupiter Systems". In: ApJ 829.2, p. 114. ISSN: 0004-637X. DOI: 10.3847/0004-637X/829/2/114. arXiv: arXiv:1511.09157.

Belokurov, V. et al. (2018). "Co-formation of the Galactic disc and the stellar halo". In: MNRAS 478.1, pp. 611–619. DOI: 10.1093/mnras/sty982. arXiv: 1802.03414. URL: http://arxiv.org/abs/1802.03414http://dx.doi.org/10.1093/mnras/sty982.

Belokurov, Vasily et al. (2017). "Clouds, Streams and Bridges. Redrawing the blueprint of the Magellanic System with Gaia DR1". In: MNRAS 466.4, stw3357. ISSN: 0035-8711. DOI: 10.1093/mnras/stw3357.

Belokurov, Vasily et al. (2020a). "The biggest Splash". In: MNRAS 494, pp. 3880–3898. ISSN: 0035-8711. DOI: 10.1093/mnras/staa876. arXiv: 1909.04679.

Belokurov, Vasily et al. (2020b). "Unresolved stellar companions with Gaia DR2 astrometry". In: MNRAS 496, pp. 1922–1940. arXiv: 2003.05467. URL: http://arxiv.org/abs/2003.05467.

Bennett, Morgan and Jo Bovy (2019). "Vertical waves in the solar neighbourhood in Gaia DR2". In: MNRAS 482.1, pp. 1417–1425. ISSN: 13652966. DOI:

10.1093/mnras/sty2813. arXiv: 1809.03507. URL: https://academic.oup.com/mnras/article/482/1/1417/5142313.

Bensby, T., S. Feltzing, and M. S. Oey (2014). "Exploring the Milky Way stellar disk : A detailed elemental abundance study of 714 F and G dwarf stars in the solar neighbourhood". In: A&A 562, A71. ISSN: 00046361. DOI: 10.1051/0004-6361/201322631.

Bilir, S. et al. (2005). "Kinematics of W Ursae Majoris type binaries and evidence of the two types of formation". In: MNRAS 357.2, pp. 497–517. ISSN: 00358711. DOI: 10.1111/j.1365-2966.2005.08609.x.

Binney, James, Ortwin Gerhard, and David Spergel (1997). "The photometric structure of the inner Galaxy". In: MNRAS 288, pp. 365–374. DOI: 10.1093/mnras/288.2.365. arXiv: 9609066 [astro-ph]. URL: http://arxiv.org/abs/astro-ph/9609066http://dx.doi.org/10.1093/mnras/288.2.365.

Bodenheimer, Peter, Olenka Hubickyj, and Jack J. Lissauer (2000). "Models of the in situ formation of detected extrasolar giant planets". In: *Icarus* 143.1, pp. 2–14. ISSN: 00191035. DOI: 10.1006/icar.1999.6246.

Boley, A. C., A. P. Granados Contreras, and B. Gladman (2016). "The In Situ Formation of Giant Planets at Short Orbital Periods". In: ApJ 817.2, p. L17. ISSN: 0004-637X. DOI: 10.3847/2041-8205/817/2/L17.

Borkovits, T. et al. (2016). "A comprehensive study of the Kepler triples via eclipse timing". In: MNRAS 455.4, pp. 4136–4165. ISSN: 0035-8711. DOI: 10.1093/mnras/stv2530.

Bouvier, J, F Rigaut, and D Nadeau (1997). "Pleiades low-mass binaries: do companions affect the evolution of protoplanetary disks?" In: A&A 323, pp. 139–150. ISSN: 0004-6361.

Bovy, Jo (2015). "galpy: A Python Library for Galactic Dynamics". In: ApJS 216.2, p. 29. DOI: 10.1088/0067-0049/216/2/29. arXiv: 1412.3451. URL: http://arxiv.org/abs/1412.3451http://dx.doi.org/10.1088/0067-0049/216/2/29.

Bovy, Jo (2017). "Galactic rotation in Gaia DR1". In: MNRAS 468, pp. L63–L67. ISSN: 0035-8711. DOI: 10.1093/mnrasl/slx027. arXiv: 1610.07610.

Bovy, Jo et al. (2016a). "ON GALACTIC DENSITY MODELING IN THE PRESENCE OF DUST EXTINCTION". In: ApJ 818.2, p. 130. ISSN: 1538-4357. DOI: 10.3847/0004-637X/818/2/130. arXiv: 1509.06751.

Bovy, Jo et al. (2016b). "THE STELLAR POPULATION STRUCTURE OF THE GALACTIC DISK". In: ApJ 823.1, p. 30. ISSN: 1538-4357. DOI: 10.3847/0004-637X/823/1/30.

Bressan, A. et al. (2012). "PARSEC: stellar tracks and isochrones with the PAdova and TRieste Stellar Evolution Code". In: MNRAS 427, pp. 127–145. ISSN: 0035-8711. DOI: 10.1111/j.1365-2966.2012.21948.x. arXiv: 1208.4498.

Bressert, E. et al. (2010). "The Spatial Distribution of Star Formation in the Solar Neighbourhood: Do all stars form in clusters?" In: MNRAS 409.1, pp. L54–L58. DOI: 10.1111/j.1745-3933.2010.00946.x. arXiv: 1009.1150. URL: http://arxiv.org/abs/1009.1150http://dx.doi.org/10.1111/j.1745-3933.2010.00946.x.

Bryan, Marta L. et al. (2016). "Statistics of Long Period Gas Giant Planets in Known Planetary Systems". In: ApJ 821.2, p. 89. ISSN: 0004-637X. DOI: 10.3847/0004-637X/821/2/89.

Capitanio, L. et al. (2017). "Three-dimensional mapping of the local interstellar medium with composite data". In: A&A 606, A65. ISSN: 14320746. DOI: 10.1051/0004-6361/201730831. arXiv: 1706.07711.

Cargile, Phillip A. et al. (2020). "MINESweeper: Spectrophotometric modeling of stars in the gaia ERA". In: ApJ 900.1, p. 28. ISSN: 23318422. DOI: 10.3847/1538-4357/aba43b. arXiv: 1907.07690. URL: https://doi.org/10.3847/1538-4357/aba43b.

Carlin, Jeffrey L. et al. (2012). "An algorithm for preferential selection of spectroscopic targets in LEGUE". In: *Research in Astronomy and Astrophysics* 12.7, pp. 755–771. ISSN: 16744527. DOI: 10.1088/1674-4527/12/7/004. arXiv: 1206.3577. URL: https://ui.adsabs.harvard.edu/abs/2012RAA....12..755C/abstract.

Casagrande, L. and Don A. VandenBerg (2018). "On the use of Gaia magnitudes and new tables of bolometric corrections". In: MNRAS 479.1, pp. L102–L107. ISSN: 17453933. DOI: 10.1093/mnrasl/sly104. arXiv: 1806.01953.

Casagrande, L. et al. (2011). "New constraints on the chemical evolution of the solar neighbourhood and Galactic disc(s): Improved astrophysical parameters for the Geneva-Copenhagen Survey". In: A&A 530, A138. ISSN: 00046361. DOI: 10.1051/0004-6361/201016276. arXiv: 1103.4651.

Chambers, K. C. et al. (2016). "The Pan-STARRS1 Surveys". In: *eprint arXiv:1612.05560*. arXiv: 1612.05560.

Chaname, Julio and Andrew Gould (2004). "Disk and Halo Wide Binaries from the Revised Luyten Catalog: Probes of Star Formation and MACHO Dark Matter". In: ApJ 601.1, pp. 289–310. ISSN: 0004-637X. DOI: 10.1086/380442.

Chandar, Rupali et al. (2017). "The Fraction of Stars That Form in Clusters in Different Galaxies". In: ApJ 849.2, p. 128. ISSN: 1538-4357. DOI: 10.3847/1538-4357/aa92ce. arXiv: 1806.11537.

Chatterjee, Sourav et al. (2008). "Dynamical Outcomes of Planet-Planet Scattering". In: ApJ 686.1, pp. 580–602. ISSN: 0004-637X. DOI: 10.1086/590227. arXiv: 0703166 [astro-ph].

Chen, Xiaodian et al. (2018). "Wide-field Infrared Survey Explorer (WISE) Catalog of Periodic Variable Stars". In: ApJS 237.2, p. 28. ISSN: 1538-4365. DOI: 10.3847/1538-4365/aad32b.

Cheng, Sihao, Jeffrey D. Cummings, and Brice Ménard (2019). "A cooling anomaly of high-mass white dwarfs". In: AJ 886, p. 100. arXiv: 1905.12710.

Choi, Jieun et al. (2016). "MESA ISOCHRONES AND STELLAR TRACKS (MIST). I. SOLAR-SCALED MODELS". In: ApJ 823.2, p. 102. ISSN: 1538-4357. DOI: 10.3847/0004-637x/823/2/102. arXiv: 1604.08592. URL: http://openmp.org/wp/.

Conroy, Charlie et al. (2019a). "Mapping the Stellar Halo with the H3 Spectroscopic Survey". In: ApJ 883.1, p. 107. ISSN: 1538-4357. DOI: 10.3847/1538-4357/ab38b8. arXiv: 1907.07684. URL: https://doi.org/10.3847/1538-4357/ab38b8.

Conroy, Charlie et al. (2019b). "Resolving the Metallicity Distribution of the Stellar Halo with the H3 Survey". In: ApJ 887.2, p. 237. ISSN: 1538-4357. DOI: 10.3847/1538-4357/ab5710. arXiv: 1909.02007.

Coronado, Johanna et al. (2018). "A distant sample of halo wide binaries from SDSS". In: MNRAS 480.4, pp. 4302–4313. ISSN: 13652966. DOI: 10.1093/MNRAS/STY2141. arXiv: 1804.06851. URL: http://skyserver.sdss.org/casjobs/.

Cowperthwaite, P. S. et al. (2017). "The Electromagnetic Counterpart of the Binary Neutron Star Merger LIGO/Virgo GW170817. II. UV, Optical, and Near-infrared Light Curves and Comparison to Kilonova Models". In: ApJ 848.2, p. L17. ISSN: 2041-8213. DOI: 10.3847/2041-8213/aa8fc7. arXiv: 1710.05840. URL: http://arxiv.org/abs/1710.05840http://dx.doi.org/10.3847/2041-8213/aa8fc7http://stacks.iop.org/2041-8205/848/i=2/a=L17?key=crossref.855984494ac6a42b7e9da44c6a1f3a12.

Cutri, R. M. et al. (2011). "Explanatory Supplement to the WISE Preliminary Data Release Products". In: *Technical reports, Explanatory Supplement to the WISE Preliminary Data Release Products*.

Daniel, Kathryne J. and Rosemary F.G. Wyse (2018). "Constraints on radial migration in spiral galaxies - II. Angular momentum distribution and

preferential migration". In: MNRAS 476.2, pp. 1561–1580. ISSN: 13652966. DOI: 10.1093/MNRAS/STY199. arXiv: 1801.08455.

David, Trevor J. et al. (2015). "HII 2407: AN ECLIPSING BINARY REVEALED BY K2 OBSERVATIONS OF THE PLEIADES". In: ApJ 814.1, p. 62. ISSN: 1538-4357. DOI: 10.1088/0004-637X/814/1/62.

David, Trevor J. et al. (2016). "NEW PLEIADES ECLIPSING BINARIES AND A HYADES TRANSITING SYSTEM IDENTIFIED BY K2". In: AJ 151.5, p. 112. ISSN: 1538-3881. DOI: 10.3847/0004-6256/151/5/112. arXiv: 1602.01901.

David, Trevor J. et al. (2019). "Age Determination in Upper Scorpius with Eclipsing Binaries". In: AJ 872, p. 161. DOI: 10.3847/1538-4357/aafe09. arXiv: 1901.05532.

Dawson, Rebekah I. and John Asher Johnson (2018). "Origins of Hot Jupiters". In: ARA&A 56.1, pp. 175–221. ISSN: 0066-4146. DOI: 10.1146/annurev-astro-081817-051853. arXiv: 1801.06117.

De Silva, G. M. et al. (2015). "The GALAH survey: Scientific motivation". In: MNRAS 449.3, pp. 2604–2617. ISSN: 13652966. DOI: 10.1093/mnras/stv327. arXiv: 1502.04767.

Deacon, N. R. and A. L. Kraus (2020). "Wide binaries are rare in open clusters". In: MNRAS 496, p. 5176. arXiv: 2006.06679. URL: http://arxiv.org/abs/2006.06679.

Dehnen, Walter and James Binney (1998). "Local stellar kinematics from Hipparcos data". In: MNRAS 298, pp. 387–394. ISSN: 0035-8711. DOI: 10.1046/j.1365-8711.1998.01600.x. arXiv: 9710077 [astro-ph].

Deng, Li Cai et al. (2012). "LAMOST experiment for galactic understanding and exploration (LEGUE) - The survey's science plan". In: *Research in Astronomy and Astrophysics* 12.7, pp. 735–754. ISSN: 16744527. DOI: 10.1088/1674-4527/12/7/003. arXiv: 1206.3578.

Dotter, Aaron (2016). "MESA ISOCHRONES AND STELLAR TRACKS (MIST) 0: METHODS FOR THE CONSTRUCTION OF STELLAR ISOCHRONES". In: ApJS 222.1, p. 8. ISSN: 1538-4365. DOI: 10.3847/0067-0049/222/1/8. arXiv: 1601.05144. URL: http://mesa.sourceforge.net.

Dotter, Aaron et al. (2017). "The influence of atomic diffusion on stellar ages and chemical tagging". In: ApJ 840.2, p. 99. ISSN: 23318422. DOI: 10.3847/1538-4357/aa6d10. arXiv: 1704.03465. URL: https://doi.org/10.3847/1538-4357/aa6d10.

Drake, A. J. et al. (2014). "The Catalina Surveys Periodic Variable Star Catalog". In: ApJS 213, p. 9. ISSN: 0067-0049. DOI: 10.1088/0067-0049/213/1/9. arXiv: 1405.4290.

Drimmel, R., A. Cabrera-Lavers, and M. Lopez-Corredoira (2003). "A three-dimensional Galactic extinction model". In: A&A 409, pp. 205–215. ISSN: 0004-6361. DOI: 10.1051/0004-6361:20031070. arXiv: 0307273 [astro-ph]. URL: http://arxiv.org/abs/astro-ph/0307273http://dx.doi.org/10.1051/0004-6361:20031070.

Drimmel, Ronald and Eloisa Poggio (2018). "On the Solar Velocity". In: *Research Notes of the American Astronomical Society* 2.4, p. 210. DOI: 10.3847/2515-5172/aaef8b.

Duchêne, Gaspard and Adam Kraus (2013). "Stellar Multiplicity". In: ARA&A 51, pp. 269–310. ISSN: 0066-4146. DOI: 10.1146/annurev-astro-081710-102602. arXiv: 1303.3028.

Duquennoy, A. and M Mayor (1991). "Multiplicity among solar-type stars in the solar neighbourhood. II - Distribution of the orbital elements in an unbiased sample. - NASA/ADS". In: A&A 248, pp. 485–524. URL: https://ui.adsabs.harvard.edu/abs/1991A%26A...248..485D/abstract.

Eggen, Olin J. and Icko Jr. Iben (1989). "Starbursts, blue stragglers, and binary stars in local superclusters and groups. II - The old disk and halo populations". In: AJ 97, p. 431. ISSN: 00046256. DOI: 10.1086/114993.

Eggleton, P. P. (1983). "Approximations to the radii of Roche lobes". In: ApJ 268, p. 368. ISSN: 0004-637X. DOI: 10.1086/160960.

Eggleton, Peter P. and Ludmila Kiseleva-Eggleton (2001). "Evolution in Binary and Triple Stars, with an application to SS Lac". In: ApJ 562, pp. 1012–1030. ISSN: 0004-637X. DOI: 10.1086/323843. arXiv: 0104126 [astro-ph].

Eggleton, Peter P. and Ludmila Kisseleva-Eggleton (2006). "A mechanism for producing short-period binaries". In: Ap&SS 304.1-4, pp. 75–79. ISSN: 0004640X. DOI: 10.1007/s10509-006-9078-z.

El-Badry, Kareem and Hans-Walter Rix (2018). "Imprints of white dwarf recoil in the separation distribution of Gaia wide binaries". In: MNRAS 480, p. 4884. ISSN: 0035-8711. DOI: 10.1093/mnras/sty2186. arXiv: 1807.06011.

El-Badry, Kareem and Hans-Walter Rix (2019). "The wide binary fraction of solar-type stars: emergence of metallicity dependence at a < 200 AU". In: MNRAS 482, pp. L139–L144. ISSN: 0035-8711. DOI: 10.1093/mnrasl/sly206. arXiv: 1809.06860. URL: http://arxiv.org/abs/1809.06860http://dx.doi.org/10.1093/mnrasl/sly206.

El-Badry, Kareem, Hans-Walter Rix, and Tyler M. Heintz (2021). "A million binaries from Gaia eDR3: sample selection and validation of Gaia parallax uncertainties". In: MNRAS. arXiv: 2101.05282. URL: http://arxiv.org/abs/2101.05282.

El-Badry, Kareem et al. (2018). "Discovery and Characterization of 3000+ Main-Sequence Binaries from APOGEE Spectra". In: MNRAS 476, pp. 528–553. ISSN: 0035-8711. DOI: 10.1093/mnras/sty240. arXiv: 1711.08793.

El-Badry, Kareem et al. (2019). "Discovery of an equal-mass "twin" binary population reaching 1000+ AU separations". In: MNRAS 489, pp. 5822–5857. arXiv: 1906.10128.

Elliott, P. and A. Bayo (2016). "The crucial role of higher-order multiplicity in wide binary formation: A case study using the β-Pictoris moving group". In: MNRAS 459.4, pp. 4499–4507. DOI: 10.1093/mnras/stw926. arXiv: 1604.06094. URL: http://arxiv.org/abs/1604.06094http://dx.doi.org/10.1093/mnras/stw926.

Elmegreen, Bruce G. and Yuri N. Efremov (1997). "A Universal Formation Mechanism for Open and Globular Clusters in Turbulent Gas". In: ApJ 480.1, pp. 235–245. ISSN: 0004-637X. DOI: 10.1086/303966. URL: https://ui.adsabs.harvard.edu/abs/1997ApJ...480..235E/abstract.

Endl, Michael et al. (2014). "Kepler-424 b: A "Lonely" Hot Jupiter that Found a Companion". In: ApJ 795.2, p. 151. ISSN: 0004-637X. DOI: 10.1088/0004-637X/795/2/151.

Evans, D. F. et al. (2016). "High-resolution Imaging of Transiting Extrasolar Planetary systems (HITEP): I. Lucky imaging observations of 101 systems in the southern hemisphere". In: A&A 589, A58. ISSN: 14320746. DOI: 10.1051/0004-6361/201527970. arXiv: 1603.03274.

Evans, D. W. et al. (2018). "Gaia Data Release 2: Photometric content and validation". In: A&A 616, A4. ISSN: 0004-6361. DOI: 10.1051/0004-6361/201832756.

Fabricius, Claus et al. (2020). "Gaia Early Data Release 3: Catalogue Validation". In: A&A. arXiv: 2012.01742. URL: http://arxiv.org/abs/2012.01742.

Fabrycky, Daniel and Scott Tremaine (2007). "Shrinking Binary and Planetary Orbits by Kozai Cycles with Tidal Friction". In: ApJ 669.2, pp. 1298–1315. ISSN: 0004-637X. DOI: 10.1086/521702.

Fall, S. Michael, Rupali Chandar, and Bradley C. Whitmore (2005). "The Age Distribution of Massive Star Clusters in the Antennae Galaxies". In: ApJ 631.2, pp. L133–L136. ISSN: 0004-637X. DOI: 10.1086/496878.

Feng, Yi and Mark R. Krumholz (2014). "Early turbulent mixing as the origin of chemical homogeneity in open star clusters". In: Nature 513.7519, pp. 523–525. ISSN: 14764687. DOI: 10.1038/nature13662. arXiv: 1408.6543. URL: https://ui.adsabs.harvard.edu/abs/2014Natur.513..523F/abstract.

Fischer, Debra A. and Geoffrey W. Marcy (1992). "Multiplicity among M dwarfs". In: ApJ 396, p. 178. ISSN: 0004-637X. DOI: 10.1086/171708. URL: https://ui.adsabs.harvard.edu/abs/1992ApJ...396..178F/abstract.

Fischer, Debra A. and Jeff Valenti (2005). "The Planet-Metallicity Correlation". In: ApJ 622.2, pp. 1102–1117. ISSN: 0004-637X. DOI: 10.1086/428383.

Fisher, Robert T. (2004). "A Turbulent Interstellar Medium Origin of the Binary Period Distribution". In: ApJ 600.2, pp. 769–780. ISSN: 0004-637X. DOI: 10.1086/380111.

Flannery, Brian P. (1976). "A Cyclic Thermal Instability in Contact Binary Stars". In: ApJ 205, p. 217. ISSN: 0004-637X. DOI: 10.1086/154266.

Flewelling, H. A. et al. (2016). "The Pan-STARRS1 Database and Data Products". In: *The Pan-STARRS1 Database and Data Products*. arXiv: 1612.05243.

Fong, W. and E. Berger (2013). "THE LOCATIONS OF SHORT GAMMA-RAY BURSTS AS EVIDENCE FOR COMPACT OBJECT BINARY PROGENITORS". In: ApJ 776.1, p. 18. ISSN: 0004-637X. DOI: 10.1088/0004-637X/776/1/18. arXiv: 1307.0819.

Ford, Eric B. and Frederic A. Rasio (2006). "On the Relation between Hot Jupiters and the Roche Limit". In: ApJ 638.1, pp. L45–L48. ISSN: 0004-637X. DOI: 10.1086/500734.

Frankel, Neige et al. (2018). "Measuring Radial Orbit Migration in the Galactic Disk". In: ApJ 865.2, p. 96. ISSN: 1538-4357. DOI: 10.3847/1538-4357/aadba5. URL: https://doi.org/10.3847/1538-4357/aadba5.

Frankel, Neige et al. (2020). "Keeping It Cool: Much Orbit Migration, yet Little Heating, in the Galactic Disk". In: ApJ 896.1, p. 15. ISSN: 1538-4357. DOI: 10.3847/1538-4357/ab910c. arXiv: 2002.04622. URL: https://doi.org/10.3847/1538-4357/ab910c.

Freeman, Ken and Joss Bland-Hawthorn (2002). *The new Galaxy: Signatures of its formation*. DOI: 10.1146/annurev.astro.40.060401.093840. arXiv: 0208106 [astro-ph]. URL: https://ui.adsabs.harvard.edu/abs/2002ARA%26A..40..487F/abstract.

Fressin, François et al. (2013). "The false positive rate of Kepler and the occurrence of planets". In: ApJ 766.2, p. 81. ISSN: 15384357. DOI: 10.1088/0004-637X/766/2/81. arXiv: 1301.0842.

Gaia Collaboration et al. (2016). "The Gaia mission". In: A&A 595, A1. ISSN: 0004-6361. DOI: 10.1051/0004-6361/201629272. URL: http://www.aanda.org/10.1051/0004-6361/201629272.

Gaia Collaboration et al. (2018a). "Gaia Data Release 2". In: A&A 616, A1. ISSN: 0004-6361. DOI: 10.1051/0004-6361/201833051.

Gaia Collaboration et al. (2018b). "Gaia Data Release 2: Observational Hertzsprung-Russell diagrams". In: A&A 616, A10. ISSN: 0004-6361. DOI: 10.1051/0004-6361/201832843. arXiv: 1804.09378.

Gaia Collaboration et al. (2019). "Gaia Data Release 2: Variable stars in the colour-absolute magnitude diagram". In: A&A 623, A110. arXiv: 1804.09382. URL: http://arxiv.org/abs/1804.09382.

Gaia Collaboration et al. (2020). "Gaia Early Data Release 3: Summary of the contents and survey properties". In: A&A 61. arXiv: 2012.01533. URL: http://arxiv.org/abs/2012.01533.

Ghez, A. M., G. Neugebauer, and K. Matthews (1993). "The multiplicity of T Tauri stars in the star forming regions Taurus-Auriga and Ophiuchus-Scorpius: A 2.2 micron speckle imaging survey". In: AJ 106, p. 2005. ISSN: 00046256. DOI: 10.1086/116782. URL: https://ui.adsabs.harvard.edu/abs/1993AJ....106.2005G/abstract.

Gies, D. R. et al. (2012). "A Search for Hierarchical Triples using Kepler Eclipse Timing". In: AJ 143.6, p. 137. ISSN: 0004-6256. DOI: 10.1088/0004-6256/143/6/137.

Goldreich, P. and S. Tremaine (1980). "Disk-satellite interactions". In: ApJ 241, p. 425. ISSN: 0004-637X. DOI: 10.1086/158356.

Gonzalez, Guillermo (1997). "The stellar metallicity-giant planet connection". In: MNRAS 285, pp. 403–412. URL: https://ui.adsabs.harvard.edu/abs/1997MNRAS.285..403G/abstract.

Goodman, Jeremy and Piet Hut (1993). "Binary-single-star scattering. V - Steady state binary distribution in a homogeneous static background of single stars". In: ApJ 403, p. 271. ISSN: 0004-637X. DOI: 10.1086/172200. URL: https://ui.adsabs.harvard.edu/abs/1993ApJ...403..271G/abstract.

Goodwin, Simon P. (2009). "The effect of the dynamical state of clusters on gas expulsion and infant mortality". In: *Astrophysics and Space Science* 324.2, pp. 259–263. ISSN: 0004640X. DOI: 10.1007/s10509-009-0116-5. URL: https://ui.adsabs.harvard.edu/abs/2009Ap%26SS.324..259G/abstract.

Goodwin, Simon P. and Nate Bastian (2006). "Gas expulsion and the destruction of massive young clusters". In: MNRAS 373.2, pp. 752–758. ISSN: 00358711. DOI: 10.1111/j.1365-2966.2006.11078.x. URL: https://ui.adsabs.harvard.edu/abs/2006MNRAS.373..752G/abstract.

Graham, Matthew J. et al. (2013). "A comparison of period finding algorithms". In: MNRAS 434, pp. 3423–3444. ISSN: 0035-8711. DOI: 10.1093/mnras/stt1264. arXiv: 1307.2209.

Gravity Collaboration et al. (2019). "A geometric distance measurement to the Galactic center black hole with 0.3 percent uncertainty?" In: A&A 625, p. L10. ISSN: 14320746. DOI: 10.1051/0004-6361/201935656. arXiv: 1904.05721. URL: https://doi.org/10.1051/0004-6361/201935656.

Green, Gregory M. et al. (2015). "A Three-Dimensional Map of Milky-Way Dust". In: ApJ 810, p. 25. ISSN: 0004-637X. DOI: 10.1088/0004-637X/810/1/25. arXiv: 1507.01005. URL: http://arxiv.org/abs/1507.01005http://dx.doi.org/10.1088/0004-637X/810/1/25.

Grether, Daniel and Charles H. Lineweaver (2007). "The Metallicity of Stars with Close Companions". In: ApJ 669.2, pp. 1220–1234. ISSN: 0004-637X. DOI: 10.1086/521714. arXiv: 0612172 [astro-ph].

Guinan, Edward F. and David H. Bradstreet (1988). "Kinematic Clues to the Origin and Evolution of Low Mass Contact Binaries". In: *Formation and Evolution of Low Mass Stars. NATO ASI Series (Series C: Mathematical and Physical Sciences)*. Ed. by A.K. Dupree and M.T.V.T. Lago. Vol. 241. Springer, Dordrecht, p. 345. URL: https://ui.adsabs.harvard.edu/abs/1988ASIC..241..345G/abstract.

Hamer, Jacob H. and Kevin C. Schlaufman (2019). "Hot Jupiters are Destroyed by Tides While Their Host Stars are on the Main Sequence". In: arXiv: 1908.06998.

Han, Doo Ri et al. (2020). "Insights into the Formation and Evolution History of the Galactic Disk System". In: ApJ 896.1, p. 14. ISSN: 1538-4357. DOI: 10.3847/1538-4357/ab919a. arXiv: 2005.04866.

Harrington, R. S. (1968). "Dynamical evolution of triple stars." In: AJ 73, p. 190. ISSN: 00046256. DOI: 10.1086/110614.

Harris, William E. and Ralph E. Pudritz (1994). "Supergiant molecular clouds and the formation of globular cluster systems". In: ApJ 429, p. 177. ISSN: 0004-637X. DOI: 10.1086/174310. URL: https://ui.adsabs.harvard.edu/abs/1994ApJ...429..177H/abstract.

Hartman, Zachary D. and Sébastien Lépine (2020). *The SUPERWIDE catalog: A catalog of 99,203 wide binaries found in gaia and supplemented by the SUPERBLINK high proper motion catalog*. DOI: 10.3847/1538-4365/ab79a6. arXiv: 2002.08850. URL: https://doi.org/10.3847/1538-4365/ab79a6.

Hawkins, Keith et al. (2020). "Identical or fraternal twins? the chemical homogeneity of wide binaries from Gaia DR2". In: MNRAS 492.1, pp. 1164–1179. ISSN: 13652966. DOI: 10.1093/mnras/stz3132. arXiv: 1912.08895.

Hebb, L. et al. (2010). "MML 53: a new low-mass, pre-main sequence eclipsing binary in the Upper Centaurus-Lupus region discovered by SuperWASP". In: A&A 522, A37. ISSN: 0004-6361. DOI: 10.1051/0004-6361/201014059.

Heggie, D. C. (1975). "Binary evolution in stellar dynamics". In: MNRAS 173, p. 729. URL: https://ui.adsabs.harvard.edu/abs/1975MNRAS.173..729H/abstract.

Helmi, Amina (2008). "The stellar halo of the Galaxy". In: A&A Rev. 15.3, pp. 145–188. ISSN: 09354956. DOI: 10.1007/s00159-008-0009-6. arXiv: 0804.0019. URL: https://ui.adsabs.harvard.edu/abs/2008A%26ARv.15..145H/abstract.

Helmi, Amina (2020). *Streams, Substructures, and the Early History of the Milky Way*. DOI: 10.1146/annurev-astro-032620-021917. arXiv: 2002.04340. URL: https://doi.org/10.1146/annurev-astro-032620-.

Helmi, Amina et al. (2018). "The merger that led to the formation of the Milky Way's inner stellar halo and thick disk". In: Nature 563.7729, pp. 85–88. ISSN: 14764687. DOI: 10.1038/s41586-018-0625-x. arXiv: 1806.06038. URL: https://ui.adsabs.harvard.edu/abs/2018Natur.563...85H/abstract.

Hernandez, X., M. A. Jiménez, and C. Allen (2012). "Wide binaries as a critical test of classical gravity". In: *European Physical Journal C* 72.2, pp. 1–8. ISSN: 14346052. DOI: 10.1140/epjc/s10052-012-1884-6. arXiv: 1105.1873. URL: https://ui.adsabs.harvard.edu/abs/2012EPJC...72.1884H/abstract.

Hoffman, D. I. et al. (2012). "VARIABILITY FLAGGING IN THE WIDE-FIELD INFRARED SURVEY EXPLORER PRELIMINARY DATA RELEASE". In: AJ 143.5, p. 118. ISSN: 0004-6256. DOI: 10.1088/0004-6256/143/5/118. URL: http://stacks.iop.org/1538-3881/143/i=5/a=118?key=crossref.782906ed58f6c4aba19ab11ee1216ae4.

Holmberg, J., B. Nordström, and J. Andersen (2009). "The Geneva-Copenhagen Survey of the Solar neighbourhood III. Improved distances, ages, and kinematics". In: A&A 501, pp. 941–947. ISSN: 0004-6361. DOI: 10.1051/0004-6361/200811191. arXiv: 0811.3982.

Hosokawa, Takashi and Kazuyuki Omukai (2009). "Low-metallicity protostars and the maximum stellar mass resulting from radiative feedback: Spherically symmetric calculations". In: ApJ 703.2, pp. 1810–1818. ISSN: 15384357. DOI: 10.1088/0004-637X/703/2/1810.

Hwang, Hsiang-Chih and Nadia Zakamska (2020). "Lifetime of short-period binaries measured from their Galactic kinematics". In: MNRAS 493, pp. 2271–2286. arXiv: 1909.06375. URL: http://arxiv.org/abs/1909.06375.

Hwang, Hsiang-Chih et al. (2020a). "Varstrometry for Off-nucleus and Dual sub-Kpc AGN (VODKA): Methodology and Initial Results with Gaia DR2". In: ApJ 888.2, p. 73. arXiv: 1908.02292.

Hwang, Hsiang-Chih et al. (2020b). "Very wide companion fraction from Gaia DR2: a weak or no enhancement for hot jupiter hosts, and a strong enhancement for contact binaries". In: MNRAS 497, p. 2250. arXiv: 2007.03688. URL: http://arxiv.org/abs/2007.03688.

Hwang, Hsiang Chih et al. (2021). "The non-monotonic, strong metallicity dependence of the wide-binary fraction". In: MNRAS 501.3, pp. 4329–4343. ISSN: 23318422. DOI: 10.1093/mnras/staa3854. arXiv: 2010.02920. URL: https://ui.adsabs.harvard.edu/abs/2021MNRAS.501.4329H/abstract.

Iben, I. Jr. and A. V. Tutukov (1984). "Supernovae of type I as end products of the evolution of binaries with components of moderate initial mass (M not greater than about 9 solar masses)". In: ApJS 54, p. 335. ISSN: 0067-0049. DOI: 10.1086/190932. URL: http://adsabs.harvard.edu/doi/10.1086/190932.

Ida, S. and D. N. C. Lin (2008). "Toward a Deterministic Model of Planetary Formation. V. Accumulation Near the Ice Line and Super-Earths". In: ApJ 685.1, pp. 584–595. ISSN: 0004-637X. DOI: 10.1086/590401. arXiv: 0802.1114.

Jao, Wei-Chun et al. (2009). "Cool Subdwarf Investigations II: Multiplicity". In: AJ 137.4, pp. 3800–3808. DOI: 10.1088/0004-6256/137/4/3800. arXiv: 0902.0555. URL: http://arxiv.org/abs/0902.0555http://dx.doi.org/10.1088/0004-6256/137/4/3800.

Jiang, Yan-Fei and Scott Tremaine (2010). "The evolution of wide binary stars". In: MNRAS 401.2, pp. 977–994. ISSN: 00358711. DOI: 10.1111/j.1365-2966.2009.15744.x.

Jiménez-Esteban, F. M., E. Solano, and C. Rodrigo (2019). "A catalog of wide binary and multiple systems of bright stars from Gaia-DR2 and the Virtual Observatory". In: AJ 157, p. 78. DOI: 10.3847/1538-3881/aafacc. arXiv: 1901.03730.

Jofre, Paula and Achim Weiss (2011). "The age of the Milky Way halo stars from the Sloan Digital Sky Survey". In: A&A 533, A59. DOI: 10.1051/0004-6361/201117131. arXiv: 1105.2022. URL: http://arxiv.org/abs/1105.2022http://dx.doi.org/10.1051/0004-6361/201117131.

Joncour, Isabelle, Gaspard Duchêne, and Estelle Moraux (2017). "Multiplicity and clustering in Taurus star-forming region. I. Unexpected ultra-wide pairs of high-order multiplicity in Taurus". In: A&A 599, A14. DOI: 10.1051/0004-6361/201629398. arXiv: 1612.02098. URL: http://arxiv.org/abs/1612.02098http://dx.doi.org/10.1051/0004-6361/201629398.

Jurić, Mario and Scott Tremaine (2008). "Dynamical Origin of Extrasolar Planet Eccentricity Distribution". In: ApJ 686.1, pp. 603–620. ISSN: 0004-637X. DOI: 10.1086/590047. arXiv: 0703160 [astro-ph].

Kalirai, Jason (2012). "The Age of the Milky Way Inner Halo". In: Nature 486.7401, pp. 90–92. DOI: 10.1038/nature11062. arXiv: 1205.6802. URL: http://arxiv.org/abs/1205.6802http://dx.doi.org/10.1038/nature11062.

Kamdar, Harshil et al. (2019). "Stars that Move Together Were Born Together". In: ApJ 884, p. L42. arXiv: 1904.02159. URL: http://arxiv.org/abs/1904.02159.

Kamdar, Harshil et al. (2020). "Spatial and Kinematic Clustering of Stars in the Galactic Disk". In: arXiv: 2007.10990. URL: http://arxiv.org/abs/2007.10990.

Katz, D. et al. (2019). "Gaia Data Release 2: Properties and validation of the radial velocities". In: A&A 622, A205. arXiv: 1804.09372.

Kirk, Brian et al. (2016). "KEPLER ECLIPSING BINARY STARS. VII. THE CATALOG OF ECLIPSING BINARIES FOUND IN THE ENTIRE KEPLER DATA SET". In: AJ 151.3, p. 68. ISSN: 1538-3881. DOI: 10.3847/0004-6256/151/3/68.

Kiseleva, L. G., P. P. Eggleton, and S. Mikkola (1998). "Tidal friction in triple stars". In: MNRAS 300.1, pp. 292–302. ISSN: 0035-8711. DOI: 10.1046/j.1365-8711.1998.01903.x.

Knutson, Heather A. et al. (2014). "Friends of Hot Jupiters. I. A Radial Velocity Search for Massive, Long-period Companions to Close-in Gas Giant Planets". In: ApJ 785.2, p. 126. ISSN: 0004-637X. DOI: 10.1088/0004-637X/785/2/126.

Koch, Andreas, Eva K. Grebel, and Sarah L. Martell (2019). "Purveyors of fine halos: Re-assessing globular cluster contributions to the Milky Way halo buildup with SDSS-IV". In: A&A 625, A75. ISSN: 0004-6361. DOI: 10.1051/0004-6361/201834825. arXiv: 1904.02146. URL: https://doi.org/10.1051/0004-6361/201834825.

Köhler, R. et al. (2000). "Multiplicity of X-ray selected T Tauri stars in the Scorpius-Centaurus OB association". In: A&A 356, pp. 541–558. ISSN: 0004-6361. URL: https://ui.adsabs.harvard.edu/abs/2000A&A...356..541K/abstract.

Koleva, Mina et al. (2009). "ULySS: A Full Spectrum Fitting Package". In: A&A 501, p. 1269. DOI: 10.1051/0004-6361/200811467. arXiv: 0903.2979. URL: http://arxiv.org/abs/0903.2979http://dx.doi.org/10.1051/0004-6361/200811467.

Kordopatis, G. et al. (2015). "The Rich Are Different: Evidence from the RAVE Survey for Stellar Radial Migration". In: MNRAS 447.4, pp. 3526–3535. DOI: 10.1093/mnras/stu2726. arXiv: 1412.5649. URL: http://arxiv.org/abs/1412.5649http://dx.doi.org/10.1093/mnras/stu2726.

Kouwenhoven, M. B.N. et al. (2010). "The formation of very wide binaries during the star cluster dissolution phase". In: MNRAS 404.4, pp. 1835–1848. ISSN: 00358711. DOI: 10.1111/j.1365-2966.2010.16399.x. arXiv: 1001.3969.

Kozai, Yoshihide (1962). "Secular perturbations of asteroids with high inclination and eccentricity". In: AJ 67, p. 591. ISSN: 00046256. DOI: 10.1086/108790. URL: http://adsabs.harvard.edu/cgi-bin/bib_query?1962AJ.....67..591K.

Kratter, Kaitlin M. and Christopher D. Matzner (2006). "Fragmentation of massive protostellar discs". In: MNRAS 373.4, pp. 1563–1576. ISSN: 1365-2966. DOI: 10.1111/j.1365-2966.2006.11103.x.

Kraus, Adam L. and Lynne A. Hillenbrand (2009). "Unusually Wide Binaries: Are They Wide or Unusual?" In: ApJ 703.2, pp. 1511–1530. DOI: 10.1088/0004-637X/703/2/1511. arXiv: 0908.1385. URL: http://arxiv.org/abs/0908.1385http://dx.doi.org/10.1088/0004-637X/703/2/1511.

Kraus, Adam L. et al. (2011). "Mapping the shores of the brown dwarf desert. II. multiple star formation in Taurus-Auriga". In: ApJ 731.1, p. 8. ISSN: 15384357. DOI: 10.1088/0004-637X/731/1/8. arXiv: 1101.4016. URL: https://ui.adsabs.harvard.edu/abs/2011ApJ...731....8K/abstract.

Kraus, Adam L. et al. (2012). "The role of multiplicity in disk evolution and planet formation". In: ApJ 745.1, p. 19. ISSN: 15384357. DOI: 10.1088/0004-637X/745/1/19. arXiv: 1109.4141.

Kraus, Adam L. et al. (2016). "THE IMPACT OF STELLAR MULTIPLICITY ON PLANETARY SYSTEMS. I. THE RUINOUS INFLUENCE OF CLOSE BINARY COMPANIONS". In: AJ 152.1, p. 8. ISSN: 0004-6256. DOI: 10.3847/0004-6256/152/1/8. arXiv: 1604.05744.

Kravtsov, Andrey V. and Oleg Y. Gnedin (2005). "Formation of Globular Clusters in Hierarchical Cosmology". In: ApJ 623.2, pp. 650–665. ISSN: 0004-637X. DOI: 10.1086/428636. URL: https://ui.adsabs.harvard.edu/abs/2005ApJ...623..650K/abstract.

Kroupa, Pavel (1995). "Inverse Dynamical Population Synthesis and Star Formation". In: MNRAS 277.4, pp. 1491–1506. DOI: 10.1093/mnras/277.4.1491. arXiv: 9508117 [astro-ph]. URL: http://arxiv.org/abs/astro-ph/9508117http://dx.doi.org/10.1093/mnras/277.4.1491.

Kruijssen, J. M. D. (2014). "Globular cluster formation in the context of galaxy formation and evolution". In: *Classical and Quantum Gravity* 31.24, p. 244006. ISSN: 13616382. DOI: 10.1088/0264-9381/31/24/244006. arXiv: 1407.2953. URL: https://ui.adsabs.harvard.edu/abs/2014CQGra..31x4006K/abstract.

Kruijssen, J. M.Diederik (2012). "On the fraction of star formation occurring in bound stellar clusters". In: MNRAS 426.4, pp. 3008–3040. ISSN: 00358711. DOI: 10.1111/j.1365-2966.2012.21923.x. arXiv: 1208.2963. URL: https://academic.oup.com/mnras/article-abstract/426/4/3008/1014654.

Lada, Charles J. and Elizabeth A. Lada (2003). "Embedded Clusters in Molecular Clouds". In: ARA&A 41.1, pp. 57–115. ISSN: 0066-4146. DOI: 10.1146/annurev.astro.41.011802.094844. arXiv: 0301540 [astro-ph]. URL: https://ui.adsabs.harvard.edu/abs/2003ARA&A..41...57L/abstract.

Lamers, Henny J.G.L.M and Emily M Levesque (2017). *Understanding Stellar Evolution*. IOP Publishing. ISBN: 978-0-7503-1278-3. DOI: 10.1088/978-0-7503-1278-3. URL: http://iopscience.iop.org/book/978-0-7503-1278-3.

Larsen, Søren S., Jean P. Brodie, and Deidre A. Hunter (2004). "Dynamical Mass Estimates for Five Young Massive Stellar Clusters". In: AJ 128.5, pp. 2295–2305. ISSN: 0004-6256. DOI: 10.1086/424538.

Larson, R. B. (1969). "Numerical Calculations of the Dynamics of a Collapsing Proto-Star*". In: MNRAS 145.3, pp. 271–295. ISSN: 0035-8711. DOI: 10.1093/mnras/145.3.271.

Latham, David W. et al. (2002). "A Survey of Proper-Motion Stars. XVI. Orbital Solutions for 171 Single-lined Spectroscopic Binaries". In: AJ 124.2, pp. 1144–1161. ISSN: 00046256. DOI: 10.1086/341384.

Law, Nicholas M. et al. (2010). "The High-Order-Multiplicity of Unusually Wide M-dwarf Binaries: Eleven New Triple and Quadruple Systems". In: ApJ 720.2, pp. 1727–1737. DOI: 10.1088/0004-637X/720/2/1727. arXiv:

1007.3735. URL: http://arxiv.org/abs/1007.3735http://dx.doi.org/10.1088/0004-637X/720/2/1727.

Lee, Eve J. and Eugene Chiang (2016). "Breeding Super-Earths and Birthing Super-puffs in Transitional Disks". In: ApJ 817.2, p. 90. ISSN: 0004-637X. DOI: 10.3847/0004-637X/817/2/90. arXiv: arXiv:1510.08855.

Lee, Jeong Eun et al. (2017). "Formation of wide binaries by turbulent fragmentation". In: *Nature Astronomy* 1, p. 0172. ISSN: 23973366. DOI: 10.1038/s41550-017-0172. arXiv: 1707.00233.

Lidov, M.L. (1962). "The evolution of orbits of artificial satellites of planets under the action of gravitational perturbations of external bodies". In: *Planetary and Space Science* 9.10, pp. 719–759. ISSN: 00320633. DOI: 10.1016/0032-0633(62)90129-0.

Lin, D. N. C. and John Papaloizou (1986). "On the tidal interaction between protoplanets and the protoplanetary disk. III - Orbital migration of protoplanets". In: ApJ 309, p. 846. ISSN: 0004-637X. DOI: 10.1086/164653.

Lin, D. N.C., P. Bodenheimer, and D. C. Richardson (1996). "Orbital migration of the planetary companion of 51 Pegasi to its present location". In: Nature 380.6575, pp. 606–607. ISSN: 00280836. DOI: 10.1038/380606a0.

Lin, Jane et al. (2020). "The GALAH survey: Temporal chemical enrichment of the galactic disc". In: MNRAS 491.2, pp. 2043–2056. ISSN: 13652966. DOI: 10.1093/mnras/stz3048. arXiv: 1911.05221.

Lindegren, L. et al. (2018). "Gaia Data Release 2: The astrometric solution". In: A&A 616, A2. arXiv: 1804.09366.

Lodieu, N., M. R. Zapatero Osorio, and E. L. Martin (2009). "Lucky Imaging of M subdwarfs". In: A&A 499.3, pp. 729–736. DOI: 10.1051/0004-6361/200911708. arXiv: 0903.4057. URL: http://arxiv.org/abs/0903.4057http://dx.doi.org/10.1051/0004-6361/200911708.

Lucy, L. B. (1968). "The Structure of Contact Binaries". In: ApJ 151, p. 1123. ISSN: 0004-637X. DOI: 10.1086/149510. URL: http://adsabs.harvard.edu/doi/10.1086/149510.

Ma, Xiangcheng et al. (2020). "Self-consistent proto-globular cluster formation in cosmological simulations of high-redshift galaxies". In: MNRAS 493.3, pp. 4315–4332. ISSN: 13652966. DOI: 10.1093/mnras/staa527. arXiv: 1906.11261. URL: https://ui.adsabs.harvard.edu/abs/2020MNRAS.493.4315M/abstract.

Mackereth, J. Ted and Jo Bovy (2018). "Fast Estimation of Orbital Parameters in Milky Way-like Potentials". In: PASP 130.993, p. 114501. ISSN: 0004-6280. DOI: 10.1088/1538-3873/AADCDD. arXiv: arXiv:1802.02592. URL: https://ui.adsabs.harvard.edu/abs/2018PASP..130k4501M/abstract.

Mainzer, A. et al. (2014). "INITIAL PERFORMANCE OF THE NEOWISE REACTIVATION MISSION". In: ApJ 792.1, p. 30. ISSN: 1538-4357. DOI: 10.1088/0004-637X/792/1/30.

Majewski, Steven R. et al. (2017). "The Apache Point Observatory Galactic Evolution Experiment (APOGEE)". In: AJ 154.3, p. 94. ISSN: 0004-6256. DOI: 10.3847/1538-3881/aa784d. arXiv: 1509.05420.

Marks, Michael and Pavel Kroupa (2011). "Dynamical population synthesis: Constructing the stellar single and binary contents of galactic field populations". In: MNRAS 417.3, pp. 1702–1714. ISSN: 00358711. DOI: 10.1111/j.1365-2966.2011.19519.x. arXiv: 1109.2896. URL: https://academic.oup.com/mnras/article/417/3/1702/1085380.

Marks, Michael and Pavel Kroupa (2012). "Inverse dynamical population synthesis: Constraining the initial conditions of young stellar clusters by studying their binary populations". In: A&A 543, A8. DOI: 10.1051/0004-6361/201118231. arXiv: 1205.1508. URL: http://arxiv.org/abs/1205.1508http://dx.doi.org/10.1051/0004-6361/201118231.

Marks, Michael, Pavel Kroupa, and Seungkyung Oh (2011). "An analytical description of the evolution of binary orbital-parameter distributions in N-body computations of star clusters". In: MNRAS 417.3, pp. 1684–1701. DOI: 10.1111/j.1365-2966.2011.19257.x. arXiv: 1106.5050. URL: http://arxiv.org/abs/1106.5050http://dx.doi.org/10.1111/j.1365-2966.2011.19257.x.

Marrese, P. M. et al. (2019). "Gaia Data Release 2. Cross-match with external catalogues - Algorithms and results". In: A&A 621, A144. DOI: 10.1051/0004-6361/201834142. arXiv: 1808.09151.

Marshall, D. J. et al. (2006). "Modelling the Galactic Interstellar Extinction Distribution in Three Dimensions". In: A&A 453, pp. 635–651. ISSN: 0004-6361. DOI: 10.1051/0004-6361:20053842. arXiv: 0604427 [astro-ph]. URL: http://arxiv.org/abs/astro-ph/0604427http://dx.doi.org/10.1051/0004-6361:20053842.

Martell, S. L. and E. K. Grebel (2010). "Light-element abundance variations in the Milky Way halo". In: A&A 519.1, A14. ISSN: 00046361. DOI: 10.1051/0004-6361/201014135. arXiv: 1005.4070. URL: https://ui.adsabs.harvard.edu/abs/2010A&A...519A..14M/abstract.

Martell, Sarah L. et al. (2011). "Building the Galactic halo from globular clusters: evidence from chemically unusual red giants". In: A&A 534, p. 136. DOI: 10.1051/0004-6361/201117644. arXiv: 1109.3916. URL: http://arxiv.org/abs/1109.3916http://dx.doi.org/10.1051/0004-6361/201117644.

Martell, Sarah L. et al. (2016). "CHEMICAL TAGGING IN THE SDSS-III/APOGEE SURVEY: NEW IDENTIFICATIONS OF HALO STARS WITH GLOBULAR CLUSTER ORIGINS". In: ApJ 825.2, p. 146. DOI: 10.3847/0004-637x/825/2/146. URL: http://www.sdss.org/dr12/algorithms/.

Martig, Marie et al. (2016). "Red giant masses and ages derived from carbon and nitrogen abundances". In: MNRAS 456.4, pp. 3655–3670. ISSN: 13652966. DOI: 10.1093/mnras/stv2830. arXiv: 1511.08203. URL: https://academic.oup.com/mnras/article/456/4/3655/1030597.

Mathieu, Robert D. (1994). "Pre-Main-Sequence Binary Stars". In: ARA&A 32.1, pp. 465–530. ISSN: 0066-4146. DOI: 10.1146/annurev.aa.32.090194.002341.

Matson, Rachel A. et al. (2018). "Stellar Companions of Exoplanet Host Stars in K2". In: AJ 156.1, p. 31. ISSN: 0004-6256. DOI: 10.3847/1538-3881/aac778. arXiv: 1805.08844.

Mayor, M. et al. (2011). "The HARPS search for southern extra-solar planets XXXIV. Occurrence, mass distribution and orbital properties of super-Earths and Neptune-mass planets". In: arXiv: 1109.2497. URL: http://arxiv.org/abs/1109.2497.

Mayor, Michel and Didier Queloz (1995). "A jupiter-mass companion to a solar-type star". In: Nature 378.6555, pp. 355–359. ISSN: 00280836. DOI: 10.1038/378355a0.

Mazzola, Christine N. et al. (2020). "The Close Binary Fraction as a Function of Stellar Parameters in APOGEE: A Strong Anti-Correlation With α Abundances". In: MNRAS 499, p. 1607. arXiv: 2007.09059. URL: http://arxiv.org/abs/2007.09059.

Melo, C. H. F. et al. (2001). "On the pre-main sequence circularization period". In: A&A 378.3, pp. 898–906. ISSN: 0004-6361. DOI: 10.1051/0004-6361:20011262.

Mengel, S. et al. (2005). "Star-formation in NGC 4038/4039 from broad and narrow band photometry: Cluster destruction?" In: A&A 443.1, pp. 41–60. ISSN: 00046361. DOI: 10.1051/0004-6361:20052908.

Minchev, I. et al. (2018). "Estimating stellar birth radii and the time evolution of Milky Way's ISM metallicity gradient". In: MNRAS 481.2, pp. 1645–1657.

ISSN: 13652966. DOI: 10.1093/mnras/sty2033. arXiv: 1804.06856. URL: https://academic.oup.com/mnras/article/481/2/1645/5063589.

Mochnacki, S. W. (1981). "Contact binary stars". In: ApJ 245, p. 650. ISSN: 0004-637X. DOI: 10.1086/158841.

Moe, Maxwell and Rosanne Di Stefano (2017). "Mind your Ps and Qs: the Interrelation between Period (P) and Mass-ratio (Q) Distributions of Binary Stars". In: ApJS 230, p. 15. ISSN: 0067-0049. DOI: 10.3847/1538-4365/aa6fb6. arXiv: 1606.05347.

Moe, Maxwell and Kaitlin M. Kratter (2018). "Dynamical Formation of Close Binaries During the Pre-main-sequence Phase". In: ApJ 854, p. 44. ISSN: 0004-637X. DOI: 10.3847/1538-4357/aaa6d2. arXiv: 1706.09894.

Moe, Maxwell and Kaitlin M. Kratter (2019). "Impact of Binary Stars on Planet Statistics – I. Planet Occurrence Rates, Trends with Stellar Mass, and Wide Companions to Hot Jupiter Hosts". In: arXiv: 1912.01699. URL: http://arxiv.org/abs/1912.01699.

Moe, Maxwell, Kaitlin M. Kratter, and Carles Badenes (2019). "The Close Binary Fraction of Solar-type Stars is Strongly Anti-correlated with Metallicity". In: ApJ 875, p. 61. arXiv: 1808.02116.

Moeckel, Nickolas and Cathie J. Clarke (2011). "The formation of permanent soft binaries in dispersing clusters". In: MNRAS 415.2, pp. 1179–1187. DOI: 10.1111/j.1365-2966.2011.18731.x. arXiv: 1103.2306. URL: http://arxiv.org/abs/1103.2306http://dx.doi.org/10.1111/j.1365-2966.2011.18731.x.

Monroy-Rodríguez, Miguel A. and Christine Allen (2014). "The end of the macho era, revisited: New limits on macho masses from halo wide binaries". In: ApJ 790.2, p. 159. ISSN: 15384357. DOI: 10.1088/0004-637X/790/2/159. arXiv: 1406.5169.

Morbidelli, Alessandro et al. (2012). "Building Terrestrial Planets". In: *Annual Review of Earth and Planetary Sciences* 40.1, pp. 251–275. DOI: 10.1146/annurev-earth-042711-105319. arXiv: 1208.4694.

Murphy, Simon J. et al. (2019). "Gaia-derived luminosities of Kepler A/F stars and the pulsator fraction across the δ Scuti instability strip". In: MNRAS 485.2, pp. 2380–2400. ISSN: 13652966. DOI: 10.1093/mnras/stz590. arXiv: 1903.00015.

Naidu, Rohan P. et al. (2020). "Evidence from the H3 Survey that the Stellar Halo is Entirely Comprised of Substructure". In: ApJ 901, p. 48. arXiv: 2006.08625. URL: http://arxiv.org/abs/2006.08625.

Naoz, Smadar (2016). "The Eccentric Kozai-Lidov Effect and Its Applications". In: ARA&A 54, pp. 441–489. ISSN: 0066-4146. DOI: 10.1146/annurev-astro-081915-023315. arXiv: 1601.07175.

Naoz, Smadar and Daniel C. Fabrycky (2014). "MERGERS AND OBLIQUITIES IN STELLAR TRIPLES". In: ApJ 793.2, p. 137. ISSN: 1538-4357. DOI: 10.1088/0004-637X/793/2/137. arXiv: 1405.5223.

Naoz, Smadar, Will M. Farr, and Frederic A. Rasio (2012). "On the formation of hot jupiters in stellar binaries". In: ApJ 754.2, p. L36. ISSN: 20418205. DOI: 10.1088/2041-8205/754/2/L36. arXiv: 1206.3529.

Naoz, Smadar et al. (2011). "Hot Jupiters from secular planet-planet interactions". In: Nature 473.7346, pp. 187–189. ISSN: 00280836. DOI: 10.1038/nature10076. arXiv: 1011.2501.

Naoz, Smadar et al. (2013a). "Resonant Post-Newtonian Eccentricity Excitation in Hierarchical Three-body Systems". In: ApJ 773, p. 187. ISSN: 0004-637X. DOI: 10.1088/0004-637X/773/2/187. arXiv: 1206.4316.

Naoz, Smadar et al. (2013b). "Secular Dynamics in Hierarchical Three-Body Systems". In: MNRAS 431, pp. 2155–2171. ISSN: 0035-8711. DOI: 10.1093/mnras/stt302. arXiv: 1107.2414.

Nelson, R. P. et al. (2000). "The migration and growth of protoplanets in protostellar discs". In: MNRAS 318.1, pp. 18–36. ISSN: 0035-8711. DOI: 10.1046/j.1365-8711.2000.03605.x. URL: https://academic.oup.com/mnras/article-lookup/doi/10.1046/j.1365-8711.2000.03605.x.

Nelson, Tyler et al. (2021). "Distant Relatives: The Chemical Homogeneity of Comoving Pairs Identified in Gaia". In: arXiv: 2104.12883. URL: http://arxiv.org/abs/2104.12883.

Ness, M. et al. (2015). "The Cannon: A data-driven approach to Stellar Label Determination". In: ApJ 808.1, p. 16. ISSN: 0004-637X. DOI: 10.1088/0004-637X/808/1/16.

Netopil, M. et al. (2016). "On the metallicity of open clusters. III. Homogenised sample". In: A&A 585, A150. ISSN: 0004-6361. DOI: 10.1051/0004-6361/201526370. arXiv: 1511.08884.

Neveu-Vanmalle, M. et al. (2014). "WASP-94 A and B planets: Hot-Jupiter cousins in a twin-star system". In: A&A 572, A49. ISSN: 14320746. DOI: 10.1051/0004-6361/201424744. arXiv: 1409.7566.

Ngo, Henry et al. (2016). "FRIENDS OF HOT JUPITERS. IV. STELLAR COMPANIONS BEYOND 50 au MIGHT FACILITATE GIANT PLANET FORMATION, BUT MOST ARE UNLIKELY TO CAUSE KOZAI–LIDOV MIGRATION". In: ApJ 827.1, p. 8. DOI: 10.3847/0004-637x/827/1/8.

Nordström, B. et al. (2004). "The Geneva-Copenhagen survey of the Solar neighbourhood: Ages, metallicities, and kinematic properties of 14,000 F and G dwarfs". In: A&A 418, pp. 989–1019. ISSN: 0004-6361. DOI: 10.1051/0004-6361:20035959. arXiv: 0405198 [astro-ph]. URL: http://arxiv.org/abs/astro-ph/0405198http://dx.doi.org/10.1051/0004-6361:20035959.

O'Briain, Teaghan et al. (2020). "Interpreting Stellar Spectra with Unsupervised Domain Adaptation". In: arXiv: 2007.03112. URL: http://arxiv.org/abs/2007.03112.

Offner, Stella S. R. et al. (2010). "The Formation of Low-mass Binary Star Systems Via Turbulent Fragmentation". In: ApJ 725.2, p. 1485. ISSN: 0004-637X. DOI: 10.1088/0004-637X/725/2/1485.

Oh, Semyeong et al. (2017). "Comoving Stars in Gaia DR1: An Abundance of Very Wide Separation Comoving Pairs". In: AJ 153.6, p. 257. ISSN: 0004-6256. DOI: 10.3847/1538-3881/aa6ffd. arXiv: 1612.02440.

Olling, Rob P. and Walter Dehnen (2003). "The Oort Constants Measured from Proper Motions". In: ApJ 599, pp. 275–296. ISSN: 0004-637X. DOI: 10.1086/379278. arXiv: 0301486 [astro-ph].

Paczynski, B. et al. (2006). "Eclipsing binaries in ASAS catalog". In: MNRAS 368, pp. 1311–1318. ISSN: 0035-8711. DOI: 10.1111/j.1365-2966.2006.10223.x. arXiv: 0601026 [astro-ph].

Padoan, Paolo and Ake Nordlund (2002). "The Stellar IMF from Turbulent Fragmentation". In: ApJ 576.2, pp. 870–879. DOI: 10.1086/341790. arXiv: 0011465 [astro-ph]. URL: http://arxiv.org/abs/astro-ph/0011465http://dx.doi.org/10.1086/341790.

Peñarrubia, Jorge et al. (2016). "Wide binaries in ultrafaint galaxies: A window on to dark matter on the smallest scales". In: MNRAS 461.1, pp. L72–L76. ISSN: 17453933. DOI: 10.1093/mnrasl/slw090. arXiv: 1605.09384. URL: https://academic.oup.com/mnrasl/article-abstract/461/1/L72/2589565.

Perets, Hagai B. and Daniel C. Fabrycky (2009). "ON THE TRIPLE ORIGIN OF BLUE STRAGGLERS". In: ApJ 697.2, pp. 1048–1056. ISSN: 0004-637X. DOI: 10.1088/0004-637X/697/2/1048.

Pineda, Jaime E. et al. (2015). "The formation of a quadruple star system with wide separation". In: Nature 518.7538, pp. 213–215. ISSN: 14764687. DOI: 10.1038/nature14166. URL: https://ui.adsabs.harvard.edu/abs/2015Natur.518..213P/abstract.

Pinsonneault, M. H. and K. Z. Stanek (2006). "Binaries Like to Be Twins: Implications for Doubly Degenerate Binaries, the Type Ia Supernova Rate, and Other Interacting Binaries". In: ApJ 639.2, pp. L67–L70. ISSN: 0004-637X. DOI: 10.1086/502799.

Piskorz, Danielle et al. (2015). "Friends of Hot Jupiters. III. An Infrared Spectroscopic Search for Low-mass Stellar Companions". In: ApJ 814.2, p. 148. ISSN: 0004-637X. DOI: 10.1088/0004-637X/814/2/148.

Pribulla, Theodor and Slavek M. Rucinski (2006). "Contact Binaries with Additional Components.I. The Extant Data". In: AJ 131, pp. 2986–3007. ISSN: 0004-6256. DOI: 10.1086/503871. arXiv: 0601610 [astro-ph].

Price-Whelan, Adrian et al. (2020). "adrn/gala: v1.3". In: *zndo*. DOI: 10.5281/ZENODO.4159870. URL: https://ui.adsabs.harvard.edu/abs/2020zndo...4159870P/abstract.

Prša, Andrej et al. (2011). "KEPLER ECLIPSING BINARY STARS. I. CATALOG AND PRINCIPAL CHARACTERIZATION OF 1879 ECLIPSING BINARIES IN THE FIRST DATA RELEASE". In: AJ 141.3, p. 83. ISSN: 0004-6256. DOI: 10.1088/0004-6256/141/3/83.

Prugniel, Ph and C. Soubiran (2001). "A database of high and medium-resolution stellar spectra". In: A&A 369.3, pp. 1048–1057. ISSN: 00046361. DOI: 10.1051/0004-6361:20010163. arXiv: 0101378 [astro-ph].

Prugniel, Ph. et al. (2007). "New release of the ELODIE library: Version 3.1". In: arXiv: 0703658 [astro-ph]. URL: http://arxiv.org/abs/astro-ph/0703658.

Quinn, D. P. and M. C. Smith (2009). "A Strip Search for New Very Wide Halo Binaries". In: MNRAS 400.4, pp. 2128–2134. DOI: 10.1111/j.1365-2966.2009.15607.x. arXiv: 0908.3640. URL: http://arxiv.org/abs/0908.3640http://dx.doi.org/10.1111/j.1365-2966.2009.15607.x.

Quinn, D. P. et al. (2009). "On the reported death of the MACHO era". In: MNRAS 396.1, pp. L11–L15. ISSN: 17453933. DOI: 10.1111/j.1745-3933.2009.00652.x. arXiv: 0903.1644. URL: https://ui.adsabs.harvard.edu/abs/2009MNRAS.396L..11Q/abstract.

Rafikov, Roman (2006). "Atmospheres of protoplanetary cores: critical mass for nucleated instability". In: ApJ 648.1, pp. 666–682. DOI: 10.1086/505695. arXiv: 0405507 [astro-ph]. URL: http://arxiv.org/abs/astro-ph/0405507http://dx.doi.org/10.1086/505695.

Rafikov, Roman R. (2005). "Can Giant Planets Form by Direct Gravitational Instability?" In: ApJ 621.1, pp. L69–L72. ISSN: 0004-637X. DOI: 10.1086/428899. arXiv: 0406469 [astro-ph].

Raghavan, Deepak et al. (2010). "A Survey of Stellar Families: Multiplicity of Solar-Type Stars". In: ApJS 190, pp. 1–42. ISSN: 0067-0049. DOI: 10.1088/0067-0049/190/1/1. arXiv: 1007.0414.

Rasio, F. A. et al. (1996). "Tidal Decay of Close Planetary Orbits". In: ApJ 470, p. 1187. ISSN: 0004-637X. DOI: 10.1086/177941.

Rasio, Frederic A. and Eric B. Ford (1996). "Dynamical instabilities and the formation of extrasolar planetary systems". In: *Science* 274.5289, pp. 954–956. ISSN: 00368075. DOI: 10.1126/science.274.5289.954.

Rastegaev, D. A. et al. (2008). "Speckle interferometry of metal-poor stars in the solar neighborhood. II". In: *Astrophysical Bulletin* 63.3, pp. 278–289. ISSN: 1990-3413. DOI: 10.1134/s1990341308030085. URL: https://ui.adsabs.harvard.edu/abs/2008AstBu..63..278R/abstract.

Reid, M. J. et al. (2009). "TRIGONOMETRIC PARALLAXES OF MASSIVE STAR-FORMING REGIONS. VI. GALACTIC STRUCTURE, FUNDAMENTAL PARAMETERS, AND NONCIRCULAR MOTIONS". In: ApJ 700.1, pp. 137–148. ISSN: 0004-637X. DOI: 10.1088/0004-637X/700/1/137.

Reipurth, Bo and Seppo Mikkola (2012). "Formation of the widest binary stars from dynamical unfolding of triple systems". In: Nature 492.7428, pp. 221–224. ISSN: 00280836. DOI: 10.1038/nature11662.

Retterer, J. M. and I. R. King (1982). "Wide binaries in the solar neighborhood". In: ApJ 254, p. 214. ISSN: 0004-637X. DOI: 10.1086/159725.

Riello, M. et al. (2018). "Gaia Data Release 2: Processing of the photometric data". In: A&A 616, A3. ISSN: 0004-6361. DOI: 10.1051/0004-6361/201832712. URL: https://www.aanda.org/10.1051/0004-6361/201832712.

Riello, M. et al. (2020). "Gaia Early Data Release 3: Photometric content and validation". In: A&A. arXiv: 2012.01916. URL: http://arxiv.org/abs/2012.01916.

Riess, Adam G. et al. (1998). "Observational Evidence from Supernovae for an Accelerating Universe and a Cosmological Constant". In: AJ 116, pp. 1009–1038. ISSN: 0004-6256. DOI: 10.1086/300499. arXiv: 9805201 [astro-ph].

Rimoldini, L. et al. (2019). "All-sky classification of high-amplitude pulsating stars". In: A&A 625, A97. ISSN: 14320746. DOI: 10.1051/0004-6361/201834616. arXiv: 1811.03919.

Robertson, J. A. and P. P. Eggleton (1977). "The evolution of W Ursae Majoris systems". In: MNRAS 179.3, pp. 359–375. ISSN: 0035-8711. DOI: 10.1093/mnras/179.3.359.

Robin, A. C. et al. (2003). "A synthetic view on structure and evolution of the Milky Way". In: A&A 409.2, pp. 523–540. ISSN: 0004-6361. DOI: 10.1051/0004-6361:20031117.

Robitaille, Thomas P. et al. (2013). "Astropy: A community Python package for astronomy". In: A&A 558, A33. ISSN: 00046361. DOI: 10.1051/0004-6361/201322068. arXiv: 1307.6212.

Rucinski, Slavek M. (1998). "Contact Binaries of the Galactic Disk: Comparison of the Baade's Window and Open Cluster Samples". In: AJ 116.6, pp. 2998–3017. ISSN: 00046256. DOI: 10.1086/300644. arXiv: 9806154 [astro-ph].

Rucinski, Slavek M., Theodor Pribulla, and Marten H. van Kerkwijk (2007). "Contact Binaries with Additional Components. III. A Search Using Adaptive Optics". In: AJ 134.6, pp. 2353–2365. ISSN: 0004-6256. DOI: 10.1086/523353.

Rybizki, Jan et al. (2018). "A Gaia DR2 Mock Stellar Catalog". In: PASP 130.989, p. 074101. ISSN: 0004-6280. DOI: 10.1088/1538-3873/aabd70. arXiv: 1804.01427.

Salim, Samir and Andrew Gould (2002). "Improved Astrometry and Photometry for the Luyten Catalog. II. Faint Stars and the Revised Catalog". In: ApJ 582.2, pp. 1011–1031. DOI: 10.1086/344822. arXiv: 0206318 [astro-ph]. URL: http://arxiv.org/abs/astro-ph/0206318http://dx.doi.org/10.1086/344822.

Santerne, A. et al. (2016). "SOPHIE velocimetry of Kepler transit candidates: XVII. The physical properties of giant exoplanets within 400 days of period". In: A&A 587, A64. ISSN: 14320746. DOI: 10.1051/0004-6361/201527329. arXiv: 1511.00643.

Santos, N. C., G. Israelian, and M. Mayor (2004). "Spectroscopic [Fe/H] for 98 extra-solar planet-host stars. Exploring the probability of planet formation". In: A&A 415.3, pp. 1153–1166. ISSN: 00046361. DOI: 10.1051/0004-6361:20034469. arXiv: 0311541 [astro-ph].

Schlaufman, Kevin C. (2018). "Evidence of an Upper Bound on the Masses of Planets and Its Implications for Giant Planet Formation". In: ApJ 853.1, p. 37. ISSN: 1538-4357. DOI: 10.3847/1538-4357/aa961c. arXiv: 1801.06185.

Schönrich, Ralph, James Binney, and Walter Dehnen (2010). "Local kinematics and the local standard of rest". In: MNRAS 403.4, pp. 1829–1833. ISSN: 00358711. DOI: 10.1111/j.1365-2966.2010.16253.x.

Schwarzenberg-Czerny, A. (1996). "Fast and Statistically Optimal Period Search in Uneven Sampled Observations". In: ApJ 460.2, pp. L107–L110. ISSN: 0004637X. DOI: 10.1086/309985.

Sellwood, J. A. and J. J. Binney (2002). "Radial Mixing in Galactic Discs". In: MNRAS 336.3, pp. 785–796. DOI: 10.1046/j.1365-8711.2002.05806.x. arXiv: 0203510 [astro-ph]. URL: http://arxiv.org/abs/astro-ph/0203510http://dx.doi.org/10.1046/j.1365-8711.2002.05806.x.

Sharma, S. et al. (2014). "Kinematic modelling of the Milky Way using the RAVE and GCS stellar surveys". In: ApJ 793, p. 51. ISSN: 0004-637X. DOI: 10.1088/0004-637X/793/1/51. arXiv: 1405.7435.

Sharma, Sanjib et al. (2011). "GALAXIA: A CODE TO GENERATE A SYNTHETIC SURVEY OF THE MILKY WAY". In: ApJ 730.1, p. 3. ISSN: 0004-637X. DOI: 10.1088/0004-637X/730/1/3.

Shaya, Ed J. and Rob P. Olling (2011). "Very Wide Binaries and Other Comoving Stellar Companions: A Bayesian Analysis of the Hipparcos Catalogue". In: ApJS 192.1, p. 2. ISSN: 0067-0049. DOI: 10.1088/0067-0049/192/1/2. arXiv: arXiv:1007.0425.

Shibata, Masaru and Keisuke Taniguchi (2006). "Merger of binary neutron stars to a black hole: Disk mass, short gamma-ray bursts, and quasinormal mode ringing". In: Phys. Rev. D 73.6, p. 064027. ISSN: 1550-7998. DOI: 10.1103/PhysRevD.73.064027. arXiv: 0603145 [astro-ph].

Silva Aguirre, V et al. (2018). "Confirming chemical clocks: asteroseismic age dissection of the Milky Way disk(s)". In: MNRAS 475, p. 548. ISSN: 0035-8711. DOI: 10.1093/mnras/sty150. arXiv: 1710.09847.

Simon, M. (1997). "Clustering of Young Stars in Taurus, Ophiuchus, and the Orion Trapezium". In: ApJ 482.1, pp. L81–L84. ISSN: 0004637X. DOI: 10.1086/310678. URL: https://ui.adsabs.harvard.edu/abs/1997ApJ...482L..81S/abstract.

Slawson, Robert W. et al. (2011). "KEPLER ECLIPSING BINARY STARS. II. 2165 ECLIPSING BINARIES IN THE SECOND DATA RELEASE". In: AJ 142.5, p. 160. ISSN: 0004-6256. DOI: 10.1088/0004-6256/142/5/160.

Smartt, S. J. et al. (2017). "A kilonova as the electromagnetic counterpart to a gravitational-wave source". In: Nature 551.7678, pp. 75–79. ISSN: 0028-0836. DOI: 10.1038/nature24303. arXiv: 1710.05841.

Stepien, K. (1995). "Loss of angular momentum of cool close binaries and formation of contact systems". In: MNRAS 274, pp. 1019–1028. ISSN: 1365-2966. DOI: 10.1093/mnras/274.4.1019.

Stepien, K. and K. Gazeas (2012). "Evolution of Low Mass Contact Binaries". In: Acta Astron. 62, pp. 153–177. URL: https://ui.adsabs.harvard.edu/abs/2012AcA....62..153S/abstract.

Stepien, Kazimierz and Marcin Kiraga (2015). "Model computations of blue stragglers and W UMa-type stars in globular clusters". In: A&A 577, A117. ISSN: 0004-6361. DOI: 10.1051/0004-6361/201425550. arXiv: 1503.07758.

Tanaka, Kei E. I. and Kazuyuki Omukai (2014). "Gravitational instability in protostellar disks at low metallicities". In: MNRAS 439, pp. 1884–1896. ISSN: 0035-8711. DOI: 10.1093/mnras/stu069. arXiv: 1401.2993.

Teske, Johanna K., Sandhya Khanal, and Ivan Ramírez (2016). "THE CURIOUS CASE OF ELEMENTAL ABUNDANCE DIFFERENCES IN THE DUAL HOT JUPITER HOSTS WASP-94A AND B". In: ApJ 819.1, p. 19. ISSN: 1538-4357. DOI: 10.3847/0004-637x/819/1/19. arXiv: 1601.01731.

Tian, Hai-Jun et al. (2020). "The Separation Distribution of Ultrawide Binaries across Galactic Populations". In: ApJS 246.1, p. 4. ISSN: 1538-4365. DOI: 10.3847/1538-4365/ab54c4. arXiv: 1909.04765.

Ting, Yuan-Sen, Charlie Conroy, and Alyssa Goodman (2015). "PROSPECTS for CHEMICALLY TAGGING STARS in the GALAXY". In: ApJ 807.1, p. 104. ISSN: 15384357. DOI: 10.1088/0004-637X/807/1/104. arXiv: 1504.03327.

Ting, Yuan-Sen and Hans-Walter Rix (2019). "The Vertical Motion History of Disk Stars throughout the Galaxy". In: ApJ 878.1, p. 21. ISSN: 1538-4357. DOI: 10.3847/1538-4357/ab1ea5. arXiv: 1808.03278. URL: https://doi.org/10.3847/1538-4357/ab1ea5.

Ting, Yuan-Sen et al. (2017a). "Measuring 14 elemental abundances with R=1,800 LAMOST spectra". In: ApJ 849, p. L9. DOI: 10.3847/2041-8213/aa921c. arXiv: 1708.01758. URL: http://arxiv.org/abs/1708.01758http://dx.doi.org/10.3847/2041-8213/aa921c.

Ting, Yuan-Sen et al. (2017b). "Prospects for Measuring Abundances of >20 Elements with Low-resolution Stellar Spectra". In: ApJ 843.1, p. 32. ISSN: 1538-4357. DOI: 10.3847/1538-4357/aa7688. arXiv: 1706.00111.

Ting, Yuan-Sen et al. (2019). "The Payne: self-consistent ab initio fitting of stellar spectra". In: ApJ 879, p. 69. DOI: 10.3847/1538-4357/ab2331. arXiv: 1804.01530. URL: http://arxiv.org/abs/1804.01530http://dx.doi.org/10.3847/1538-4357/ab2331.

Tobin, John et al. (2016a). "A Triple Protostar System Formed via Fragmentation of a Gravitationally Unstable Disk". In: Nature 538, pp. 483–486. ISSN: 0028-0836. DOI: 10.1038/nature20094. arXiv: 1610.08524.

Tobin, John J. et al. (2016b). "The VLA Nascent Disk and Multiplicity Survey of Perseus Protostars (VANDAM). II. Multiplicity of Protostars in the Perseus Molecular Cloud". In: ApJ 818.1, p. 73. DOI: 10.3847/0004-637X/818/1/73. arXiv: 1601.00692. URL: http://arxiv.org/abs/1601.00692http://dx.doi.org/10.3847/0004-637X/818/1/73.

Tohline, Joel E. (2002). "The Origin of Binary Stars". In: ARA&A 40.1, pp. 349–385. ISSN: 0066-4146. DOI: 10.1146/annurev.astro.40.060401.093810.

Tokovinin, A. and O. Kiyaeva (2016). "Eccentricity distribution of wide binaries". In: MNRAS 456.2, pp. 2070–2079. ISSN: 13652966. DOI: 10.1093/mnras/stv2825. arXiv: 1512.00278.

Tokovinin, A. et al. (2006). "Tertiary companions to close spectroscopic binaries". In: A&A 450, pp. 681–693. ISSN: 0004-6361. DOI: 10.1051/0004-6361:20054427. arXiv: 0601518 [astro-ph].

Tokovinin, A. A. (1997). "On the multiplicity of spectroscopic binary stars". In: *Astronomy Letters* 23.6, p. 727.

Tokovinin, A. A. (2000). "On the origin of binaries with twin components". In: A&A 360, pp. 997–1002. URL: https://ui.adsabs.harvard.edu/abs/2000A%26A...360..997T/abstract.

Tokovinin, Andrei (2014a). "From binaries to multiples I: Data on F and G dwarfs within 67 pc of the Sun". In: AJ 147.4, p. 86. DOI: 10.1088/0004-6256/147/4/86. arXiv: 1401.6825. URL: http://arxiv.org/abs/1401.6825http://dx.doi.org/10.1088/0004-6256/147/4/86.

Tokovinin, Andrei (2014b). "FROM binaries to multiples. II. Hierarchical multiplicity of F and G dwarfs". In: AJ 147.4, p. 87. ISSN: 00046256. DOI: 10.1088/0004-6256/147/4/87. arXiv: 1401.6827.

Tokovinin, Andrei (2017). "Formation of wide binary stars from adjacent cores". In: MNRAS 468.3, pp. 3461–3467. ISSN: 0035-8711. DOI: 10.1093/mnras/stx707. arXiv: 1703.06794.

Tokovinin, Andrei (2020). "Eccentricity distribution of wide low-mass binaries". In: MNRAS 496, p. 993. arXiv: 2004.06570. URL: http://arxiv.org/abs/2004.06570.

Tokovinin, Andrei and Sébastien Lépine (2012). "Wide Companions to Hipparcos Stars within 67 pc of the Sun". In: AJ 144.4, p. 102. ISSN: 0004-6256. DOI: 10.1088/0004-6256/144/4/102.

Tokovinin, Andrei and Maxwell Moe (2020). "Formation of close binaries by disc fragmentation and migration, and its statistical modeling". In: MNRAS 491, pp. 5158–5171. arXiv: 1910.01522. URL: http://arxiv.org/abs/1910.01522.

Torres, G. (2003). "Discovery of a Bright Eclipsing Binary in the Pleiades Cluster". In: *Information Bulletin on Variable Stars* 5402, p. 1.

Tylenda, R. et al. (2011). "V1309 Scorpii: merger of a contact binary". In: A&A 528, A114. ISSN: 0004-6361. DOI: 10.1051/0004-6361/201016221.

Van, K. X., N. Ivanova, and C. O. Heinke (2019). "Low-mass X-ray binaries: The effects of the magnetic braking prescription". In: MNRAS 483.4, pp. 5595–5613. ISSN: 13652966. DOI: 10.1093/mnras/sty3489. arXiv: 1812.08239.

Van, Kenny X. and Natalia Ivanova (2019). "Evolving LMXBs: CARB Magnetic Braking". In: ApJ 886.2, p. L31. ISSN: 2041-8213. DOI: 10.3847/2041-8213/ab571c.

VanderPlas, Jacob T. (2018). "Understanding the Lomb–Scargle Periodogram". In: ApJS 236.1, p. 16. ISSN: 1538-4365. DOI: 10.3847/1538-4365/aab766.

Veer, F. van't (1979). "The angular momentum controlled evolution of solar type contact binaries." In: A&A 80, p. 287.

Wang, Ji et al. (2014a). "Influence of stellar multiplicity on planet formation. I. evidence of suppressed planet formation due to stellar companions within 20 AU and validation of four planets from the kepler multiple planet candidates". In: ApJ 783.1, p. 4. ISSN: 15384357. DOI: 10.1088/0004-637X/783/1/4. arXiv: 1309.7097.

Wang, Ji et al. (2014b). "Influence of stellar multiplicity on planet formation. II. Planets are less common in multiple-star systems with separations smaller than 1500 AU". In: ApJ 791.2, p. 111. ISSN: 15384357. DOI: 10.1088/0004-637X/791/2/111. arXiv: 1407.3344.

Warner, Brian (1995). *Cataclysmic variable stars*. Cambridge Astrophysics Series. Cambridge Univ. Press, Cambridge, New York.

Webbink, R. F. (1976). "The evolution of low-mass close binary systems. I - The evolutionary fate of contact binaries". In: ApJ 209, p. 829. ISSN: 0004-637X. DOI: 10.1086/154781.

Webbink, R. F. (1984). "Double white dwarfs as progenitors of R Coronae Borealis stars and Type I supernovae". In: ApJ 277, p. 355. ISSN: 0004-637X. DOI: 10.1086/161701.

Weidenschilling, Stuart J. and Francesco Marzari (1996). "Gravitational scattering as a possible origin for giant planets at small stellar distances". In: Nature 384.6610, pp. 619–621. ISSN: 00280836. DOI: 10.1038/384619a0.

Weinberg, Martin D., Stuart L. Shapiro, and Ira Wasserman (1987). "The dynamical fate of wide binaries in the solar neighborhood". In: ApJ 312, p. 367. ISSN: 0004-637X. DOI: 10.1086/164883.

Whelan, John and Jr. Iben, Icko (1973). "Binaries and Supernovae of Type I". In: ApJ 186, p. 1007. DOI: 10.1086/152565.

Widmark, Axel and Giacomo Monari (2019). "The dynamical matter density in the solar neighbourhood inferred from Gaia DR1". In: MNRAS 482.1, pp. 262–277. ISSN: 13652966. DOI: 10.1093/mnras/sty2400. arXiv: 1711.07504.

Wojno, Jennifer et al. (2016). "Chemical separation of disc components using RAVE". In: MNRAS 461.4, pp. 4246–4255. ISSN: 13652966. DOI: 10.1093/mnras/stw1633. arXiv: 1603.09339.

Wright, Edward L. et al. (2010). "The Wide-field Infrared Survey Explorer (WISE): Mission Description and Initial On-orbit Performance". In: AJ 140, pp. 1868–1881. ISSN: 0004-6256. DOI: 10.1088/0004-6256/140/6/1868. arXiv: 1008.0031.

Wright, J. T. et al. (2012). "The frequency of hot jupiters orbiting nearby solar-type stars". In: ApJ 753.2, p. 160. ISSN: 15384357. DOI: 10.1088/0004-637X/753/2/160. arXiv: 1205.2273.

Wu, Y. and N. Murray (2003). "Planet Migration and Binary Companions: The Case of HD 80606b". In: ApJ 589.1, pp. 605–614. ISSN: 0004-637X. DOI: 10.1086/374598. arXiv: 0303010 [astro-ph].

Wu, Yue et al. (2011a). "Automatic Determination of Stellar Atmospheric Parameters and Construction of Stellar Spectral Templates of the Guoshoujing Telescope (LAMOST)". In: *Research in Astronomy and Astrophysics* 11.8, pp. 924–946. DOI: 10.1088/1674-4527/11/8/006. arXiv: 1105.2681. URL: http://arxiv.org/abs/1105.2681http://dx.doi.org/10.1088/1674-4527/11/8/006.

Wu, Yue et al. (2011b). "Coude-feed stellar spectral library - atmospheric parameters". In: A&A 525, A71. DOI: 10.1051/0004-6361/201015014. arXiv: 1009.1491. URL: http://arxiv.org/abs/1009.1491http://dx.doi.org/10.1051/0004-6361/201015014.

Wyse, Rosemary F. G., Maxwell Moe, and Kaitlin M. Kratter (2020). "The Rich Lack Close Neighbours: The Dependence of Blue-Straggler Fraction on Metallicity". In: MNRAS 493, pp. 6109–6118. DOI: 10.1093/mnras/staa731. arXiv: 2004.00066. URL: http://arxiv.org/abs/2004.00066http://dx.doi.org/10.1093/mnras/staa731.

Xiang, Maosheng et al. (2019). "Abundance Estimates for 16 Elements in 6 Million Stars from LAMOST DR5 Low-Resolution Spectra". In: ApJS 245.2, p. 34. DOI: 10.3847/1538-4365/ab5364. arXiv: 1908.09727.

Yakut, K., B. Kalomeni, and C. A. Tout (2008). "Angular momentum loss by magnetic braking and gravitational radiation in relativistic binary stars". In: ISSN: 13138502. arXiv: 0811.0455.

Yakut, Kadri and Peter P. Eggleton (2005). "Evolution of Close Binary Systems". In: ApJ 629.2, pp. 1055–1074. ISSN: 0004-637X. DOI: 10.1086/431300.

Yanny, Brian et al. (2009). "SEGUE: A spectroscopic survey of 240,000 stars with g = 14-20". In: AJ 137.5, pp. 4377–4399. ISSN: 00046256. DOI: 10.1088/0004-6256/137/5/4377. arXiv: 0902.1781. URL: https://ui.adsabs.harvard.edu/abs/2009AJ....137.4377Y/abstract.

Yildiz, Mutlu (2014). "Origin of W UMa-type contact binaries - age and orbital evolution". In: MNRAS 437.1, pp. 185–194. ISSN: 0035-8711. DOI: 10.1093/mnras/stt1874. arXiv: 1310.5526.

Yildiz, Mutlu and Tuncay Dogan (2013). "On the origin of W UMa type Contact binaries - a new method for computation of initial masses". In: MNRAS 430.3, pp. 2029–2038. ISSN: 1365-2966. DOI: 10.1093/mnras/stt028. arXiv: 1301.6035.

Yoo, Jaiyul, Julio Chaname, and Andrew Gould (2004). "The End of the MACHO Era: Limits on Halo Dark Matter from Stellar Halo Wide Binaries". In: ApJ 601.1, pp. 311–318. ISSN: 0004-637X. DOI: 10.1086/380562. arXiv: 0307437 [astro-ph].

Yuan, Haibo et al. (2015). "Stellar loci II. a model-free estimate of the binary fraction for field FGK stars". In: ApJ 799, p. 135. ISSN: 0004-637X. DOI: 10.1088/0004-637X/799/2/135. arXiv: 1412.1233.

Zakamska, Nadia L. and Scott Tremaine (2004). "Excitation and Propagation of Eccentricity Disturbances in Planetary Systems". In: AJ 128.2, pp. 869–877. ISSN: 0004-6256. DOI: 10.1086/422023.

Zapatero Osorio, M. R. and E. L. Martin (2004). "A CCD Imaging Search for Wide Metal-Poor Binaries". In: A&A 419.1, pp. 167–180. DOI: 10.1051/0004-6361:20035907. arXiv: 0402310 [astro-ph]. URL: http://arxiv.org/abs/astro-ph/0402310http://dx.doi.org/10.1051/0004-6361:20035907.

Zhang, X. B., L. Deng, and P. Lu (2009). "TX Cnc AS A MEMBER OF THE PRAESEPE OPEN CLUSTER". In: AJ 138.2, pp. 680–685. ISSN: 0004-6256. DOI: 10.1088/0004-6256/138/2/680.

Zhang, Z. H. et al. (2013). "A spectroscopic and proper motion search of sloan digital sky survey: Red subdwarfs in binary systems". In: MNRAS 434.2, pp. 1005–1027. ISSN: 00358711. DOI: 10.1093/mnras/stt1030. URL: https://academic.oup.com/mnras/article/434/2/1005/1062934.

Zhao, Gang et al. (2012). "LAMOST spectral survey — An overview". In: *Research in Astronomy and Astrophysics* 12.7, p. 723. ISSN: 1674-4527. DOI: 10.1088/1674-4527/12/7/002.

Zhou, G. et al. (2019). "Two New HATNet Hot Jupiters around A Stars and the First Glimpse at the Occurrence Rate of Hot Jupiters from TESS". In: AJ 158.4, p. 141. ISSN: 1538-3881. DOI: 10.3847/1538-3881/ab36b5. arXiv: 1906.00462.

Ziegler, Carl et al. (2015). "Multiplicity of the Galactic Senior Citizens: A high-resolution search for cool subdwarf companions". In: ApJ 804, p. 30. DOI: 10.1088/0004-637X/804/1/30. arXiv: 1411.3336. URL: http://arxiv.org/abs/1411.3336http://dx.doi.org/10.1088/0004-637X/804/1/30.

Ziegler, Carl et al. (2019). "SOAR TESS Survey. I: Sculpting of TESS planetary systems by stellar companions". In: arXiv: 1908.10871. URL: http://arxiv.org/abs/1908.10871.

Zinnecker, H, R Köhler, and H Jahreiß (2004). "BINARY STATISTICS AMONG POPULATION II STARS". In: *RevMexAA* 21, pp. 33–36. URL: https://ui.adsabs.harvard.edu/abs/2004RMxAC..21...33Z/abstract.